OPEN ACCESS

University of BRISTOL

This electronic thesis or dissertation has been downloaded from Explore Bristol Research, http://research-information.bristol.ac.uk

Author:
Reolizo, Lien Mari P.

Title:
Potential of Proline Rich Homeodomain (PRH) to inhibit intimal thickening

General rights
Access to the thesis is subject to the Creative Commons Attribution - NonCommercial-No Derivatives 4.0 International Public License. A copy of this may be found at https://creativecommons.org/licenses/by-nc-nd/4.0/legalcode This license sets out your rights and the restrictions that apply to your access to the thesis so it is important you read this before proceeding.

Take down policy
Some pages of this thesis may have been removed for copyright restrictions prior to having it been deposited in Explore Bristol Research. However, if you have discovered material within the thesis that you consider to be unlawful e.g. breaches of copyright (either yours or that of a third party) or any other law, including but not limited to those relating to patent, trademark, confidentiality, data protection, obscenity, defamation, libel, then please contact collections-metadata@bristol.ac.uk and include the following information in your message:

• Your contact details
• Bibliographic details for the item, including a URL
• An outline nature of the complaint

Your claim will be investigated and, where appropriate, the item in question will be removed from public view as soon as possible.

POTENTIAL OF PROLINE RICH HOMEODOMAIN (PRH) TO INHIBIT INTIMAL THICKENING

LIEN MARI P. REOLIZO

A dissertation submitted to the University of Bristol in accordance with the requirements of the degree of Doctor of Philosophy (Translational Health Sciences) in the Faculty of Health Sciences, Bristol Medical School, Research Floor Level 7, Queens' Building, Bristol Royal Infirmary, Upper Maudlin St, Bristol, BS2 8HW

JANUARY 2021

Word count: 64, 989

ABSTRACT

Autologous human saphenous vein (HSV) is commonly used as a conduit for coronary artery bypass grafting in patients with ischemic heart disease. However, the primary patency of venous grafts is poor, with 30-50% of grafted conduits failing within 10 years post-implantation. Early vein graft failure is caused in 10-15% of grafts by thrombosis whilst the remainder fail due to late vein graft failure instigated by intimal thickening. The Achilles heel of this surgical technique is vascular injury resulting from endothelial cell (EC) damage and inflammation which promotes aberrant, uncontrolled migration and proliferation of vascular smooth muscle cells (VSMCs) within the intimal layer of the blood vessel wall. Consequent intimal thickening triggers the narrowing of the lumen and causes susceptibility of the bypass graft to superimposed atherosclerosis and restenosis. Therefore, there is a pressing unmet clinical need to identify new approaches that reduce VSMC proliferation and intimal thickening without having detrimental effects on endothelial coverage.

Proline Rich Homeodomain (PRH) protein is a transcription factor required for cell growth and differentiation. Previous work by our laboratory demonstrated that adenovirus-mediated overexpression of S163C:S177C PRH in rat VSMCs and neointimal ex vivo human saphenous vein organ cultures effectively prevented intimal thickening of the venous grafts. In this thesis, we investigated whether adenovirus-mediated delivery of mutant non-phosphorylated PRH protein using Ad: PRH S163C:S177C attenuates VSMC proliferation without detrimental effects on the endothelial cells. We observed that overexpression of Ad: PRH S163C:S177C in human saphenous vein VSMCs significantly inhibited proliferation, migration and promoted the contractile phenotype. Importantly, we also showed that overexpression of Ad: PRH S163C:S177C impaired carotid artery ligation induced neointimal proliferation and thickening. Importantly, Ad: PRH S163C:S177C did not significantly affect HSV endothelial cell (HSVEC) proliferation, migration and apoptosis. However, interestingly, the expression of TNFα-induced vascular cell adhesion molecule 1 (VCAM-1) and Intercellular Adhesion Molecule 1 (ICAM-1) proteins were significantly reduced in Ad: PRH S163C:S177C treated HSVECs and was associated with significantly reduced monocyte adhesion. Other inflammation-related molecules such as interleukin-6 (IL-6) and monocyte chemotactic factor-1 (MCP-1) measured by ELISA were also significantly attenuated, indicative of suppression of a pro-inflammatory response to TNFα. To identify novel PRH S163C:S177C-regulated target genes in HSV VSMCs, we have utilised Next Generation Sequencing. Our findings revealed Signal

transducer and activator of transcription 1 (STAT-1) and Histone deacetylase 9 (HDAC-9) as novel targets of PRH which were validated by in vitro and in vivo analyses.

Taken together, this study has revealed that overexpression of PRH S163C:S177C attenuated VSMC proliferation, migration and apoptosis and induced a contractile VSMC phenotype, whilst promoting the endothelial cell repair and anti-inflammatory properties. Importantly, we have shown that overexpression of PRH S163C:S177C in vivo attenuated intimal thickening without affecting endothelial coverage in a validated mouse carotid artery ligation model. Moreover, this study has enabled the identification of novel mechanisms that beneficially regulate VSMC behaviour and preserve the endothelial function. These findings have the potential to translate into novel therapeutics for the reduction of late vein graft failure in the future.

DEDICATION AND ACKNOWLEDGEMENTS

First and foremost, I would like to express my deepest appreciation and gratitude to Professor Sarah Jane George for providing me this opportunity. I am honoured to have worked with her research group under her guidance and supervision. Her time and devotion to my project is greatly appreciated and I cannot thank her enough for being an amazing mentor. I would also like extend my sincerest appreciation to my co-supervisors Dr. Jason Johnson, Professor Kevin Gaston and Dr. Padma Sheela Jayaraman.

I could not have completed my research project without the guidance of Dr. Bethan Brown for being approachable and her tireless help with training me in experimental techniques and advice which I have learnt so much from. I am deeply grateful and indebted to Dr. Kerry Wadey for her laboratory teaching and time dedicated to editing this thesis. I would like to further acknowledge Dr. Helen Williams for helping me complete my *in vivo* studies despite the COVID-19 disruption. I would also like to thank Dr. Graciela Sala-Newby and Tom Hathway for generating the adenoviruses utilised throughout this project. My colleagues, Dr. Silvia Boyajian, Dr. Nadiah Suleiman, Ze Li, Georgios Kremastiosis, Alexandros Stroutzas, Aleksandra Frankow, Tessa Forbes, Dr. Rosaria Bianco, Dr. Karina Di Gregoli, Dr. Andy Bond and Dr. Mark Bond are thanked for creating an exhilarating atmosphere and providing support throughout this project.

Most importantly, I would like to dedicate this work to my parents, Mr. Neil Reolizo and Mrs. Maricele Reolizo. I would not be where I am today if it weren't for the unwavering love, patience, support and sacrifices you have made over the years. I am truly grateful for all that you do. Thank you for seeing me in all things I can still become and continue having faith that I can do and be whatever I want. To my siblings, Aaron, JB and Brooke, a very huge thank you for providing me with love, laughter, and support.

Finally, I would like to give special thanks to the British Heart foundation for supporting and funding this research project. I am grateful for giving me the chance and opportunity.

AUTHOR'S DECLARATION

I declare that the work in this thesis was carried out in accordance with the requirements of the University's *Regulations and Code of Practice for Research Degree Programmes* and that it has not been submitted for any other academic award. Except where indicated by specific reference in the text, the work is the candidate's own work. Work done in collaboration with, or with the assistance of, others, is indicated as such. Any views expressed in this thesis are those of the author.

SIGNED: ..... DATE: 22nd January 2021 .....

PUBLICATION LIST

Unpublished Papers

REOLIZO, L.M., WADEY, K.S., WILLIAMS, H., FRANKOW, A., GASTON, K., JAYARAMAN, P.S., JOHNSON, J.L. and GEORGE, S.J. 2020. The potential of PRH to inhibit intimal thickening. Unpublished.

BROWN, B.A., REOLIZO, L.M., WILLIAMS, H., FRANKOW, A., JAYARAMAN, P.S., ZAKKAR, M., PULA, G., GASTON, K. and GEORGE, S.J. 2020. CX-4945 and TBCA Paper. Unpublished.

Conference Attended

Bristol Heart Institute "Rising to the Challenge" Conference, 2020, Bristol, UK.

Future Physiology Annual Conference, 2019, Liverpool, UK.

Bristol Endothelial Annual Meeting, 2019, Bristol, UK.

British Heart Foundation Fellow's Meeting, 2019, University of Cambridge, UK.

British Atherosclerosis Society, 2019, University of Oxford, UK.

Annual Bristol Heart Institute (BHI) Specialist Research Institute Meeting, 2018, Bristol, UK.

Awards

Young Investigator's Award (2nd Prize) at the Bristol Heart Institute "Rising to the Challenge" Conference, University of Bristol 2020.

Special Commendation Poster Presentation Award at the British Heart Foundation Fellow's Meeting, University of Cambridge 2019.

TABLE OF CONTENTS

LIST OF FIGURES

LIST OF TABLES

LIST OF SUPPLEMENTARY MATERIALS

LIST OF ABBREVIATIONS

A

Ad	adenovirus
αSMA	α smooth muscle actin
ACTA2	smooth muscle-a-actin
AML	Acute myelogenous leukaemia
ANOVA	Analysis of variance
ApoE	Apolipoprotein E
ARRIVE	Animal Research: Reporting of In Vivo Experiments
ATP	Adenosine triphosphate
AUC	Analytical ultracentrifugation

B

BMS	Bare Metal Stents
BCA	Bicinchoninic acid
BHF	British Heart Foundation
BrdU	Bromodeoxyuridine
BSA	Bovine serum albumin

C

CABG	Coronary artery bypass graft
CAD	Coronary artery disease
cAMP	Cyclic adenosine 3’,5’-cyclic monophosphate
CAR	Coxsackievirus and adenovirus receptor
CASCADE	Clopidogrel after Surgery for Coronary Artery Disease
CC-3	Cleaved caspase-3
CCN1	Calponin
CD31	Cluster of differentiation 31
ChIP	Chromatin immunoprecipitation
CK2	Casein kinase II
CKI	Cyclin-dependent kinase inhibitor
CLL	Chronic lymphocytic leukaemia
CPB	Cardiopulmonary bypass
CRE	cAMP responsive element
CREB	cAMP responsive element binding protein
CT	Cycle threshold

CTCL	Cutaneous T-cell lymphoma
CVD	Cardiovascular disease

D

DAB	3,3’-diaminobenzidine
DAPI	4’,6-diamidino-2-phenylindole
DEG	Differentially regulated gene
DES	Drug-eluting stents
DE	Differential expression
DMAT	2-dimethylamino-4,5,6,7-tetrabromo-1H-benzimidazole
DMEM	Dulbecco’s modified eagle’s medium
DMSO	Dimethyl sulfoxide
DPBS	Dulbecco’s phosphate-buffered saline

E

E2F	E2 factor
EC	Endothelial Cell
ECM	Extracellular matrix
EDTA	Ethylene diamine tetraacetic acid
EDU	5-ethynyl-2'-deoxyuridine
EEL	External elastic lamina
Eh-1	Engrailed homology 1
eIF-4E	Eukaryotic initiation factor 4E
ELISA	Enzyme-linked immunosorbent assay
EOMA	Murine Hemangioendothelioma Endothelial Cells
ES	Embryonic stem
ESM-1	Endothelial cell-specific molecule -1
EVG	Miller’s Elastic van Giesen

F

FBS	Foetal bovine serum
FDR	False Rate Discovery
FRTL-5	Fischer rat thyroid cell line-5

G

G6PD	Glucose-6-phosphate dehydrogenase

H

HAT	Histone acetyltransferase
HDAC	Histone deacetylase
HDAC-9	Histone deacetylase 9
Hex/Hhex	Haematopoietically expressed homeobox
HIV	Human immunodeficiency virus
HMG-CoA	3-hydroxy-3-methylglutaryl-coenzyme A
HNF-1α	Hepatocyte nuclear factor 1α
HRP	Horseradish peroxidase
HSV	Human saphenous vein
HSVEC	Human saphenous vein endothelial cell
HUVEC	Human umbilical vein endothelial cell

I

ICC	Immunocytochemistry
ICAM	Intercellular adhesion molecule 1
IEL	Internal elastic lamina
IF	Immunofluorescence
IgG	Immunoglobulin-G
IHC	Immunohistochemistry
IMA	Internal mammary artery
IL-1β	Interleukin 1 beta
IL-6	Interleukin 6
IL-8	Interleukin 8
IPA	Ingenuity Pathway Analysis
IRF9	Interferon Regulatory Factor 9
ITA	Internal thoracic artery

K

kDa	Kilodaltons

L

LAD	Left anterior descending
LDL	Low-density lipoprotein
LMO2	LIM domain only 2
LIMA	Left internal mammary artery

LITA	Left internal thoracic artery
L-PK	Liver pyruvate kinase
LSS	Low shear stress

M

MAPK	Mitogen-activated protein kinase
MALAT1	Metastasis Associated Lung Adenocarcinoma Transcript 1
MCP-1	Monocyte Chemotactic Protein-1
MDS	Myelodysplastic syndrome
MI	Myocardial Infarction
MMP	Matrix-degrading metalloproteinase
M.O.M	Mouse on mouse
MYH11	Myosin heavy chain

N

NGS	Next Generation Sequencing
NIS	Sodium iodide symporter
NMHC-B	Non-muscle myosin heavy chain B
NS	Not significant
NTCP	Sodium-taurocholate co-transporting polypeptide
NTT	“No-touch” technique

P

PAGE	Polyacrylamide gel electrophoresis
PBS	Phosphate-buffered saline
PCI	Percutaneous coronary intervention
PCR	Polymerase chain reaction
PFA	Paraformaldehyde
pfu	Plaque-forming units
PLGA	Polyactide-co-glycolide
PML	Promyelocytic leukaemic
pRb	Rb protein
PRH	Proline-rich homeodomain
PTCL	Peripheral T-cell lymphoma.

Q

qPCR	Quantitative polymerase chain reaction

R

RBP1	Retinol binding protein 1
RPKM	Reads per kilobase million (RPKM)
RPMI-1640	Roswell Park Memorial Institute-1640
RT	Room temperature
RT	Reverse transcription
RT-PCR	Reverse transcription polymerase chain reaction

S

SATB1	Special AT-rich binding protein 1
SDS	Sodium dodecyl sulphate
SELDI-TOF-MS	Surface-enhancer laser desorption/ionisation time-of-flight mass spectrophotometry
SEM	Standard error of the mean
SM22α	Smooth muscle protein 22α
SMTN	Smoothelin
SRF	Serum-response factor
STAT	Signal Transducer and Activator of Transcription
STAT-1	Signal Transducer and Activator of Transcription 1
SYBR	Synergy Brands, Inc.
SVG	Saphenous vein graft
SVGF	Saphenous vein graft failure

T

TAGLN	Transgelin
TBB	4,5,6,7 tetrabromo-1H-benzotriazole
TBP	TATA-box-binding protein
TBS	Tris-buffered saline
TBS-T	Tris-buffered saline-tween
TGFR2	Transforming growth factor-beta receptor type-2
TGS	Tris/Glycine/SDS
TIE	Tyrosine kinase with immunoglobulin-like
TIMP	Tissue inhibitor of metalloproteinase
TLE	Transducin-like enhancer of split
TMB	3,3',5,5'-tetramethylbenzidine
TNFα	Tumour necrosis factor α

Tg	Thyroglobulin

U

uPA	Urokinase-type PA

V

VCAM	Vascular cell adhesion molecule
VEGF	Vascular endothelial growth factor
VEGFR	Vascular endothelial growth factor receptor
VEGFR-1	Vascular endothelial growth factor receptor 1
VGF	Vascular Graft Failure
VPA	Valproic acid
VSMC	Vascular smooth muscle cells
v/v	Volume per volume

W

WB	Western Blotting
Wnt	Wingless/Int
w/v	Weight per volume

X

Xtle4	Xenopus Tle4
Xnr	Xenopus nodal-related genes

1.

INTRODUCTION

1. INTRODUCTION

1.1 CARDIOVASCULAR DISEASES

Cardiovascular disease (CVD) is a class of diseases affecting the heart and circulatory system (Bhatnagar *et al.,* 2015), and includes stroke and coronary artery disease (CAD). The underlying pathology responsible for the majority of CVDs is atherosclerosis. Atherosclerosis is characterised by accumulation of lipids, inflammatory cells and a fibrous cap in the innermost layer of arteries and results in the formation of an atherosclerotic lesion or plaque (see review by Lusis, 2000). The subsequent progression of atherosclerotic disease can result in critical narrowing or complete occlusion of arteries. When this occurs in one or more of the coronary arteries it can inhibit adequate supply of oxygen-rich blood to the myocardium and may lead to the symptoms of angina. Rupture of a coronary artery atherosclerotic plaque and ensuing thrombosis which partially or completely occludes the artery can cause catastrophic clinical consequences of myocardial infarction (MI), more commonly known as a heart attack, or even death (Khan, Farah and Domb, 2012).

According to the World Health Organization (WHO), the most prevalent cause of mortality worldwide is CVD, which accounts for 31% of all global deaths (World Heart Day 2017). It is estimated as one of the common causes of death in the United Kingdom by claiming 27% of deaths (CVD Statistics– BHF UK Factsheet, 2020). The British Heart Foundation (BHF) documented that there are currently 7.4 million people living with CVD in the UK (CVD Statistics– BHF UK Factsheet, 2020). This equated to an average of 170,000 deaths per annum with one death every three minutes. Furthermore, 2.3 million people in the UK suffer from CAD, and hospital admissions due to stroke were estimated at around 240,000 cases (CVD Statistics– BHF UK Factsheet, 2020).

As one of the leading public health problems in the UK, CVD is a substantial clinical and economic burden costing the British economy approximately £19 billion annually (CVD Statistics– BHF UK Factsheet, 20120. Despite the significant decline in mortality as a result of CVD over the years, it must be emphasised that prescriptions and operations for CVD are rising strikingly with time (CVD Statistics– BHF UK Factsheet, 2020). Hence, there has been increasing pressure to identify improved therapies for patients with CVD.

1.1.1 History of Myocardial Revascularization

Preventative measures and treatments such as lifestyle management, medical therapies and myocardial revascularization have yielded clinical benefit for patients with CAD, although, these have not eradicated atherosclerosis and the incidence of major adverse cardiovascular events. A strong emphasis on mortality caused by CAD have resulted in the development and utilisation of cardiac surgical procedures (Bhatnagar *et al.,* 2015). For example, surgical interventions to treat coronary artery disease include intracoronary stenting or coronary artery bypass graft surgery (CABG) (Schwartz *et al.,* 1995 and Wallitt *et al.,* 2007) to unblock coronary stenosis. In percutaneous coronary intervention (PCI), drug-eluting stents (DES) demonstrated clear superiority compared to bare metal stents (BMS) because it has better survival rates and less adverse event (Khan *et al.,* 2012). Despite success, issues with safety and efficacy of DES have been associated with late stent thrombosis and graft occlusion rates have not improved over time (Taniwaki *et al.,* 2012; Conte, 2007). Although there has been advancement in stenting technology, there remains an unmet challenge faced by the clinicians and basic scientists for the development of appropriate materials with preferred specifications. For this reason, CABG remains the gold standard therapy for patients with left main disease, multivessel coronary artery disease and those with diabetes (Harskamp *et al.,* 2013).

In the late 1930s, cardiac surgery was in its infancy but became more feasible as the first ever heart-lung machine was developed by Dr John Gibbon which enabled cardiopulmonary bypass (CPB) (Cooper, 2011). Following on from this success, CABG has become one of the most important and most utilised surgical revascularizations in the history of medicine. CABG involves grafting a section of a blood vessel or vascular conduits from the aorta to the coronary artery distal to the stenosed (atherosclerotic) region, to restore blood flow, thereby revascularizing the cardiac tissue. Vineberg was the first to pioneer bypass graft surgery in 1946 by implanting an internal mammary artery (IMA) as the conduit for the treatment of cardiac ischemia and angina in dogs (Thomas, 1999). In 1953, Dr Gordon Murray introduced experimental arterial-coronary grafting using internal thoracic artery (ITA) in the coronary circulation (Murray *et al.,* 1954). The first successful harvest and use of saphenous vein as an aorto-coronary conduit was accomplished by Sidney Smith (Smith *et al.,* 1957). The first human coronary artery bypass operation was performed in 1961 by Robert Goetz using left ITA (Goetz *et al.,* 1961). Major breakthroughs in the field of cardiothoracic surgery persisted during the 1960s including the innovative success of left internal mammary artery (LIMA) to the left anterior descending (LAD) artery anastomoses in the absence of CPB by Kolesov (Konstantinov, 2004). In 1967, René Favaloro led a novel, ground-breaking surgical technique to treat coronary stenosis by reconstructing the right coronary artery, and for the first time,

using saphenous vein graft interposition (Captur, 2004). During the late 20th century, the evolution of surgical procedures and conduits contributed to the increased prevalence of CABG and to improve survival of patients by successfully diverting the flow of blood from the aorta to the coronary artery, distal to the stenosis caused by an atherosclerotic plaque (Gulielmos, 2004; Duhaylongsod, Mayfield and Wolf, 1998).

1.1.2 Coronary Artery Bypass Graft (CABG)

The choice of graft conduit is imperative to the success of CABG since the patency of the conduit is an important determinant of normal postoperative outcome and patient survival (Loop, Lytle and Cosgrove, 1986).

To date, the most commonly used vessel conduit or graft is the autologous saphenous vein, in particular, for patients with multi-vessel disease where 75% of grafts utilise saphenous vein (Wan *et al.,* 2012). Though patients experience improved survival and symptomatic relief post-CABG surgery, long-term success is hindered by the high prevalence of vein graft failure (VGF). At one year post implantation of saphenous vein grafts the occlusion prevalence is 10% to 15% (Fitzgibbon *et al.,* 1996). While 5-10 years following CABG, implanted vein graft patency is approximately 50-60% (Sabik, 2011). Consequently, there is a high incidence of patients undergoing repeat CABG surgery compared to the former surgical procedure (Yap *et al.,* 2009). Therefore, CABG cannot be considered a cure but rather a useful palliative treatment (Bourassa *et al.,* 1985). Nonetheless, the usage of venous conduits remains a fundamental requirement for CABG and are still the most frequently used owing to its length and ease of harvesting (Sabik, 2011).

Arterial grafts such as left internal thoracic artery (LITA) exhibit improved long-term patency and survival rates compared to venous grafts. Hence, total arterial revascularization has gained much prominence for coronary bypass graft surgery (Al-Sabti *et al.,* 2013; Taggart, D'Amico and Altman, 2001; Buxton *et al.,* 1998). Despite the striking resistance to the development of intimal thickening and super-imposed atherosclerosis of arterial grafts, use of these conduits carries the risk of mediastinitis, a severe complication involving inflammation of the tissues in the mid-chest, which inevitably presents a significant drawback. In addition, there is a lack of sufficient arterial material to achieve multiple grafts, thus, signifying the need to utilise venous grafts (Al-Sabti *et al.,* 2013).

In summary, VGF reduces the long-term success of CABG surgery as it can result in recurrent angina and MI which may precipitate the requirement for further treatments including repeat

revascularization. This is not only detrimental to CABG patients, but such a clinical burden clearly represents a significant strain on the NHS.

1.1.2 Arteries and Veins

The vascular system is composed of arteries and veins; two separate components which differ structurally and functionally (Szasz *et al.,* 2007). In general arteries transport oxygenated blood under a high pressure away from the heart into the systemic circulation. Large arteries branch off from the aorta and form smaller divisions known as arterioles. The arterioles distribute oxygenated blood to capillary beds, which permit the exchange of oxygen and carbon dioxide along with nutrients and metabolic waste products. The capillaries lead back to small vessels, termed venules, that flow into the larger veins, which transport blood towards the heart from the tissues.

Both arteries (FIGURE 1.1A) and veins (FIGURE 1.1B) consist of a tri-laminar structure: tunica externa, tunica media and tunica intima surrounding a central blood-containing space called the lumen (Betts *et al.,* 2013). The internal and external elastic membrane separate the three tunicae (Kloc and Ghobrial *et al.,* 2014). The tunica externa also known as the adventitia is the external substantive layer of a blood vessel, and is comprised of fibroblasts, macrophages, nerves and connective tissue, predominantly collagen, which acts as a supportive element by anchoring the blood vessel, preventing overexpansion and imparting tensile strength. In veins, it is the thickest layer (FIGURE 1.1B). Also characteristic of this tunica is the network of nourishing micro-vessels called the vasa vasorum (FIGURE 1.1B), which supplies nutrients to the vascular walls of larger arteries and veins (Brown, Williams and George, 2017). The tunica media is the middle layer of a blood vessel characterised by the presence of quiescent, contractile vascular smooth muscle cells (VSMCs) positioned within a collagen-rich extracellular matrix (ECM) and surrounded by the external elastic lamina (EEL). The EEL is commonly present in larger arteries but not smaller arteries or veins (FIGURE 1). This muscular medial layer is responsible for regulating blood pressure by controlling the arterial calibre. The tunica media is generally the thickest layer in arteries, and it is much thicker in arteries than veins enabling them to withstand high blood pressure. Moreover, the elastic lamina that are present in arteries as continuous layers of elastic but fenestrated in veins (Betts *et al.,* 2013) (FIGURE 1A). The innermost layer of a blood vessel is called the tunica intima and is formed of a monolayer of endothelial cells (ECs) also known as the endothelium delimited by the internal elastic lamina (IEL), which is not apparent in veins but present in arteries. To achieve satisfactory blood circulation under low pressure, many veins possess semilunar folds in the tunica intima known as the venous valves which prevent retrograde flow

(Betts *et al.,* 2013). In arteries, the tunica intima has an undulating structure due to partial constriction exerted by the tunica media, whereas in veins, it characteristically appears smooth (FIGURE 1.1C) (Betts *et al.,* 2013).

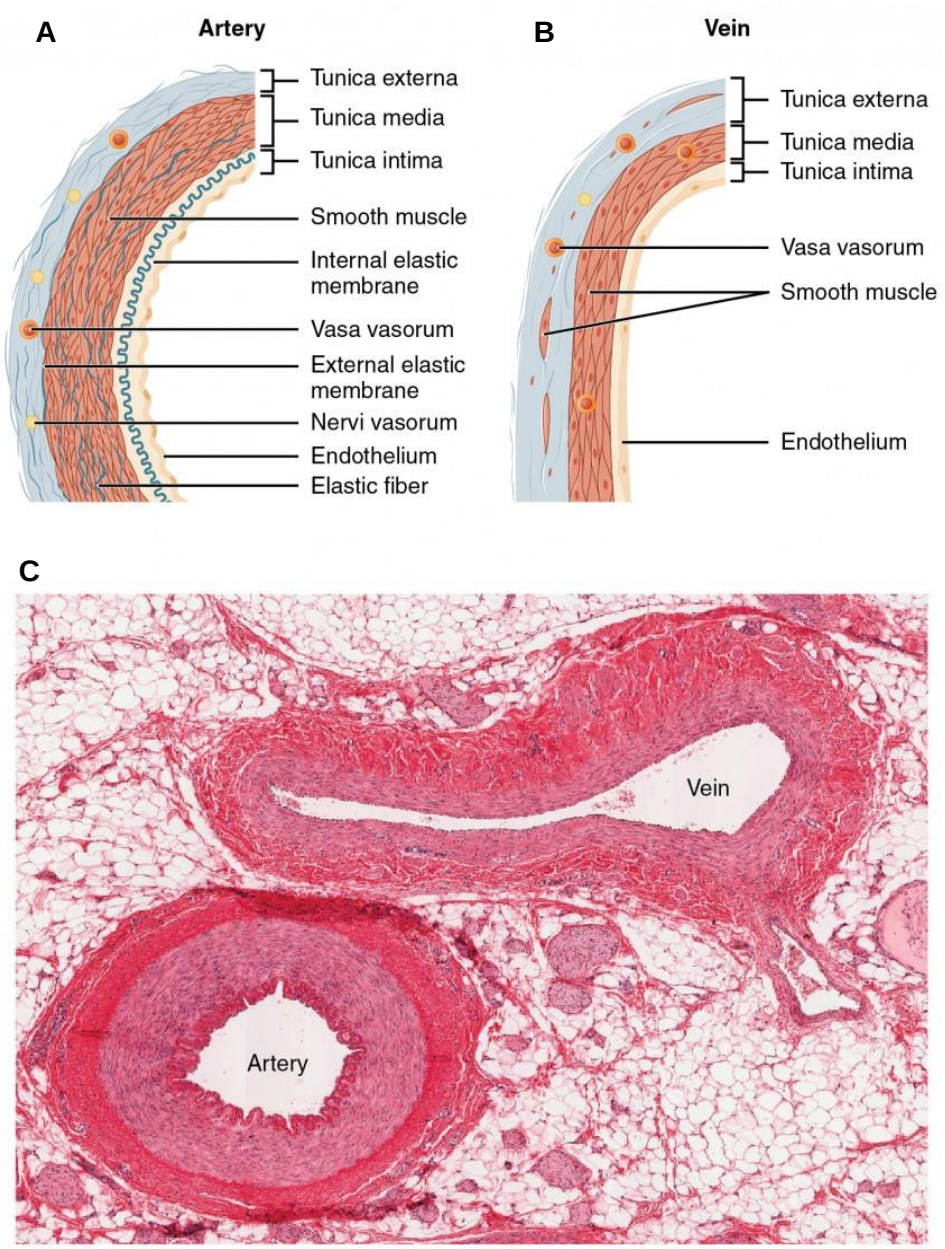

FIGURE 1.1: Anatomy of the Blood Vessel Wall

(**A**) Arteries and (**B**) veins contain three structural layers, tunica externa, tunica media and tunica intima. The structure and thickness of each layer varies between the vessel types.

(**C**) Cross section of a vein and artery. The smooth muscle and connective tissue of the vessels are visible in this photomicrograph. Original figure from Betts *et al.,* 2013.

The different properties of arterial and venous grafts used in CABG surgery have inspired research to compare these vessel types in an attempt to achieve superior patency rates. The higher patency rates of arterial grafts have been considered as a fundamental advantage compared with saphenous vein grafts (SVGs). However, SVGs remains to be the preferred conduit of choice due to the need for multiple grafts when there is either insufficient arterial material or time to do the more complex arterial surgery. More importantly, in emergency situations and for patients at higher operative risk due to the complicated and time-consuming nature of arterial grafting (Cuminetti *et al.,* 2017). In addition to structural differences of arteries and veins including thickness, presence of elastic membrane and ECM composition, inherent differences exist between venous VSMCs and arterial VSMCs. For example, arterial VSMCs exhibit a lower growth rate than VSMCs isolated from saphenous veins (Yang *et al.,* 1998) which may contribute to the improved patency of arterial grafts.

1.2 PATHOPHYSIOLOGY OF VEIN GRAFT FAILURE (VGF)

The pathophysiology underlying SVG failure (SVGF) is complex and has not been fully defined. Multiple biological processes comprising of acute thrombosis, neointimal hyperplasia and atherosclerosis are considered to be the primary contributors to graft failure (FIGURE 1.2) (Ward *et al.,* 2017; Shuhaiber *et al.,* 2002). SVGF can be divided into three distinct phases: early, intermediate and late graft failure (Motwani and Topo, 1998).

1.2.1 Early Vein Graft Failure

Early SVGF occurs within one-year post-implantation in 10-15% of venous grafts (Sabik, 2011). It is considered that the surgical preparation of saphenous vein causes injury to the endothelium triggering early occlusion (Shukla and Jeremy, 2012). Within the first month following CABG, the risk of thrombosis is elevated by surgical errors associated with harvesting, sites of anastomoses or vessels with poor runoff (Conte, 2010) (FIGURE 3). During conventional harvesting of SV used as bypass conduits, vascular spasm is triggered when the cushion of perivascular fat surrounding the adventitia is stripped off. Consequently, uncontrolled hydrostatic distension is required to dilate the vessel leading to extensive damage to the endothelium (Hinokiyama *et al.,* 2006). To address this concern, an innovative “no-touch” technique (NTT) for vein harvesting was used to ameliorate the physical damage

due to dissection, side branch ligation and handling/distension, all of which damage the delicate endothelium (Souza, 2002a; Souza 2003).

Implantation of the SVG into the high-pressure arterial circulation exposes the vein to different haemodynamic parameters such as shear “hydrostatic” stress, increased wall tension and turbulent flow and results in endothelial injury within the graft (Angelini *et al.,* 1987). Removal of or damage to the endothelium during vein graft preparation as well as after implantation exposes the intimal and medial layers of the vessel wall. These adverse conditions permit the adherence and activation of blood cells such as platelets, neutrophils and monocytes to the vein graft. Further damage the endothelial layer depletes its synthesis and secretion of atheroprotective compounds including nitric oxide and prostacyclin, encouraging vasospasm and loss of graft patency (Ishiwata *et al.,* 1997). Endothelial injury and dysfunction also enhance expression of anti-fibrinolytic proteins including thromboxane A2, fibronectin, thrombospondin etc. which promote thrombosis (Wan *et al.,* 2012; Tsui and Dashwood, 2002).

1.2.2 Intermediate to late-stage Vein Graft Failure

Intermediate (1 month–1-year post-surgery) and late (beyond 1-year post-surgery) graft failure occurs in 15–30% of reported cases, respectively (Sabik, 2011). By 10 years post-implantation, 50-60% of grafts become blocked and a further 30% develop compromised flow (Jeremy, Gasdon and Shukla, 2007; Favaloro, 1998; Motwani and Topol, 1988). Intermediate to late vein graft failure is commonly attributed to neointimal hyperplasia, particularly at the proximal/distal anastomoses, which can lead to late vein graft failure as a result of prolonged development of superimposed atherosclerosis (Sabik, 2011).

The injury to the endothelium not only leads to early thrombosis but precipitates longer term effects including inflammation and VSMC activation that contribute to intermediate and late vein graft failure. Endothelial damage leads to enhances expression of adhesion molecules including vascular cell adhesion molecule 1 (VCAM-1) and intercellular adhesion molecule 1 (ICAM-1), which facilitate monocyte adhesion and therefore monocyte recruitment and inflammation (Wan *et al.,* 2012; Tsui and Dashwood, 2002). Initial vein harvesting from the circulation removes the blood supply provided via the vasa vasorum and thereby causes susceptibility to hypoxic injury within the first day after surgery which activates VSMCs (Vlovader and Edwards, 1971).

Intact and functional endothelium releases factors that are key inhibitors of VSMC proliferation and thereby intimal thickening (Angelini, Soyombo and Newby, 1991). For instance, there is

an insufficient endothelial regrowth after denuding injury to the artery which can compromise its vascular function and integrity as a result of altered arterial haemodynamic forces. Haemodynamic forces are capable of modulating the physiology and disease progression of the vascular wall. In addition, activated ECs are a source of VSMC mitogens thereby promoting VSMC proliferation (Angelini *et al.,* 1987). Hence, endothelial loss and dysfunction is recognised to affect the long-term efficacy of SVG in addition to early vein graft failure.

The principal cause underlying intermediate to late graft failure is the progressive intimal hyperplasia due to VSMC accumulation and ECM deposition, as described in Figure 3 (Southerland, 2013). Unlike skeletal and cardiac muscle cells, which are terminally differentiated, VSMCs have a remarkable characteristic of plasticity that enables them to reversibly switch to a less “contractile” phenotype or “synthetic” phenotype (de-differentiation) in response to altering environmental cues (Rensen *et al.,* 2007). In the healthy blood vessel, ‘contractile’ VSMCs exhibit a low rate of proliferation, low synthetic activity and express a unique set of contractile proteins, essential for the contraction and relaxation of the vascular wall. These proteins either act as structural components of the contractile apparatus or as regulators of contraction and include: transgelin (TAGLN), smooth muscle-a-actin (ACTA2), calponin (CNN1), smoothelin (SMTN) and smooth muscle myosin heavy chain (MYH11) (Rensen *et al.,* 2007).

Upon injury or insult, the synthetic phenotype is typically characterized by loss of expression of contractile proteins and increased expression of synthetic proteins such as osteopontin (Alexander and Owens, 2012). Such phenotypic switching is required to maintain vascular homeostasis and regulate vascular response to injury and inflammation. "Synthetic" VSMCs are characterised and identified by their loss of contractile marker expression and the upregulation of selective gene sets, including pro-inflammatory cytokines and matrix metalloproteinases (MMPs), leading to increased cell migration, proliferation and secretion of pro-inflammatory cytokines (Alexander and Owens, 2012; Clarke *et al.,* 2010; Owens *et al.,* 2004). Within 24 hours of vein graft insertion, VSMCs exit the quiescent G_0 phase and proceed into the G_1 and G_2/S phases of the cell cycle (Bochaton-Piallat *et al.,* 1996). As a response to vascular injury, switching of VSMCs from “contractile” or differentiated phenotype to “synthetic” or dedifferentiated state is a hallmark in the pathogenesis of VGF. The synthetic, migratory and proliferative phenotype enhances the production of inflammatory cytokines and growth factors which serve as paracrine factors to stimulate surrounding VSMCs and inflammatory cells (Nguyen *et al.,* 2013; Owens *et al.,* 2004). Activated platelets on the denuded surface of the vein, and recruitment of macrophages and other inflammatory cells into the damaged intimal surface results in the release of mitogens and chemotactic agents

which initiate VSMC migration into the intima and further proliferation of VSMCs. In addition, the production and activation of matrix-degrading metalloproteinases (MMPs) by VSMCs and macrophages enable digestion of ECM and facilitate VSMC migration and proliferation (Newby, 2005; George *et al.,* 2000). The VSMC migration and proliferation is observed early after implantation and in a rat model migration of VSMCs from the media into the intimal layer of the graft was observed on post-operative day 7 (Allaire and Clowes, 1997). Once within the intima, VSMCs proliferate and secrete abundant quantities of ECM (collagen and proteoglycans, but not elastin) (Mitra, Gangahar and Agrawal, 2006).

Atherosclerosis leads to the development of an atheromatous plaque within the intima composed of a necrotic core encapsulated by a fibrous cap. A crucial initiating stage in atherosclerosis is the accumulation of oxidatively modified LDL in the subendothelial matrix contributing to the monocyte recruitment and foam-cell formation. The newly deposited matrix proteins in the intima are known to enable the trapping of lipid in the intima and act as a soil for atherosclerosis. Superimposed atherosclerosis occurs in vein grafts beyond the first year after bypass surgery (FIGURE 1.2). The thickened intima resulting from aberrant VSMC and ECM accumulation serves as the foundation for the development of superimposed atherogenesis (Motwani and Topol, 1998). Compared to native coronary artery atheromas, SVG atherosclerosis contains a higher number of foam and inflammatory cells (Southerland *et al.,* 2013, Chiu and Chien, 2011). Superimposed and accelerated atherosclerosis is more diffuse and concentric yet contains less calcification and lacked fibrous caps than native atherosclerotic lesions. Of interest, SVG atherosclerosis is located at either the aorto-ostial or the main shaft of the graft. Evaluation of SVG shaft lesions revealed an association with increased death rates, MI, enhanced plaque rupture and no-reflow (Hong *et al.,* 2013; Sano *et al.,* 2006).

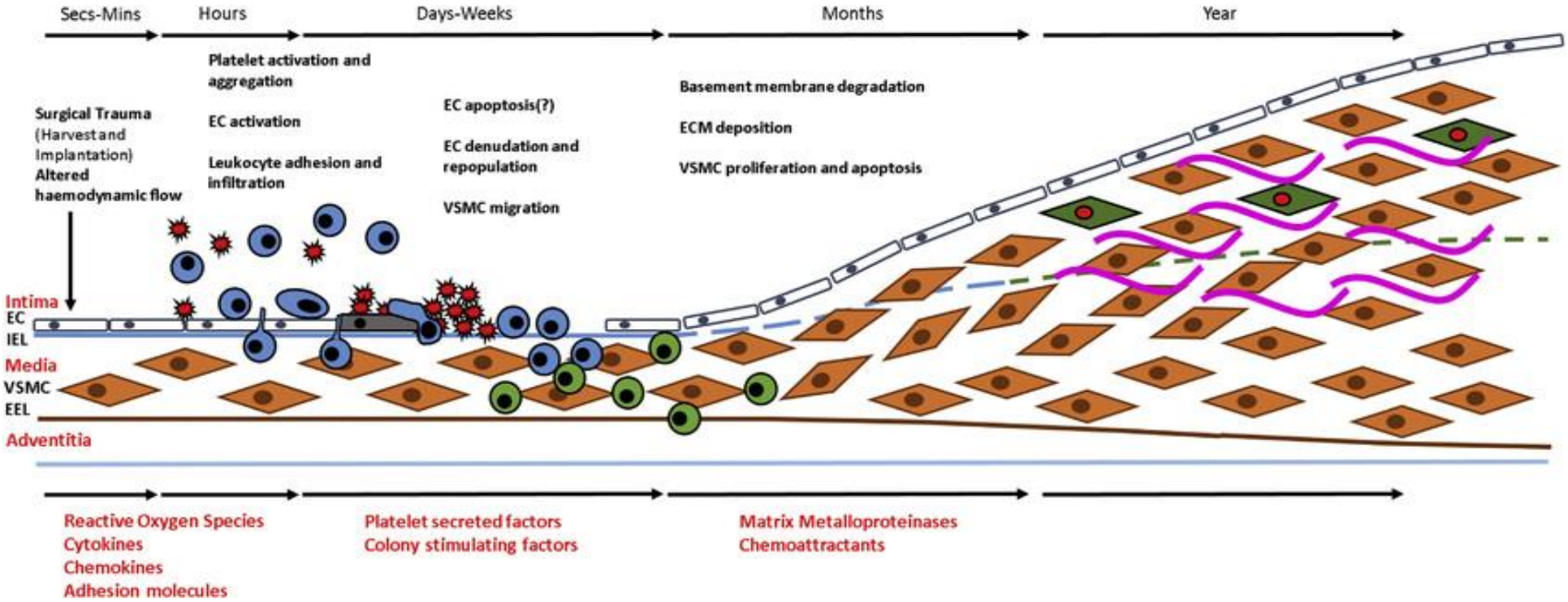

FIGURE 1.2: Schematic diagram of the events that contribute to Vein Graft Failure

Early graft failure primarily occurs when the SVG is exposed to altered haemodynamics and surgical trauma which result in endothelial injury. Resultant endothelial dysfunction induces leukocyte recruitment and their subsequent release of a plethora of vasoactive mediators, chemotactic agents and growth factors initiating VSMC de-differentiation, proliferation, and migration. This leads to progressive intimal thickening. Late vein graft failure is a much slower process predominantly due to intimal thickening and superimposed atherosclerosis. EC, endothelial cell; ECM, extracellular matrix; VSMC, vascular smooth muscle cell; IEL, internal elastic lamina; EEL, external elastic lamina. Original figure from Ward *et al.,* 2017.

1.3 CURRENT STRATEGIES TO PREVENT VGF

Preventive measures and interventional strategies for preservation of vein graft patency is essential for long-term surgical success (McKavanagh*et al.,* 2017). This may be accomplished through perioperative measures, lifestyle modifications, prescription medication, percutaneous coronary intervention (PCI) and repeat CABG surgery. Despite this, such interventions have not eliminated the problem of SVGF thereby driving the need to advance strategies to improve coronary revascularization (Thomas, Angelini and Zakkar, 2016).

As mentioned previously, NTT resulted in minimal surgical complications with less endothelial damage and less neointimal hyperplasia thereby improving patency in CABG in comparison to the conventional harvesting techniques. However, it is postulated that NTT is only effective for early, but not late VGF (Souza *et al.,* 2006; Souza *et al.,* 2002b).

Beyond surgery, optimal secondary prevention involving lifestyle modifications includes cessation of smoking, a diet low in saturated fats and carbohydrates and regular exercise continues to have an important role in reducing thrombotic risk and management of vein graft degeneration (Thomas, Angelini and Zakkar, 2016). In addition, pharmacological intervention including aspirin and/or clopidogrel has emerged to prevent SVGF and reduce the need to reoperate failed SVGs (McKavanagh *et al.,* 2017; Wijins *et al.,* 2010; Wallentin *et al.,* 2009). Aggressive lipid-lowering therapy has been proven to help lower the incidence of early SVGF (Kang *et al.,* 2013). The administration of statin therapy following CABG intervention correlates to improving the patency of the graft (Kang *et al.,* 2013; Hillis *et al.,* 2012).

Irrespective of the established pharmacotherapy, intimal thickening persists to be a clinical burden (Engelberger *et al.,* 2008). Recognition of the significant unmet clinical need in this area presents the potential of gene therapy to improve patency rates of bypass graft by inhibiting cellular proliferation that causes intimal hyperplasia (Mann *et al.,* 1999; George *et al.,* 2011). Initial optimism to attenuate intimal thickening was observed in the PREVENT II study involving 200 patients undergoing CABG surgery in which vein conduits were treated *ex vivo* with edifoligide, an E2F transcription factor decoy that retards VSMC proliferation (Grube et al. 2001). However, the success was dampened by a phase 3 randomized, double-blind, placebo-controlled trial, PREVENT IV, enrolling 3014 patients. The researchers found edifoligide was no more effective than placebo in preventing clinical consequences of VGF (Alexander *et al.,* 2005). In fact, another study from our research group in Bristol illustrated that TIMP-3 possess a pro-apoptotic function that retards the development of intimal thickening if porcine vein grafts for up to 3 months (George *et al.,* 2011). Of interest, a Medical Research Council (MRC)/British Heart Foundation (BHF)-funded clinical trial for TIMP-3 is

planned to explore its therapeutic potential in reducing vein graft failure. Other pharmacological agents such as nitric oxide-donating aspirin (Wan *et al.,* 2007) and endothelin-1 receptor antagonists (Wan *et al.,* 2004) have been tested in pre-clinical studies for the treatment of vein graft failure in porcine models. Although, these have not been examined in clinical trials.

Despite the success of identifying a plethora of genes that modulate VSMC proliferation, migration and apoptosis, these genes often fail to promote reendothelialization due to lack of cell specificity (George *et al.,* 1998; George *et al.,* 2000). As a result, the scope of this strategy has potential shortcomings regarding potential translation into a clinical setting (Conte, 2007; Harskamp *et al.,* 2013). Preservation of endothelial cell function and structure by inducing endothelial cell regrowth on the vein graft is fundamental to sustain the balance between inhibition and encouragement of the migration and proliferation of VSMCs in addition to platelet aggregation and adhesion (Sena, Pereira and Seiça, 2013).

In the absence of clinically proven strategies to block VGF, the search for novel therapeutic approaches to improve SVG patency and long-term clinical success after CABG are urgently needed. Most importantly, anti-proliferative therapies that inhibit VSMC accumulation within the inner, intimal layer of the vessel wall whilst preventing damage to the endothelium is an attractive strategy to alleviate intimal thickening in the venous bypass graft and enhance patency.

1.4 PROLINE RICH HOMEODOMAIN (PRH)

1.4.1 Overview of PRH

The proline rich homeodomain protein (PRH), also known as haematopoietically expressed homeobox (HHEX), is a highly conserved transcription factor and belongs to a family of proteins that serve key regulatory functions in cellular development and differentiation via both transcriptional and post-transcriptional mechanisms. Formerly discovered in screens to identify novel homeobox genes in human, mouse and avian hematopoietic cells [Crompton *et al.,* 1992; Bedford *et al.,* 1993; Hromas *et al.,* 1993], PRH has since been found to contain high sequence similarity between various species including mouse (Hex), xenopus (Xhex), zebrafish (hhex) and rat (Ho *et al.,* 1999; Newman, Chia and Krieg., 1997; Tanaka *et al.,* 1999). Evidence from analysis of mRNA and protein in adulthood indicates that PRH is preferentially expressed in pluripotent myelomonocytic cells, erythroid cells and B-cell

progenitors although absent in T-cell lineages (Manfioletti *et al.,* 1995; Bedford *et al.,* 1993). During embryonic development, PRH is essential for the development of vital organs such as the forebrain, heart, liver, thyroid and thymus; it is also required for the formation of the sagittal axis at the earlier stages of embryogenesis (Gaston *et al.,* 2016; Keng *et al.,* 2000). In support of this notion, in Hhex-null mouse embryos, haematopoiesis, vasculogenesis, forebrain and liver generation were impaired, and embryos were unable to survive gestation (Hallaq *et al.,* 2004). PRH can affect multiple processes since it regulates the expression of a number of genes, Table 1 summarizes the list of genes known to be repressed or activated by PRH (Soufi and Jayaraman, 2008).

Table 1: PRH Target Genes

Gene	Regulation	Model	Method	References
Goosecoid	Repressed	Xenopus embryos ES tissue cultured cells	Ectopic expression Transient transfection	Brickman *et al.,* 2000
Chordin	Repressed	Xenopus embryos	Ectopic expression	Brickman *et al.,* 2000
Xtle4, Nodal (Xnr1, Xnr2)	Repressed	Xenopus embryos ES tissue cultured cells	In situ hybridization Ectopic expression Conditional expression Affymetrix gene chips	Zamparini *et al.,* 2006
Tg	Repressed	FRTL-5 tissue cultured cells	Transient transfection	Pellizzari *et al.,* 2000
VEGF, VEGFR-1, VEGFR-2, TIE-1, TIE-2, neuropilin-1, integrin αV	Repressed	HUVEC tissue cultured cells ES tissue cultured cells	Adenoviral infection cDNA microarray analysis, quantitative real-time RT-PCR	Guo *et al.,* 2003 Kubo *et al.,* 2005 Nakagawa *et al.,* 2003
ESM-1	Repressed	EOMA and HUVEC tissue cultured cells	Transient transfection Adenoviral infection Quantitative real-time RT (reverse transcription)–PCR OMM16K Gene chip microarray	Cong *et al.,* 2006
NTCP	Activated	PRH knockout in E10.5 embryos	Transient transfection	Denson *et al.,* 2000
L-PK	Activated	Hep G2 tissue cultured cells HeLa cells Rat cultured hepatocytes	Transient transfection Adenoviral infection	Tanaka *et al.,* 2005
NIS	Activated	HeLa cultured cells	Transient transfection	Puppin *et al.,* 2006

Key words: *Xtle4; xenopus Tle4, Xnr; xenopus nodal-related genes, Tg; thyroglobulin, VEGFR; vascular endothelial growth factor receptor, TIE; tyrosine kinase with immunoglobulin-like and EGF-like domains, ESM-1; endothelial cell specific molecule, NTCP; sodium-dependent bile acid co-transporter, L-PK; liver pyruvate kinase, NIS; sodium iodide symporter, ES; embryonic stem, FRTL-5; Fischer rat thyroid cell line-5, EOMA; murine hemangioendothelioma, HUVEC; human umbilical vein endothelial cells, PCR; polymerase chain reaction, RT; reverse transcription. Table adapted from Soufi and Jayaraman, 2008.*

1.4.2 PRH Structure

Human PRH protein encoded by *HHEX* gene, located on human chromosome 10, is 270 amino acids in length and is detected as a single band with molecular weight of ~37 kDa (Gaston *et al.,* 2016). Over recent years, success in biophysical analysis have provided structural data on PRH which forms highly stable homo-oligomeric complexes (Soufi and Jayaraman, 2008). The PRH protein is highly conserved: a comparison between the human and avian PRH homeodomain discovered a 97% homology, whereas the human and murine PRH homeodomain differ by only a single amino acid (Crompton *et al.,* 1992). In accordance with the general structural modularity found in most transcription factors, the PRH monomer consist of three functional domains: N-terminal domain, homeodomain, and C-terminal domain (FIGURE 1.3).

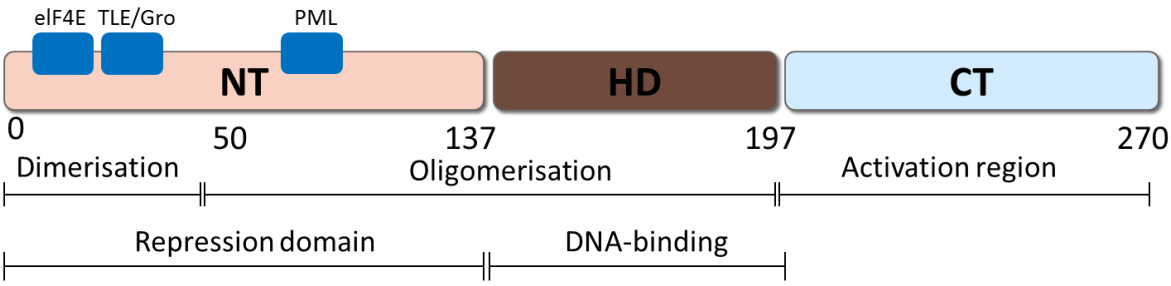

FIGURE 1.3: The domain organization of PRH

PRH protein is approximately 270 amino acids in length and contains three domains: N-terminal transcription repression domain (left; NT) required for oligomerisation and serves as an interface for protein-protein interactions, homeodomain (middle; HD) that facilitates DNA binding and acidic C-terminal domain that facilitates transcription activation (right; CT). Numbers indicate position of amino acid residues.

1.4.3 N-terminal domain of PRH

The glycine- (10%), alanine- (15%) and proline-(20%) rich N-terminal domain (amino acids 1–136) possess dimerization ability as discovered via gel filtration chromatography and analytical ultracentrifugation (AUC) studies (Soufi *et al.,* 2006). Amongst its unique properties, the N-terminal dimer is partially resistant to SDS (sodium dodecyl sulphate) denaturation which

results in PRH appearing as a protein band at 37 kDa on a Western blot rather than the predicted 30 kDa from its amino acid content.

To further characterise its functional diversity, deletion studies, mutagenesis and pulldown assays have been performed and verified that the dimerised N-terminal domain of PRH can repress transcriptional activity once tethered onto a heterologous DNA-binding domain. For example, formation of the PRH-GAL4 complex can block transcriptional activity (Soufi *et al.,* 2009). A strong repression domain has been identified between amino acids 45 and 136 in the proline-rich N-terminal domain of rat PRH or the domain that lies downstream of amino acid 50 in the N-terminus of avian PRH (Guiral *et al.,* 2001; Tanaka *et al.,* 1999). Furthermore, the N-terminal domain operates as an interface to a variety of proteins such as the growth control protein promyelocytic leukaemic (PML), protein kinase CK2, eukaryotic initiation factor 4E (eIF-4E), proteosome subunit C8 and family of the Groucho/TLE (transducin-like enhancer) co-repressor proteins (Swingler *et al.,* 2004; Topisirovic *et al.,* 2003; Bess *et al.,* 2003; Topcu *et al.,* 1999). In support of this notion, it has been demonstrated that the PML interaction domain acts as a co-repressor via functional interaction with other transcription factors such as special AT-rich binding protein 1 (SATB1) (Bischof et. al., 2007). *In vitro* and *in vivo*, the N-terminal repression domain of PRH can interact with TLE1 via a short sequence situated within the N-terminus (amino acids 32–38) that bares reassembly to an Engrailed homology (Eh-1) motif. The interaction between TLE1 and PRH is essential for increased transcriptional suppression by PRH. In contrast, the repression ability of PRH declines through a Grg5-mediated titration of endogenous TLE proteins, presumably because Grg5 retains the ability to tetramerize with full-length TLE proteins (Wang *et al.,* 2000). Hence, PRH can co-repress transcription with TLE proteins (Swingler *et al.,* 2004).

1.4.4 Homeodomain of PRH

The homeodomain of PRH, comprised of approximately 60 amino acids, mediates sequence-specific DNA binding. The homeodomain itself consists of an N-terminal arm and three alpha-helices forming of a helix-turn-helix motif. Of interest, the two N-terminal α-helices are anti-parallel and lie approximately perpendicular to the third helix (Crompton *et al.,* 1992). The N-terminal arm and third alpha helix form specific contacts with the base pairs in the minor and major groove of the DNA, respectively. With the application of computational modelling, glutamine, and asparagine at residues 50 and 51, respectively, have been implicated to have a key role in establishing PRH-DNA interactions (Jalili and Karami, 2012). These interactions are distinctively important such that a single mutation of asparagine to alanine at position 187

within the PRH homeodomain significantly decreases DNA binding activity, thus, rendering PRH defective in repression and activation against its direct target genes. The N187A mutant has been characterised to have a trans-dominant negative activity over wild type PRH for transcriptional repression by sequestration of TLE proteins into sub-nuclear domains (Desjobert *et al.,* 2009; Jankovic *et al.,* 2003).

In the context of VSMC phenotype modulation it is interesting that the interaction between PRH homeodomain with serum-response factor (SRF) induced the expression of α smooth muscle actin (αSMA) and smooth muscle protein 22α (SM22α) in embryonic fibroblasts (Oyama *et al.,* 2004). Activation of the of smooth muscle myosin heavy chain (SMemb/NMHC-B) gene in VSMCs has also been shown to be homeodomain-dependent (Sekiguchi *et al.,* 2001). Moreover, forced expression of CREB (CRE (cAMP-response-element)-binding protein) upregulated PRH-induced SMemb promoter activity but it is unclear whether PRH binds to the PRH-binding domains or to the CRE element within the SMemb promoter (Sekiguchi *et al.,* 2001). Thus, this may explain that PRH may regulate transcription of its downstream genes via multiple mechanisms.

1.4.5 C-terminal domain of PRH

The C-terminal domain of PRH also plays a role in regulation of target genes. PRH can activate transcription of some genes via association with other transcription factors to act as a transcriptional co-activator, rather than direct binding to promoter domains. For instance, stimulation of hepatic nuclear factor 1 alpha (HNF-1α) required interaction with the homeodomain and C-terminal domain of PRH at the liver pyruvate kinase gene promoter in HeLa cells (Tanaka *et al.,* 2005). Similarly, the C-terminal domain is required for the transcriptional activation of the sodium-dependent bile acid co-transporter (NTCP) gene. It activates transcription using the homeodomain (amino acids 137–196) and the C-terminal domain (amino acids 197–271) and deletion studies have demonstrated a C-terminal domain encompassing residue 255–271 is of high importance for activating NTCP promoter (Kasamatsu *et al.,* 2004). The mechanism by which PRH affects NTCP activation remains to be precisely defined although interaction of the homeodomain and C-terminal domain with transcription factor TBP (TATA-box-binding protein) is thought to be involved (Kasamatsu *et al.,* 2004; Guiral *et al.,* 2001).

1.4.6 PRH Oligomerisation

Oligomerisation of PRH in cells is facilitated by the interaction between the N-terminal domain and PRH homeodomain. Recombinant PRH has also been reported to be highly aggregated and allows for self-association behaviour when examined under electron microscope. PRH self-assembles into larger aggregates due to a dimerization domain that corresponds to N-terminal 50 amino acids and a homeodomain association domain (50-137 residues) (Soufi *et al.,* 2006). *In vivo* cross-linking data have demonstrated the oligomerisation of PRH, and *in vitro* gel filtration chromatography and analytical ultracentrifugation experiments imply formation of discrete disc-shaped octameric complexes and more spherical double octamers (hexadecamers) in solution (Soufi *et al.,* 2010). In this respect, a monomeric full-length recombinant PRH can access a single DNA binding site, however, binding usually occurs with low affinity (Soufi *et al.,* 2006). Conversely, oligomeric forms of PRH allow association to DNA fragments with a greater binding affinity; the requirement here for multiple binding sites also improves specificity (Williams et al. 2008). Additionally, the promoter regions of several genes repressed by PRH, e.g., Goosecoid and endothelial cell specific molecule-1 (ESM-1), include tandem arrays of consensus and non-consensus PRH binding sites (Cong *et al.,* 2006; Zamparini *et al.,* 2006; Brickman *et al.,* 2000). This indicates that binding of oligomeric PRH is assisted by multiple clustered sites, the nature of which determines the relative importance of PRH association and the recruitment other PRH-interacting proteins and to regulate gene expression (Jayaraman *et al.,* 2018).

1.5 THE REGULATION OF PRH

PRH is regulated by Protein Kinase CK2, also termed “casein kinase-2 or casein kinase II” which phosphorylates two serine residues in PRH. CK2 is a constitutively active and ubiquitously expressed serine/threonine kinase implicated in the regulation of a wide array of physiological and pathological processes in cells including proliferation, migration and invasion and stress responses (Ahmed, Gerber and Cochet, 2002). CK2 phosphorylates protein substrates with a minimal consensus target sequence of Ser/Thr – X – X – Asp/Glu/pSer, where X denotes any non-basic amino acid. It appears as a hetero-tetrameric enzyme composed of composed of two catalytic and two regulatory β subunits, or in a monomeric form. Human CK2 has two well-characterised isoenzymic forms of the catalytic subunit, designated as CK2α and CK2α’, and a third one, i.e., CK2α’’ which is less well-

understood (Maslyk *et al.,* 2017). The regulatory subunit, CK2β, is responsible for the control of substrate specificity (Jayaraman *et al.,* 2018).

Using yeast two hybrid screening, the N-terminal domain (1-98 residues) of both human and avian PRH have been identified to interact with CK2β and is a target for phosphorylation by the CK2α. It has been implicated PRH/Hhex as a substrate for protein kinase CK2 (Noy *et al.,* 2012; Soufi *et al.,* 2009). Attempts for immunoprecipitation of c-myc tagged-PRH from chronic myeloid leukaemia K562 cells, followed by separation of proteins by SDS-PAGE and identification by mass spectrophotometry revealed three peptides originating from PRH (Soufi *et al.,* 2009). Of interest, the slowest migrating and most prominent PRH band was established as phosphorylated by staining with Pro-Q Diamond Phosphoprotein Stain. Therefore, PRH can exist as a phosphoprotein in cells (Soufi *et al.,* 2009).

Substantiating these findings further, incubation with CK2 inhibitors 2-dimethylamino-4,5,6,7-tetrabromo-1H-benzimidazole (DMAT) or 4,5,6,7-tetrabromo-1H-benzotriazole (TBB) significantly decreased the amount of hyper-phosphorylated PRH without influencing hypo-phosphorylated PRH (Noy *et al.,* 2012). Remarkably, surface enhanced laser desorption/ionization-time of flight-mass spectrometry (SELDI-TOF-MS) technology facilitated the discovery of CK2 phosphorylation sites within PRH using purified, human PRH protein incubated with CK2 and adenosine triphosphate (ATP) (Soufi *et al.,* 2009). These findings have shown phosphorylation at two sites residing within the homeodomain: S163 (CK2 consensus target motif) and S177 (non-consensus site) (FIGURE 1.4). Phosphorylation of PRH at said sites has been demonstrated to abrogate DNA-binding affinity, impair repression of transcription of multiple PRH target genes as well as affect intracellular protein localisation and reduce stability (Noy *et al.,* 2012; Soufi *et al.,* 2009). Diminished DNA binding activity mediated by CK2 phosphorylation can be restored with calf intestinal alkaline phosphatase. Hence, PRH phosphorylation by CK2 is recognised as a reversible switch for DNA binding (Soufi *et al.,* 2009).

Ectopic overexpression of wild-type PRH in K652 cells repressed the targeted transcription of VEGF and VEGF receptor 1 (VEGFR-1) and this effect has been shown to be revoked upon co-transduction with CK2α and CK2β transgenes (Noy *et al.,* 2012). A mutant PRH protein, PRH S163C:S177C (PRH S163C:S177C), was generated for preventing phosphorylation by CK2 at these positions (FIGURE 1.4) (Noy *et al.,* 2012). As expected, co-transfection of PRH S163C:S177C with CK2α and CK2β transgenes revealed an increase in the repression activity of VEGFR-1 transcription; CK2 overexpression was unable to counteract this repression (Noy *et al.,* 2012). In contrast to wild-type PRH, quantitative chromatin immunoprecipitation (ChIP)

analysis was carried out to show that binding of PRH S163C:S177C to VEGFR-1 promoter cannot be supressed with CK2 overexpression (Noy *et al.,* 2012).

Phosphorylation by protein kinase CK2 additionally lowers nuclear retention, stability and activity of PRH (Noy *et al.,* 2012). In fact, *in situ* cell fractionation and biochemical fractionation confirmed the influence of phosphorylation in regard to the intracellular localisation of PRH protein. Firstly, the wild-type PRH and PRH S163C:S177C are observed tightly bound within the nuclear fraction, while the phosphomimetic-CC (PRH EE; replacement of serine residues with glutamic acid) is present within cytoplasmic and loosely held nuclear fractions (Noy, *et al.,* 2012). In addition, the expression of hypo-phosphorylated PRH was prolonged upon incubation with an inhibitor of translation, anisomycin in comparison to hyper-phosphorylated PRH (Noy *et al.,* 2012). Hyper-phosphorylated PRH stability was enhanced upon incubation with proteasome inhibitors such as MG132 and Lactacystin (Noy *et al.,* 2012). Thus, phosphorylation of PRH by CK2 leads to proteasome-mediated proteolysis of PRH. CK2-dependent phosphorylation of PRH leads to the formation of a stable, truncated product that lacks the C-terminal domain, PRHΔC, due to proteasome-mediated protein cleavage (Noy, *et al.,* 2012). Interestingly, forced expression of CK2 increases the production of the PRHΔC protein which functions as a trans-dominant negative regulator of PRH by sequestering TLE proteins (Noy, *et al.,* 2012).

To summarise, CK2-dependent phosphorylation of Ser163 and Ser177 within the PRH homeodomain significantly damages DNA-binding potential, transcriptional regulation, and nuclear localisation (Soufi *et al.,* 2009, Noy *et al.,* 2012). Notably, the mutant PRH S163C:S177C maintains putative enhanced stability in the presence of CK2 (Noy *et al.,* 2012), hence, may be more valuable than wild-type PRH for therapeutic utility.

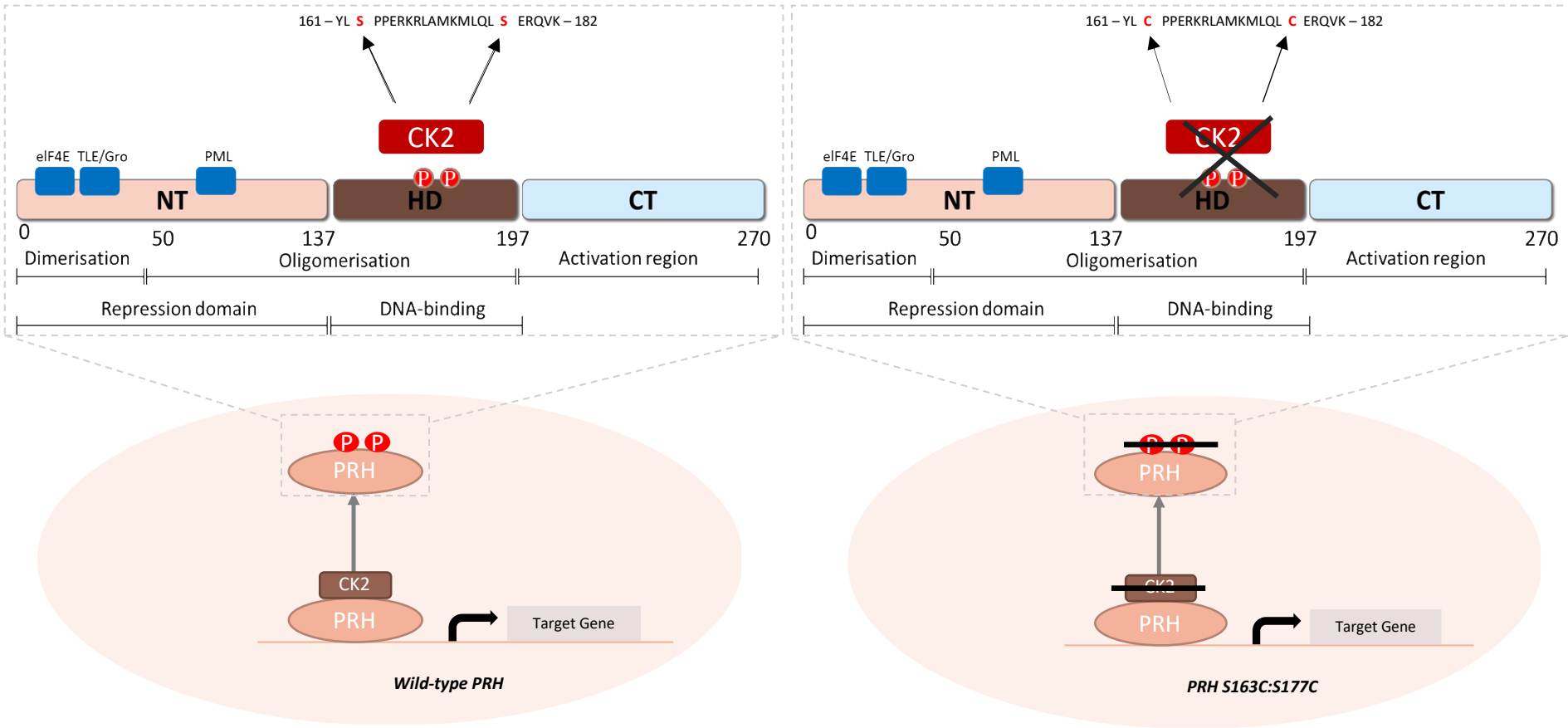

FIGURE 1.4: Protein Kinase CK2 phosphorylates two serine residues in PRH (S163 and S177)

SELDI-TOF-MS analysis and mutation studies revealed two protein kinase CK2 phosphorylation sites located within the PRH homeodomain, Ser163 and Ser177. Mutation of both serine residues to cysteines, PRH *S163C:S177C,* is preventative of phosphorylation. NT; N-terminal, HD; homeodomain, CT; C-terminal.

1.5.1 PRH in cell proliferation and cell survival

PRH has been implicated in the control of cell proliferation and cell survival via multiple mechanisms in different cell types (Gaston *et al.,* 2016; Soufi and Jayaraman, 2008). For example, PRH can repress the transformation and growth-promoting effects of eIF4E by inhibiting the transport of eIF-4E-dependent cyclin d1 transcripts in U937 leukemic cells (Topisirovic *et al.,* 2003). In keeping with an inhibitory role of PRH on proliferation, knockdown of PRH in K562 cells upregulates vascular endothelial growth factor (VEGF) autocrine signalling leading to increased cell survival (Noy *et al.,* 2010). Additionally, in this study it was demonstrated that cessation of expression of *Vegf*, *Vegfr-1*, and *Vegfr-2* occurred upon overexpression of PRH levels in tumourigenic MCF-7 breast cells (Noy *et al.,* 2010). PRH deficiency resulted in attenuated proliferation in T- and B-cell progenitors. Similarly, these findings correspond to its role as an oncogene in the T-cell lineage situated downstream of LIM domain only 2 (LMO2) (Goodings *et al.,* 2015; McCormack *et al.,* 2010). More recently, data suggests an anti-proliferative role for PRH in conditional PRH knockout stem and progenitor cell populations under conditions of stress haematopoiesis. (Goodings *et al.,* 2015).

With regards to hepatocyte proliferation, adenovirus mediated PRH overexpression in liver cancer cells attenuated hepatocarcinoma growth in a xenograft mouse model (Su *et al.,* 2012). Moreover, direct interaction with c-myc indicates PRH functions as a negative regulator of hepatocyte proliferation (Marfil *et al.,* 2015). Moreover, binding of PRH to a transmembrane protein known to regulate cellular proliferation and motility, CD81, results in sequestration into the hepatocyte cytoplasm at hepatocyte proliferation peak thereby downregulates proliferation (Bhave *et al.,* 2013). Clearly, PRH presents divergent actions in the control of proliferation in multiple cell types.

1.5.2 PRH in cell migration

To investigate whether loss of PRH activity alters cell migration, atrioventricular explants obtained from a null mutation of PRH in Hhex$^{-/-}$ mice were utilised. They revealed an increase in the quantity of collagen-invasive cells in the absence of PRH, suggesting a role in migration (Hallaq *et al.,* 2004). It has been demonstrated that PRH induces the movement of breast and prostate epithelial cells in part via the direct transcriptional regulation of endoglin, since PRH-dependent decrease in endoglin expression induces migration and enhanced invasion of cancerous cells in Matrigel layer (Kershaw *et al.,* 2013). In addition, overexpression of CK2 prevents PRH from inhibiting prostate cancer cell motility. This inhibition occurs through

phosphorylation of CK2 phosphorylation sites that lie within the PRH homeodomain and thereby the anti-migratory and anti-invasive actions of PRH are lost due to CK2-dependent phosphorylation and inactivation of PRH (Siddiqui *et al.,* 2017).

1.5.3 PRH in Vascular Development

Microarray experiments in PRH deficient embryoid bodies have shown upregulated levels of vascular endothelial growth factor (VEGF) mRNA which is essential for vascular development (Guo et al, 2003). PRH mRNA and protein levels appears to be downregulated throughout the differentiation of most haematopoietic lineages (Soufi *et al.,* 2008). Interestingly in human umbilical vein endothelial cells (HUVECs), PRH overexpression results in repression of angiogenesis-related genes FLT1 (*VegfR1*), KDR (*VegfR2*) and VEGF coreceptor neuropilin-1 gene (Nakagawa *et al.,* 2003). For *Vegfr-2*, repression occurs via an interaction with the transcription factor GATA-2 in endothelial cells (Minami *et al.,* 2004). Studies in vascular endothelial cells have also implicated that xenopus PRH overexpression leads to disorganization of the vasculature and increases vascular progenitors suggesting PRH could possibly stimulate the proliferation of early endothelial progenitors (Newman, Chia and Krieg, 1997).

Collectively, these findings suggest PRH as a negative regulator of vascular and hematopoietic cellular growth. Analysis to uncover the features contributing to these associations revealed PRH is necessary for controlling cell proliferation and differentiation in several tissues.

1.6 OVEREXPRESSION OF PRH RETARDS VSMC PROLIFERATION

In a previous study by Sekiguchi and co-workers, the expression of PRH protein during neointimal hyperplasia has been assessed in balloon-injured rat aorta model. It was observed that PRH was significantly induced in neointimal VSMCs; although expression was absent in normal, healthy aortas. This study also demonstrated that PRH transactivated SMemb/NMHC-B, known to be a marker of dedifferentiated VSMC synthetic phenotype, thereby facilitating neointima formation (Sekiguchi *et al.,* 2001).

However, these findings and conclusions are contradicted by a subsequent study in which it was demonstrated that PRH is anti-proliferative in VSMCs as observed in other cell types as outlined above. Firstly wild-type PRH overexpression in primary cultures of rat aortic VSMCs blocked cell cycle progression (Wadey *et al.,* 2017). Secondly, siRNA-induced knockdown of PRH stimulated VSMCs proliferation (Wadey *et al.,* 2017). Most remarkably, overexpression of PRH S163C:S177C allowed for a prolonged cell cycle arrest for up to 96 h post-nucleofection compared to wild-type PRH which is stable for up to 24 h post-nucleofection (Wadey *et al.,* 2017).

It was previously stated that CK2-dependent phosphorylation of PRH lowers DNA-binding potential, transcriptional regulation, and nuclear localisation of PRH (Noy *et al.,* 2012). Knockdown of CK2α and α' catalytic subunits retarded VSMC proliferation (Wadey *et al.,* 2017). Correspondingly, pharmacological inhibition of CK2 using the synthetic inhibitor K66 (1-carboxymethyl-2-dimethylamino-4,5,6,7-tetrabromo-benzimidazole), significantly hindered VSMC proliferation *in vitro*. To ascertain that the effects of CK2 were mediated at least in part by PRH, CK2 was inhibited in either control VSMC or VSMC with depleted PRH. Results demonstrated that inhibition of CK2 showed an anti-proliferative action only in cells expressing PRH (Wadey *et al.,* 2017).

1.7 OVEREXPRESSION OF PRH RETARDS NEOINTIMA FORMATION *EX VIVO*

Since PRH retarded VSMC proliferation it was assessed whether PRH had the capacity to attenuate neointima formation. Adenovirus-mediated gene delivery of PRH S163C:S177C impaired intimal thickening and VSMC proliferation in segments of human saphenous vein (Wadey *et al.,* 2017). Quantification of bromodeoxyuridine (BrdU) incorporation exhibited clear depletion in neointimal and medial proliferation compared to the controls. Moreover, scratch wound assays and cleaved caspase-3 immunocytochemistry revealed that PRH S163C:S177C intervention did not influence migratory and apoptotic state respectively in primary cultures of rat aortic VSMCs (Wadey *et al.,* 2017). These findings suggested that overexpression of PRH S163C:S177C may be beneficial for reducing intimal thickening and incidences of SVGF via inhibition of VSMC proliferation.

However, it is important that strategies to reduce VSMC proliferation do not have a detrimental effect on endothelial coverage of the saphenous vein graft. Endeavours to preserve endothelial cell integrity and function must be considered when identifying new targets for

therapeutic intervention. In cultured endothelial cells, human umbilical vein endothelial cells (HUVECs) and human saphenous vein endothelial cells (HSVECs), inhibition of CK2 activity using K66 antagonised cell cycle progression by only ~25% but did not influence cell migration and apoptotic rate (Wadey *et al.,* 2017). With regards to PRH overexpression, via jet-PEI-HUVEC-mediated transfection or adenovirus-mediated delivery, no significant effect on either the proliferative, apoptotic and migratory rate of cultured endothelial cells was observed (Wadey *et al.,* 2017).

In summary, these data indicate CK2-dependent phosphorylation as a potent mediator of PRH inactivation and a potential mechanism for the regulation of cell proliferation. Recent work is consistent with this hypothesis and highlights the anti-proliferative properties of non-phosphorylatable PRH S163C:S177C mutant in VSMCs and could thereby abrogate accelerated intimal thickening in the vein graft without causing further damage to the endothelium.

1.8 JUSTIFICATION OF RESEARCH

Bypass surgery is extremely beneficial in the short-term, however long-term success is reduced by vein graft failure. In particular, intimal thickening and resultant superimposed atherosclerosis remains a clinical concern. Considering the considerable burden of cardiovascular diseases and wide use of SVG, there is a pressing unmet need to discover therapeutic whether over-expression PRH S163C:S177C can effectively retard smooth muscle proliferation and migration and intimal thickening without damaging endothelial function has been investigated.

1.9 HYPOTHESIS

It is hypothesised that local overexpression of PRH protein with enhanced stability could be advantageous to prevent the development of intimal thickening without impairing endothelial function. Furthermore, it is hypothesised that the identification of PRH target genes in VSMCs will reveal potential targets for therapeutic interventions to sustain long-term SVG patency.

1.10 EXPERIMENTAL AIMS

1. To determine the effect of overexpression of non-phosphorylatable PRH S163C:S177C on human SV (HSV) EC and VSMC proliferation, migration and apoptosis *in vitro*.

2. To determine the effect of overexpression of non-phosphorylatable PRH S163C:S177C on phenotypic switching in HSV VSMCs *in vitro*.

3. To determine the effect of overexpression of non-phosphorylatable PRH S163C:S177C on vascular inflammation in HSV ECs *in vitro*.

4. To compare PRH target genes in HSV VSMCs and ECs and thereby identify genes that specifically repress VSMC proliferation.

5. To validate PRH target genes repress HSV VSMC proliferation *in vitro*.

6. To determine the effect of overexpression of non-phosphorylatable PRH S163C:S177C on intimal thickening and EC coverage *in vivo*.

2.

MATERIALS AND METHODS

2. MATERIALS AND METHODS

2.1 MATERIALS

Laboratory reagents were purchased from Sigma Aldrich unless specified otherwise in the text. All reagents purchased were of the highest possible quality and purity.

2.1.1 Tissue Culture Media

Table 2.1 The composition of media for culture of human saphenous vein VSMCs

10% (v/v) Foetal Bovine Serum (FBS)/DMEM	Dulbecco's Modified Eagle's Medium (DMEM: 1.0g/L glucose, without L-glutamine; catalogue number: E15-005) and DPBS (Ca2+ and Mg2+ free; catalogue number: D8537) were purchased from GE Healthcare and Sigma, respectively. Foetal bovine serum (FBS) gold (catalogue number: A15-151), L-glutamine (catalogue number: M11-004), penicillin and streptomycin (catalogue number: P11-010), and gentamicin (catalogue number: P11-004) were acquired from PAA Laboratories.

Table 2.2 The composition of media for culture of human saphenous vein ECs

2% (v/v) Foetal Bovine Serum (FBS)/Serum-Free Endothelial Cell Growth Medium	Endothelial Cell Basal Medium (catalogue number: C-22210) were purchased from Promocell. Penicillin and streptomycin (PAA Laboratories; catalogue number: P11-010) and Foetal bovine serum (FBS) gold (catalogue number: A15-151).
Endothelial Cell Growth Medium	Endothelial Cell Growth Medium Kit (catalogue number: C-22010), Endothelial Cell Growth Supplement (ECGS: catalogue number: C-22010, includes bovine hypothalamic extract, but contains basic Fibroblast Growth Factor, Insulin-like Growth Factor (Long R3 IGF-1), and Vascular Endothelial Growth Factor. Endothelial Cell Basal Medium (catalogue number: C-22210) were purchased from Promocell. Penicillin and streptomycin (PAA Laboratories; catalogue number: P11-010).

Table 2.3 The composition of media for culture of human saphenous vein VSMCs

RPMI Medium	Roswell Park Memorial Institue-1640 medium (RPMI-1640 buffered with 25mM HEPES; catalogue number: 42401018) was used purchased from Gibco. Other tissue culture reagents included: 10% (v/v) heat-inactivated FBS (Gibco; catalogue number: 10082147), 2mM L-glutamine (PAA Laboratories; catalogue number: M11-004), and 100µg/mL penicillin and 100IU/mL streptomycin (PAA Laboratories; catalogue number: P11-010).

2.1.2 Immunochemical Reagents

The immunochemical reagents utilised in the experiments outlined in this thesis are listed in Table 2.4 & 2.5.

Table 2.4: Primary Antibodies used for Western Blotting
Antibodies were diluted in 1% (w/v) bovine serum albumin (BSA) / phosphate buffered saline (PBS), 5% (w/v) BSA/PBS, 5% (w/v) BSA/ tris-buffered saline (TBS), 5% (w/v) BSA/ tris-buffered saline-tween (TBS-T) or 5% (w/v) skimmed milk powder in TBS-T (5% milk/TBS-T) depending on manufacturer's instructions or in-house optimisation.

Antibody	Host Species	Dilution	Working Concentration	Company	Catalogue Number
Anti-Calponin	Rabbit	1:1000 5% (w/v) milk/TBS-T	0.1µg/mL	Novus Biologicals	NBP1-87029
Anti-C-Myc-Tag	Mouse	1:1000 5% (w/v) BSA/TBS-T	0.56µg/ml	Cell Signalling	2276
Anti-Cyclin D1	Rabbit	1:500 5% (w/v) BSA/TBS-T	0.1µg/mL	Cell Signalling	2978
Anti-HDAC-9	Rabbit	1:500 5% (w/v) BSA/TBS-T	0.5µg/mL	Abcam	Ab239979
Anti-ICAM-1	Rabbit	1:2000 5% (w/v) BSA/TBS	0.3µg/mL	Abcam	Ab53013
Anti-P21	Rabbit	1:1000 5% (w/v) BSA/TBS-T	0.1µg/mL	Cell Signalling	2947
Anti-Smoothelin	Rabbit	1:1000 5% (w/v) BSA/TBS-T	0.5µg/mL	Novus Biologicals	NBP2-3797
Anti-STAT-1	Rabbit	1:1000 5% (w/v) BSA/TBS-T	0.1µg/mL	Cell Signalling	14994S
Anti-VCAM-1	Rabbit	1:1000 5% (w/v) BSA/TBS-T	0.44µg/mL	Abcam	Ab134047

Abbreviations. HRP: Horseradish Peroxidase; ICAM-1: Intercellular Adhesion Molecule 1; HDAC-9: Histone Deacetylase 9; STAT-1: Signal Transducer And Activator Of Transcription 1; VCAM-1: Vascular cell adhesion protein

Table 2.5: Secondary Antibodies used for Western Blotting
Antibodies were diluted in PBS, 5% (w/v) BSA/TBS-T or 5% milk/TBS-T depending on manufacturer's instructions or in-house optimisation.

Antibody	Host Species	Dilution	Company	Catalogue Number
Anti-Mouse IgG-HRP	Rabbit	WB: 1:2000 5% (w/v) BSA/TBS-T	Dako	P0260
Anti-Mouse IgG-HRP	Horse	WB: 1:2000 5% (w/v) milk/TBS-T	Cell Signalling	7076
Anti-Rabbit IgG-HRP	Swine	WB: 1:5000 5% (w/v) BSA/TBS-T	Dako	P0217
Anti-Rabbit IgG-HRP	Goat	WB: 1:2000 5% (w/v) milk/TBS-T	Cell Signalling	7074

Abbreviations. HRP: Horseradish Peroxidase; IgG: Immunoglobulin-G; WB: Western Blotting.

Table 2.6: Primary Antibodies used for Immunocytochemistry, Immunohistochemistry and Immunofluorescence

Antibody	Host Species	Working Concentration	Company	Catalogue Number
Anti-Cleaved Caspase-3	Rabbit	ICC: 1µg/ml	R & D systems	AF835
Anti-Myc Tag	Mouse	ICC: 4µg/mL	Millipore	16244
Anti-α Smooth Muscle Cell Actin	Mouse	IF: 3.1µg/mL	Sigma Aldrich	A2547
Anti-BrdU	Mouse	IHC: 8.6µg/mL	Sigma Aldrich	B2531
Anti-C-Myc-Tag	Mouse	IHC: 22.4ng/mL	Cell Signalling	2276
Anti-Calponin	Rabbit	ICC: 1ug/mL IHC: 0.2ug/mL	Novus Biologicals	NBP1-87029
Anti-CD31	Rabbit	IHC: 0.4ug/mL	Abcam	Ab28364
Anti-HDAC-9	Rabbit	IHC: 1ug/mL	Abcam	Ab239979
Anti-Smoothelin	Rabbit	ICC: 1µg/mL IHC: 1ug/mL	Novus Biologicals	NBP2-37971
Anti-STAT-1	Rabbit	IHC: 1ug/mL	Cell Signalling	14994S

Abbreviations. HRP: Horseradish Peroxidase; ICC: Immunocytochemistry; IF: Immunofluorescence; IHC: Immunohistochemistry; BrdU: 5-bromo-2'-deoxyuridine; CD31: Cluster of Differentiation 31; HDAC-9: Histone Deacetylase 9; STAT-1: Signal Transducer And Activator Of Transcription 1.

Table 2.7: Secondary and Tertiary Antibodies used for Immunocytochemistry, Immunohistochemistry and Immunofluorescence

Antibody	Company	Catalogue Number
AlexaFluor-488 goat anti-rabbit IgG	Invitrogen	A11008
DyLight-488 goat anti-rabbit IgG	Vector	D1-1488
Biotinylated goat anti-mouse IgG	Vector	BA-9200
Biotinylated goat anti-rabbit IgG	Sigma Aldrich	B7389
Dylight-488 Streptavidin	Vector	SA-5488
ExtrAvidin-peroxidase	Sigma Aldrich	E2886

Abbreviations. HRP: Horseradish Peroxidase; IgG: Immunoglobulin-G.

2.1.3 Details of Suppliers

The location and website details of suppliers of laboratory reagents and equipment are summarised in Table 2.8.

Table 2.8: Contact details of suppliers from which Immunochemical Reagents were acquired

Company	Location	Website
2B Scientific	Upper Heyford, UK	2bscientific.com
Abcam	Cambridge, UK	www.abcam.com
Addgene	Middlesex, UK	www.addgene.org
Bio-Rad	Hertfordshire, UK	www.bio-rad.com
Cell Signalling Technologies	Hertfordshire, UK	www.cellsignal.com
Dako	Cambridgeshire, UK	www.dako.com
Enzo Life Sciences	Exeter, UK	www.enzolifesciences.com
GE Healthcare (including PAA)	Buckinghamshire, UK	www.gehealthcare.com
Geneflow	Staffordshire, UK	www.geneflow.co.uk
Generon	Slough, UK	www.generon.co.uk
Life Technologies (including Ambion, Applied Biosystems, Gibco, Invitrogen, Molecular Probes)	Paisley, UK	www.lifetechnologies.com
Merck Millipore (including Calbiochem)	Hertfordshire, UK	www.merckmillipore.com
Qiagen	Manchester, UK	www.qiagen.com
R&D Systems	Oxfordshire, UK	www.rndsystems.com
Sigma Aldrich	Dorset, UK	www.sigmaaldrich.com
Roche	West Sussex, UK	www.roche.com
Stratech	Cambridge, UK	https://stratech.co.uk/
Thermo Fisher Scientific	Massachusetts, USA	www.thermoscientific.com
Vector Laboratories	Peterborough, UK	www.vectorlabs.com
VWR	Leicestershire, UK	uk.vwr.com

2.1.4 Adenoviruses

In this study, replication-defective adenovirus (Ad) based on the adenovirus type-5 vector were used. The recombinant adenoviral constructs were depleted of ΔE_1E_3 by site-specific FLP-mediated recombination and create replication incompetence. The empty adenoviral vector lacking a transgene (Ad: Control) and c-myc-tagged S163C:S177C mutant PRH (Ad: PRH S163C:S177C) were prepared using the shuttle vector pDC 515 (Microbix Biosystems; catalogue number) by Dr. Graciela Sala-Newby and Tom Hathaway (University of Bristol). Plaque-pure viruses were propagated on HEK293 cells, purified by caesium chloride density gradient centrifugation and the number of plaques forming units (pfu) per ml was titred using the end-point dilution assay (Anderson *et al.,* 2000). All Ad: PRH S163C:S177C preparations were tested for transgene production using Western blotting, lack of toxicity and ability to inhibit VSMC proliferation as previously reported (Wadey *et al.,* 2017) in isolated VSMCs *in vitro.* Adenoviral stocks were stored at -70°C in aliquots and thawed immediately before use.

2.1.5 Infection of cultured cells with adenoviruses

Cells were infected with Ad: PRH S163C:S177C diluted in the cell type specific culture medium to a final concentration of at 5 x 10^8 pfu/ml in VSMCs, and a combined dose of 4 x 10^8 pfu/ml Ad: Control and 1 x 10^8 pfu/ml in HSVECs. The controls for both cell types were cells infected with 5 x 10^8 pfu/ml of Ad: Control or uninfected cells (media alone). Cell culture medium was refreshed 18 h after infection.

2.2 METHODS: CULTURE OF HSV VSMCs

2.2.1 Isolation and primary culture of HSV VSMCs

With Research Ethical Committee approval (number 04/Q2007/6), human saphenous vein (HSV) VSMCs were isolated using a medial explant method. Briefly, segments of human saphenous veins, obtained from patients undergoing coronary artery bypass surgery, were collected in 10% (v/v) FBS/DMEM. Prior to dissection of veins immersed in 10% (v/v) FBS/DMEM in a glass petri dish with set Sylgard resin, the cannulae were removed by cutting the vein segment at the end of the cannula with micro-scissors. Veins were cut longitudinally and pinned using 23-gauge syringe needles to the resin endothelium uppermost. Removal of the endothelial layer was performed by rubbing the endothelial surface with firm pressure using the insert of a 1ml syringe. The medial layer was isolated from the adventitia using a

scalpel and forceps, then cut into approximately 2mm x 2mm explants. The explants were transferred into T25 tissue culture flasks and allowed to adhere onto the growth surface of the flasks for 30 minutes. Then, explants were covered with 10% (v/v) FBS/DMEM and incubated at 37°C and 5% CO_2. Fresh VSMC culture media was provided on a weekly basis until the VSMCs reached confluency.

2.2.2 Cell Passage of VSMCs

Cell passage by trypsin digestion was performed on fully confluent cell culture flasks for further propagation of primary VSMCs. VSMCs were briefly washed with Dulbecco's phosphate-buffered saline (DPBS: Ca2+ and Mg2+ free; company; catalogue number: D8537) before incubation with 0.05% (w/v) trypsin-ethylene diamine tetraacetic acid (EDTA: PAA Laboratories; catalogue number: L11-003) at 37°C for 4 minutes. After incubation, VSMCs were checked under a microscope to ensure the detachment of adherent cells from the culture flask. Subsequently, trypsin was quenched with an equal volume of 10% (v/v) FBS/DMEM to neutralise trypsin activity. For gentle mechanical removal, adherent VSMCs were scraped from the flask using a cell scraper. VSMCs were then centrifuged at 433g for 5 minutes. The supernatant was removed, and the cell pellet re-suspended in 1ml 10% (v/v) FBS/DMEM. Cells were then re-cultured in a larger flask or split into two flasks containing VSMC culture medium and incubated at 37°C and 5% CO_2. VSMC culture medium was routinely changed once a week to optimize growth. All experiments were performed with VSMCs between passages 2 and 8.

2.2.3 Cell Freezing

Confluent VSMCs were detached from cell culture flasks with 0.05% (w/v) Trypsin-EDTA as described above and centrifuged at 433g for 5 minutes. Supernatant was discarded and the cell pellet re-suspended in fresh VSMC culture medium supplemented with 10% (v/v) dimethyl sulfoxide (DMSO). The cell suspension was quickly transferred to a sterile cryovial and frozen to -80°C in a freezing chamber overnight to enable 1°C decrease per minute, then moved to liquid nitrogen for long-term storage.

2.2.4 Cell Counting

Cells in suspension were counted using a cover-slipped Neubauer haemocytometer. The following formula was employed to calculate cell density:

$$\textit{Average cell count per } 1mm^2 = \textit{Number of cells per mL} \times 10^4$$

2.2.5 Revival of frozen HSV VSMCs

HSV VSMCs were thawed rapidly by holding a vial of cells under running hot water. The vial contents were transferred to a centrifuge tube containing 9 mL of pre-warmed VSMC culture medium and centrifuged at 433g for 5 minutes. The cell pellet was resuspended in 1 mL of pre-warmed VSMC culture medium and added to an appropriate culture flask already containing 10-12 mL pre-warmed VSMC culture growth medium and incubated at 37°C and 5% CO_2.

2.3 METHODS: CULTURE OF HSVECs

2.3.1 Culture of HSVECs

Primary human saphenous vein endothelial cells (HSVECs, Promocell; catalogue number: C-12231 and Stratech; catalogue number: HEC18) were obtained from single donors. HSVECs were cultured in endothelial cell growth medium and incubated at 37°C and 5% CO_2. The experiments were performed with cells at passage 3-6.

2.3.2 Cell Passage

Cell passage by trypsin digestion was performed on fully confluent cell culture flasks for further propagation of primary HSVECs. HSVECs were briefly washed with DPBS before incubation with 0.05% (w/v) Trypsin-EDTA at 37°C for 1-2 minutes. After incubation, HSVECs were checked under a microscope to ensure detachment of adherent cells from the culture flask. Subsequently, trypsin was quenched with an equal volume of endothelial cell growth medium to neutralise trypsin activity. For gentle mechanical removal, adherent cells were scraped from the flask using a cell scraper. HSVECs were then centrifuged at 330 g for 4 minutes as recommended by the manufacturer's instructions. The supernatant was removed, and the cell pellet re-suspended in 1ml endothelial cell growth medium. HSVECs were then re-cultured in

a larger flask or split into two flasks containing endothelial cell culture media and incubated at 37°C and 5% CO_2. Endothelial cell culture media was routinely changed once every 2-3 days to optimize growth. All experiments were performed with ECs between passage 3 and 6.

2.3.3 Cell Freezing

Confluent cells were detached from cell culture flasks with 0.05% (w/v) Trypsin-EDTA as described above and centrifuged at 330 g for 4 minutes. Supernatant was discarded and the cell pellet re-suspended in fresh endothelial cell culture media supplemented with 10% (v/v) DMSO. The cell suspension was quickly transferred to a sterile cryovial, frozen to -80°C in a freezing chamber overnight, then moved to liquid nitrogen for long-term storage.

2.3.4 Cell Counting

HSVECs in suspension were counted using a cover-slipped Neubauer haemocytometer. The following formula was employed to calculate cell density:

$$\textit{Average cell count per } 1mm^2 = \textit{Number of cells per mL} \times 10^4$$

2.3.5 Revival of frozen HSVECs

HSVECs were thawed rapidly by holding a vial of cells under running hot water. The vial contents were transferred to a centrifuge tube containing 9 mL of pre-warmed endothelial cell growth medium and centrifuged at 330 g for 4 minutes. The cell pellet was resuspended in 1 mL of pre-warmed endothelial cell growth medium and added to an appropriate culture flask already containing 10-12 mL pre-warmed endothelial cell growth medium and incubated at 37°C and 5% CO_2.

2.4 METHODS: CULTURE OF THP-1 CELLS

2.4.1 Culture of THP-1 cells

THP-1 human monocytic-like cells obtained from THP-1 ATCC® TIB-202™ (lgcstandards-atcc.org) were cultured in suspension in RPMI medium. THP-1 cells were incubated at 37°C and 5% CO_2.

2.4.2 Cell Passage

For sub-culturing, every 3 to 4 days, cell density was assessed by cell counting and a density above 1×10^6 cells/mL was prevented. Briefly, any loosely adhered cells were dislodged using a cell scraper and the cell suspension was centrifuged at 300 g for 5 minutes, the supernatant was discarded, and cell-pellet re-suspended in 1 mL pre-warmed RPMI medium, a further 14 mL was added to the cell suspension, prior to cell counting as described in 2.2.4 and 2.3.4. Cells were then seeded into flasks containing 20 mL of pre-warmed RPMI at a density of 1×10^5 cells/mL.

2.4.3 Cell Freezing

For cryopreservation, cells were sub-cultured as described in 2.4.2 and resuspended at a density of 1×10^5 cells/mL in 1 mL 10% (v/v) DMSO in RPMI medium. The cell suspension was quickly transferred to a sterile cryovial, frozen to -80°C in a freezing chamber overnight, then moved to liquid nitrogen for long-term storage.

2.4.4 Cell Counting

Cells in suspension were counted using a cover-slipped Neubauer haemocytometer. The following formula was employed to calculate cell density:

$$\textit{Average cell count per } 1mm^2 = \textit{Number of cells per mL} \times 10^4$$

2.4.5 Revival of frozen THP-1 CELLS

For resuscitation, THP-1 cells were thawed rapidly by holding a vial of cells under running hot water. The vial contents were transferred into 20-25 mL pre-warmed RPMI medium in a T175 flasks and incubated at 37°C and 5% CO2. RPMI medium was replaced on a weekly basis.

2.5 METHODS: WESTERN BLOTTING

2.5.1. Protein Extraction

Cells were washed twice with DPBS and then sodium dodecyl sulphate (SDS) lysis buffer (50 mM Tris-HCl (pH 8), 10% (v/v) glycerol, 5% (w/v) SDS) added. Wells were scraped with the

insert of a 1 mL syringe and lysates transferred to eppendorf tubes. Samples were kept on ice until protein quantification or stored at -80°C.

2.5.2 Protein Quantification

The protein concentrations of cell lysates were determined using the Micro Bicinchoninic Acid (BCA) Assay Kit (Thermo Scientific; catalogue number: 23235). In a 96-well plate, 1 µL of cell lysate was diluted in 140 µL of HPLC water. The protein concentration of cell lysates was determined in duplicate wells by reference to a standard curve consisting of known concentrations of BSA: 0, 0.1, 0.25, 0.5, 1.0, 2.5, 5.0 and 10 µg/mL. Prior to incubation at 37°C for 30-60 minutes, 150µl of Micro BCA reagent (reagents A: B: C in a ratio of 25:24:1) was added to each well. Absorbance of each well was read at 560 nm wavelength using the GloMax® Explorer Multimode Microplate Reader (Promega; catalogue number: GM3500).

2.5.3 Gel Electrophoresis

To immunologically detect specific proteins, cell lysates were first separated by size using SDS–polyacrylamide gel electrophoresis (PAGE). Cell lysates were prepared by adding HPLC water to ensure equal protein concentration and volume. One volume Laemmli Sample Buffer (Bio-Rad; catalogue number: 161-0737) with 5% (v/v) β-mercaptoethanol was added to each of the samples, followed by heating to 95°C for 5 minutes. 5 µL of BLUeye Prestained Protein Ladder (Geneflow; catalogue number: S6-0024) with 5% (v/v) β-mercaptoethanol was also heated to 95°C for 5 minutes and served as a molecular weight marker. Samples and marker were electrophoresed on a 4-12% Mini-PROTEAN TGX Gels (Bio-Rad; catalogue number: 456-1084) using 1X Tris/Glycine/SDS (TGS) running buffer (Bio-Rad; catalogue number: 161-0772) and 300 V for 15-20 minutes.

2.5.4 Stain-free Gel

Stain-free technology allows for immediate visualisation of proteins following electrophoresis and normalisation of bands to total protein (refer to http://www.bio-rad.com/en-uk/product/mini-protean-precast-gels/mini-protean-tgx-stain-free-precast-gels for more details). Immediately after electrophoresis, the gel was removed from the cassette and placed directly into the ChemiDoc MP System (Bio-Rad; catalogue number: 170-8280). To acquire a stain-free gel image, 1 minute UV activation provided adequate signal intensity.

2.5.5 Protein Transfer

Following protein separation by SDS-PAGE and stain-free imaging, gels were transferred to Trans-Blot Mini Nitrocellulose Membranes (Bio-Rad; catalogue numbers: 170-4158 and 170-4159, respectively) using the Trans-Blot Turbo Transfer Starter System (Bio-Rad; catalogue number: 170-4155) for fast and efficient electrophoretic protein transfer, following the manufacturer's instructions.

2.5.6 Antibody Labelling

To reduce non-specific binding, nitrocellulose membranes were placed in blocking solution consisting of 5% (w/v) fat-free milk powder diluted in TBS-T (20mM Tris, 137mM NaCl, 0.1% (v/v) Tween 20; pH 7.6) for 30 minutes at room temperature (RT). The membranes were incubated with diluted primary antibodies detailed in Table 2.1, overnight at 4°C. Following incubation, the nitrocellulose membranes were washed with TBS-T for 5, 10 and 20 minutes prior to incubation in diluted horseradish peroxidase (HRP)-labelled secondary antibodies detailed in Table 2.2 for 1 hour at RT. Following three more washes with TBS-T for 5, 10 and 20 minutes, membranes were incubated with Luminata Forte Western HRP substrate (Merck Millipore; catalogue number: WBLUF0100) for 1 minute to detect bound antibodies. Finally, the luminescence was detected using the ChemiDoc MP System (Bio-Rad, 170-8280) with 1 minute length of exposure to avoid saturation of bands.

2.5.7 Densitometry

Quantification of the density of the detected protein band was performed using Image Lab Software (Bio-Rad, 170-8280). Optical density was expressed in units of mm^2 (OD x mm^2) and normalised to the most prominent stain-free band in the same MW range for the sample.

2.6 METHODS: IMMUNOASSAYS

For ELISA assays, primary HSVECs conditioned media was collected and was either stored at -80^{o}C or analysed immediately. Quantikine ELISA (enzyme-linked immunosorbent assay) kits were used to detect the following pro-inflammatory mediators: human IL-6 Quantikine ELISA Kit (R&D Systems; catalogue number: D6050), human IL-8 Quantikine ELISA Kit (R&D Systems; catalogue number: D8000C) and human CCL2/MCP-1 Quantikine ELISA Kit (R&D

Systems; catalogue number: DCP00). Conditioned media was diluted with Calibrator Diluent RD6Q to ensure detection within the linear range of the standard curve. 50 µL of Assay Diluent RD1-83 was added to each well. Then, 200µl of standard, sample or control was added per well followed by sealing the plate with the adhesive strip and incubation for 2 hours at RT.

Each well was aspirated and washed using 400 µL Wash Buffer repeating the process twice for a total of three washes. To ensure complete removal of liquids, the ELISA plate was inverted and blotted against clean paper towel. Subsequently, 200 µL of human IL-6, IL-8 or MCP-1 Conjugate was added to each well. The plate was covered by an adhesive strip followed by incubated for 1 hour at RT. Wells were aspirated and washed with 400 µL Wash buffer three times. Subsequently, 200 µL of Substrate Solution was added to each well followed by a 30-minute incubation at RT protected from the light. This was followed by the addition of 50 µL of Stop Solution to each well to encourage a colour change from blue to yellow. To ensure thorough mixing the plate was tapped. The absorbance of each well was determined at 450 nm wavelength using a GloMax® Explorer Multimode Microplate Reader within 30 minutes. The concentration of the detected protein was calculated by the average of duplicate readings for each standard, control, and sample and subtract the average zero standard absorbance.

2.7 METHODS: IMMUNOCYTOCHEMISTRY

2.7.1 Immunocytochemistry for c-myc tagged PRH

Primary HSVECs or HSV VSMCs (2 x 10^4 cells) were seeded on glass coverslips in a 24-well plate. Cells were washed twice in PBS prior to fixation in 250 µL of 3% (w/v) paraformaldehyde/PBS (PFA/PBS) for 10 minutes. Cells were rinsed once with PBS and permeabilised with three 5-minute washes in 500 µL of 0.2% (v/v) Triton X-100/PBS, then rinsed twice with PBS and blocked in 250 µL of 20% (v/v) goat serum/PBS for 30 minutes at RT. Cells were washed again with PBS followed by incubation with 4 mg/mL of anti-c-myc-tag antibody, clone 4A6, Alexa Fluor 488 Conjugate (Millipore; catalogue number: 16-244) diluted in 5% (w/v) BSA/PBS, overnight at 4°C. 4 µg/mL of non-immune mouse IgG diluted in 5% (w/v) BSA/PBS was used as a negative control. Following three PBS washes, cells were mounted with Prolong Gold Antifade Reagent with 4',6-diamidino-2-phenylindole (DAPI) (Molecular Probes; catalogue number: P36931), then stored at 4°C in the dark until visualisation using fluorescence microscopy.

The cells were imaged using an Olympus BX41 microscope and Q-capture pro 6.0 software. Cells with nuclear and cytoplasmic c-myc-tagged staining (green) were identified as positive. Cells without distinct green staining were denoted as negative. Overall, 20 images were taken in 20x magnification to represent approximately 200-400 cells per condition. The number of c-myc-tag-positive cells was expressed as a percentage of the total number of cells counted.

2.7.2 Immunocytochemistry for EdU - Proliferation Assay

Proliferative cells were identified using the Click-iT 5-ethynyl-2'-deoxyuridine (EdU) Alexa Fluor 488 Imaging Kit (Invitrogen; catalogue number: C10337). Unlike traditional cell proliferation assays, the Click-iT® Plus EdU proliferation assay does not rely on radioactivity or antibodies for detection of the newly incorporated deoxyribonucleoside. Primary HSVECs or HSV VSMCs were seeded at 2 x 10^4 in 24-well plates with an appropriate cell growth medium supplemented with 10 µM EdU. Cells were washed twice in PBS and then fixed with 250 µL of 3% (w/v) PFA/PBS for 15 minutes. Following a single wash in PBS, cells were incubated in 500 µL of 0.5% (v/v) Triton X-100/PBS to permeabilise the cells for 20 minutes prior to rinsing twice in 3% (w/v) BSA/PBS. The Click-iT reaction cocktail was prepared as stated in the Click-iT handbook such that the final Click-iT reaction cocktail contained 758 µL deionised water, 100 µL reaction buffer, 40 µL catalyst solution, 2 µL Alexa Fluor azide and 100 µL buffer additive, all prepared in the said order for optimal performance. 250 µL of Click-iT reaction cocktail was added to cells within 15 minutes of preparation and incubated for 30 minutes at RT, protected from day light. Cells were washed thrice in PBS. To stain nuclei, cells were mounted with Prolong Gold Antifade Reagent with DAPI (Molecular Probes; catalogue number: P36931), then stored at 4°C in the dark until visualisation using a fluorescent microscope.

The cells were imaged using an Olympus BX41 microscope and Q-capture pro 6.0 software. EdU-positive cells were identified as those with green-coloured nuclei whereas negative cells were those with only blue-coloured (DAPI) nuclei. To determine the proliferative rate per condition, the percentage of EdU-positive cells was calculated. Overall, 20 images were taken in 20x magnification to represent approximately 200-400 cells per condition. The number of EdU-positive cells was expressed as a percentage of the total number of cells counted.

2.7.3 Immunocytochemistry for Cleaved Caspase-3 - Apoptosis Assay

Primary HSVECs or HSV VSMCs at a cell seeding density of 2 x 10^4 were seeded in 24-well plates. As a positive control, cells were incubated with 200 ng/mL human recombinant Fas-ligand (Enzo Life Sciences; catalogue number: ALX-522-020-C005) to induce apoptosis. Cells were washed twice in PBS and then fixed in 250 µL of 3% (w/v) PFA/PBS for 15 minutes. Following a single wash in PBS, cells were permeabilised with three 5-minute washes in 500 µL of 0.2% (v/v) Triton X-100/PBS then rinsed twice with PBS and blocked in 250 µL of 20% (v/v) goat serum/PBS for 30 minutes at RT. Cells were washed once with PBS and incubated with 250 µL of 1 mg/mL rabbit anti-cleaved caspase-3 antibody (R & D systems; Catalogue number: MAB835) diluted in 1% (w/v) BSA/PBS, overnight at 4°C. Following three PBS washes, cells were incubated with 250 µL of biotinylated goat-anti-rabbit (Sigma; Catalogue number: B7389) diluted 1:200 in PBS for 1 hour at RT. Following another two PBS washes, cells were incubated with 250 µL of Streptavidin-488 antibody (Vector Laboratories; catalogue numbers: SA-5488-1) diluted 1:200 in PBS for 1 hour at RT, protected from day light. Following two washes with PBS, cells were mounted with Prolong Gold Antifade Reagent with DAPI (Molecular Probes; catalogue number: P36931), then stored at 4°C in the dark until visualisation using fluorescence microscopy.

The cells were imaged using an Olympus BX41 microscope and Q-capture pro 6.0 software. Cells with nuclear cleaved caspase-3 (green) were identified as apoptotic. All nuclei were stained blue with DAPI. To determine the apoptotic rate per condition, the percentage of cleaved caspase-3 positive cells was calculated. Overall, 20 images were taken in 20x magnification to represent approximately 200-400 cells per condition. The number of cleaved caspase-3 positive cells was expressed as a percentage of the total number of cells counted.

2.8 METHODS: MIGRATION ASSAY

Cell migration was analysed by measuring the decrease in wound size 24 hours after scratching a wound on the monolayer of cells. Firstly, primary HSVECs (4x10^4 cells) or HSV VSMCs (4x10^4 cells) were seeded on fibronectin-coated glass coverslips in a 24-well plate and cultured in the appropriate cell growth medium. Following infection with the adenovirus for 18 hours, wells were washed twice in PBS and then the confluent cells were scratched using a 1 mL pipette tip to create two parallel straight lines, simulating a wound. Cells were washed once with PBS to remove debris, then treated with 2 mM hydroxyurea to prevent cell proliferation. Using the EVOS FL Color Imaging System (Thermo Fisher Scientific; Catalogue

number: AMEFC4300) with a 10x objective lens, images of the wound edges were taken immediately after wounding and 24 hours post incubation at 37°C in 5% CO_2.

Four fields were photographed per condition and five measurements taken per field at each time point. Migration was quantified and expressed as the distance migrated in pixels between 0 and 24 hours.

2.9 METHODS: MONOCYTE ADHESION ASSAY

2.9.1 Monocyte Adhesion Assay: Static Condition

Monocyte adherence to an endothelial monolayer was assessed using THP-1 monocytes under static conditions. HSVECs (2 x 10^4 cells) were seeded in wells of 24-well plates and grown to confluency. Following infection with the adenovirus for 18 hours, wells were washed twice in PBS. Then, cells were incubated with 10ng/ml recombinant human Tumor Necrosis Factor α (TNFα) (PromoKine; Catalogue number: C-63721) in 2% (v/v) FBS endothelium cell medium for 24 hours. After 24 hours, THP-1 cells were fluorescence-labelled with 100 µM calcein-AM by incubation for 30 minutes at 37°C amd 5% CO_2. Then, 2 x 10^4 calcein-labelled THP-1 monocytes were added to each well of confluent HSVECs and then co-incubated for 1 hr at 37°C adn 5% CO_2 in 2% (v/v) FBS endothelium cell medium. Non-adherent cells were then removed by washing wells twice with PBS. Ten fields were photographed per condition. Adhered THP-1 cells (green) were visualised and counted using the EVOS FL Colour Imaging System (Thermo Fisher Scientific; Catalogue number: AMEFC4300) and divided by the total number of HSVECs in the viewing channels.

2.9.2 Monocyte Adhesion Assay: Low Shear Stress Model

Monocyte adherence to an endothelial monolayer was assessed using THP-1 monocytes under ‘low shear stress’ conditions. HSVECs (2 x 10^4 cells) were seeded in wells of 24-well plates and grown to confluency. Following infection with the adenovirus for 18 hours, wells were washed twice in PBS and endothelial cell growth medium was replenished. Then, cells were subjected to ‘low shear stress’ for 24 hours at 37°C and 5% CO2 using fixed-angle platform rocker (Grant Instruments, Fisher Scientific, UK) with a maximum tilt angle of 7° at 10 oscillations per minute. ‘Static’ control group were kept in the same incubator but were not subjected to ‘low shear stress’. After 24 hours, THP-1 cells were fluorescence-labelled with 100 µM calcein-AM by incubation for 30 minutes at 37°C and 5% CO_2. Then, 2 x 10^4 calcein-

labelled THP-1 monocytes were added to each well of confluent HSVECs and then co-incubated for 1 hr at 37°C and 5% CO_2 in 2% (v/v) FBS endothelium cell medium. Non-adherent cells were then removed by washing wells twice with PBS. Ten fields were photographed per condition. Adhered THP-1 cells (green) were visualised and counted using the EVOS FL Colour Imaging System (Thermo Fisher Scientific; Catalogue number: AMEFC4300) and divided by the total number of HSVECs in the viewing channels.

2.10 METHODS: TRANSWELL PERMEABILITY ASSAY

To measure endothelial permeability, HSVECs (4 x 10^4 cells) were seeded on in Transwell inserts (Corning, catalogue number: 3413) suspended within a 24-well plate and cultured in endothelial cell growth medium. To ensure the maximal growth of the HSVEC monolayer, cell growth medium was replenished every two days. Endothelial cell growth medium was replaced with 2% (v/v) FBS endothelial basal media containing streptavidin-HRP (R&D Systems, catalogue number: DY998) followed by a 5-minute incubation at 37°C and 5% CO_2. Then, 20 µL of media from the lower chamber was collected and added to a 96 well plate in triplicate. 50 µL of 3,3',5,5'-tetramethylbenzidine (TMB) substrate (Sigma-Aldrich, catalogue number: T0440) was added into each well of the 96 well plate followed by incubation at RT for 5 minutes. 25 µL of stop solution (2N H_2SO_4 water solution) (Sigma-Aldrich, catalogue number: 30743) was added to each well and absorption was determined at 450 nm wavelength using a GloMax® Explorer Multimode Microplate Reader. The absorption readings were normalised to control.

2.11 METHODS: COLLAGEN GEL CONTRACTION ASSAY

VSMC contractile capability was assessed using Cell Biolabs' Collagen-based Contraction Assay Kit (Cell Biolabs; Catalogue Number: CBA-201) following the manufacturer's instructions. Primary HSV VSMCs at a cell seeding density of 1 x 10^5 were seeded in wells of a 24-well plate. Post adenoviral infection as described in 2.1.7, VSMCs were detached using 0.05% (w/v) Trypsin-EDTA at 37°C for 5 minutes and resuspended in desired 10% (v/v) FBS/DMEM at 0.5 x 10^5 cells/mL. Cold collagen gel working solution was prepared by mixing the following components in this order collagen solution, 5 x PBS and neutralizing solution. The collagen gel working solution and VSMCs at 0.5 x 10^5 cells/mL were mixed on ice at a ratio of 1:4. Following this, 500 µL of the final mixture was cast into each well of a 24-well

culture plate. The solution was then allowed to polymerize at RT, which generally completed in 30 minutes, then 1.0 mL of culture medium was added atop each collagen gel lattice. After polymerization for 48 hours, using a sterile needle, the gels were gently released from the plates in which they were cast to allow contraction. The gels were photographed at different time-points after collagen release and the diameter of each gel was measured using Image J. Data were expressed as the distance of contraction (arbitrary units).

2.12 METHODS: *IN VIVO* EXPERIMENTS

2.12.1 Intimal thickening in C57BL/6 mice

To address whether PRH S163C:S177C expression affected intimal thickening, VSMC proliferation, migration and VSMC differentiation *in vivo*, mouse carotid artery ligation was performed. Intimal lesions are predominantly formed of VSMCs in this well-established model (Johnson *et al*, 2005; Tsaousi *et al*, 2011; Williams *et al*, 2016). Male and female, 8-week-old C57BL/6 mice were purchased from Charles River and housed in the University of Bristol animal unit. Mice were anaesthetized by inhalation of isofluorane in 100% oxygen for 30 minutes after intraperitoneal administration of 1.5 µg buprenorphine hydrochloride for analgesia (Vetergesic). The left common carotid artery was isolated and the first 5-0 silk suture was placed at the bifurcation of the common carotid artery (Singh *et al*, 2001). Right carotid arteries acted as unligated controls. The exposed left carotid arteries were coated with 100 µl of 30% (w/v) pluronic gel containing 1.33 x 10^8 pfu of the Ad: PRH S163C:S177C (with c-myc-tag) or Ad: Control. Mini osmotic pumps (model 2004 Alzet) were primed with BrdU and inserted into the mice to quantify proliferation. After suturing the wound, animals were left for 28 days. At 7 days, very little intimal formation is detectable however medial VSMC migration and proliferation is activated, while at 28 days a substantial intima is formed (reference). After allowing 28 days for intimal thickening to occur, mice were culled using 20 mg pentobarbital sodium (Euthatal). The left and right carotid arteries were fixed in 10% (v/v) formalin/PBS for 24 hours, then transferred into PBS and stored at 4°C until processing. The carotid arteries were paraffin wax-embedded longitudinally and then subjected to histological staining to enable accurate analysis of the lesion size as described below. All *in vivo* work was performed by Dr Helen Williams.

2.12.2 Histological Analysis

The arteries were gently held upright (7-day study) and horizontal (28-day study) in heated molten agar using forceps until the agar solidified. The agar plugs containing the arteries were then processed using the Shandon Excelsior Tissue Processor (Thermo Electron Corporation). Arteries were then embedded in paraffin wax using the Shandon Histocentre 3 (Thermo Electron Corporation). Blocks were cooled to -20°C using a block cooler (Elstat Electronics Limited) for at least 30 minutes and then 3-4 µm transverse sections (7-day study) and longitudinal sections (28 days study) were cut using a Reichert-Jung 2030 Biocut microtome or Bright M3500 microtome and dried onto Superfrost Plus slides (Thermo Fischer Scientific, catalogue number: 10149870).

2.12.2.1 Elastic Van Gieson Staining

Elastic van Gieson (EVG) staining was performed to stain elastin and collagen to enable measurement of the intimal area and the cross-sectional area of the left carotid arteries. EVG staining was performed in a Shandon Varistain 24-4 Automatic Slide Stainer (Thermo Scientific), in accordance with the protocol outlined in Table 2.9. Slides were mounted in DPX mounting medium (Thermo Fisher Scientific, catalogue number: 10050080), cured overnight and imaged using an Olympus BX40 microscope at x40 magnification using Q-capture pro 6.0 software. EVG stained vessel parameters were measured by using ImageJ software (imagej.nih.gov/ij).

Table 2.9: EVG Staining Protocol

Solution	Incubation time
Clearene	2 x 3 minutes
100% (v/v) alcohol (industrial methylated spirits: IMS)	2 x 3 minutes
Tap water	5 minutes
0.5% (w/v) potassium permanganate	10 minutes
Distilled water	3 minutes
1% (w/v) oxalic acid	5 minutes
Distilled water	3 minutes
70% (v/v) alcohol (industrial methylated spirits: IMS)	2 minutes
50% (v/v) Millers elastin stain (Pioneer Research Chemical Limited, PRC/R/108)	60 minutes
70% (v/v) alcohol (industrial methylated spirits: IMS)	2 minutes
Running tap water	3 minutes
Van Gieson stain (Thermo Scientific, LAMB/400-D)	20 seconds
100% (v/v) alcohol (industrial methylated spirits: IMS)	2 x 5 minutes
Clearene	2 x 5 minutes

2.12.2.2 Image Analysis

The borders of the lumen and internal elastic lamina (IEL) were traced on a digitizing board and analysed using the Image J software. The intimal area was calculated by subtracting the luminal area from the IEL area (Figure 2.1). The ratio of intimal/medial area (I/M ratio) was calculated by dividing the intimal area by medial area. Percentage occlusion was calculated on the basis of dividing the intimal area by the IEL and expressed as %.

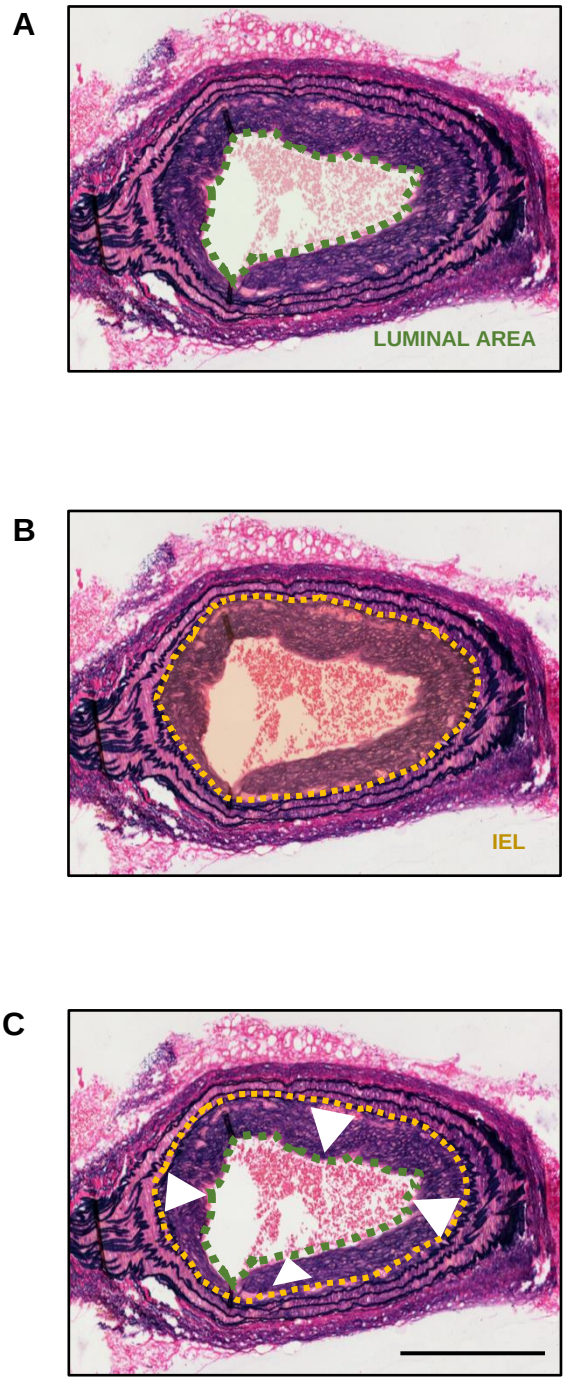

FIGURE 2.1: Visual representation of the parameters used to calculate neointimal area in EVG stained ligated carotid artery

Representative images of left carotid arteries of C57B/L6 mice 28 days after ligation stained with EVG. Green dashed lines indicates the luminal area boundary; Yellow dashed lines indicate IEL boundary. White arrows indicate the neointimal area Scale bar represents 200μm.

2.12.3 Immunostaining of tissue sections

2.12.3.1 Immunofluorescence for c-myc tagged PRH

Paraffin-wax sections (3-4μm) were de-waxed by three 5-minute incubations in 100% (v/v) clearene and rehydrated by two consecutive 5-minute washes in 100% (v/v) alcohol, a single 5-minute wash in 70% (v/v) alcohol and then distilled water. Slides were then briefly washed in distilled water then antigen retrieval was achieved by submerging the slides submerged in 10mM citrate buffer (pH 6.0) and microwaving at 800 W for 5 minutes. Distilled water was then added if necessary, to re-submerge slides, and slides were microwaved for a further 5 minutes at 800 W and then allowed to cool for 30 minutes at RT. Afterwards, the slides were transferred to cold running tap water for 5 minutes, then washed three times with PBS and sections were delineated using a hydrophobic pen. Following three washes of PBS, sections were incubated with approximately 50 μL/section of Image-iT FX Signal Enhancer (Molecular Probes; catalogue number: I-36933) for 30 minutes at RT. Sections were incubated overnight at 4°C with 50 μL/section of 1 μg/mL anti-c-myc-tag antibody (Cell Signalling; catalogue number: 2276) or non-immune rabbit IgG diluted in PBS. Slides were then washed three times in PBS. Sections were incubated with 50 μL/section of biotinylated goat anti-rabbit IgG diluted 1:200 in 1% (w/v) BSA/PBS and incubated for 45 minutes at RT. Slides were again washed three times in PBS followed by incubation with 50 μL of Dylight 488 Streptavidin (Vector Laboratories; catalogue number: SA-5488-1) diluted 1:200 in PBS for 45 minutes at RT, protected from day light. Slides were then washed four times with PBS and then mounted with Prolong Gold Antifade Reagent with DAPI (Molecular Probes; catalogue number: P-36931) overnight at 4°C in the dark until analysis.

The following day the sections were imaged using an Olympus BX41 microscope and four images of the vessel wall were taken at x60 magnification using Q-capture pro 6.0 software. C-myc-tag positive nuclei appeared green whilst all nuclei were stained blue with DAPI. The number of c-myc-tag positive nuclei were counted and expressed as a percentage of the total number of medial cells in the four images and the average calculated per artery.

2.12.3.2 Immunofluorescence for α smooth muscle cell actin

Paraffin-wax sections (3-4μm) were de-waxed by three 5-minute washes in 100% (v/v) clearene and rehydrated by two consecutive 5-minute washes in 100% (v/v) alcohol, a single 5-minute wash in 70% (v/v) alcohol and then distilled water. Slides were then briefly washed in distilled water then antigen retrieval was achieved by submerging the slides submerged in

10mM citrate buffer (pH 6.0) and microwaving at 800 W for 5 minutes. Distilled water was then added if necessary, to re-submerge slides, and slides were microwaved for a further 5 minutes at 800 W and then allowed to cool for 30 minutes at RT. Afterwards, the slides were transferred to cold running tap water for 5 minutes, then washed three times with PBS and sections were delineated using a hydrophobic pen. The Fluorescein Vector mouse-on-mouse (M.O.M) Immunodetection Kit (Vector Laboratories; catalogue number: FMK-2201) was utilised since the anti-αSMA antibody (Sigma Aldrich, catalogue number: A2547) was raised in mouse, following the manufacturer's instruction to inhibit non-specific binding of the antibody to mouse tissue. Slides were incubated with M.O.M mouse IgG blocking reagent for 1 hour at RT. Then slides were washed three times in PBS then incubated in M.O.M diluent for 5 minutes at room temperature. The diluent was then gently removed with tissue paper and 50 µL/section 3.1 µg/mL of anti-αSMA antibody (Sigma Aldrich, catalogue number: A2547) diluted in M.O.M diluent was added for 30 minutes at room temperature. As a negative control, the primary antibody was not added. Slides were washed three times in PBS and then incubated in 50 µL/section of M.O.M biotinylated anti-mouse IgG reagent for 10 minutes at room temperature. Following two washes in PBS, 50 µL/section of Fluorescein Avidin DCS was added for 5 minutes at room temperature. Finally, the slides were then washed twice in PBS and mounted in Prolong Gold with DAPI (Invitrogen, catalogue number: P36931).

The following day the sections were imaged using an Olympus BX41 microscope and Q-capture pro 6.0 software. Four images at x60 magnification were taken of each vessel. α-SMA-positive cells were identified as those with green-coloured whereas negative cells were those with only blue-coloured (DAPI). The number of nuclei associated with a green cytoplasm was counted in each x60 image and expressed as a percentage of the total nuclei present. To calculate the mean percentage of α-SMA positive cells per vessel, the percentage from all 4 images was averaged. In addition, one image at x20 magnification was taken of blue DAPI staining to permit quantification of total cell number and cell density.

2.12.3.3 Immunohistochemistry for BrdU

Paraffin-wax sections (3-4µm) were de-waxed by three 5-minute washes in 100% (v/v) clearene and rehydrated by two consecutive 5-minute washes in 100% (v/v) alcohol, a single 5-minute wash in 70% (v/v) alcohol and then distilled water. Slides were then briefly washed in distilled water then antigen retrieval was achieved by submerging the slides submerged in 10mM citrate buffer (pH 6.0) and microwaving at 800 W for 5 minutes. Distilled water was then added if necessary, to re-submerge slides, and slides were microwaved for a further 5 minutes at 800 W and then allowed to cool for 30 minutes at RT. Afterwards, the slides were transferred

to cold running tap water for 5 minutes, then washed three times with PBS and sections were delineated using a hydrophobic pen. Next, the slides were incubated in 2N HCL at 37°C for 30 minutes, then washed three times with PBS. To inhibit endogenous peroxidase activity, slides were incubated with 0.3% (v/v) H_2O_2 for 7 minutes at RT. Following three washes of PBS, sections were incubated with approximately 50 µL/section of 20% (v/v) goat serum/PBS for 30 minutes at RT. The goat serum was then removed and 50 µL/section of 1 µg/mL anti-Bromodeoxyuridine (BrdU) antibody (Sigma; catalogue number: B2531) or non-immune rabbit IgG diluted in 1% (w/v) BSA/PBS was added and incubated overnight at 4°C. Slides were then washed three times in PBS. Sections were incubated with 50 µL/section of biotinylated goat anti-rabbit IgG (Sigma Aldrich, catalogue number: B7389) diluted 1:200 in 1% (w/v) BSA/PBS and incubated for 30 minutes at RT. Following three washes of PBS, the slides were incubated with ExtrAvidin-peroxidase (Sigma Aldrich, catalogue number: E2886) diluted 1:200 in 1% (w/v) BSA/PBS and incubated for 30 minutes at RT. Slides were again washed three times in PBS followed by incubation with the HRP substrate, SigmaFast 3,3'-diaminobenzidine (DAB: Sigma Aldrich, catalogue number: D4293) for 2 minutes at RT. The ExtrAvidin-peroxidase-DAB reaction produces a brown precipitate. Slides were washed twice distilled water, and then stained with Mayer's haematoxylin for 2-5 minutes. Haematoxylin was washed off with tap water until the water appeared clear and blue colour is produced in nuclei. Slides were then dehydrated by one 5-minute incubation in 70% (v/v) alcohol, two 5-minute incubation in 100% (v/v) alcohol and then three 5-minute incubations in 100% (v/v) clearene. Slides were then mounted in DPX mounting medium (Thermo Fisher Scientific, catalogue number: 10050080) overnight at RT.

2.12.3.4 Immunohistochemistry for Smoothelin and Calponin

Paraffin-wax sections (3-4µm) were de-waxed by three 5-minute washes in 100% (v/v) clearene and rehydrated by two consecutive 5-minute washes in 100% (v/v) alcohol, a single 5-minute wash in 70% (v/v) alcohol and then distilled water. Slides were then briefly washed in distilled water then antigen retrieval was achieved by submerging the slides submerged in 10mM citrate buffer (pH 6.0) and microwaving at 800 W for 5 minutes. Distilled water was then added if necessary, to re-submerge slides, and slides were microwaved for a further 5 minutes at 800W and then allowed to cool for 30 minutes at RT. Afterwards, the slides were transferred to cold running tap water for 5 minutes, then washed three times with PBS and sections were delineated using a hydrophobic pen. To inhibit endogenous peroxidase activity, slides were incubated with 0.3% (v/v) H_2O_2 for 7 minutes at RT. Following three washes of PBS, sections were incubated with approximately 50 µL/section of 20% (v/v) goat serum/PBS for 30 minutes

at RT. The goat serum was then removed and 50 µL/section of 0.2 µg/mL anti-calponin (Novus Biologicals; catalogue number: NBP1-87029) or non-immune rabbit IgG diluted in 1% (w/v) BSA/PBS was added and incubated overnight at 4°C. To stain for smoothelin protein, 1µg/mL anti-smoothelin (Novus Biologicals; catalogue number: NBP2-3797) or non-immune rabbit IgG diluted in 1% (w/v) BSA/PBS was added and incubated overnight at 4°C. Slides were then washed three times in PBS. Sections were incubated with 50 µL/section of biotinylated goat anti-rabbit IgG (Sigma Aldrich, catalogue number: B7389) diluted 1:200 in 1% (w/v) BSA/PBS and incubated for 30 minutes at RT. Following three washes of PBS, the slides were incubated with ExtrAvidin-peroxidase (Sigma Aldrich, catalogue number: E2886) diluted 1:200 in 1% (w/v) BSA/PBS and incubated for 30 minutes at RT. Slides were again washed three times in PBS followed by incubation with the HRP substrate, SigmaFast 3,3'-diaminobenzidine (DAB: Sigma Aldrich, catalogue number: D4293) for 2 minutes at RT. The ExtrAvidin-peroxidase-DAB reaction produces a brown precipitate. Slides were washed twice distilled water, and then stained with Mayer's haematoxylin for 30 seconds – 2 minutes. Haematoxylin was washed off with tap water until the water appeared clear and blue colour is produced in nuclei. Slides were then dehydrated by one 5-minute wash in 70% (v/v) alcohol, two 5-minute washes in 100% (v/v) alcohol and then three 5-minute washes in 100% (v/v) clearene. Slides were then mounted in DPX mounting medium (Thermo Fisher Scientific, catalogue number: 10050080) overnight at RT.

2.12.3.5 Immunohistochemistry for STAT-1

Paraffin-wax sections (3-4µm) were de-waxed by three 5-minute washes in 100% (v/v) clearene and rehydrated by two consecutive 5-minute washes in 100% (v/v) alcohol, a single 5-minute wash in 70% (v/v) alcohol and then distilled water. Slides were then briefly washed in distilled water then antigen retrieval was achieved by submerging the slides submerged in 10mM citrate buffer (pH 6.0) and microwaving at 800 W for 5 minutes. Distilled water was then added if necessary, to re-submerge slides, and slides were microwaved for a further 5 minutes at 800 W and then allowed to cool for 30 minutes at RT. Afterwards, the slides were transferred to cold running tap water for 5 minutes, then washed three times with PBS and sections were delineated using a hydrophobic pen. To inhibit endogenous peroxidase activity, slides were incubated with 0.3% (v/v) H_2O_2 for 7 minutes at RT. Following three washes of PBS, sections were incubated with approximately 50 µL/section of 20% (v/v) goat serum/PBS for 30 minutes at RT. The goat serum was then removed and 50 µL/section of 1 µg/mL anti-Stat-1 (Cell Signalling; catalogue number: 14994S) or non-immune rabbit IgG diluted in SignalStain® Antibody Diluent (Cell Signalling; catalogue number: 8112) was added and incubated

overnight at 4°C. Slides were then washed three times in PBS. Sections were incubated with 50 µL/section of SignalStain® Boost IHC Detection Reagent for rabbit (Cell Signalling; catalogue number: 8114P) diluted 1:200 in 1% (w/v) BSA/PBS and incubated for 45 minutes at RT. Slides were again washed three times in PBS followed by incubation with the HRP substrate, SigmaFast 3,3'-diaminobenzidine (DAB: Sigma Aldrich, D4293) for 2 minutes at RT. Slides were washed twice distilled water, and then stained with Mayer's haematoxylin for 30 seconds–2 minutes. Haematoxylin was washed off with tap water until the water appeared clear and nuclei appeared blue. Slides were then dehydrated by one 5-minute wash in 70% (v/v) alcohol, two 5-minute washes in 100% (v/v) alcohol and then three 5-minute washes in 100% (v/v) clearene. Slides were then mounted in DPX mounting medium (Thermo Fisher Scientific, catalogue number: 10050080) overnight at RT.

2.12.3.6 Immunohistochemistry for HDAC-9 and CD31

Paraffin-wax sections (3-4µm) were de-waxed by three 5-minute washes in 100% (v/v) clearene and rehydrated by two consecutive 5-minute washes in 100% (v/v) alcohol, a single 5-minute wash in 70% (v/v) alcohol and then distilled water. Slides were then briefly washed in distilled water then antigen retrieval was achieved by submerging the slides submerged in 10mM citrate buffer (pH 6.0) and microwaving at 800 W for 5 minutes. Distilled water was then added if necessary, to re-submerge slides, and slides were microwaved for a further 5 minutes at 800W and then allowed to cool for 30 minutes at RT. Afterwards, the slides were transferred to cold running tap water for 5 minutes, then washed three times with PBS and sections were delineated using a hydrophobic pen. To inhibit endogenous peroxidase activity, slides were incubated with 0.3% (v/v) H_2O_2 for 7 minutes at RT. Following three washes of PBS, sections were incubated with approximately 50 µL/section of 20% (v/v) goat serum/PBS for 30 minutes at RT. The goat serum was then removed and 50 µL/section of 1 µg/mL anti-HDAC-9 antibody (Abcam; catalogue number: ab239979) or non-immune rabbit IgG diluted in 1% (w/v) BSA/PBS was added and incubated overnight at 4°C. To stain for CD31 protein, 0.4µg/mL anti-smoothelin (Abcam; catalogue number: ab28364) or non-immune rabbit IgG diluted in 1% (w/v) BSA/PBS was added and incubated overnight at 4°C. Slides were then washed three times in PBS. Sections were incubated with 50 µL/section of biotinylated goat anti-rabbit IgG (Sigma Aldrich, catalogue number: B7389) diluted 1:200 in 1% (w/v) BSA/PBS and incubated for 30 minutes at RT. Following three washes of PBS, the slides were incubated with ExtrAvidin-peroxidase (Sigma Aldrich, catalogue number: E2886) diluted 1:200 in 1% (w/v) BSA/PBS and incubated for 30 minutes at RT. Slides were again washed three times in PBS followed by incubation with the HRP substrate, SigmaFast 3,3'-diaminobenzidine (DAB:

Sigma Aldrich, catalogue number: D4293) for 2 minutes at RT. The ExtrAvidin-peroxidase-DAB reaction produces a brown precipitate. Slides were washed twice distilled water, and then stained with Mayer's haematoxylin for 30 seconds–2 minutes. Haematoxylin was washed off with tap water until the water appeared clear and nuclei stain blue. Slides were then dehydrated by one 5-minute wash in 70% (v/v) alcohol, two 5-minute washes in 100% (v/v) alcohol and then three 5-minute washes in 100% (v/v) clearene. Slides were then mounted in DPX mounting medium (Thermo Fisher Scientific, catalogue number: 10050080) overnight at RT.

2.13 METHODS: QUANTITATIVE RT-PCR (RT-qPCR)

2.13.1 RNA Extraction

Total RNA extraction and purification was performed using the miRNeasy Mini kit (Qiagen; catalogue number: 217004). Cells were washed briefly in DPBS and lysed in 350 or 700 µL Qiazol lysis reagent (Qiagen; catalogue number: 79306) for approximately 30 seconds. The wells were scraped with the plunger of a 1mL syringe and lysates were transferred into RNAse-free eppendorfs then kept on ice or stored at -80°C until RNA purification was performed.

2.13.2 RNA Purification

According to QIAGEN's instructions, RNA was purified from cell lysates to remove DNA from total nucleic acid samples. 140 µL of chloroform was added to each sample and vortexed to disperse any visible precipitate. Then, samples were left to incubate at room temperature for 2-3 minutes then micro-centrifuged at 4°C for 15 minutes at 12,000 g. Then, the colourless upper layer from each sample was carefully removed and transferred into a new eppendorf and mixed with 1.5 volumes of 100% RNA-grade ethanol. Samples were then transferred to purification columns and micro-centrifuged at 12,000g for 15 seconds at RT. The resultant flow-through was discarded and columns were washed once with 700 µL of buffer RWT, and twice with 500 µL of buffer RPE at 12,000 g for 15 seconds each. Flow-through was discarded and spin cartridges were reinserted into new collection tubes. Samples were eluted in 30µl RNAse free water by micro-centrifuging at 12,000 g for 1-2 minutes. Then, samples were stored at -80°C until required.

2.13.3 RNA Quantification

The quality and quantity of RNA was assessed using a QIAxpert Nanodrop spectrophotometer (QIAGEN, 9023460). 2 µL of each RNA sample was added into the cassettes to the Nanodrop spectrophotometer and the absorbance at 230 nm, 260 nm and 280 nm was recorded. The RNA concentration (ng/mL) was determined by measuring the absorption at 260 nm. The 260/230 nm ratio corresponded to ethanol contamination, with a 260/230nm ratio of ≥1.8 indicative of minimal ethanol content. Meanwhile, the 260/280nm absorbance ratio describes RNA purity in which a ratio of <2.0 suggests nucleic acid contamination. If contamination was detected, samples were discarded.

2.13.4 Reverse Transcription (RT)

cDNA was synthesized from 100-500 ng/mL purified RNA using the High-Capacity RNA-to-cDNA Kit (Applied Biosystems; catalogue number: 4387406). RNA samples were made up to a total volume of 9 µL with RNAse-free water to equalise RNA concentration. In accordance with the manufacturer's instructions, 10 µL of 2 X RT Buffer Mix and 1 µL of 20 X RT Enzyme Mix was added to each RT reaction to give a final volume of 20 µL. Reactions were then incubated for 1 hour at 37°C, 5 minutes at 95°C and held at 4°C. cDNA samples were stored at -20°C until analysis.

2.13.5 Quantitative PCR

Quantitative PCR analysis was performed using the LightCycler 480 real-time PCR System (Roche) and LightCycler 480 SYBR Green I Master (Roche; catalogue number: 04707516001) in combination with primers described in Table 2.4. Each 10 µL reaction consisted of: 1µL of cDNA, 5µL 2 x SYBR green, 3µL PCR-grade water and 1 µL primer sets (0.5 µL of both forward and reverse primers). Each cDNA sample was analysed in triplicate to account for technical variation. As an internal control, the cDNA was substituted with 1 µL of PCR-grade water or 1 µL of blank RT negative control. Plates were sealed (Greiner Bio-one; catalogue number: 676040) and centrifuged for 30 seconds at 250 g (Labnet; Mini PCR plate spinner; catalogue number: C1000). The thermocycling conditions (Table 2.10) were as follows:

Table 2.10: RT-qPCR program conditions

STEP	SUB-STEP	TEMPERATURE (°C)	TIME
Pre-incubation	-	95	5 min
Amplification (45 cycles)	Denaturing	95	10 sec
	Annealing	60	10 sec
	Elongation	72	10 sec
Melting	-	95	5 sec
		65	1 min
		97	Continuous
Cooling	-	40	-1.5°C/sec

A mean cycle threshold (C_T) value was generated from cDNA samples analysed in triplicate by averaging the closest two C_T values, and then values were normalised with 36B4 RNA levels. The samples with two C_T values less than 0.5 cycle apart were included in analysis which was used to calculate fold changes in expression. The following equation was used to determine fold change:

$$Fold\ change = 2^{-\Delta C_T}$$

$$\Delta C_T = C_T\ (Target\ RNA) - C_T\ (Reference\ RNA)$$

The specificity of the real-time PCR assay can be confirmed by analysing the melting curves. All primers used throughout the study gave a single peak on the melting curves indicating that only one PCR product was being amplified.

2.13.6 Primer Design

Pre-designed primers for qPCR analysis were purchased from Qiagen or designed using Primer-BLAST software and ordered from Sigma (Table 2.11). Filters for design included:

- specificity for the target gene
- a product size of between 100 and 250 base pairs
- an optimal melting temperature (Tm) of 65°C
- an optimal primer size of between 22 and 26 base pairs
- a primer GC content of 40-65%
- a requisite for spanning exon-exon junctions
- lack of secondary structures
- lack of primer dimers

Table 2.11: Details of primers

GENE	PRIMER	SEQUENCE OR CATALOGUE NUMBER	COMPANY
ICAM-1	ICAM-1	FORWARD: GCAGACAGTGACCATCTACAGCTT	SIGMA
		REVERSE: GCCTCACACTTCACTGTCACCTC	
VCAM-1	VCAM-1	FORWARD: ACTTGATGTTCAAGGAAGAG	SIGMA
		REVERSE: TCCAGTTGAACATATCAAGC	
SMTN	Smoothelin	QT00026677	QIAGEN
CNN1	Calponin	QT00067718	QIAGEN
IL-6	Interleukin-6	FORWARD: AAATTCGGTACATCCTCGACGGCA	SIGMA
		REVERSE: TTTTCACCAGGCAAGTCTCCTCAT	
IL-8	Interleukin-8	FORWARD: TGTGAAGGTGCAGTTTTGCCAAGG	SIGMA
		REVERSE: AATTTCTGTGTTGGCGCAGTGTGG	
MCP-1	Monocyte Chemotactic Protein-1	FORWARD: CTCAGCCAGATGCAATCAATGCCC	SIGMA
		REVERSE: TTCTTTGGGACACTTGCTGCTGGT	

2.14 METHODS: TRANSCRIPTOMIC PROFILING

2.14.1 Next Generation Sequencing

In this study, we have utilized high-throughput RNA sequencing to perform genome wide analysis of transcriptional diversity and regulation using the TruSeq stranded mRNA kit (QIAGEN). Total RNA extraction, purification and quantification were performed, as described in sections 12.13.1, 12.13.2 and 12.13.3, respectively. All analysis was performed using CLC Genomics Workbench (version 12.0.2) and CLC Genomics Server (version 11.0.2). In addition, the human genome version used is hg38 with an annotation of ENSEMBL Homo_sapiens.GRCh38.97.

RNA-seq libraries were successfully prepared, quantified and sequenced for all of the samples. The collected reads were subjected to quality control, alignment and downstream analysis. The principal structure of the results data is summarized in FIGURE 2.3, which outlines the workflow of an RNA NGS service project with QIAGEN Genomic Services. The samples have been run on an Illumina NextSeq 550 and the aim was to acquire an average of 30 million reads per sample. The parameters were: 100 ng input RNA, 15 cycles of PCR in the fragment enrichment step and the loading molarity used was 1.5 pM. The sequencing was performed in accordance with the manufacturer's instructions and an overview of the protocol is briefly described in FIGURE 2.2. The sequencing company supplies an Expression Browser List of genes annotated with: Gene Name, Gene Identifier, Max Group Means, Fold Change, Log Fold Change, p-value, FDR p-value, Bonferroni and the Raw Values for each condition.

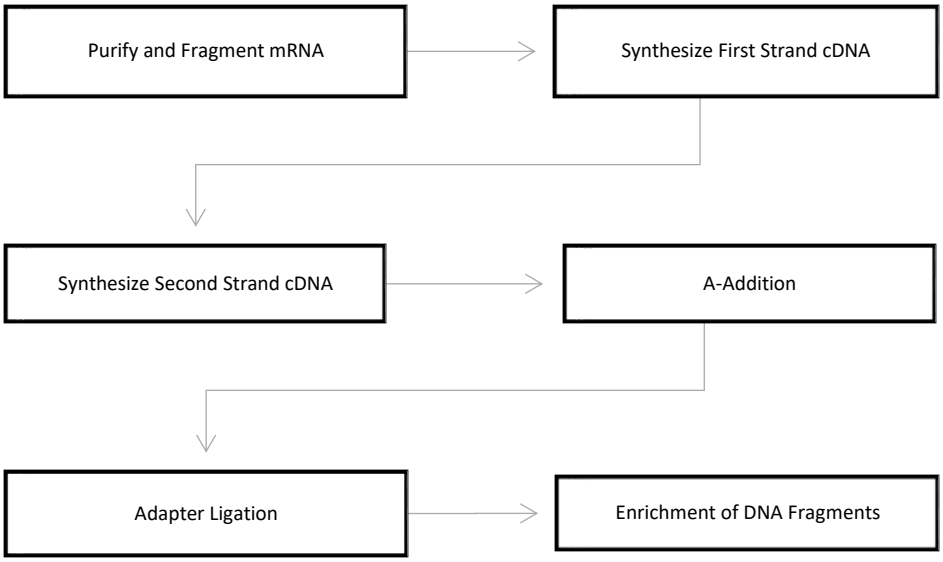

FIGURE 2.2: Schematic representation of steps taken during RNA Sequencing using Illumina NextSeq 550

The protocol for the NGS procedure: the mRNA in a total RNA sample is used to generate a library of template molecules of known strand origin using the reagents provided in an Illumina® TruSeq® Stranded mRNA library prep kit.

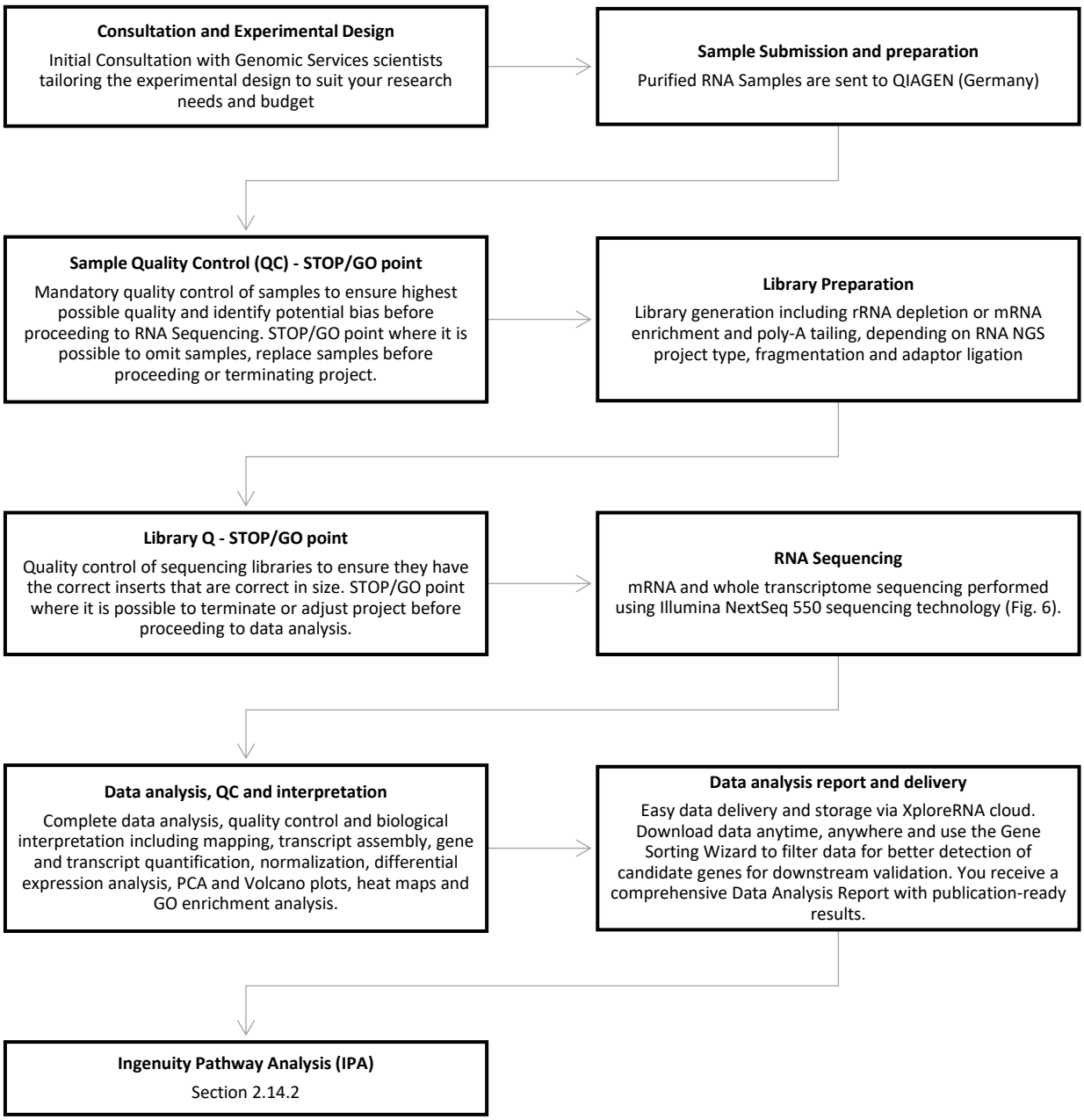

FIGURE 2.3: NGS Workflow

Simple outline of the RNA NGS service project with QIAGEN Genomic Services Information adapted from QIAGEN Genomic Services.

2.14.2 Ingenuity Pathway Analysis (IPA)

Bioinformatic analysis was used to prioritise the differentially regulated genes (DEGs) identified by NGS to determine those most likely associated to VSMC proliferation and migration. Analysing unprecedented DEGs identified through NGS is a significant challenge. The Ingenuity Pathway Analysis program (IPA version 8.0, Ingenuity Systems Inc, California, USA. www.ingenuity.com) functions to analyse, interrogate and interpret data derived from 'omics experiments such as RNA-seq. IPA was utilised to obtain a deeper understanding of the significantly altered canonical pathways and biological functions associated with the DEGs regulated by PRH S163C:S177C. IPA also creates networks where the uploaded DEGs can be connected by either direct or indirect interactions, based on published interactions. It is a powerful tool that is based on Ingenuity knowledge which is linked to published literature and QIAGEN Knowledge Base. This approach offers the advantage of identifying canonical and metabolic signalling pathways that are enriched in the data. To prioritise potential DEGs, a series of filtering strategies were implemented, outlined in the following sections and FIGURE 2.3.

2.14.2.1 Data Upload and Data Annotation

The raw RNAseq dataset files generated from NGS by QIAGEN were imported to IPA. In this study, the RNAseq dataset files were expressed in two separate datasets: Dataset A denotes DEGs obtained from HSV VSMCs infected with Ad: Control or Ad: PRH S163C:S177C whereas Dataset B denotes DEGs obtained from HSVECs infected with Ad: Control or Ad: PRH S163C:S177C. The imported 'omics data is annotated by mapping the molecules to the corresponding gene ID that exists in the IPA's Knowledge database. A dataset file may contain more than one identifier source in different columns. Multiple identifier columns, such as GenBank, Gene Symbol-Human (HUGO) and Ensembl, can be assigned to increase the chance that a row will be mapped in IPA. The raw data was then allocated to 'Observation 1' describing a single observation dataset which contains only one experimental comparison (e.g., experimental vs. control). Subsequently, the corresponding measurement values can be assigned to the correct columns. For example, the next column was mapped to reads per kilobase million (RPKM). RPKM is a normalised unit of transcription. It corrects differences in both sample sequencing depth and gene length. The 'Expression Fold Change' determines the magnitude of change between two measurements. The 'Expression Log Ratio' is the logarithm base 2 of fold change and 'Expression p-value' represents the significance of the variation in gene expression changes. Lastly, the 'Expression False Rate Discovery (FDR)' is

a p-value adjusted for multiple sets using the Benjamin-Hochberg procedure. It is a method used to conceptualise the expected proportion of false positives per transcript. Once data annotation has been completed, the dataset can be processed for the next stage of data filtering (FIGURE 2.4).

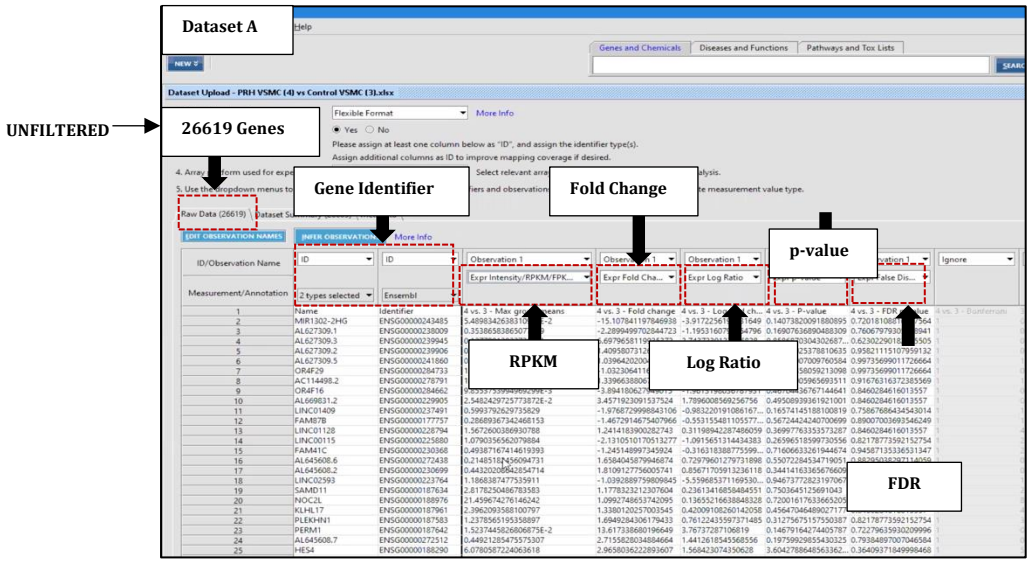

FIGURE 2.4: Data Formatting and Upload using an unfiltered Dataset A

During Data Upload, each column has been annotated with appropriate headers including Gene Identifier. The remaining columns within a dataset can be annotated manually to indicate the type of measurement value including reads per kilobase million (RPKM), false discovery rate (FDR), fold change, p-value, log ratio to help IPA assign the correct data type.

The differential expression (DE) calculation can be calculated using the following:

Recommended Log_2(ratio): $Log_2 = \left(\frac{Experimental\ Condition}{Control\ Condition} \right)$

Ratio DE: $\left(\frac{Experimental\ Condition}{Control\ Condition} \right)$

Fold Change: *Increased DE* $= \left(\frac{Experimental\ Condition}{Control\ Condition} \right)$

Decreased DE $= -1 \left(\frac{Experimental\ Condition}{Control\ Condition} \right)$

RPKM of a gene: $\left(\frac{No.\ of\ reads\ mapped\ to\ a\ gene\ x\ 10^3\ x}{Total\ no.\ of\ mapped\ reads\ from\ a\ given\ library\ x\ gene\ length\ in\ base\ pairs} \right)$

2.14.2.2 Data Filtering

The first criterion to prioritise the DEGs was data filtering. 'Ideal' set size for IPA core analysis from gene expression data is typically $\leq$3000 molecules. In the Set Cutoffs section, reasonable cut-off values can be specified to reduce the number of DEGs from $\geq$26,000 genes in each RNAseq datasets for statistical analysis. Only features that pass the cut-offs that have been specified at this step will be used for further IPA analysis. For example, set analysis parameters for each of the dataset include: $\pm$ 1.5 for Expr Fold Change (Up-regulated/Down-regulated) and 0.05/0.01 for Expr p-value, to produce statistically significant DEGs in the transcriptomic experiment.

2.14.2.3 Compare Data

Using the 'Compare Data', filtered datasets are compared to run set operations like Union (Sum), Common (Intersection) and Unique DEGs between the different datasets being compared (FIGURE 2.5). This will produce an interactive Venn diagram to display the DEGs that are VSMC-specific and EC-specific and then a 'final' dataset was created from there to run in 'Core Analysis'.

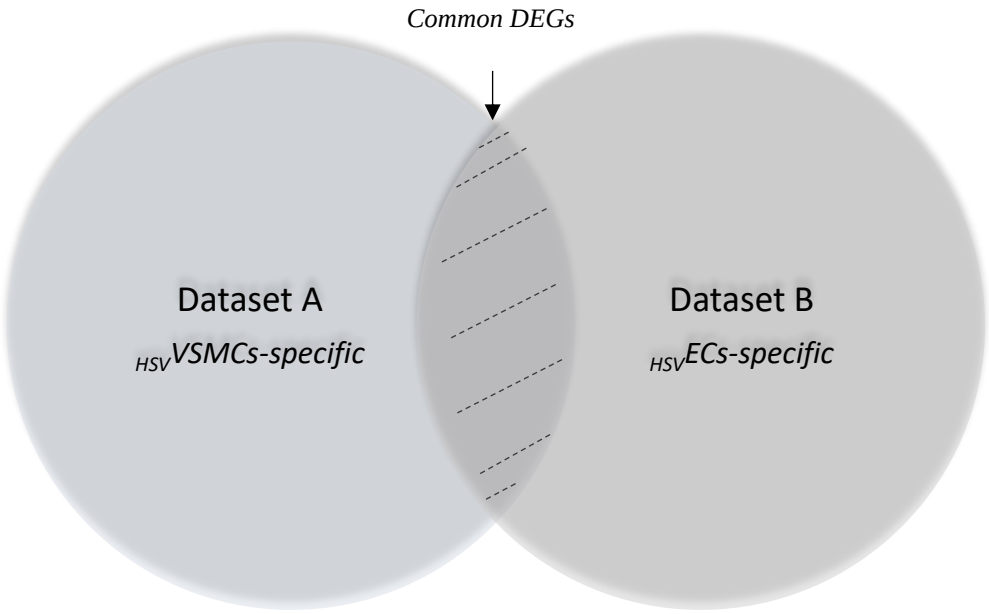

FIGURE 2.5: Interactive Venn diagram for the 'Compare Data' tool

Two entities which were the previously filtered datasets were uploaded into the 'Compare Data tool' for further filtering of DEGs which are VSMC-specific and PRH S163C:S177C-specific. A new dataset from the selected molecules can be created for the subsequent 'Core Analysis'.

2.14.2.4 Core Analysis

Core Analysis was performed on the final dataset using 'Expression Analysis'. This identifies the canonical pathways, upstream regulators, regulator effects (molecular networks), and disease and biological functions based on the changes of expression of genes or proteins relevant to a dataset. IPA calculates two distinct statistics as part of a core analysis. The P-

value was calculated using a Right-Tailed Fisher's Exact Test which determines the probability that the association or overlap between a set of significant molecules from the data and a given biological function is due to random chance. The Z-score takes into account the directional effect of one molecule on another molecule or on a process, and the direction of change of molecules in the dataset.

2.14.2.5 Canonical Pathways

The first criterion used to prioritise the DEGs was Canonical Pathways. Canonical Pathways provide information about what is known from literature to occur on the cellular level in signalling and metabolic cascades. In this study, the 15 most significant IPA Canonical Pathways have been selected determine which signalling pathways were regulated by overexpression of PRH S163C:S177C. The significance of the association between the PRH S163C:S177C DEGs and canonical pathways was assessed based on the following measures: 1) the number of occurrences of DEGs in a given canonical pathway; 2) the p-value; 3) the degree of fold change and 4) an extensive review of each DEG (Section 2.14.2.6).

2.14.2.6 Biological analysis of PRH S163C:S177C-regulated gene targets

For an in-depth literature retrieval, 'vascular smooth muscle cell', 'cell proliferation', 'cell contractility', 'phenotypic switching', 'cell migration', 'endothelial cell', and 'inflammation' was used as the keywords to search for the association of DEGs with a cellular function. The DEGs obtained from the top enriched Canonical Pathways were subjected to biological annotation to determine those most likely associated with VGF. Due to the expanse of biological information, there are a number of databases that integrate the functional interpretation of NGS molecules for target prioritisation. The following public databases were utilised to conduct searches and find relevant information from the literature. PubMed (https://pubmed.ncbi.nlm.nih.gov) utilise search interfaces to allow for interrogation of the literature. In addition, UniProtKB (https://www.uniprot.org) and The Human Protein Atlas (https://www.proteinatlas.org) are comprehensive databases that provides concise evidence about molecular function, tissue expression, protein interactions, biological process and involvement in disease. The IPA Gene View (ttps://reports.ingenuity.com/) generated by IPA also retrieves a wealth of experimental evidence for the DEGs obtained from QIAGEN Knowledge Base. IPA's Map Overlay Tool also quantitatively integrates direct and indirect

protein interactions derived from four sources: genomic context, high-throughput experiments, co-expression data and previous knowledge. Each DEG was annotated by gene name, p-value score and fold change, protein name, gene function, cellular location and association to the VSMC proliferation and migration.

2.14.2.7 Downstream Effects Analysis: Disease and Function

To identify key biological processes influenced by the DEGs within the dataset, IPA allows for a novel approach to visualize and predict biological impact of the observed gene expression changes. Using the 'Disease and Function' tab, IPA identifies a small subset of genes that were predicted to be involved in several biological processes which can be utilised to validate the DEGs which were prioritised previously (FIGURE 2.6).

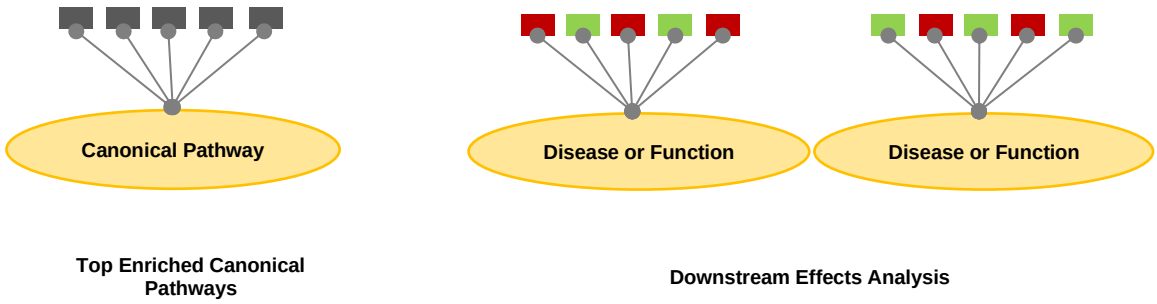

FIGURE 2.6: Schematic representation of downstream effect analysis

Prioritised DEGs from the top enriched canonical pathways were described in 'grey'. 'Inhibited' and 'Activated' DEGs identified in IPA's downstream effect analysis were described in 'red' or 'green' respectively.

2.14.2.8 Upstream Regulator and Functional Network Analysis

IPA's upstream regulator analysis function was used to identify potential transcriptional regulators that could explain the observed changes in gene expression between Ad: Control and Ad: PRH S163C:S177C (FIGURE 2.7). The extent of relevant biological functions of the prioritised DEGs was further validated using functional analysis of a network generating biological functions associated with a given network, pathway, or neighbourhood (FIGURE

2.8). This combination of filtering strategies to evaluate and validate prioritised DEGs within our dataset is powerful in leading the identification of relevant PRH S163C:S177C-regulated gene targets.

2.15 METHODS: STATISTICAL ANALYSIS

Statistical analysis was performed using Graphpad Instat statistical software. For experiments comparing the two groups, a Student's *t*-test was used for normally distributed data and a *t*-test with Welch Correction was employed for non-normally distributed data with N less than 6 or a Mann Whitney test was employed for non-normally distributed data with an N greater than 6. For experimental data comparing three or more groups, an Analysis of Variance (ANOVA) with the Student-Newman-Keuls Multiple Comparisons Test was utilised. $p<0.05$ was acknowledged as significantly different in all statistical tests. All graphical data was displayed as mean ± standard error of the mean (SEM) and charts show data points and error bars (SEM).

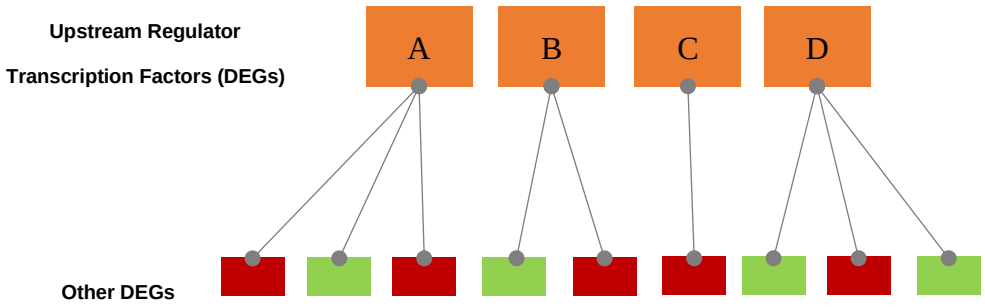

FIGURE 2.7: IPA Mechanistic Networks

The IPA Upstream Regulator computationally seeks pairs of regulators based on causal relationships predicted to affect expression of similar set of DEGs within the dataset. It also indicates the molecules predicted to be in the signalling cascade on a hypothesis basis. DEGs denotes 'Differentially Expressed Genes'.

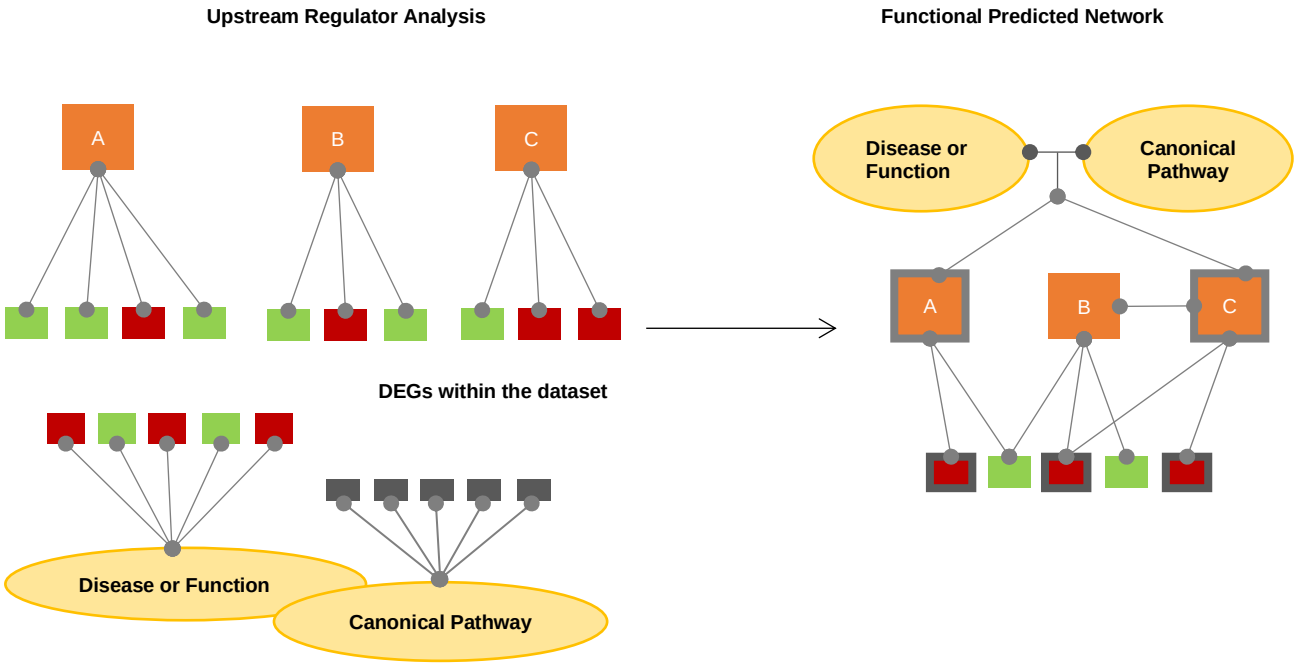

FIGURE 2.8: IPA Functional Network Analysis

Combinatorial strategy to strengthen the justification of the selected prioritised DEGs. Prioritised DEGs that have been identified in the downstream effect analysis and as an upstream regulator can be further analysed in functional network analysis.

3.

THE EFFECT OF PRH S163C:S177C ON VASCULAR SMOOTH MUSCLE CELL: PROLIFERATION, MIGRATION AND PHENOTYPE

3.1 INTRODUCTION

The PRH/HHex transcription factor is an oligomeric protein that is required for multiple processes during early development including axis formation, haematopoiesis and development of the vasculature (Kershaw *et al.,* 2017). Intima thickening is caused by VSMC migration and replication and subsequent build-up VSMCs and ECM within the intima that thickens the intima and reduces the lumen area (Harskamp *et al.,* 2013). A previous study identified PRH to be up-regulated within intima thickenings of balloon-injured rat aortae (Sekiguchi *et al.,* 2001). In apparent contradiction with these findings, knockdown and overexpression studies revealed that PRH exerted an anti-proliferative action in primary cultures of rat aortic VSMCs (Wadey *et al.,* 2017). Moreover, adenoviral-mediated expression of a mutated form of PRH S163C:S177C with enhanced stability abrogated intima thickening in human saphenous vein organ cultures (Wadey *et al.,* 2017). This suggest that overexpression of S163C:S177C PRH may present a novel therapeutic approach for reducing intima thickening in VGF.

Aberrant VSMC behaviour is a key component of multiple vascular pathologies including post-angioplasty restenosis, atherosclerosis, and aneurysms (Pahk *et al.,* 2017). In the healthy vasculature, VSMCs are typically ‘contractile’ and quiescent exhibiting very low proliferative and migratory rates. The ‘contractile’ phenotype has increased expression of contractile markers calponin, smoothelin, smooth muscle myosin heavy chain and alpha smooth muscle actin (αSMA). Vascular injury initiates phenotypic switching from the ‘contractile’ phenotype to the ‘synthetic’ phenotype and induces migration to the intima and proliferation of VSMCs. Synthetic VSMCs lose the expression of said contractile markers. Hence, de-differentiation of VSMCs results in impaired contractility and facilitates intima thickening (Petsophonsakul *et al.,* 2019). The contractile and synthetic phenotypes are characterized and distinguished by notable differences in marker expression, morphology, and activity (Petsophonsakul *et al.,* 2019; Biswas *et al.,* 2014). Unravelling ways to maintain or restore the ‘contractile’ phenotype is an attractive strategy for efficiently preventing vascular remodelling disorders.

In this chapter, I evaluated whether overexpressing the mutated form of PRH (PRH S163C:S177C) retards proliferation, apoptosis, and migration of human saphenous vein VSMCs. Additionally, VSMC de-differentiation was evaluated by quantifying the protein levels of calponin and smoothelin which are specific to the ‘contractile’ phenotype, and by measuring functional contractility.

3.2 HYPOTHESES

The hypotheses for this chapter were:

- PRH S163C:S177C overexpression reduces HSV VSMC proliferation, and migration.
- PRH S163C:S177C overexpression promotes the contractile phenotype in HSV VSMCs.

These hypotheses were tested by:

- Adenoviral-mediated overexpression of PRH S163C:S177C and quantification of VSMC proliferation, apoptosis and migration using appropriate assays (EdU; Cleaved-Caspase-3 and Scratch Wound Assays).
- Adenoviral-mediated overexpression of PRH S163C:S177C and evaluation of expression levels of contractile SMC-specific marker proteins by Western blotting.
- Adenoviral-mediated overexpression of PRH S163C:S177C and measurement of VSMC contractility using collagen contraction assay.

3.3 RESULTS

3.3.1 Adenovirus-mediated overexpression of PRH S163C:S177C in HSV VSMCs

To determine the optimal concentration of adenoviral particles for high infection efficiency and achieve maximal overexpression of PRH S163C:S177C in HSV VSMCs, a dose response was performed utilising three different adenoviral concentrations. Infection of HSV VSMCs with an adenovirus without a transgene (Ad: Control) or c-myc-tagged PRH S163C:S177C encoding recombinant adenoviruses was performed at three different viral concentrations: 1 x 10^8 pfu/mL, 2.5 x 10^8 pfu/mL and 5 x 10^8 pfu/mL. Uninfected cells served as an additional negative control. Following an 18-hour incubation to allow for viral infection of HSV VSMCs, the culture media containing the virus was removed and cells were incubated for a further 24 hours in 10% (v/v) FBS/DMEM. Subsequently, overexpression of c-myc-tagged PRH S163C:S177C was assessed using Western blotting (FIGURE 3.1) and immunofluorescence (FIGURE 3.2) for the c-myc-tagged transgene. Western blotting and immunocytochemistry showed all doses are significantly different from uninfected and Ad: Control. A significant elevation in c-myc-tagged protein expression of approximately 90% was observed in cells infected with 5 x 10^8 pfu/mL of adenoviral vector with respect to lower doses, and thus this dose was selected as the optimal viral concentration. As expected, c-myc-tagged PRH S163C:S177C was localised to the nucleus.

A

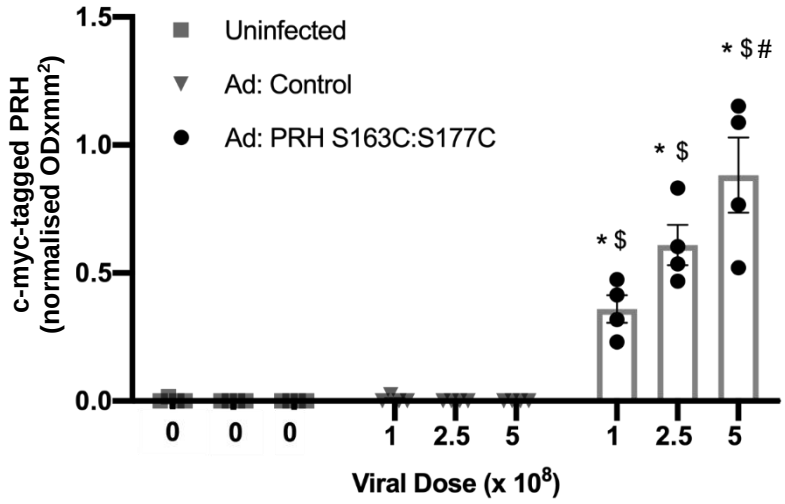

B

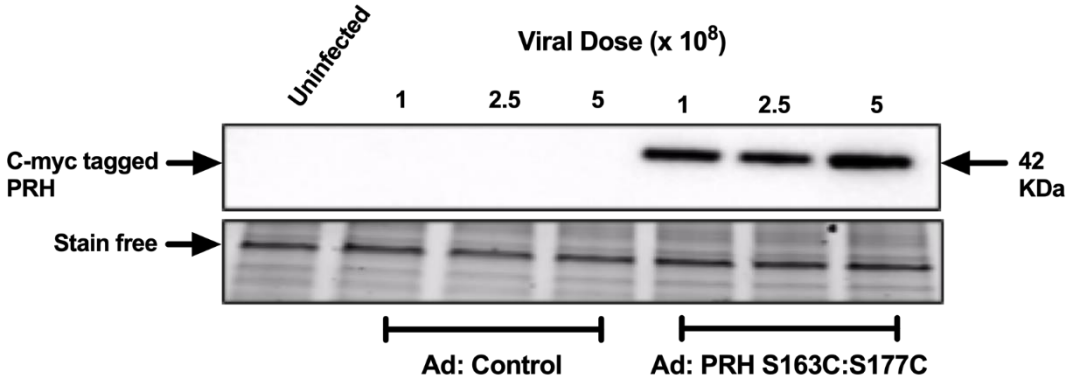

FIGURE 3.1 - Detection of c-myc-tagged PRH S163C:S177C in HSV VSMCs using Western Blotting

HSV VSMCs were either infected with 1 x 10^8 pfu/mL, 2.5 x 10^8 pfu/mL or 5 x 10^8 pfu/mL Ad: Control or Ad: PRH S163C:S177C or were left uninfected.

A – Densitometric analysis of c-myc-tagged PRH S163C:S177C protein. * indicates $p<0.05$ vs. uninfected, $ indicates $p<0.05$ vs. all Ad: Control, # indicates $p>0.05$ vs 1 x 10^8 pfu/mL and 2.5 x 10^8 pfu/mL Ad: PRH S163C:S177C, ANOVA, Student-Newman-Keuls Multiple Comparisons Test, n=4. Error bars represent standard error of mean (SEM).

B - Representative Western blot of c-myc-tagged PRH S163C:S177C protein. Stain-free bands served as a loading control. Approximate molecular weight of detected band indicated in kDa.

FIGURE 3.2 - Detection of c-myc-tagged PRH S163C:S177C in HSV VSMCs using Immunocytochemistry

HSV VSMCs were either infected with 1 x 10^8 pfu/mL, 2.5 x 10^8 pfu/mL or 5 x 10^8 pfu/mL Ad: Control or Ad: PRH S163C:S177C or were left uninfected.

A – Quantification of percentage of cells expressing c-myc-tagged PRH S163C:S177C protein. * indicates $p<0.05$ vs. uninfected, $ indicates $p<0.05$ vs. all Ad: Control, ANOVA, Student-Newman-Keuls Multiple Comparisons Test, n=4. Error bars represent SEM.

B – Representative images of immunocytochemistry for c-myc-tagged protein. Positive cells have green nuclei and examples are indicated with red arrows; all nuclei are stained blue with DAPI. Scale bar indicates 50 μm and applies to all panels.

A

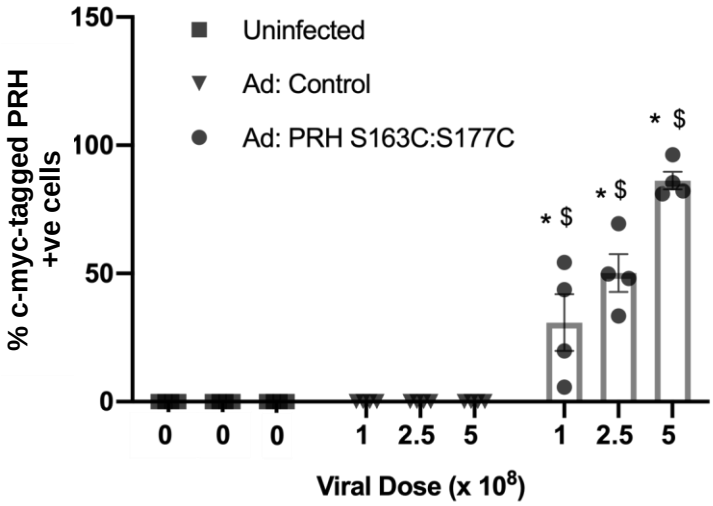
Uninfected
Ad: Control
Ad: PRH S163C:S177C
% c-myc-tagged PRH +ve cells
150
100
50
0
* $
* $
* $
0 0 0 1 2.5 5 1 2.5 5
Viral Dose (x 10^8)

B

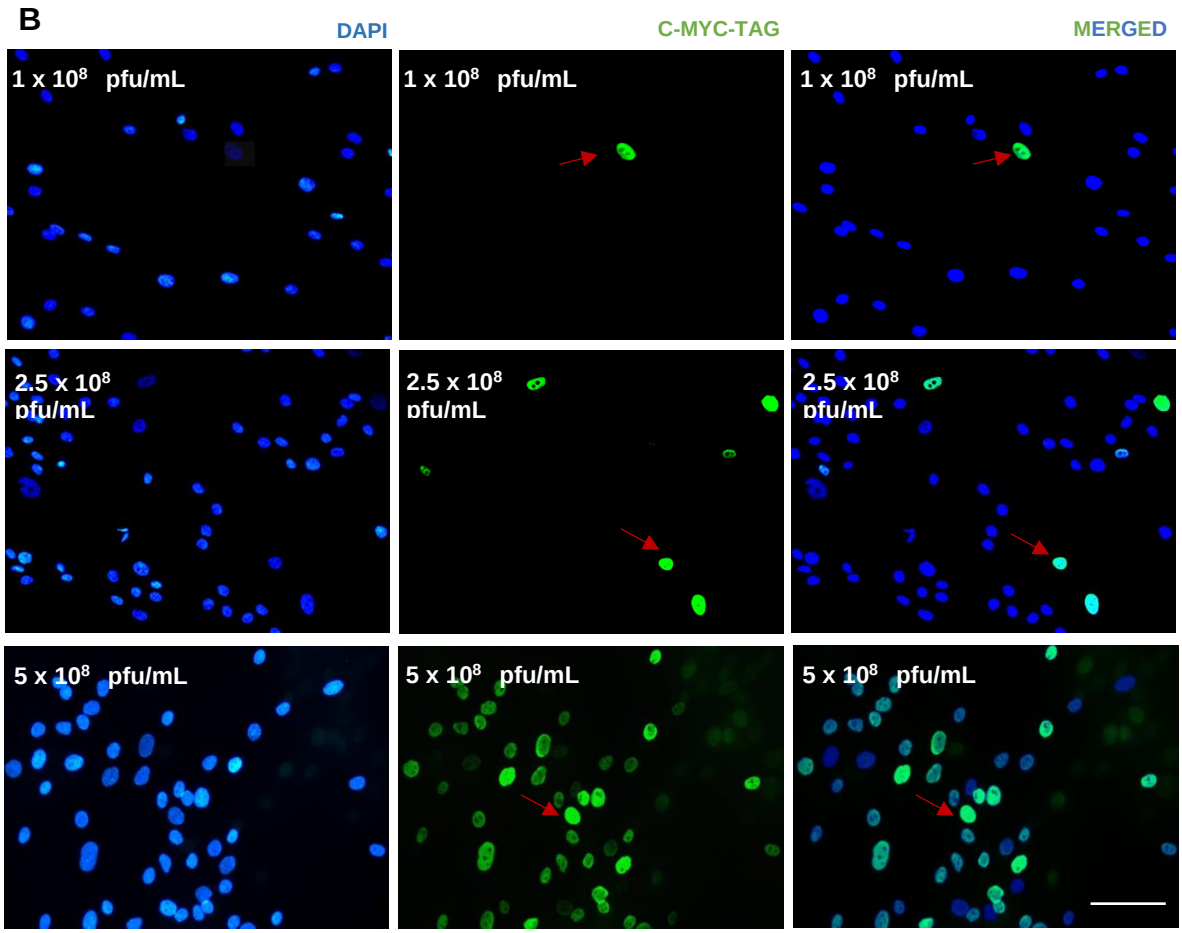
DAPI
C-MYC-TAG
MERGED
1 x 10^8 pfu/mL
1 x 10^8 pfu/mL
1 x 10^8 pfu/mL
2.5 x 10^8 pfu/mL
2.5 x 10^8 pfu/mL
2.5 x 10^8 pfu/mL
5 x 10^8 pfu/mL
5 x 10^8 pfu/mL
5 x 10^8 pfu/mL

3.3.2 PRH S163C:S177C attenuated HSV VSMCs proliferation

To investigate whether increasing PRH S163C:S177C levels affected proliferation of human saphenous vein VSMCs, cells were infected with either 5 x 10^8 pfu/mL adenovirus encoding c-myc-tagged PRH S163C:S177C and compared to VSMCs infected with Ad: Control or uninfected VSMCs. After 18 hours the culture medium was replaced with 10% (v/v) FBS/DMEM supplemented with 10 μM EdU and cells incubated for a further 8 hours for Click-iT EdU incorporation analysis, or a further 24 hours for Western blot analysis of cell cycle regulators p21 and cyclin D1. The rate of proliferation detected by EdU was similar in VSMCs infected with Ad: Control as that seen in uninfected VSMCs. Quantification of EdU incorporation showed that overexpression of PRH S163C:S177C significantly retarded the rate of proliferation in HSV VSMCs compared to cells infected with Ad: Control and uninfected cells (FIGURE 3.3). There was also no significant difference in the amount of p21 and cyclin D1 detected in the VSMCs infected with Ad: Control and uninfected VSMCs. Although, cells infected with PRH S163C:S177C showed dramatically elevated p21 protein levels (FIGURE 3.3 A&C) and suppressed cyclin D1 protein levels (FIGURE 3.2.2 B&D) with respect to uninfected cells and cells infected with Ad: Control.

FIGURE 3.3 - Overexpression of c-myc-tagged PRH S163C:S177C in HSV VSMCs retarded proliferation

HSV VSMCs were infected with 5 x 10^8 pfu/mL Ad: Control or Ad: PRH S163C:S177C or were left uninfected.

A – EdU incorporation was quantified and expressed as the percentage of EdU-positive cells. ** indicates $p<0.01$, ANOVA, Student-Newman-Keuls Multiple Comparisons Test, n=4. Error bars represent SEM.

B – Representative images of Click-iT EdU imaging assay. Positive cells are green, and examples are indicated with red arrows; all nuclei are stained blue with DAPI. Scale bar indicates 50μm and applies to all panels.

A

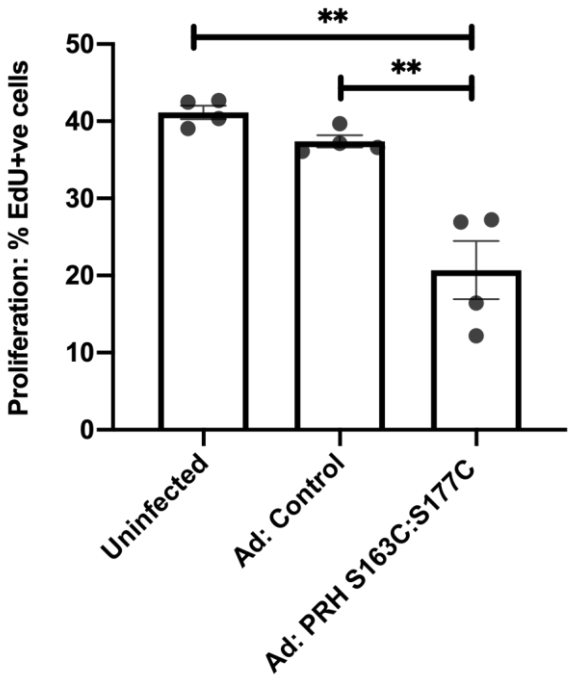
**
**
50
40
30
20
10
0
Proliferation: % EdU+ve cells
Uninfected
Ad: Control
Ad: PRH S163C:S177C

B

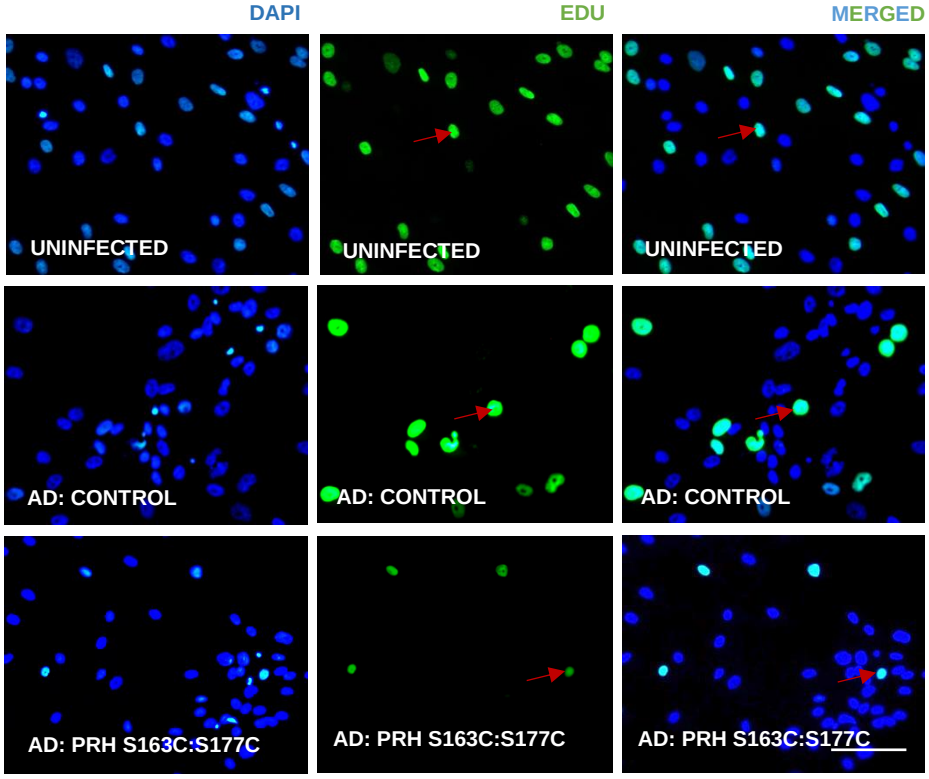
DAPI
EDU
MERGED
UNINFECTED
UNINFECTED
UNINFECTED
AD: CONTROL
AD: CONTROL
AD: CONTROL
AD: PRH S163C:S177C
AD: PRH S163C:S177C
AD: PRH S163C:S177C

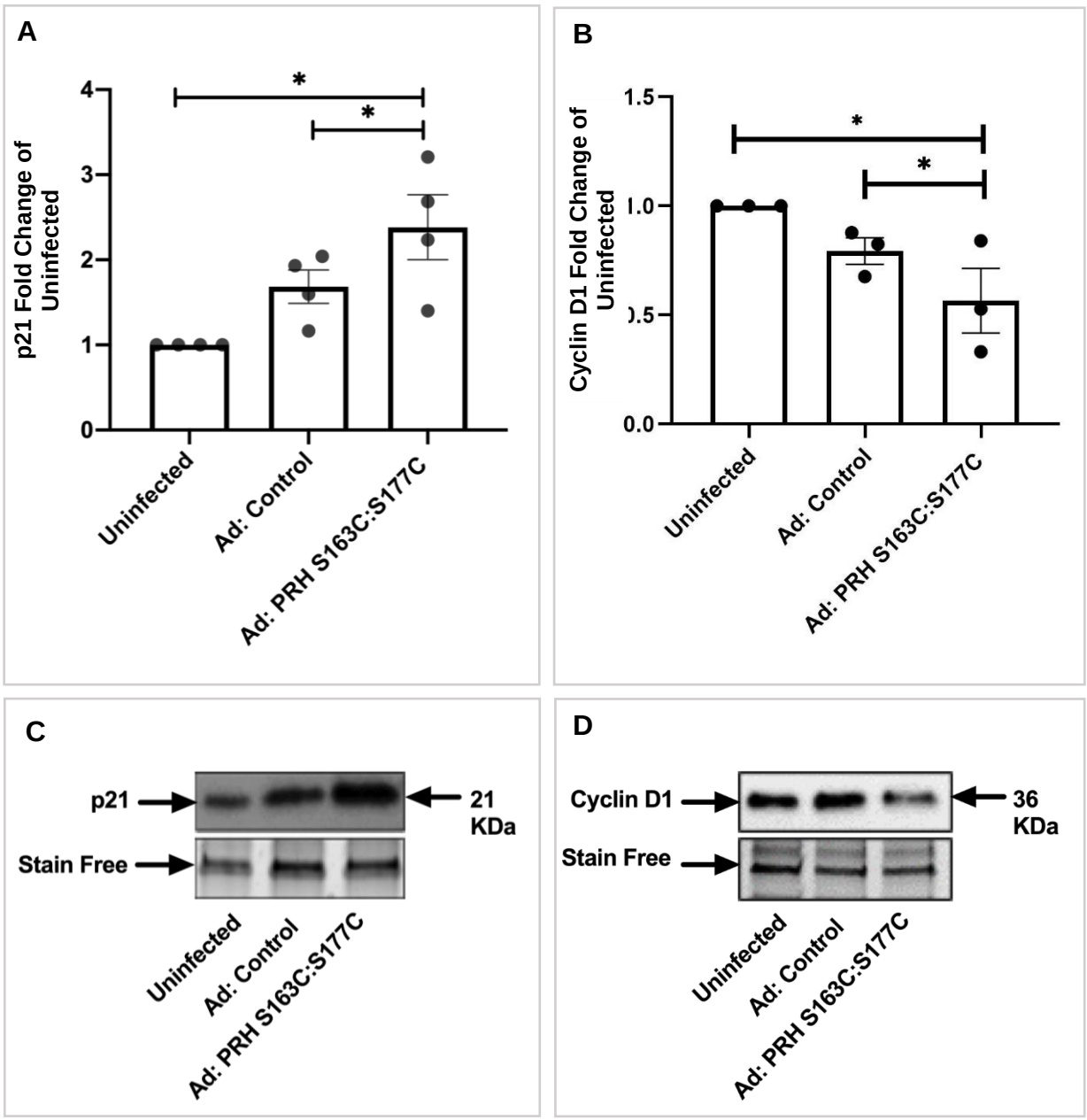

FIGURE 3.4 - Overexpression of c-myc-tagged PRH S163C:S177C in HSV VSMCs retarded proliferation

HSV VSMCs were infected with Ad: Control or Ad: PRH S163C:S177C or were left uninfected. Densitometric quantification of p21 protein (**A**) and cyclin D1 (**B**) expression by Western blotting; data was normalised by stain-free bands and expressed as a fold change from uninfected control. * indicates $p<0.05$, ANOVA, Student-Newman-Keuls Multiple Comparisons Test, n=4 (A) and n=3 (B). Error bars represent SEM.

Representative Western blot for p21 (**C**) and cyclin D1 (**D**). Stain-free bands served as a loading control. Approximate molecular weight is indicated on the right in kDa.

3.3.3 PRH S163C:S177C did not affect HSV VSMCs apoptosis

To investigate the effect of PRH S163C:S177C overexpression on VSMC apoptosis, HSV VSMCs were infected with 5 x 10^8 pfu/mL of adenovirus encoding either empty vector or c-myc-tagged PRH S163C:S177C, or were left uninfected, for 18 hours. Subsequently, cells were incubated for a further 24 hours after replenishing the 10% (v/v) FBS/DMEM. Apoptosis was then quantified via immunofluorescence for cleaved caspase-3. As a positive control, cells were incubated with 200 ng/mL human recombinant Fas-ligand in 2% (v/v) FBS/DMEM. The rate of apoptosis was similar in uninfected cells as those infected with Ad: Control with rates between 5 and 9%. Quantification of the percentage of cleaved caspase-3 (CC-3) positive cells showed that rate of apoptosis in VSMCs overexpressing PRH S163C:S177C was not significantly different from that detected in HSV VSMCs infected with Ad: Control or uninfected cells (FIGURE 3.5. Fas ligand-induced VSMCs apoptotic cell death as expected and acted as a positive control (FIGURE 3.5).

FIGURE 3.4 - Overexpression of c-myc-tagged PRH S163C:S177C did not affect HSV VSMCs apoptosis

HSV VSMCs were infected with Ad: Control or Ad: PRH S163C:S177C or were left uninfected. Fas ligand was used as a positive control.

A – The rate of apoptosis was quantified and expressed as the percentage of cleaved caspase-3-positive cells. NS denotes not significant. ANOVA, Student-Newman-Keuls Multiple Comparisons Test, n=4. Error bars represent SEM.

B – Representative images of immunocytochemistry for cleaved caspase-3 (CC-3). Positive cells (white arrow) are green, and all nuclei are stained blue with DAPI. Scale bar measures 25 μm and applies to all panels. CC-3 denotes cleaved caspase-3.

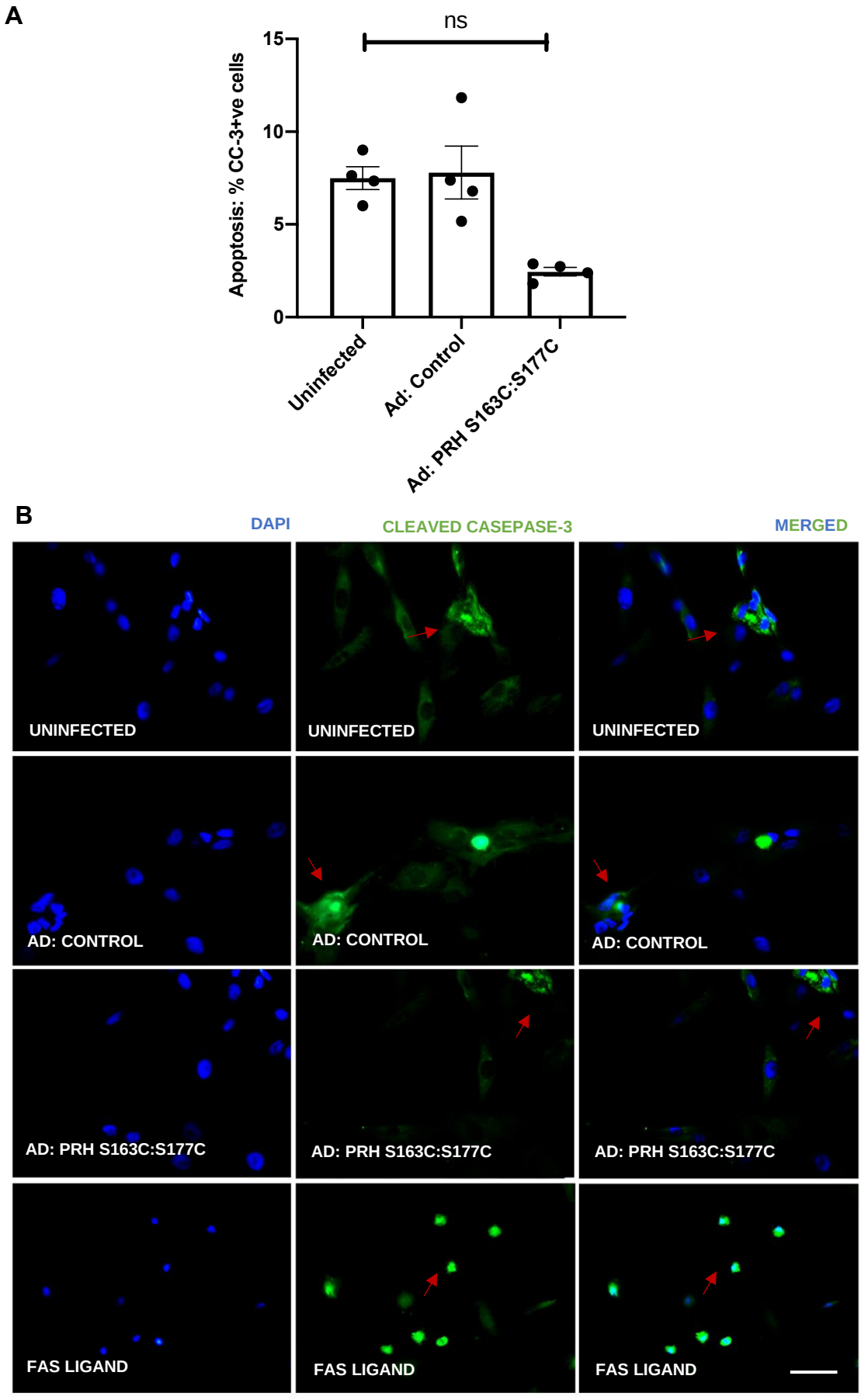
A
ns
Apoptosis: % CC-3+ve cells
15
10
5
0
Uninfected
Ad: Control
Ad: PRH S163C:S177C
B
DAPI
CLEAVED CASEPASE-3
MERGED
UNINFECTED
UNINFECTED
UNINFECTED
AD: CONTROL
AD: CONTROL
AD: CONTROL
AD: PRH S163C:S177C
AD: PRH S163C:S177C
AD: PRH S163C:S177C
FAS LIGAND
FAS LIGAND
FAS LIGAND

3.3.4 PRH S163C:S177C reduced HSV VSMCs migration

The scratch wound assay was utilised to investigate the effect of PRH S163C:S177C overexpression on VSMC migration. Confluent HSV VSMCs were wounded then incubated with 5 x 10^8 pfu/mL of adenovirus encoding either empty vector or c-myc-tagged PRH S163C:S177C, or were left uninfected, for 24 hours. Concurrent treatment with 2 mM hydroxyurea inhibited cell proliferation enabling migration to be accurately quantified. The migrated distance was quantified by measuring the wound width at 0- and 24-hours post-wounding. VSMCs migrated approximately 400 mm in uninfected cells (FIGURE 3.6). Infection with Ad: Control did not significantly affect the distance migrated (FIGURE 3.6). The distance migrated by HSV VSMCs infected with Ad: PRH S163C:S177C was significantly less than that observed in uninfected VSMCs and VSMCs infected with Ad: Control (FIGURE 3.6).

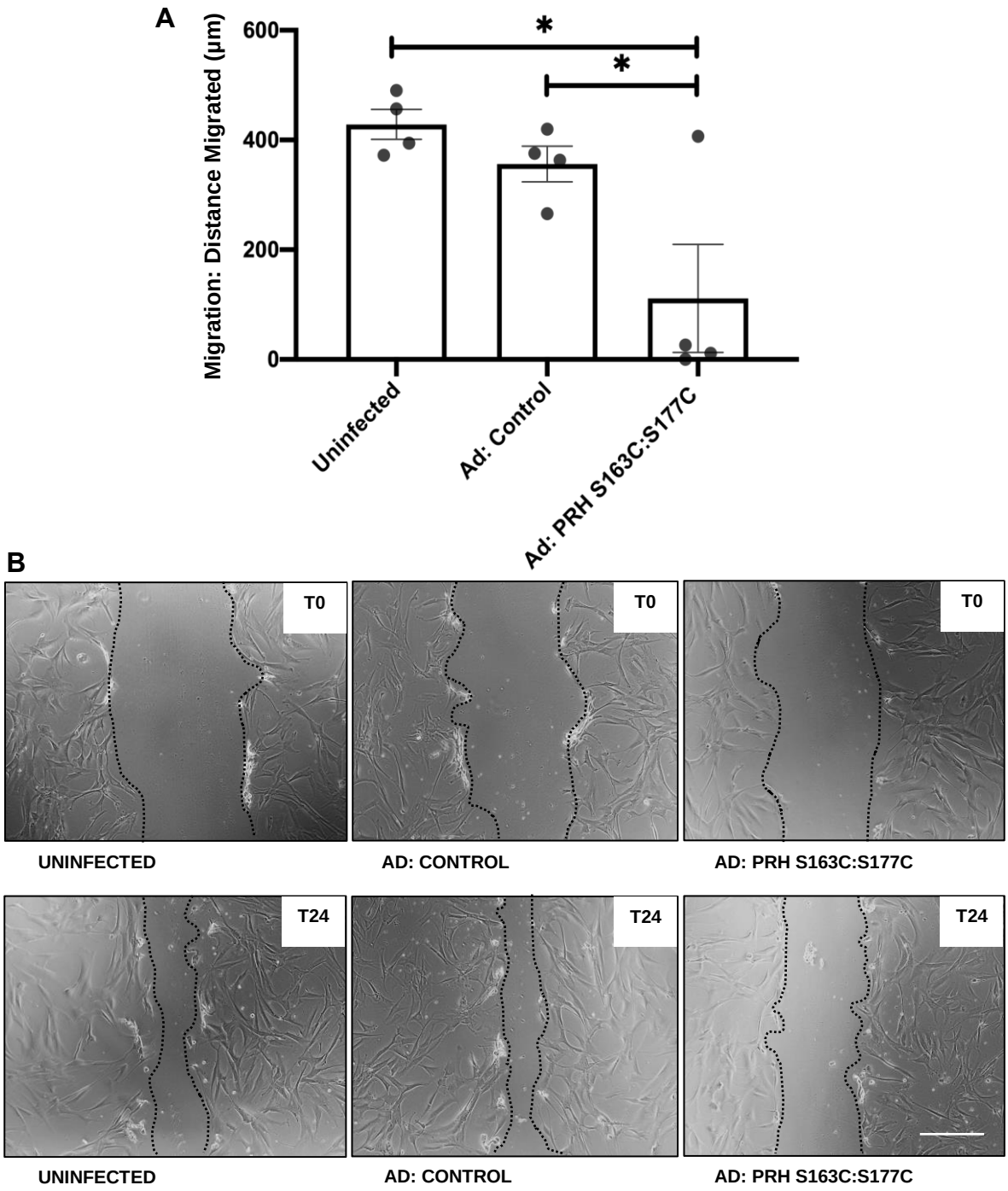

FIGURE 3.6 – Overexpression of PRH S163C:S177C reduced migration of HSV VSMCs

The scratch wound assay was used to assess migration of HSV VSMCs infected with Ad: Control or Ad: PRH S163C:S177C or were left uninfected.

A – Migration was quantified in µm; * indicates $p<0.05$. ANOVA, Student-Newman-Keuls Multiple Comparisons Test, n=4.

B – Representative images of scratch wound assay. Dashed line indicates wound edge. T0 indicates Time = 0 hr; T24 indicates Time = 24 hr. Scale bar represents 1 mm and applies to all panels.

3.3.5 PRH S163C:S177C induced protein expression of contractile markers

The contractile markers smoothelin and calponin were quantified using Western blotting. HSV VSMCs were infected with 5 x 10^8 pfu/mL of adenovirus encoding either empty vector or c-myc-tagged PRH S163C:S177C, or were left uninfected, for 18 hours. Subsequently, cells were incubated for a further 24 hours after replenishing the culture medium. Smoothelin and calponin proteins were detected at a similar level in both uninfected VSMCs and VSMCs infected with Ad: Control (FIGURE 3.7). Both smoothelin and calponin proteins were significantly upregulated in the PRH S163C:S177C-infected VSMCs compared to uninfected VSMCs and VSMCs infected with the Ad: Control (FIGURE 3.7). This finding indicates that ectopic overexpression of PRH S163C:S177C in VSMCs promotes the contractile and differentiated VSMC phenotype via, at least in part, the upregulation of smoothelin and calponin.

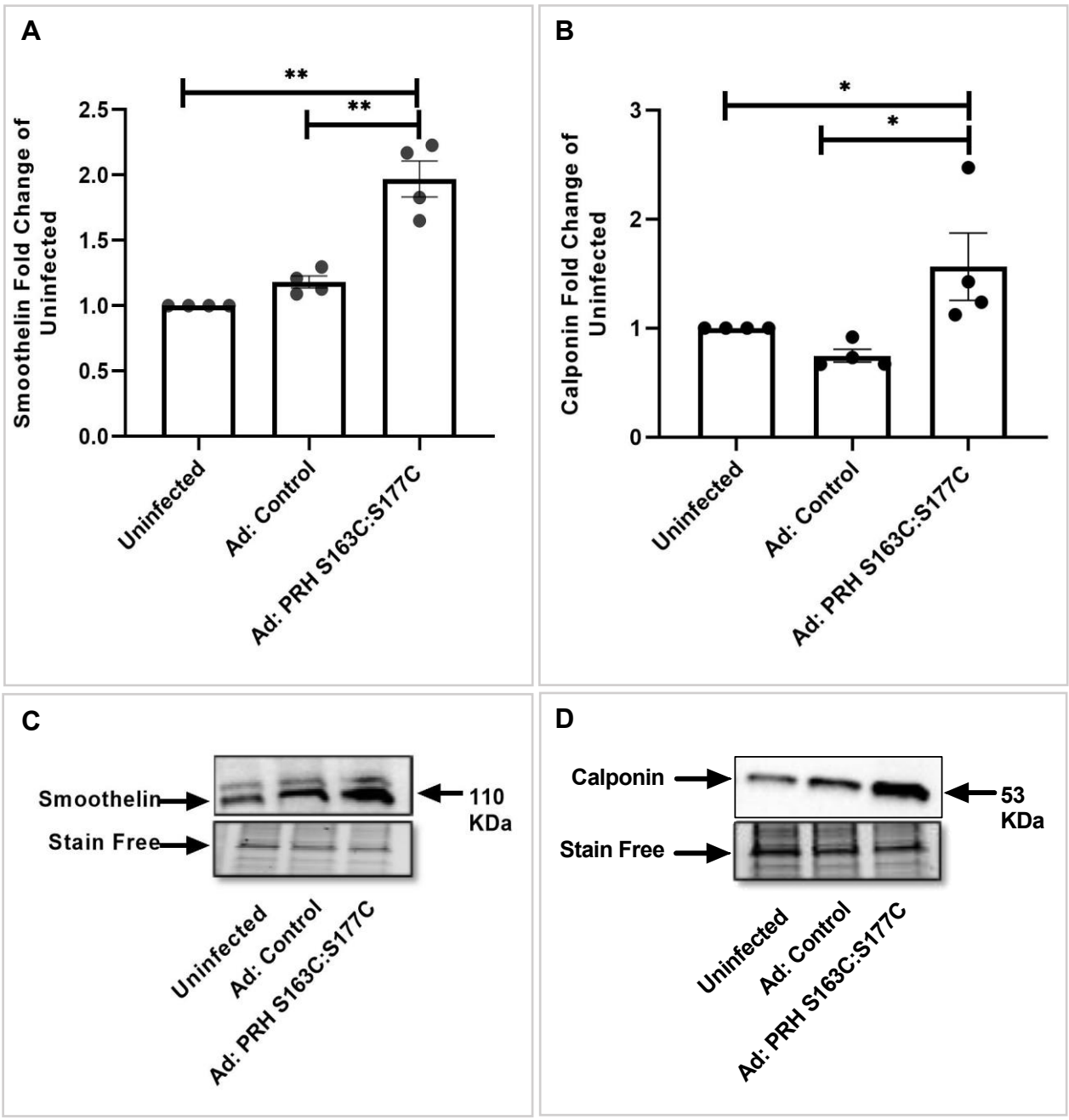

FIGURE 3.7 – The effect of PRH S163C:S177C on contractile protein markers in HSV VSMCs

HSV VSMCs were infected with Ad: Control or Ad: PRH S163C:S177C or were left uninfected. Quantification of smoothelin (**A**) and calponin (**B**) protein expression by Western blotting. Data was normalised by stain-free bands and expressed as a fold change from uninfected control. * indicates $p<0.05$ vs. uninfected, ** indicates $p<0.01$. ANOVA, Student-Newman-Keuls Multiple Comparisons Test, n=4. Error bars represent SEM. Representative Western blots for smoothelin (**C**) and calponin (**D**) proteins. Stain-free bands served as a loading control. Approximate molecular weights are indicated on the right in kDa.

3.3.6 PRH S163C:S177C facilitated HSV VSMCs contraction

The observation of increased amounts of contractile proteins as a result of PRH S163C:S177C overexpression is suggestive of increased contractile potential, and therefore contraction was quantified using a collagen contraction assay. HSV VSMCs were infected with 5 x 10^8 pfu/mL of Ad: Control or Ad: PRH S163C:S177C, or were left uninfected, for 18 hours. Post-infection, cells were detached by 0.05% (w/v) Trypsin-EDTA. The collagen gel working solution and VSMCs at 0.5 x 10^5 cells/mL were mixed on ice at a ratio of 1:4. After polymerization for 48 hours, gels were gently released to allow contraction and then photographed to quantify time-specific gel contraction. As expected, collagen gel diameter at time 0 was similar in all treatment groups and contraction was evident at each time point from 24, 48 and 72 hours in all treatment groups (FIGURE 3.8). However, contraction was significantly greater in VSMCS infected with Ad: PRH S163C:S177C compared to the uninfected and adenovirus controls at each time point examined (FIGURE 3.8).

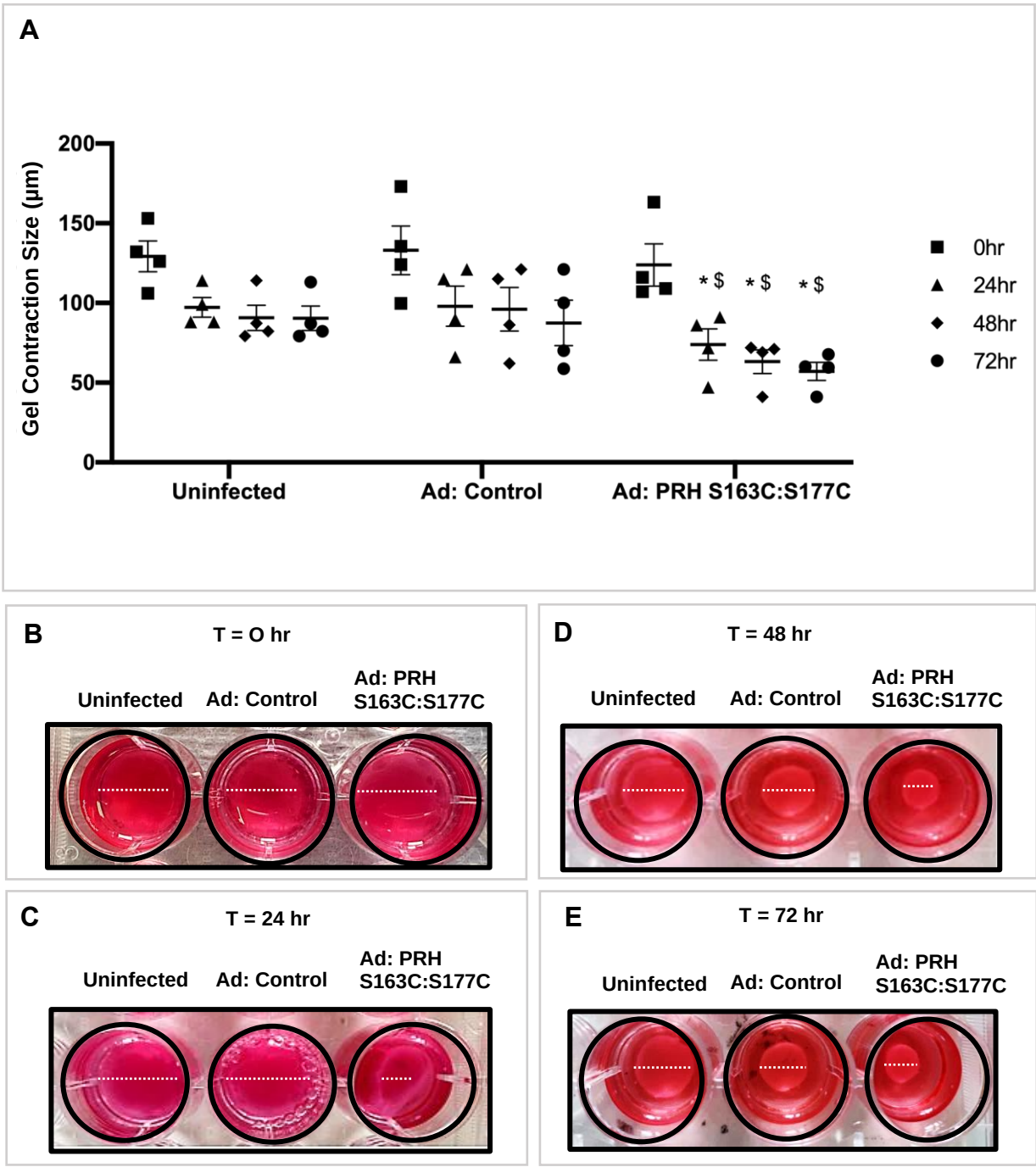

FIGURE 3.8 – Adenovirus-mediated delivery of Ad: PRH S163C:S177C enhanced contraction of VSMCs

A - Contraction was measured by the relative changes in collagen gel diameter. Serial changes in gel area at time 0hr (**B**), 24hr (**C**), 48hr (**D**) and 72hr (**E**) with an uninfected control, Ad: Control and Ad:PRH S163C:S177C. White lines indicate the size of gel diameter for quantification. Error bars indicate SEM. * indicates $p<0.01$ vs. uninfected, $ indicates $p<0.01$ vs. Ad: Control. ANOVA, Student-Newman-Keuls Multiple Comparisons Test, n=4.

3.4 DISCUSSION

The first objective was to determine the optimal adenoviral concentration for high transfection efficiency of adenovirus to achieve high levels of overexpression of S163C:S177C mutant PRH (PRH S163C:S177C) *in vitro* using HSV VSMCs. The second aim was to ascertain whether overexpressing PRH S163C:S177C affected the following cell behaviour indices: proliferation, apoptosis and migration. The final aim was to discover the effects of PRH S163C:S177C on VSMC phenotype. The ability of PRH S163C:S177C to significantly reduce VSMC proliferation and migration without affecting cell death would be attractive properties for reducing intima thickening and thereby treating late vein graft failure. A previous study from our group found that PRH S163C:S177C can reduce VSMC proliferation and migration without affecting cell death in rat cultured VSMCs. For this to be translatable in human grafts, it is important to validate these findings in human cells. Hence, the current study utilises human saphenous vein VSMCs to investigate the effect of PRH S163C:S177C on VSMC behaviour and function.

3.4.1 PRH S163C:S177C was overexpressed in HSV VSMCs

It is important to reiterate the advantage of the constitutively active, non-phosphorylatable PRH S163C:S177C mutant form over the wild-type PRH counterpart. Wadey and colleagues previously demonstrated PRH S163C:S177C PRH was resistant to CK2 phosphorylation and therefore exhibited an extended half-life and effectively suppressed rat aortic VSMC proliferation and intima thickening in HSV organ cultures (Wadey *et al.,* 2017). For these reasons, PRH S163C:S177C was selected for this study.

The current project assesses the efficiency of PRH S163C:S177C overexpression using adenoviral-mediated delivery *in vitro.* The feasibility of vascular gene transfer was first established by Nabel *et al.,* in 1989 by seeding retrovirally transduced endothelial cells in porcine arteries to study atherosclerosis. Since then, the potential of gene therapy has been proclaimed (Williams and Kingston, 2011). Several pre-clinical VGF gene therapy trials for potential molecular targets including tissue inhibitor of MMPs (TIMPs), MCP-1 and eNOS (George *et al.,* 1998; George *et al.,* 2000; West *et al.,* 2001; Turner *et al.,* 2005; Akowuah *et al.,* 2005; Schepers *et al.,* 2006; George *et al.,* 2011) have shown promising results. Nonetheless, up to the present time, the PREVENT-IV study (Lopes *et al.,* 2005) remains as the sole randomised clinical trial for VGF which utilises gene expression modification. The PREVENT-IV study utilised edifoligide, an E2F transcription decoy, acknowledged to inhibit

neointimal lesion formation (Lopes *et al.,* 2005). Despite the promising initial results, the trial failed at stage IV as edifoligide did not prevent VGF or adverse events (Lopes *et al.,* 2005).

Viral vectors are typically used to deliver genetic information to cells (Southerland *et al.,* 2013). The viral vector system must perform genetic transfer efficiently and safely. Adenovirus-based gene therapy emerges to be a valuable strategy into ameliorating vein graft disease due to its features that permit efficient infection of cells. Adenoviruses can be used to effectively deliver transgenes into both dividing and quiescent cells (Lee *et al.,* 2017). This feature is advantageous for vein graft gene therapy since many cells within the saphenous vein are quiescent, and also following transplantation, a population of VSMCs adopt a proliferative phenotype (Mali, 2013). These advantages make adenoviral vectors a good candidate for gene therapy for saphenous vein graft failure (Mali, 2013).

Dose-response experiments were performed in this study to achieve a high infection efficiency and assess the functional effects of PRH S163C:S177C without the virus causing cell toxicity. To directly ascertain that the effect was specifically due to PRH S163C:S177C, a recombinant adenovirus expressing an empty vector (Ad: Control) was utilised as well as an uninfected control cell. The ΔE1E3 empty construct within Ad: Control is the identical vector to Ad: PRH S163C:S177C and as it is an empty vector it does not express a transgene. Previous findings in primary rat aortic VSMCs revealed overexpression of wild-type PRH and PRH S163C:S177C via AMAXA plasmid transfection reduced VSMC proliferation (Wadey *et al.,* 2017). In this current study 5 x 10^8 pfu/mL was selected as the optimal concentration for high transfection efficiency of HSV VSMCs to achieve overexpression of PRH S163C:S177C. Western blotting showed that the level of c-myc-tagged PRH S163C:S177C protein was significantly elevated in lysates obtained from HSV VSMCs infected with an Ad: PRH S163C:S177C compared with those from uninfected VSMCs or VSMCs infected with Ad: Control. In addition, immunocytochemistry showed $\geq$80% of cells were positive for c-myc-tagged PRH S163C:S177C protein. Staining was restricted to the nuclear compartment suggesting that PRH S163C:S177C is of the hypo-phosphorylated, active state and more stable compared to its wild-type protein counterpart.

3.4.2 PRH S163C:S177C retarded VSMC proliferation and migration

A previous report demonstrated that in adult male Wistar rats, PRH protein expression was undetectable in healthy aorta though abundant levels were observed in neointimal VSMCs of

aortas injured with a balloon embolectomy catheter. Reportedly, expression of PRH reached its peak 2 weeks following injury then declined thereafter (Sekiguchi *et al.,* 2001). In addition, PRH induced expression of a dedifferentiated VSMCs marker, SMemb/NMHC-B (Sekiguchi *et al.,* 2001). As a result, it was proposed that PRH mediates intima thickening in-part via promotion of VSMC dedifferentiation (Sekiguchi *et al.,* 2001), although this was not directly verified. By way of contradiction, the works of Wadey *et al.,* directly showed that rather than inducing intima thickening, ectopic overexpression of PRH S163C:S177C reduced VSMC proliferation in cultured rat aortic VSMCs and retarded intima thickening in human saphenous vein organ cultures measured by BrdU Assay (Wadey *et al.,* 2017). These data support an anti-proliferative role for PRH, contradicting what was previously postulated by Sekiguchi and colleagues. It was therefore proposed by Wadey et al. that the PRH protein accumulates in proliferating VSMCs of the neointima of injured vessels in order to prevent uncontrolled cell proliferation. The results of this current study from EdU incorporation and markers of cell cycle progression corroborate the observations of Wadey et al clearly illustrating the anti-proliferative effects of PRH.

It has been shown that PRH S163C:S177C exerted a prolonged anti-proliferative action with respect to wild-type PRH when transiently transfected into primary rat aortic VSMCs (Wadey *et al.,* 2017). As mentioned previously, mutation of Ser163 and Ser177 within the PRH homeodomain to cysteine residues is preventative of CK2 proliferation therefore increasing protein stability, DNA binding potential and transcriptional activity (Noy *et al.,* 2012; Soufi *et al.,* 2009).

In support of the anti-proliferative effect of PRH S163C:S177C on EdU incorporation cell cycle progression proteins were quantified by Western blotting. Cell cycle progression is a tightly controlled event regulated positively by cyclin-dependent kinases and their cyclin- regulatory subunits, and negatively by cyclin-dependent kinase inhibitor (CKI) (Andres, 2004). p21 is a potent cyclin-dependent kinase inhibitor (CKI) that promotes G1 or G2/M cell cycle arrest in response to a variety of stimuli (Andres, 2004). On the other hand, cyclin D1 is another important regulator of cell cycle progression that inhibits cell cycle arrest at the G1 phase (Topisirovic *et al.,* 2003). A number of reports have demonstrated that p21 inhibits VSMC proliferation and injury-induced intima thickening (Bond *et al.,* 2006; Han *et al.,* 2015; Xie *et al.,* 2017). Interestingly, it has been previously reported that PRH can repress cyclin D1 protein production implicating PRH to arrest cells during the cell cycle phase by decreasing the transport of cyclin D1 mRNA via elF4e and PML nuclear bodies (Topisirovic *et al.,* 2003; Gaston *et al.,* 2016). The findings in the current study uncover the role of PRH S163C:S177C in regulating the levels of cell cycle proteins p21 and cyclin D1 and reveal the proliferative

state of VSMCs. The results thus indicate that the antiproliferative effect of PRH S163C:S177C in HSV VSMCs is attributable to arrest of the cell cycle in G0/G1 caused, in turn, by upregulation of p21 and inhibition of cyclin D1. In line with our proliferation data, PRH S163C:S177C have been shown to alleviate the migration of HSV VSMCs.

To determine the role of PRH S163C:S177C in apoptosis and hence cell survival, the presence of cleaved caspase-3 protein was quantified. The results showed that PRH S163C:S177C had no effect on the number of cells positive for cleaved caspase-3, an apoptotic marker, hence, the rate of apoptosis was altered. In agreement with this finding, Wadey *et al.,* was unable to detect changes in apoptosis with overexpression of PRH.

3.4.3 PRH S163C:S177C stimulates the contractile phenotype in VSMCs

In this chapter, PRH S163C:S177C was discovered to be a novel regulator VSMC phenotype. VSMCs are highly differentiated cells with a low proliferative rate and maintain vascular tone in mature vessels. In a healthy vessel wall, VSMCs are in a 'contractile' state with low proliferation and migration rates. However, in disease, they can dedifferentiate into a 'synthetic' phenotype, where they become highly proliferative and migratory, and increase ECM protein production. This process is called phenotypic switching and is often the first step in vascular pathology (Petsophonsakul *et al.,* 2019). Previous findings by Oyama *et al.,* demonstrated induced transcription of the SM22a and smooth muscle α-actin genes in response to wild-type PRH using rat embryonic fibroblast cells (Oyama *et al.,* 2004). Yet, expression of other contractile markers including calponin and smooth muscle myosin heavy chain 1 and 2 did not change in murine embryonic fibroblasts (Oyama *et al.,* 2004). Contrary to these findings, the present study found a pronounced increase in smoothelin and calponin protein expression following PRH S163C:S177C overexpression. These were further validated by the functional collagen contraction assay. For the first time, we have shown that cells overexpressing PRH S163C:S177C induced VSMC collagen gel contractile function. Conversely, no significant changes were seen in the expression of smooth muscle myosin heavy chain 10 and α-SMA (data not shown). Contrary to SM22a and SM α-actin, calponin and smoothelin genes are induced at the later stage of differentiation (Beamish *et al.,* 2010). Since expression patterns of SM22a and α-SMA occur at the early stages on differentiation, difference in our findings could be due to the rate limiting factor of PRH S163C:S177C to activate the late stage of VSMC differentiation via SRF. A study by Zhang *et al.,* reported that Interferon Regulatory Factor 9 (IRF9) deficiency by IRF9-KO mice have illustrated increased

expression of SM22α, α-SMA, and smoothelin in addition to IRF9 overexpression being reported to promoting VSMC proliferation, migration and intimal hyperplasia (Zhang *et al.,* 2014). In another study, loss of glucose-6-phosphate dehydrogenase (G6PD) was reported to upregulate the expression of contractile proteins including MYH11, calponin and SM22α in the isolated coronary arteries treated with G6PD inhibitor (Chettimada *et al.,* 2016). Most importantly, it is essential to note that Oyama's group performed the experiment using pluripotent embryonic fibroblasts in comparison to the present study that utilised HSV VSMCs which is more representative the context of vein graft disease. Collectively, the current findings show that PRH S163C:S177C regulates VSMC proliferation, migration and survival as well as restoring their dedifferentiated, contractile phenotype.

3.4.4 Chapter Summary

The results of this chapter show that PRH S163C:S177C promoted the contractile phenotype, and inhibited migration and proliferation in primary HSV VSMCs. The findings indicate that gene therapy to induce elevated levels of PRH could be effective in preventing early-to-mid stage VGF, additional methods for increasing levels of PRH S163C:S177C and stabilising the protein long-term is attractive when considering therapies for VGF. Hence, the results in this chapter provided further evidence that PRH S163C:S177C is a valuable candidate for gene therapy in saphenous vein graft failure. Furthermore, it is important to assess the effect of PRH S163C:S177C on endothelial cells as endothelial dysfunction could lead to incidences of thrombosis. It would be of interest to determine the underlying mechanisms responsible for the effect of PRH on VSMC behaviour, hence in Chapter 6, Next Generation Sequencing (NGS) was utilised to identify a molecular link and/or mechanism responsible for the effects of PRH S163C:S177C.

4.

THE EFFECT OF PRH S163C:S177C ON ENDOTHELIAL CELLS: PROLIFERATION, MIGRATION, APOPTOSIS, AND INFLAMMATORY RESPONSES

4.1 INTRODUCTION

The endothelium acts as a crucial functional barrier by controlling the interchange of materials between blood and the vessel wall, as well as influencing inflammatory processes, vascular tone, thrombogenesis and growth of blood vessels (Ward *et al.,* 2017). During coronary artery bypass graft (CABG) surgery, damage to the endothelium occurs as a result of transient ischaemia, high pressure distention and tissue handling (Angelini *et al.,*1987; Conte, 2010). Following implantation, exposure of venous endothelial cells to the arterial circulation and turbulent blood flow around the sites of anastomoses further exacerbates endothelial dysfunction (Gosling *et al.,* 1999, Ward *et al.,* 2017). Disruption of the endothelium is the initial step in the pathogenesis of autologous vein graft disease and ultimately restricts the long-term efficacy of this surgical intervention (Ward *et al.,* 2017; Favero, 2014, Fitzgibbon *et al.,*1996, Sabik, 2011). Re-endothelialisation begins rapidly after CABG surgery; therefore, it is essential that any potential therapy does not retard this process or heighten endothelial dysfunction (Ward *et al.,* 2017). Hence, interventions that do not interfere with re-endothelialisation or can help restore an intact endothelium and normal endothelial function, as well as prevent neointima formation and restenosis, are highly desirable to retard VGF.

Typically, investigation into endothelial dysfunction in disease entails the usage of cultured human umbilical vein endothelial cells (HUVECs) (Siow, 2012). HUVECs can be obtained relatively easily from umbilical cords which are routinely available from labour and delivery wards; however, there is some controversy surrounding whether these cells are representative of the adult endothelium as these are isolated from immune-privileged foetal tissue (Zhang *et al.,* 2017). HUVECs express high levels of Fas ligand, which is assumed to encourage apoptosis of activated maternal lymphocytes which present the Fas ligand receptor (Guller et *al.,* 1999; Zhang *et al.,* 2017). Tan *et al.*, previously reported that HUVECs are very responsive to proinflammatory cytokines but have less sensitivity to ox-LDL when compared to adult HSVECs (Tan *et al.,* 2004). HSVECs are isolated from excess saphenous vein segments remaining after CABG surgery and may therefore be more appropriate for investigating the characteristics of the adult large vessel endothelium and for studying the pathogenesis of HSV VGF. Thus, the experiments in this current study were conducted in primary cultures of HSVECs.

It has been previously demonstrated that adenovirus-mediated delivery of PRH S163C:S177C retarded neointima formation in human saphenous vein organ cultures thereby identifying PRH S163C:S177C as a candidate for gene therapeutics in preventing VGF (Wadey *et al.,* 2017). This study also highlighted that this approach may not impair re-endothelialisation post CABG surgery as cell replication, motility and survival was not affected in cultured HUVECs

or HSVECs overexpressing wild-type PRH (Wadey *et al.,* 2017); however, the effects of introducing PRH S163C:S177C remain to be investigated as well as its impact on other aspects of endothelial function including monocyte adhesion and inflammatory cytokine production.

In this chapter, the effect of overexpressing PRH S163C:S177C on endothelial cell behaviour, including cellular proliferation, apoptosis and migration was evaluated. Moreover, to discern whether PRH S163C:S177C has favourable anti-inflammatory properties, its effects on monocyte adhesion, expression of pro-inflammatory cytokines and barrier function was investigated.

4.2 HYPOTHESES

The hypotheses for this chapter were:

- PRH S163C:S177C does not affect HSVEC proliferation, apoptosis and migration.
- PRH S163C:177C plays a role in inflammatory responses in HSVECs including monocyte adhesion, cytokine release and permeability.

These hypotheses were tested by:

- Quantification of EdU incorporation and Western blotting for proliferative markers p21 and cyclin D1 was employed to determine the effect of adenovirus-mediated overexpression of PRH S163C:S177C on proliferation of HSVECs.
- Immunofluorescence for cleaved caspase-3 was utilised to test the effect of adenovirus-mediated overexpression of PRH S163C:S177C on apoptosis of HSVECs.
- The scratch wound assay was utilised to assess the effect of adenovirus-mediated overexpression of PRH S163C:S177C on migration of HSVECs.
- Monocyte adhesion assays, qPCR and ELISAs for inflammatory cytokines, and permeability assays were used to evaluate the effect of adenovirus-mediated overexpression of PRH S163C:S177C on inflammatory responses in HSVECs.

4.3 RESULTS

4.3.1 Adenovirus-mediated overexpression of PRH S163C:S177C in HSVECs

Previously in Chapter 3, in HSV VSMCs, an approximate 80% infection efficiency was achieved with 5 x 10^8 pfu/ml of adenovirus encoding PRH S163C:S177C. In order to determine a concentration for achieving a similar infection efficiency in endothelial cells, HSVECs were subjected to infection with c-myc-tagged PRH S163C:S177C expressing recombinant adenoviruses at three different viral doses: 0.25 x 10^8 pfu/ml, 0.50 x 10^8 pfu/ml and 1 x 10^8 pfu/ml. Both uninfected HSVECs and HSVECs infected with identical doses of adenovirus encoding an empty vector served as negative controls. Subsequent to an 18-hour incubation, culture medium was refreshed with endothelial cell growth medium, and cells were incubated for a further 24 hours. Overexpression of the c-myc-tagged PRH S163C:S177C protein was assessed via Western blotting and immunofluorescence for c-myc-tagged protein (FIGURE 4.1 and FIGURE 4.2). As expected, c-myc-tagged protein was not detected in uninfected cells or cells subjected to infection with Ad: Control via either Western blotting or immunofluorescence (FIGURE 4.1 and FIGURE 4.2). The c-myc-tagged PRH S163C:S177C were detected at 42 kDa on Western blots. Immunofluorescence for c-myc-tagged protein revealed an approximate infection efficiency of 80% in cells infected with 1 x 10^8 pfu/ml of Ad: PRH S163C:S177C, thus a comparable efficiency was obtained in HSVECs and HSV VSMCs (FIGURE 4.2).

To investigate whether comparable levels of PRH S163C:S177C protein expression is achieved between the two cell types, HSVECs and HSV VSMCs were infected with an adenovirus encoding c-myc-tagged PRH S163C:S177C as described previously. As the viral load must be identical for comparative experiments, HSVECs were infected 1 x 10^8 pfu/ml Ad: PRH S163C:S177C and supplemented with 4 x 10^8 pfu/ml of Ad: Control to achieve a final viral concentration of 5 x 10^8 pfu/ml as this was used for infection of HSV VSMCs with Ad: PRH S163C:S177C. For both cell types, cells were cultured with the virus for 18 hours and then were cultured for a further 24 hours in fresh cell growth medium. Subsequently, cell lysates were collected for Western blot analysis of the c-myc-tagged PRH S163C:S177C transgene. Analysis of Western blots revealed comparable levels of PRH S163C:S177C protein in HSVECs to HSV VSMCs (FIGURE 4.3).

A

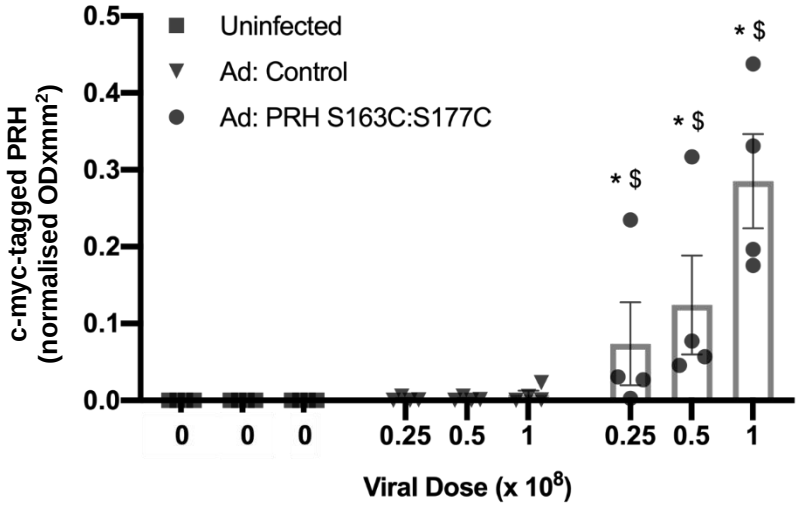

B

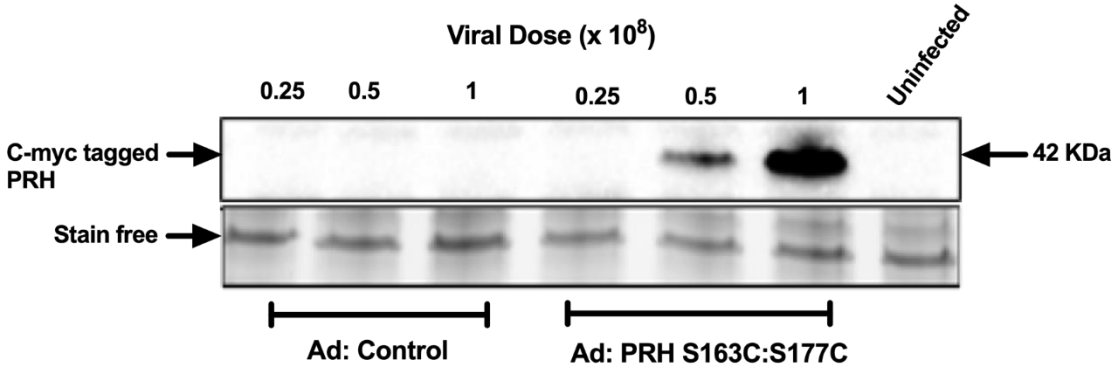

FIGURE 4.1 - Detection of c-myc-tagged PRH S163C:S177C in HSVECs using Western Blotting

HSVECs were either infected with 0.25 x 10^8 pfu/mL, 0.5 x 10^8 pfu/mL or 1 x 10^8 pfu/mL Ad: Control or Ad: PRH S163C:S177C or were left uninfected.

A – Densitometry analysis of c-myc-tagged PRH S163C:S177C protein expression normalised to stain free gel. * indicates $p<0.05$ vs. uninfected, $ indicates $p<0.05$ vs. Ad: Control, ANOVA, Student-Newman-Keuls Multiple Comparisons Test, n=4. Error bars represent standard error of mean SEM.

B - Representative Western blot of c-myc-tagged PRH S163C:S177C protein. Stain-free bands served as a loading control. Approximate molecular weight of detected band indicated in kDa.

FIGURE 4.2 - Detection of c-myc-tagged PRH S163C:S177C in HSVECs using Immunocytochemistry.

HSVECs were either infected with 0.25 x 10^8 pfu/mL, 0.5 x 10^8 pfu/mL or 1 x 10^8 pfu/mL Ad: Control or Ad: PRH S163C:S177C or were left uninfected.

A – Quantification of percentage of cells expressing c-myc-tagged PRH S163C:S177C protein. * indicates $p<0.05$ vs. uninfected, $ indicates $p<0.05$ vs. all Ad: Control, ANOVA, Student-Newman-Keuls Multiple Comparisons Test, n=4.Error bars represent SEM.

B – Representative images of immunocytochemistry for c-myc-tagged protein. Positive cells have green nuclei and examples are indicated with red arrows; all nuclei are stained blue with DAPI. Scale bar indicates 25 μm and applies to all panels.

A

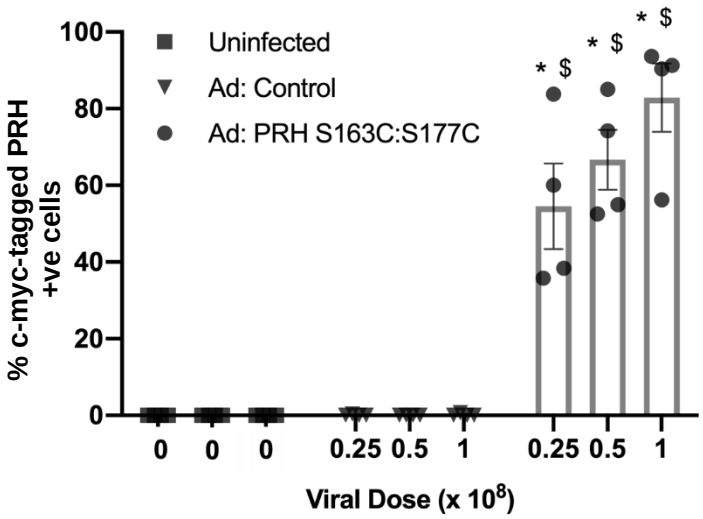
100
80
60
40
20
0
% c-myc-tagged PRH +ve cells
Uninfected
Ad: Control
Ad: PRH S163C:S177C
* $
* $
* $
0 0 0 0.25 0.5 1 0.25 0.5 1
Viral Dose (x 10^8)

B

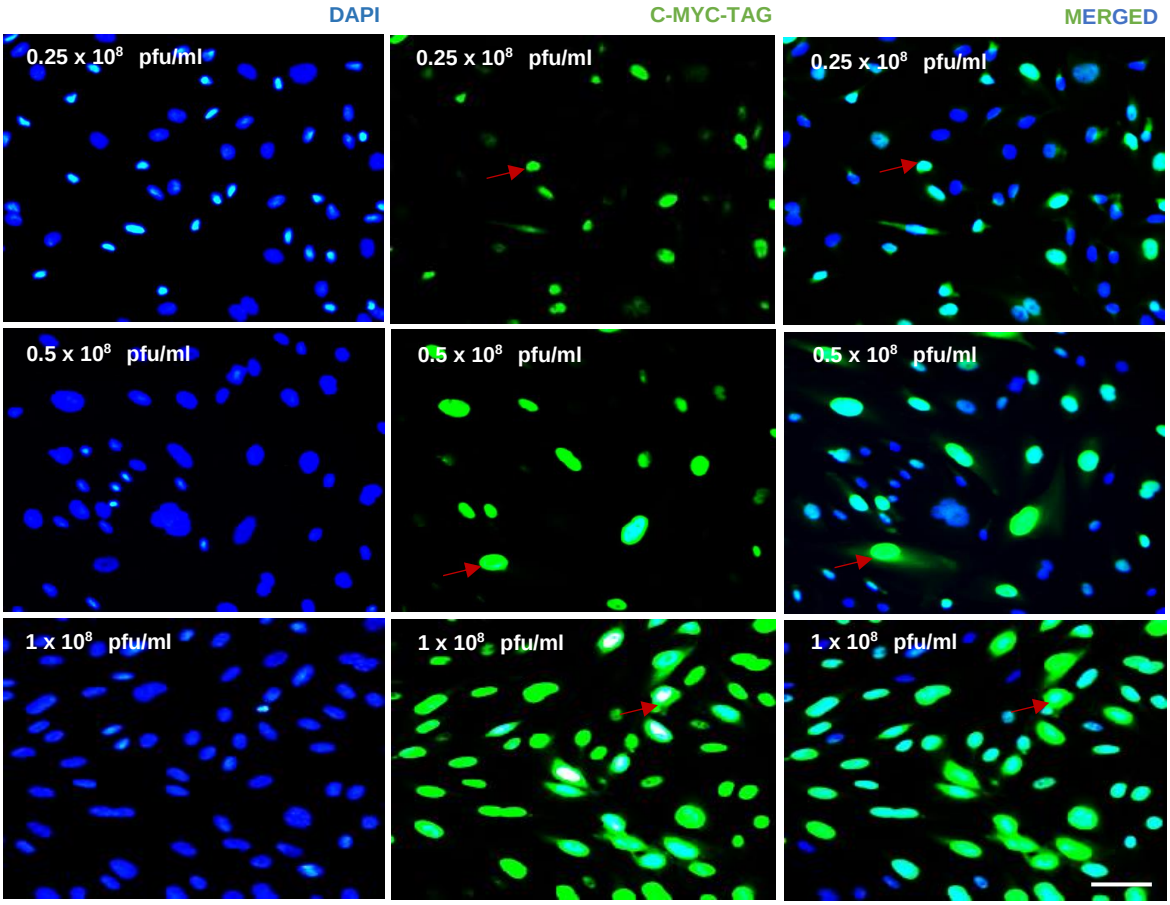
DAPI
C-MYC-TAG
MERGED
0.25 x 10^8 pfu/ml
0.25 x 10^8 pfu/ml
0.25 x 10^8 pfu/ml
0.5 x 10^8 pfu/ml
0.5 x 10^8 pfu/ml
0.5 x 10^8 pfu/ml
1 x 10^8 pfu/ml
1 x 10^8 pfu/ml
1 x 10^8 pfu/ml

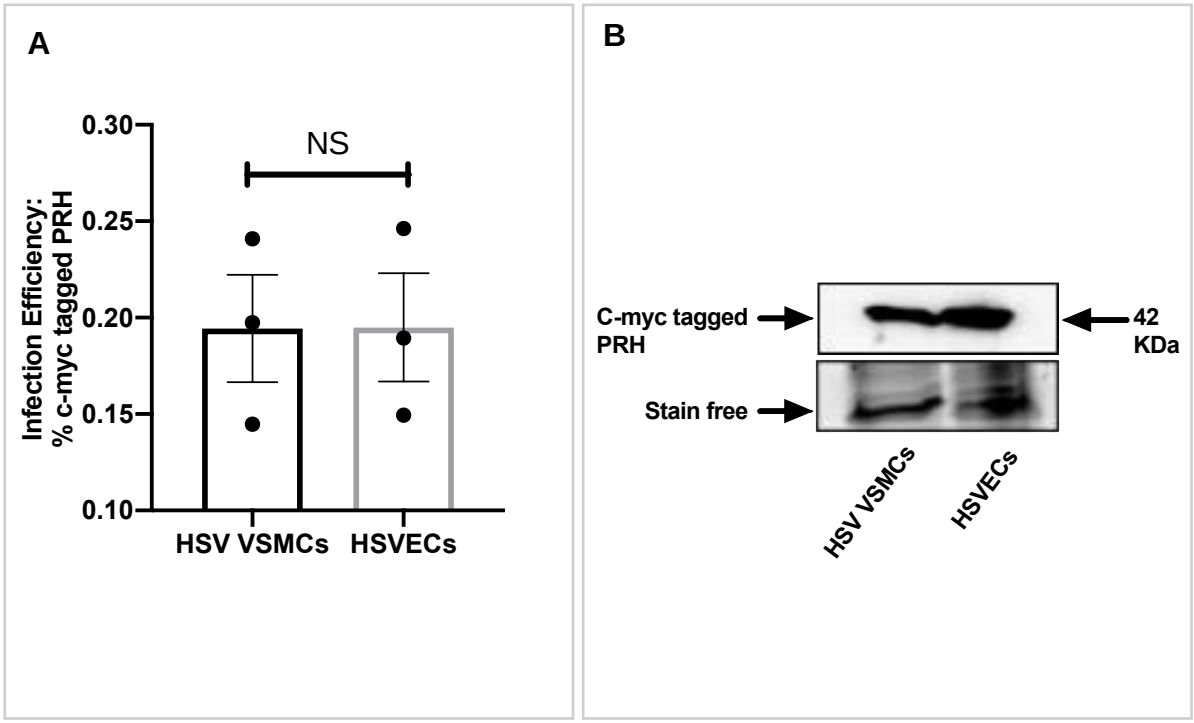

FIGURE 4.3 – Comparable overexpression of c-myc-tagged PRH S163C:S177C in HSVECs and HSV VSMCs

HSV VSMCs were infected with 5 x 10^8 pfu/mL of Ad: PRH S163C:S177C. HSVECs were infected with 1 x 10^8 pfu/mL of adenovirus encoding c-myc-tagged PRH S163C:S177C combined with 4 x 10^8 pfu/mL Ad: Control.

A - Quantification of c-myc-tagged protein by Western blotting; data was normalised by stain-free bands. NS denotes not significant, unpaired, two-tailed Student's t-test, n=4.Error bars represent SEM.

B - Representative Western blot for c-myc-tagged PRH S163C:S177C protein. Stain-free bands served as a loading control. Approximate molecular is indicated on the right in kDa.

4.3.2 PRH S163C:S177C did not affect HSVECs proliferation

To investigate whether ectopically increasing PRH S163C:S177C protein levels affects proliferation of endothelial cells, HSVECs infected with 1 x 10^8 pfu/ml Ad: PRH S163C:S177C supplemented with 4 x 10^8 pfu/ml of Ad: Control for 18 hours. The controls were HSVECs infected with 5 x 10^8 pfu/ml of Ad: Control or uninfected HSVECs. Cells were cultured for a further 24 hours in fresh endothelial cell growth medium supplemented with 10 μM EdU for Click-iT EdU, and without EdU for Western blot analysis of proliferative markers cyclin D1 and p21. Quantification of EdU incorporation showed that the rate of proliferation in HSVECs overexpressing PRH S163C:S177C was not significantly different to that detected in HSVECs infected with Ad: Control and uninfected control HSVECs (FIGURE 4.4). CyclinD1 and p21 were detected at 21 kDa and 36 kDa on Western blots, respectively. Analysis of Western blots revealed that overexpression of PRH S163C:S177C protein expression in HSVECs did not influence the levels of cyclin D1 or p21 protein compared to uninfected control HSVECs and HSVECs subjected to adenoviral delivery of an empty vector (FIGURE 4.5).

FIGURE 4.4 – Overexpression of c-myc-tagged PRH S163C:S177C in HSVECs did not affect the rate of proliferation

HSVECs were infected with 1 x 10^8 pfu/mL of Ad:PRH S163C:S177C combined with 4 x 10^8 pfu/mL Ad: Control, or 5 x 10^8 pfu/mL Ad: Control, or were left uninfected.

A – EdU incorporation was quantified and expressed as the percentage of EdU-positive cells. NS denotes not significant, ANOVA, Student-Newman-Keuls Multiple Comparisons Test, n=4. Error bars indicate SEM.

B – Representative images of Click-iT EdU imaging assay. Positive cells have green nuclei and examples are indicated with red arrows; all nuclei are stained blue with DAPI. Scale bar measures 50μm and applies to all panels.

A

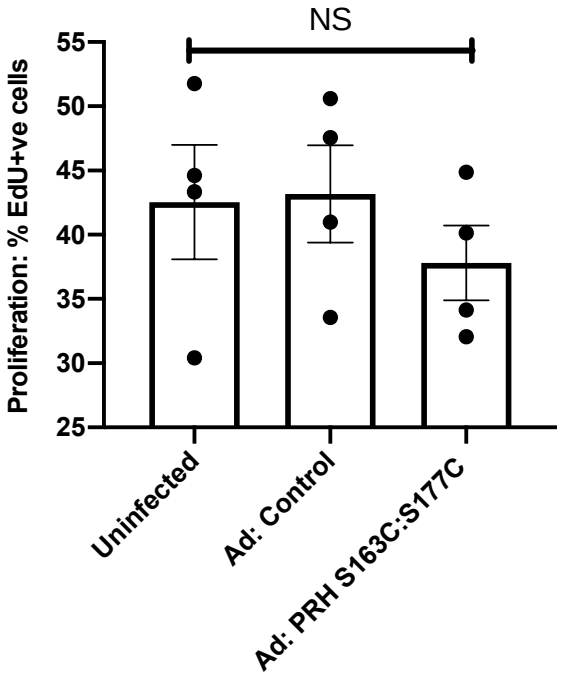
NS
Proliferation: % EdU+ve cells
55
50
45
40
35
30
25
Uninfected
Ad: Control
Ad: PRH S163C:S177C

B

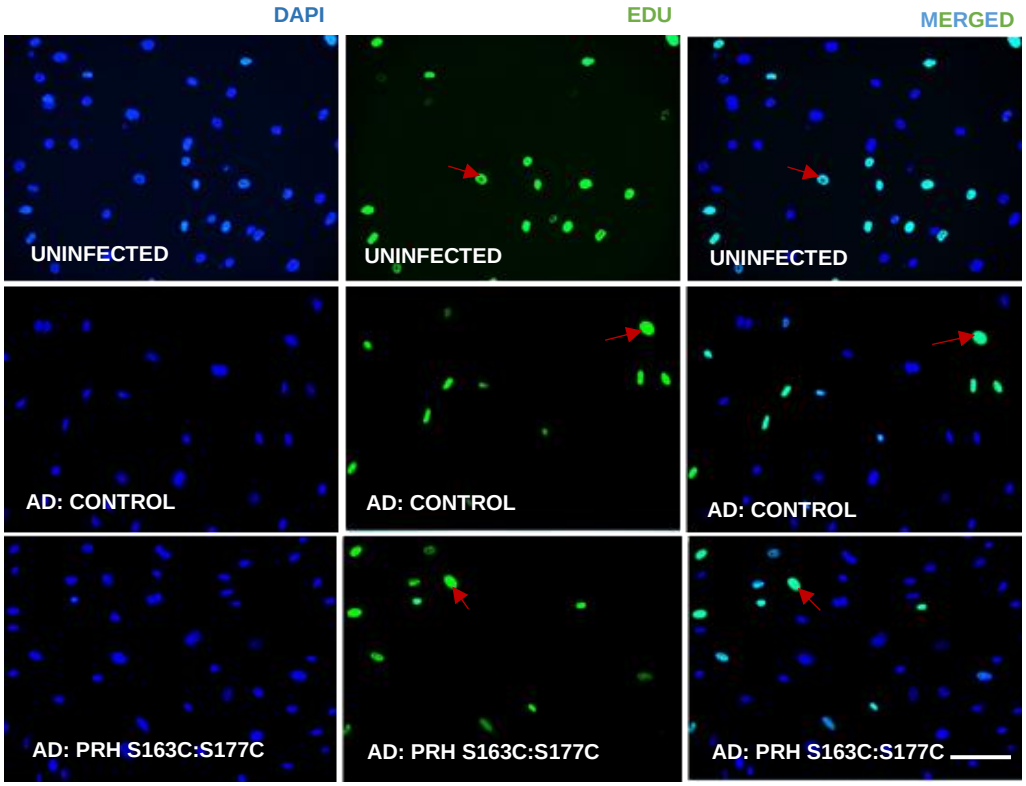
DAPI
EDU
MERGED
UNINFECTED
UNINFECTED
UNINFECTED
AD: CONTROL
AD: CONTROL
AD: CONTROL
AD: PRH S163C:S177C
AD: PRH S163C:S177C
AD: PRH S163C:S177C

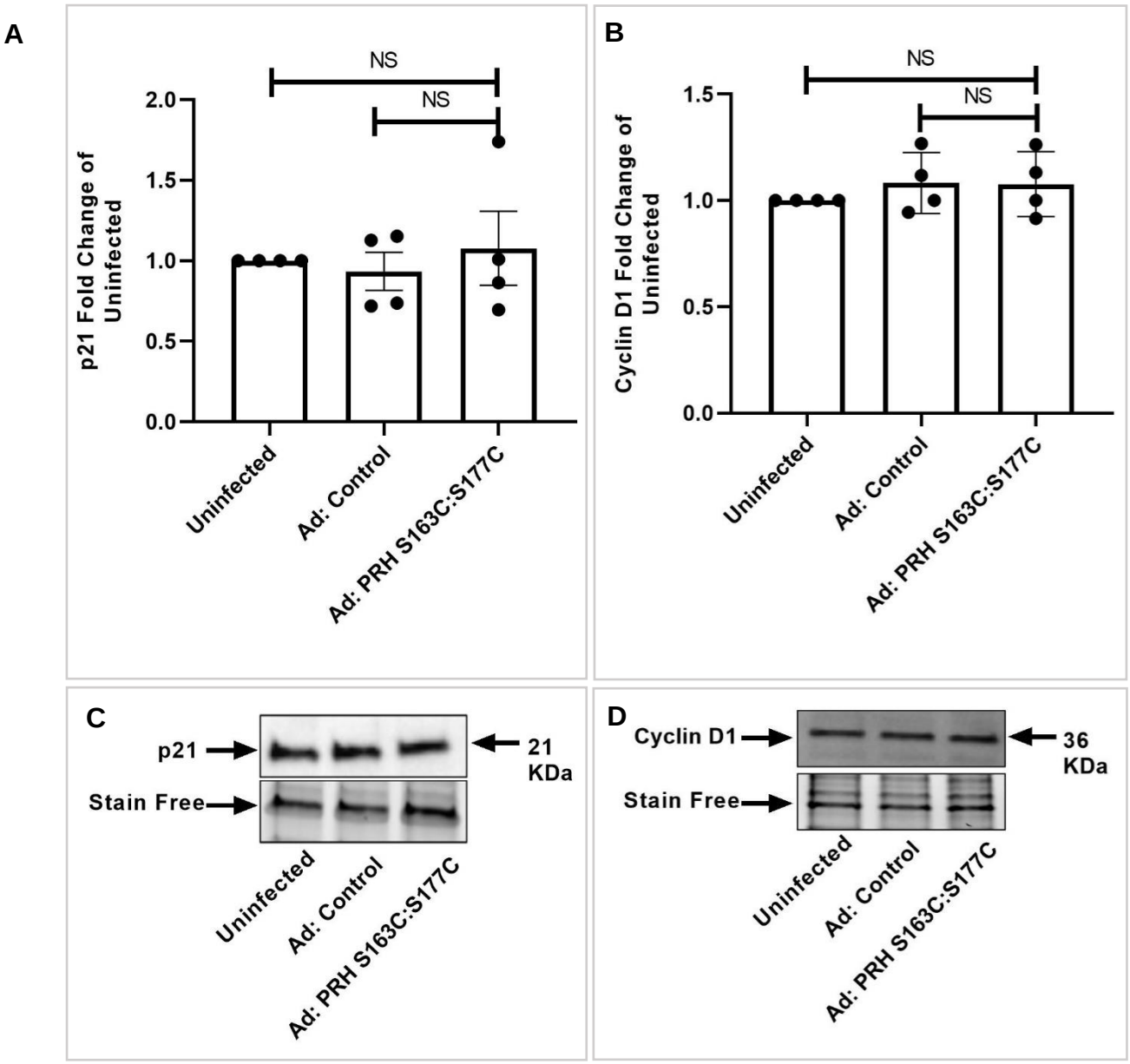

FIGURE 4.5 – Overexpression of c-myc-tagged PRH S163C:S177C in HSVECs did not cyclin D1 and p21 protein levels

HSVECs were infected with 1 x 10^8 pfu/mL Ad: PRH S163C:S177C combined with 4 x 10^8 pfu/mL Ad: Control, or 5 x 10^8 pfu/mL Ad: Control or were left uninfected.

Quantification of p21 (**A**) and Cyclin D1 (**B**) protein expression by Western blotting; data was normalised by stain-free bands and expressed as a fold change from uninfected control. NS denotes not significant, ANOVA, Student-Newman-Keuls Multiple Comparisons Test, n=4. Error bars indicate SEM. Representative Western blot for p21 (**C**) and Cyclin D1 (**D**). Stain-free bands served as a loading control. Approximate molecular weight of protein band is indicated on the right in kDa.

4.3.3 PRH S163C:S177C reduced HSVECs apoptosis

To investigate the effect of PRH S163C:S177C overexpression affected HSVEC apoptosis, HSVECs infected with 1 x 10^8 pfu/ml Ad: PRH S163C:S177C supplemented with 4 x 10^8 pfu/ml of Ad: Control, or 5 x 10^8 pfu/ml of Ad: Control or left uninfected for 18 hours. Cells were then cultured for another 24 hours after replenishing the culture medium. As a positive control, cells were incubated with 200 ng/mL human recombinant Fas ligand in 2% FBS endothelial cell growth medium. Subsequently, apoptosis was assessed via immunocytochemistry for cleaved caspase-3. As expected, Fas ligand significantly increased the rate of apoptosis compared to that observed in the control uninfected HSVECs (FIGURE 4.6). Quantification of the percentage of cleaved caspase-3 positive cells showed that rate of apoptosis in HSVECs overexpressing PRH S163C:S177C was significantly lower than the rate of apoptosis in HSVECs infected with Ad: Control or uninfected control HSVECs (FIGURE 4.6).

FIGURE 4.6 - Overexpression of c-myc-tagged PRH S163C:S177C in HSVECs reduced apoptosis

HSVECs were infected with 1 x 10^8 pfu/mL Ad: PRH S163C:S177C combined with 4 x 10^8 pfu/mL Ad: Control, or 5 x 10^8 pfu/mL Ad: Control or were left uninfected.

A – The percetage of CC-3 positive cells (apoptotic cells) was quantified. ** indicates $p<0.01$ vs. uninfected or Ad: Control. ANOVA, Student-Newman-Keuls Multiple Comparisons Test, n=4. Error bars indicate SEM.

B – Representative images of immunofluorescence for cleaved caspase-3. Positive cells have green nuclei and examples are indicated with red arrows; all nuclei are stained blue with DAPI. Scale bar measures 25 µm and applies to all panels.

A

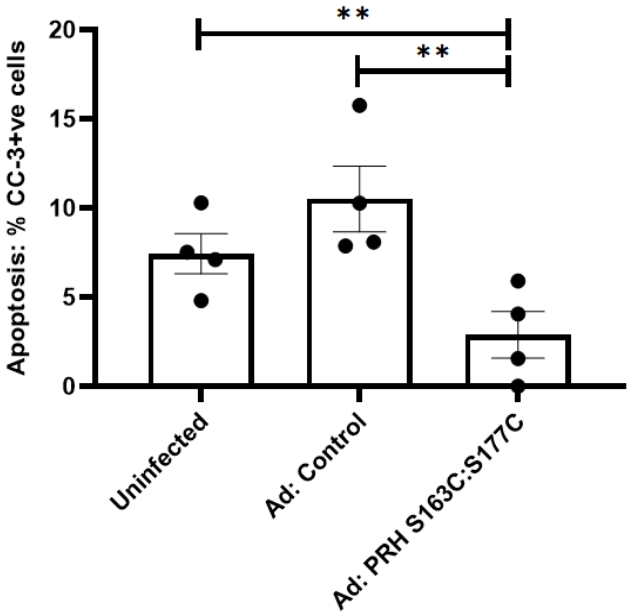
**
**
Apoptosis: % CC-3+ve cells
20
15
10
5
0
Uninfected
Ad: Control
Ad: PRH S163C:S177C

B

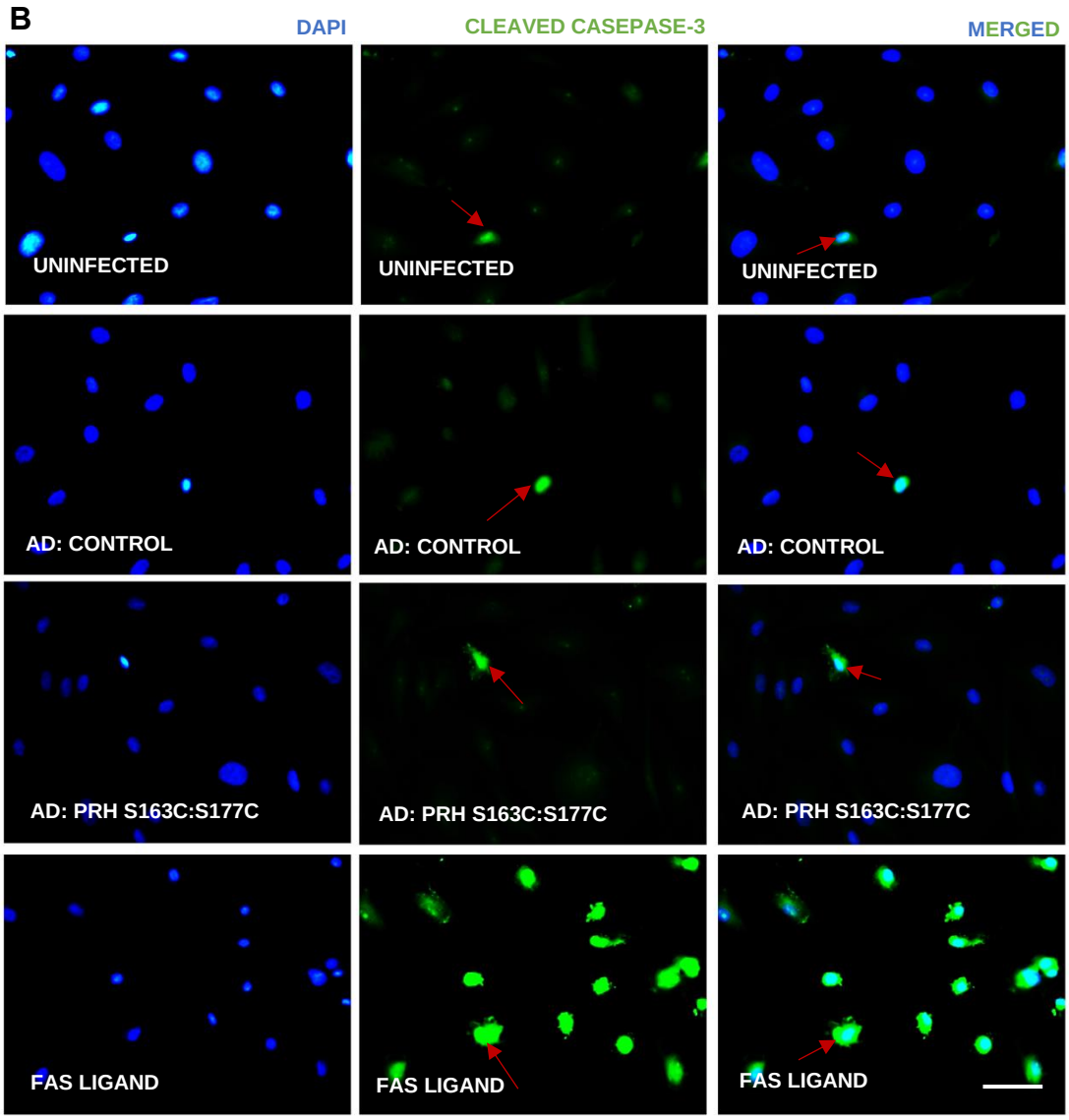
DAPI
CLEAVED CASEPASE-3
MERGED
UNINFECTED
UNINFECTED
UNINFECTED
AD: CONTROL
AD: CONTROL
AD: CONTROL
AD: PRH S163C:S177C
AD: PRH S163C:S177C
AD: PRH S163C:S177C
FAS LIGAND
FAS LIGAND
FAS LIGAND

4.3.4 PRH S163C:S177C did not affect HSVECs migration

The scratch wound assay was utilised to investigate the effect of PRH S163C:S177C overexpression on endothelial cell migration. HSVECs infected with 1 x 10^8 pfu/ml Ad: PRH S163C:S177C supplemented with 4 x 10^8 pfu/ml of Ad: Control, or 5 x 10^8 pfu/ml of Ad: Control or left uninfected for 18 hours. Subsequently, the confluent monolayers of HSVECs were wounded then incubated for a further 24 hours. Treatment with 2 mM hydroxyurea inhibited cell proliferation and enabled assessment of migration only. The distance migrated was quantified by measuring the wound at 0- and 24-hours post-wounding. No significant effect on the distance migrated was observed across all treatment conditions: uninfected or infected with either Ad: Control or Ad: PRH S163C:S177C (FIGURE 4.7).

FIGURE 4.7 – Overexpression of PRH S163C:S177C did not affect migration of HSVECs

HSVECs were infected with 1 x 10^8 pfu/mL Ad: PRH S163C:S177C combined with 4 x 10^8 pfu/mL Ad: Control, or 5 x 10^8 pfu/mL Ad: Control or were left uninfected and migration assessed using the scratch wound assay.

A – Migration was quantified and expressed as distance migrated in µm; NS denotes not significant, ANOVA, Student-Newman-Keuls Multiple Comparisons Test, n=4.Error bars indicate SEM.

B – Representative images of the scratch wound assay. Dashed line indicates wound edge. T0 indicates Time = 0 hr; T24 indicates Time = 24 hr. Scale bar represents 1 mm and applies to all panels.

A

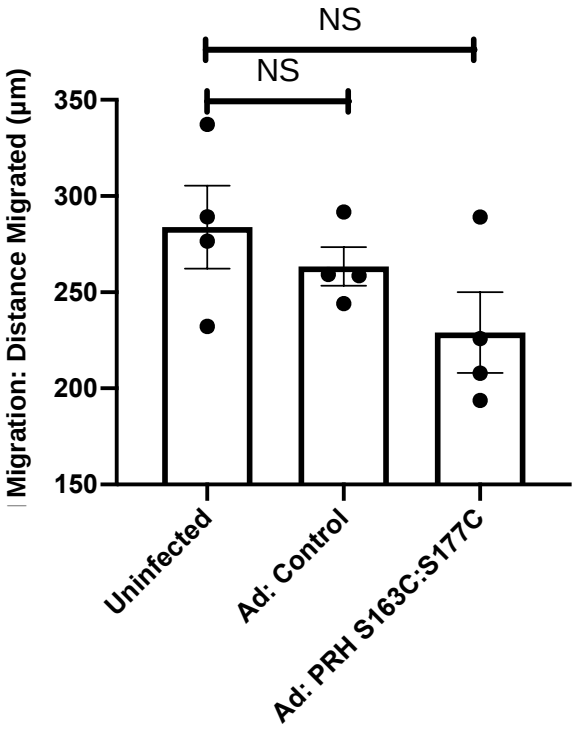
NS
NS
Migration: Distance Migrated (µm)
350
300
250
200
150
Uninfected
Ad: Control
Ad: PRH S163C:S177C

B

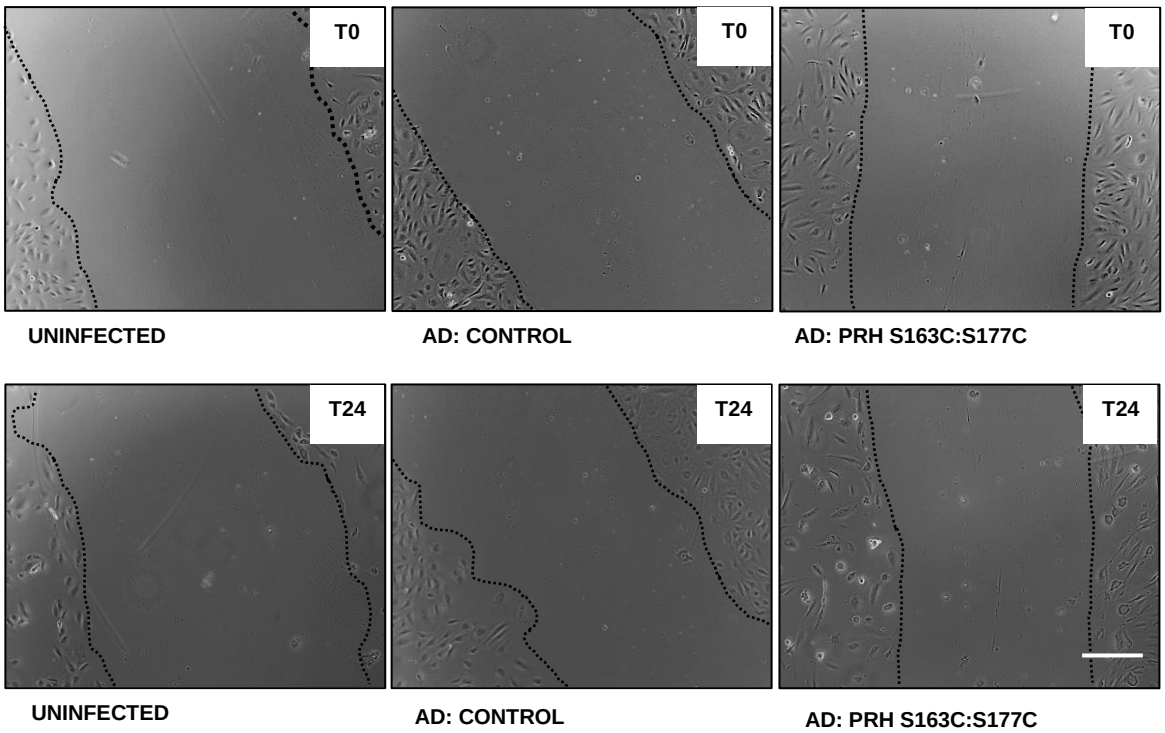
T0
T0
T0
UNINFECTED
AD: CONTROL
AD: PRH S163C:S177C
T24
T24
T24
UNINFECTED
AD: CONTROL
AD: PRH S163C:S177C

4.3.5 PRH S163C:S177C attenuated TNFα-induced monocyte adhesion

Adhesion of circulating monocytes to the endothelial surface is a key step in the onset of localised vascular inflammation and disease progression (Ley *et al.,*2007). To investigate the effect of PRH S163C:S177C expression on monocyte adhesion, HSVECs were infected with 1 x 10^8 pfu/ml Ad: PRH S163C:S177C supplemented with 4 x 10^8 pfu/ml of Ad: Control, or 5 x 10^8 pfu/ml of Ad: Control or left uninfected for 18 hours. Subsequently, cells were stimulated with 10 ng/mL TNFα for a further 24 hours to induce endothelial activation and an inflammatory response. Calcein-labelled THP-1 cells were then co-cultured with the activated endothelial monolayer for 30 minutes and the number of adherent THP-1 cells quantified. At baseline levels, HSVECs in the absence of TNFα very few THP-1 cells adhered to the HSVECs (data not shown). As expected, stimulation of HSVECs with TNFα induced an approximate 10-fold induction in THP-1 cell adhesion in uninfected HSVECs (data not shown). The number of adherent THP-1 monocytes was not affected as a result of infection of HSVECs with the control adenovirus compared to uninfected HSVECs (FIGURE 4.8). Interestingly, a significant reduction in the number of adherent monocytes was observed when TNFα-treated HSVECs were infected with Ad: PRH S163C:S177C compared to uninfected HSVECs and HSVECs infected with Ad: Control (FIGURE 4.8)

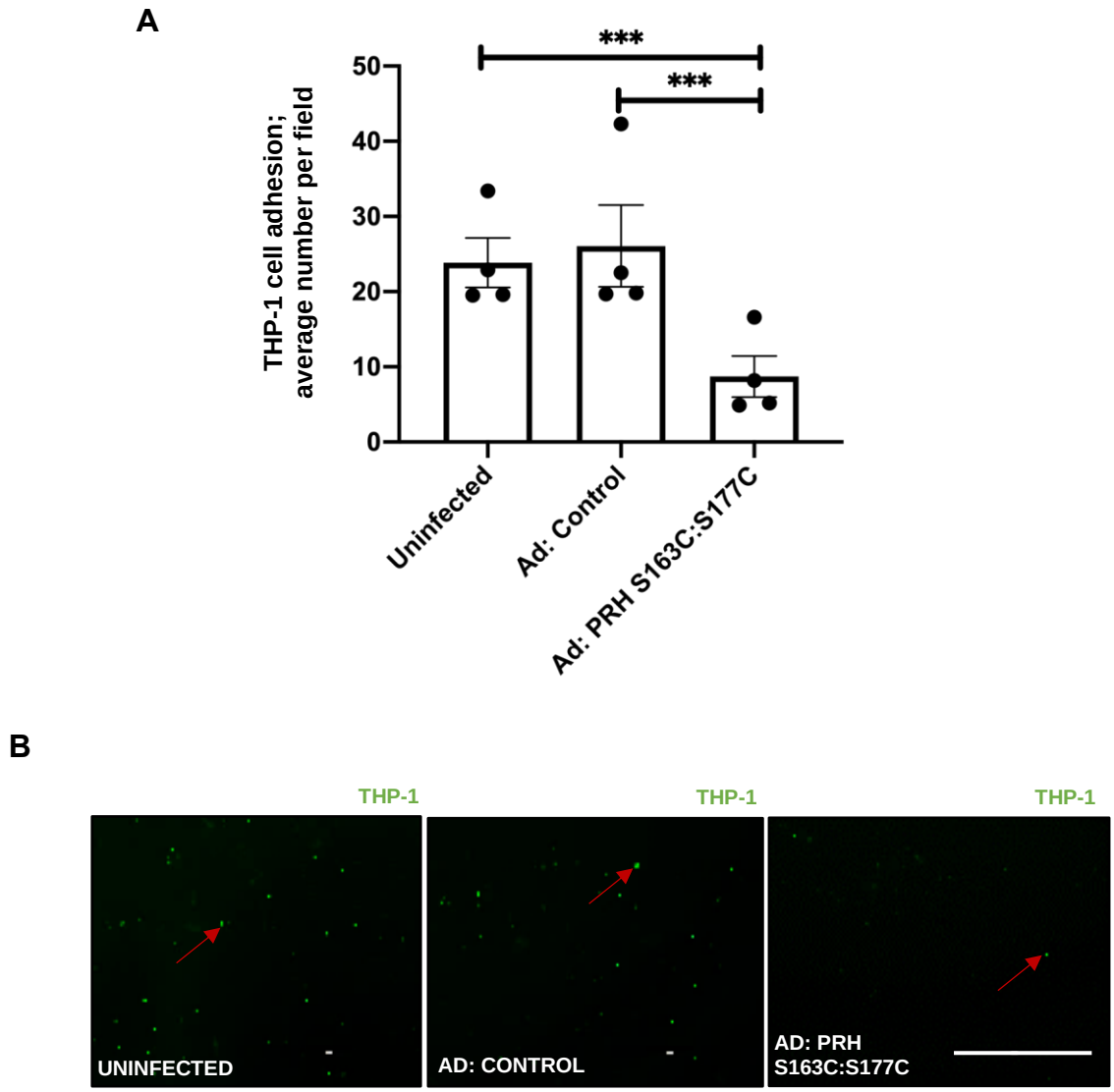

FIGURE 4.8 – Overexpression of PRH S163C:S177C attenuated monocyte adhesion in TNFα-stimulated HSVECs

HSVECs were infected with 1 x 10^8 pfu/mL Ad: PRH S163C:S177C combined with 4 x 10^8 pfu/mL Ad: Control, or 5 x 10^8 pfu/mL Ad: Control or were left uninfected. HSVECs were subsequently stimulated with TNFα for 24 hours, then co-cultured with calcein-labelled THP-1 cells to assess monocyte adhesion.

A – Monocyte adhesion was quantified and expressed as the average number of adherent cells per field viewed. *** indicates $p<0.001$, ANOVA, Student-Newman-Keuls Multiple Comparisons Test, n=4. Error bars indicate SEM.

B – Representative images showing adherent calcein-labelled THP-1 cells. Red arrow indicates some of the adherent THP-1 cell. Scale bars represent 1000µm and applies to all panels.

4.3.6 PRH S163C:S177C attenuated monocyte adhesion to HSVECs exposed to LSS

Endothelial cell activation is associated with increased low wall sheer stress (LSS) upon implantation of the vein graft into the arterial circulation and its exposure to high pulsatile pressures (Ward *et al.,* 2017). A simple rocker-induced mechanical stimulus can be utilised to mimic LSS such that is observed in atheroprone regions of the vasculature exposed to disturbed flow (Tucker *et al.,* 2014; Potter *et al.,* 2011; Dhawan *et al.,* 2010). Having shown a reduction in monocyte adhesion in TNFα-stimulated HSVECs, we then investigated the effect of ectopic overexpression of PRH S163C:S177C on monocyte adhesion in HSVECs exposed to LSS. HSVECs were infected with 1 x 10^8 pfu/ml Ad: PRH S163C:S177C supplemented with 4 x 10^8 pfu/ml of Ad: Control, or 5 x 10^8 pfu/ml of Ad: Control or left uninfected for 18 hours. A static control was also included. Then, cells were cultured for another 24 hours after replenishing the culture medium under either static or LSS conditions (30 rpm). Calcein-labelled THP-1 cells were subsequently co-cultured with HSVECs for 30 minutes and the number of adherent THP-1 cells quantified. As expected, monocyte adhesion was elevated in uninfected HSVECs subjected to LSS with respect to uninfected HSVECs cultured under static conditions (FIGURE 4.9). In addition, no significant changes in the number of adherent THP-1 cells were observed between uninfected and Ad: Control groups, where HSVECs were cultured under LSS conditions (FIGURE 4.9). The attachment of monocytes to LSS-stimulated endothelial cells was significantly attenuated by the introduction of PRH S163C:S177C in comparison to uninfected HSVECs and HSVECs infected with Ad: Control (FIGURE 4.9).

FIGURE 4.9 – Overexpression of PRH S163C:S177C attenuated monocyte adhesion in HSVECs subjected LSS

HSVECs were infected with 1 x 10^8 pfu/mL Ad: PRH S163C:S177C combined with 4 x 10^8 pfu/mL Ad: Control, or 5 x 10^8 pfu/mL Ad: Control or were left uninfected, and subsequently cultured for a further 24 hours under LSS conditions, then co-cultured with calcein-labelled THP-1 cells to assess monocyte adhesion. A static uninfected control was included.

A – Monocyte adhesion was quantified and expressed as the average number of adherent cells per field viewed.

*** indicates $p<0.001$, ANOVA, Student-Newman-Keuls Multiple Comparisons Test, n=4. Error bars indicate SEM.

B – Representative images showing adherent calcein-labelled THP-1 cells. Red arrow indicates some of the adherent THP-1 cell. Scale bars represent 1000μm and applies to all panels.

A

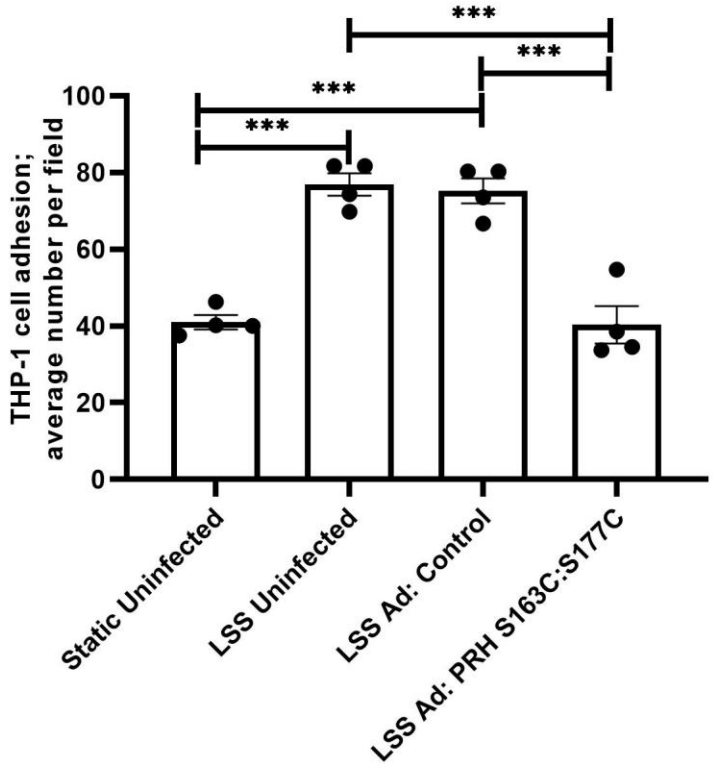
***
***
***
***
100
80
60
40
20
0
THP-1 cell adhesion; average number per field
Static Uninfected
LSS Uninfected
LSS Ad: Control
LSS Ad: PRH S163C:S177C

B

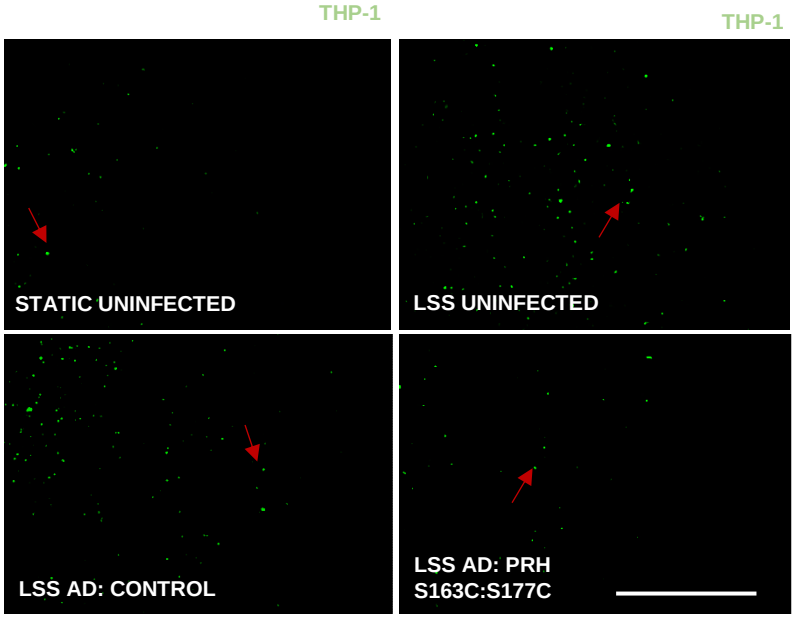
THP-1
THP-1
STATIC UNINFECTED
LSS UNINFECTED
LSS AD: CONTROL
LSS AD: PRH S163C:S177C

4.3.7 PRH S163C:S177C downregulated ICAM-1 and VCAM-1 in HSVECs

Previous studies have demonstrated that upregulation of adhesion molecules ICAM-1 and VCAM-1 facilitates recruitment and infiltration of leukocytes into the vessel wall (Kluger, 2004; van Buul *et al.,* 2007). Having demonstrated that adenoviral-mediated expression of PRH S163C:S177C reduced monocyte adhesion in TNF-α-stimulated HSVECs, down-regulation of ICAM-1 and VCAM-1 protein was investigated as a potential mechanism. To investigate the effect of PRH S163C:S177C expression on endothelial cell adhesion molecules, HSVECs infected with 1 x 10^8 pfu/ml Ad: PRH S163C:S177C supplemented with 4 x 10^8 pfu/ml of Ad: Control, or 5 x 10^8 pfu/ml of Ad: Control or left uninfected for 18 hours. Subsequently, cells were stimulated with 10 ng/mL TNFα for a further 24 hours to induce endothelial activation and an inflammatory response. Western blotting analysis demonstrated expression of ICAM-1 and VCAM-1 protein in uninfected HSVECs (FIGURE 4.10). Infection with Ad: Control did not significantly alter the amount of ICAM-1 and VCAM-1 proteins compared to uninfected HSVECs (FIGURE 4.10). However, a significant reduction in the amount of ICAM-1 and VCAM-1 proteins was observed in HSVECs overexpressing PRH S163C:S177C compared to both uninfected cells and cells infected with Ad: Control (FIGURE 4.10).

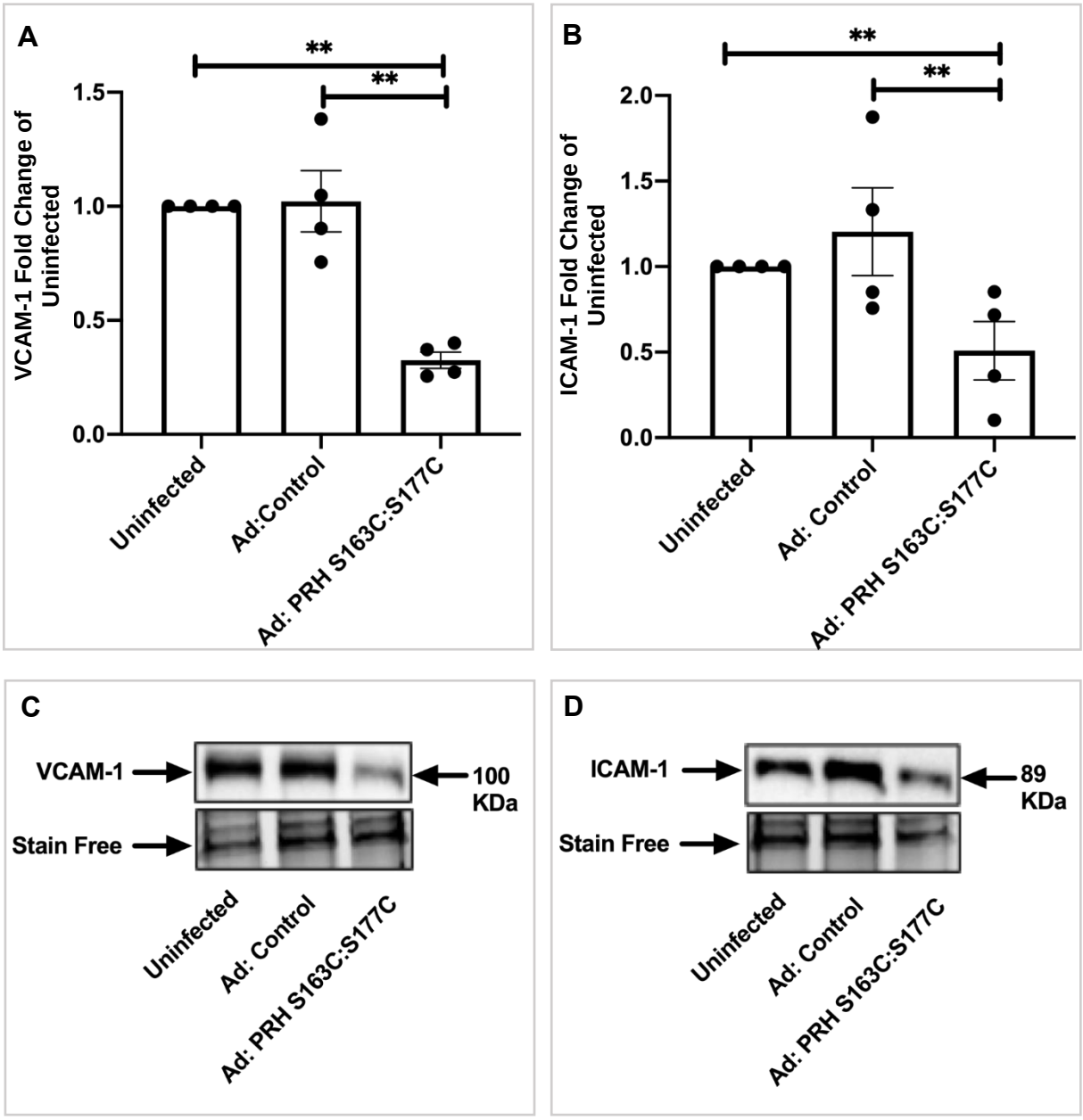

FIGURE 4.10 – Overexpression of PRH S163C:S177C reduced levels of ICAM-1 and VCAM-1 proteins in TNFα-stimulated HSVECs

HSVECs were infected with 1 x 10^8 pfu/mL Ad: PRH S163C:S177C combined with 4 x 10^8 pfu/mL Ad: Control, or 5 x 10^8 pfu/mL Ad: Control or were left uninfected. Quantification of VCAM-1 **(A)** and ICAM-1 **(B)** proteins was achieved using Western blotting. Data were normalised using stain-free bands and expressed as a fold change from uninfected control. ** indicates $p<0.01$, ANOVA, Student-Newman-Keuls Multiple Comparisons Test, n=4. Error bars indicate SEM. Representative Western blots of VCAM-1 **(C)** and ICAM-1 **(D)**. Stain-free bands served as a loading control. Approximate molecular weights are indicated on the right in kDa.

4.3.8 PRH S163C:S177C downregulated expression of IL-6 and MCP-1 in HSVECs

To ascertain whether adenovirus-mediated overexpression of PRH S163C:S177C inhibited the production of key endothelial inflammatory cytokines and mediators, the mRNA and protein levels of IL-6 and MCP-1 were quantified. HSVECs were infected with 1 x 10^8 pfu/ml Ad: PRH S163C:S177C supplemented with 4 x 10^8 pfu/ml of Ad: Control, or 5 x 10^8 pfu/ml of Ad: Control or were left uninfected for 18 hours. Cells were cultured for a further 24 hours in fresh endothelial cell growth medium. Cells were lysed and RNA was collected. IL-6 and MCP-1 mRNA levels were quantified via qPCR. Additionally, condition media was collected from cultured HSVECs to measure the levels of secreted IL-6 and MCP-1 proteins using ELISA.

qPCR analysis and ELISAs revealed that IL-6 and MCP-1 mRNAs and proteins, respectively were present in uninfected cells (FIGURE 4.11). Infection of HSVECs with Ad: Control did not significantly influence mRNA of IL-6 and MCP-1 compared to uninfected control HSVECs (FIGURE 4.11 A&B). Notably, infection of HSVECs with PRH S163C:S177C lowered levels of IL-6 and MCP-1 mRNAs with respect to HSVECs infected with Ad: Control and uninfected control HSVECs (FIGURE 4.11 A&B). ELISAs showed that compared to uninfected HSVECs, infection of HSVECs with Ad: Control did not affect levels of secreted IL-6 and MCP-1 proteins (FIGURE 4.11 C&D). Strikingly, adenovirus-mediated gene transfer of PRH S163C:S177C suppressed levels of secreted IL-6 and MCP-1 proteins with respect to both control groups (FIGURE 4.11 C&D).

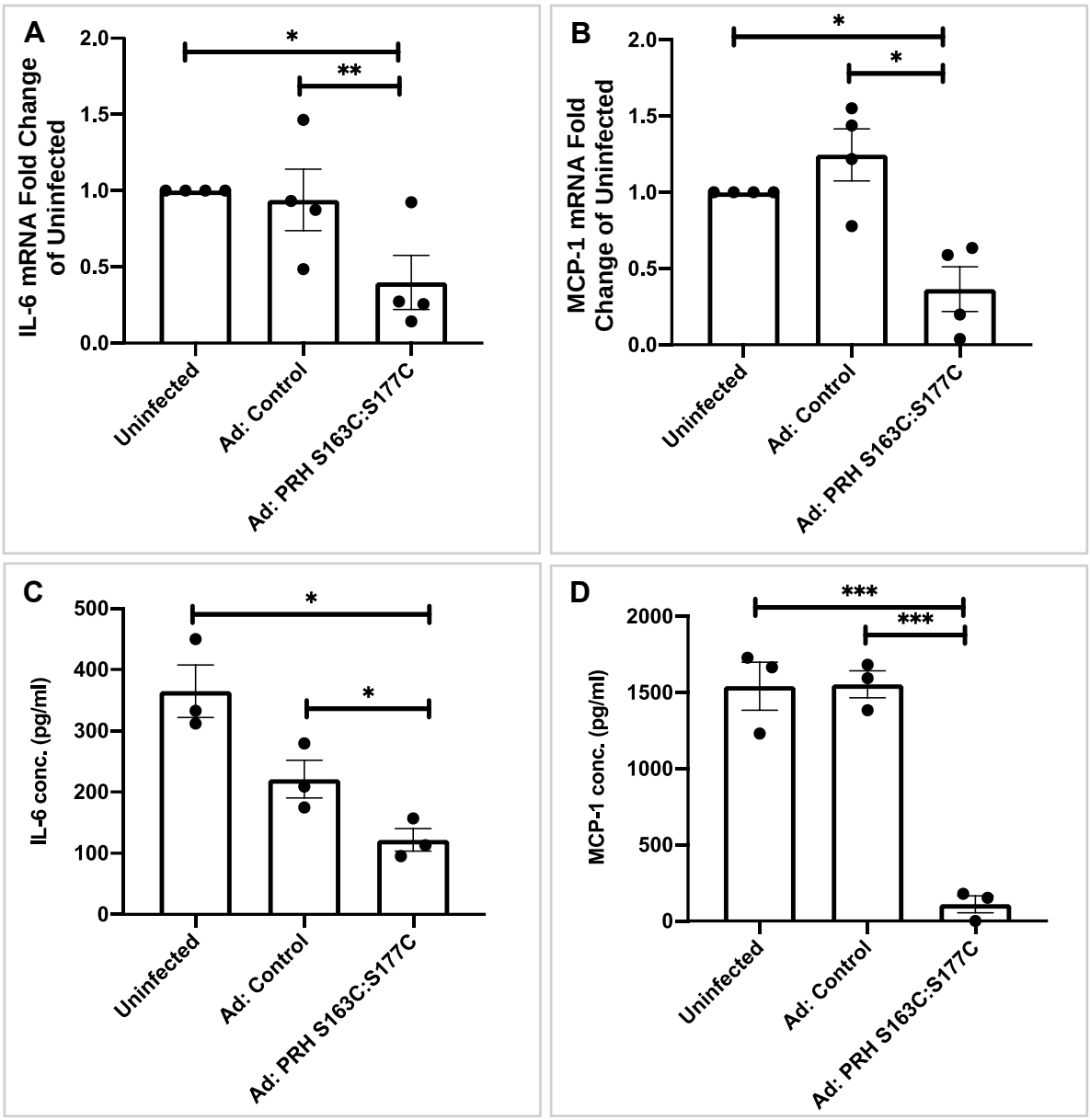

FIGURE 4.11 – Overexpression of PRH S163C:S177C downregulated IL-6 and MCP-1 mRNA and secreted protein levels in HSVECs

HSVECs were infected with 1 x 10^8 pfu/mL Ad: PRH S163C:S177C combined with 4 x 10^8 pfu/mL Ad: Control, or 5 x 10^8 pfu/mL Ad: Control or were left uninfected. Quantification of IL-6 **(A)** and MCP-1 **(B)** proteins in conditioned media by ELISA; data is expressed in pg/ml. Quantification of IL-6 **(C)** and MCP-1 **(D)** mRNA levels by qPCR. Data are normalised by 36B4-house keeping gene- and expressed as a fold change from uninfected control. * indicates $p<0.05$, ** indicates $p<0.01$, *** indicates $p<0.001$, ANOVA, Student-Newman-Keuls Multiple Comparisons Test, n=3. Error bars indicate SEM.

4.3.9 PRH S163C:S177C did not alter the permeability of a HSVEC monolayer

Regulation of permeability is maintained through an intricate network of intercellular contacts situated in the cleft between endothelial cells (Mundi *et al.,* 2018; Chen and Yeh, 2017). To ascertain whether adenovirus-mediated delivery of PRH S163C:S177C affected endothelial cell permeability, a simple permeability assay was conducted. HSVECs were infected with 1 x 10^8 pfu/ml Ad: PRH S163C:S177C supplemented with 4 x 10^8 pfu/ml of Ad: Control, or 5 x 10^8 pfu/ml of Ad: Control or were left uninfected for 18 hours. Cells were cultured for a further 24 hours in fresh endothelial cell growth medium. Treatment of HSVECs with TNFα was utilised as a positive control as it is known to significantly enhance endothelial cell permeability (Ley *et al.,* 2007). As expected, TNFα markedly enhanced HSVEC permeability compared to unstimulated HSVECs (FIGURE 4.12). Permeability was not significantly affected by infection with Ad: Control compared to uninfected HSVECs. Similarly, infection with Ad: PRH S163C:S177C did not affect endothelial cell permeability compared to uninfected control HSVECs and HSVECs infected with Ad: Control (FIGURE 4.12).

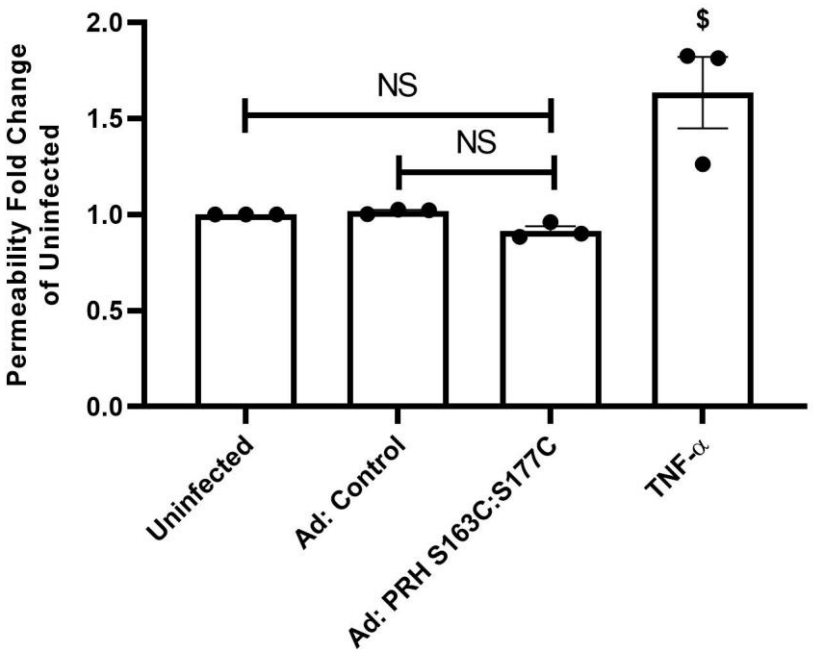

FIGURE 4.12 – Overexpression of PRH S163C:S177C did not permeability of HSVEC monolayers

HSVECs were infected with 1 x 10^8 pfu/mL Ad: PRH S163C:S177C combined with 4 x 10^8 pfu/mL Ad: Control, or 5 x 10^8 pfu/mL Ad: Control or were left uninfected. TNFα was used a positive control. Permeability of HSVECs seeded in Transwell inserts to streptavidin-HRP was quantified and expressed as fold change from uninfected. NS denotes not significant, $ indicates $p<0.05$ vs. uninfected, Ad: Control and PRH S163C:S177C, ANOVA, Student-Newman-Keuls Multiple Comparisons Test, n=3. Error bars indicate SEM.

4.4 DISCUSSION

The first aim of this chapter was to determine an appropriate viral dose for Ad: PRH S163C:S177C for achieving a comparable infection efficiency in HSVECs as achieved in HSV VSMCs. The second aim was to determine whether Ad: PRH S163C:S177C overexpression would interfere with HSVEC replication and migration, or apoptosis. The last aim was to examine whether PRH S163C:S177C overexpression affected inflammatory properties of HSVECs.

4.4.1 Comparable expression of PRH S163C:S177C in VSMCs and ECs

In Chapter 3, infection of HSV VSMCs with adenovirus encoding PRH S163C:S177C at a dose of 5 x 10^8 pfu/mL achieved a transfection efficiency of approximately 80%. Additionally, it was shown that infection of HSV VSMCs with 5 x 10^8 pfu/mL of Ad: PRH S163C:S177C or adenovirus expressing an empty vector did not induce apoptotic cell death, suggesting that the viral load was not compromising cell viability. As described in section 4.3.1, an equivalent infection efficiency was achieved in HSVECs using a much lower viral concentration of 1 x 10^8 pfu/mL of Ad: PRH S163C:S177C. Interestingly, adenovirus-mediated gene transfer of PRH S163C:S177C at a concentration of 1 x 10^8 pfu/mL was only sufficient to achieve an approximate 10% infection efficiency in primary HSV VSMCs (Section 3.3.1). However, the utilisation of different amount of virus would confound results when comparing the two cell types. Hence, in HSVECs, overexpression of PRH S163C:S177C required a combined dose of 4 x 10^8 pfu/mL Ad: Control and 1 x 10^8 pfu/mL Ad: PRH S163C:S177C to ensure an equivalent viral load was delivered as previously in HSV VSMCs.

Gene therapy for cardiovascular diseases has emerged as a potential therapy to treat vein graft stenosis. Major attention has been focused on how saphenous vein grafts can be treated *ex-vivo* prior to grafting (Owens *et al.,* 2015; George *et al.,* 2011). The goal of gene therapy is to introduce new genetic material into target cells without invoking toxicity to non-target tissues. Genetic material can be transferred via a vector or a vehicle (viral or non-viral) for delivery (Mali, 2013). However, gene transfer technologies related to efficacy and safety continue to present problems hence hindering significant progress in this field. In a non-viral approach, electroporation-mediated plasmid transfer into vein grafts *ex vivo* achieved potentially therapeutic effects (Yamoaka *et al.,* 2005). In 2014, Ohnaka and colleagues had demonstrated the ability of a non-viral and plasmid-based miR-145 gene transfer to venous grafts abrogated intimal thickening formation (Ohnaka *et al.,* 2014). Unfortunately, the efficiency of transfection to the vasculature is relatively poor limiting its success. Furthermore,

results of clinical trials of plasmid-mediated cardiovascular gene therapy to date have been disappointing as a result of their incapability to prompt high efficiency gene delivery *in vivo*. (Williams and Kingston, 2011). On the other hand, adenovirus has been used extensively for vascular gene therapy due to successful efficiencies *in vitro* and *in vivo*. Central to the entire discipline of achieving overexpression of therapeutic transgenes within the vasculature is the utility of adenovirus type-5 (George *et al.,* 2011; Kritz *et al.,*2008; George *et al.,* 2000); however, extremely high doses of adenovirus type-5 (typically $>10^{10}$ pfu per graft) are often required for successful uptake across the vessel wall. For example, it has been previously shown that adenoviral overexpression of TIMP-3 in porcine vein grafts promotes VSMCs apoptosis and retards intimal thickening (George *et al.,* 2000; George *et al.,* 2011). Although utility of adenoviruses is hampered by the potential of generating an immune response against DNA and its inability to traverse cells (Young and Dean, 2015; French *et al.,*1994; Newman *et al.,*1995), adenoviruses remain to have a clear advantage as the most efficient gene delivery vector due to it yielding high expression of the transgene which can be achieved *in vitro* and *in vivo* (Chen, Wilson and Muller, 1995; Kupfer *et al.,*1994). Hence, the present study utilised adenovirus gene transfer system to deliver the PRH S163C:S177C transgene.

Sensitivity of ECs to adenoviral vectors has been found to be much higher in comparison to VSMCs (Zhou *et al.,*1995). Reportedly, transfection rates of approximately 80% were found in ECs although a disappointing transfection efficacy of only 40% in VSMCs at the viral titre of 10×10^9 pfu/ml (Zhou *et al.,*1995). In support of this notion, profiling of receptor expression in VSMCs and ECs has illustrated vanishingly low levels of the adenovirus primary attachment receptor called as coxsackievirus and adenovirus receptor (CAR) in human VSMCs (Parker *et al.,* 2013) and an absence of expression in intact human vessels (Vigl *et al.,* 2009) which could explain the discrepancy in infection efficiencies and necessity for high input titres of adenovirus for efficient infection in VSMCs in this project and previous studies. Although there is a general lack of knowledge to explain this, Parker and colleagues suggested that at high titres, it is probable that the observed upregulation of integrin αvβ3 and αvβ5 in human VSMCs promotes adenovirus internalisation, though this does not necessarily explain the mechanism for cell attachment (Wickham *et al.,*1993).

4.4.2 PRH S163C:S177C does not have detrimental effects on HSVEC proliferation, migration and survival

In designing therapies for vein graft disease, it is essential that the intervention does not exacerbate endothelial cell loss or impair re-growth of endothelium so as to prevent postoperative thrombotic occlusion and eventual failure of the vein graft.

As mentioned previously, there is evidence to suggest that cultured HUVECs may not be representative of the adult endothelium; therefore, in this study, primary cultures of HSVECs were utilised as these are the most relevant cell type, particularly for studying HSV graft failure. Previously in our laboratory, Wadey *et al.* subjected primary cultures of HUVECs and HSVECs to plasmid-mediated overexpression of wild-type PRH to examine its effects on endothelial cell proliferation, migration and survival. Interestingly, in contrast to the effects observed in VSMCs, overexpression of wild-type PRH did not significantly affect cell cycle progression, cell motility or cell survival indices in HSVECs *in vitro* (Wadey *et al.,* 2017). Similarly, in this study, it was observed that overexpression of PRH S163C:S177C in HSVECs via adenoviral delivery did not significantly affect endothelial proliferation, migration or apoptosis (Sections 3.3.2, 3.3.3 and 3.3.4). Of interest, additional work in the recent years have been conducted investigating the effect of wild-type PRH in mouse lung microvascular endothelial cells have shown translocation of uPA to the cell nuclei through its kringle or binding motif of wild-type PRH upregulates vegfr1 and vegfr2 expression. Such transcriptional repression has been reported to induce EC motility, invasion and proliferation thereby promoting angiogenesis. Although, the mechanism of how it induces an angiogenic switch through coordinate up-and/or down-regulation of genes involved in endothelial cell proliferation, adhesion and migration warrants further investigation (Stepanova *et al.,* 2016).

In summary, these findings demonstrate that forced expression of PRH S163C:S177C did not affect apoptosis, proliferation or migration of HSVECs, indicating that using such an intervention to reduce intimal thickening via retarding VSMC proliferation should not have detrimental effects on re-endothelialisation. Future studies directly measuring re-endothelialisation may involve investigating the effect of re-endothelialisation in the vessel scaffold.

4.4.3 The anti-inflammatory properties of PRH S163C:S177C in HSVECs

The initial reaction to vascular injury is associated to the inflammation of the arterial wall. Inflammation may be multifactorial although aberrant influx of monocytes is one of the first phenomena seen as a result of vascular injury during intimal hyperplasia (Yang, Chang and Wei, 2016). The augmentation of cytokines, chemo-attractants and cell adhesion molecules has been increasingly recognised as key indicators of disturbed endothelial function (Ward *et al.,* 2017). For instance, Interleukin-6 (IL-6) and monocyte chemotactic factor-1 (MCP-1) are pro-inflammatory mediators implicated in the pathogenic mechanism of vascular disease progression (Mudau *et al.,* 2012). In addition, it is known that augmented levels of these

proinflammatory cytokines mediate the acceleration of neointimal hyperplasia within the implanted venous graft (Mudau *et al.,*2012; Ward *et al.,* 2017). Other inflammatory mediators such as the intracellular adhesion molecule-1 (ICAM-1) and vascular cellular adhesion molecule-1 (VCAM-1) as well as including those of the selectin family (E-selectin and P-selectin) permit monocyte trafficking into the blood vessel, via adherence of monocytes to the vascular endothelium, and transmigration into the vessel walls (Yang, Chang and Wei, 2016). Furthermore, vascular wall impermeability to solutes and lipoproteins is an integral property of a functional endothelium (Mundi *et al.,*2018; Chen and Yeh, 2017).

Ultimately, monocyte recruitment, cytokine release and increased permeability of the graft wall leads to compromised graft efficacy due to subsequent vein wall adaptation and abnormal functionality within the endothelium. The total sum of these processes acts as the driving mechanisms resulting hyperplastic response and pathological intimal hyperplasia and lumen loss failing vein graft (Ward *et al.,* 2017). For example, the macrophage was acknowledged as a fundamental cellular mediator of intimal thickening within the SVG in which macrophage depletion also reduces hyperplasia of vein grafts (Hoch *et al.,*1994). Focusing on the maintenance of EC functionality post-surgical trauma is integral in pre- and peri-operatively of vein grafts. Current treatments addressing the implications of these inflammatory components have received attention in the recent years. Anti-inflammatory cytokine-based therapies have emerged wherein currently, statins and aspirin treatment remain to be the only recommended primary intervention for patients with CAD (Kang *et al.,*2013; Hillis *et al.,* 2012). Statins exerts several modes of actions during cardiothoracic surgical procedure including primarily through cholesterol lowering by inhibiting β-Hydroxy β-methylglutaryl-CoA (HMG-CoA) reductase (Kulik *et al.,* 2011). These have been shown to improve endothelial function, thwart VSMC proliferation and reduce macrophage activation and improve vascular endothelial function. In the CASCADE (Clopidogrel after Surgery for Coronary Artery Disease) trial, statin therapy has been proven to improve management of post-operative hyperlipidaemia/dyslipidaemia and prevent vein graft stenosis in coronary grafts after CABG (Kulik *et al.,* 2011). Although several studies are underway to find new targets and therapies, there are somewhat key unmet needs in the field of VGF prevention. The principal findings from the CANTOS trial showed that canakinumab (150 mg), a monoclonal antibody targeting Interleukin 1 beta (IL-1β) inhibition, has demonstrated positive effects on inflammatory therapy in patients with atherosclerosis (Ridker *et al.,* 2017). Unfortunately, progress in the overall effect of this anti-inflammatory agent had been underwhelming and the prospect of targeting inflammation seems to be slim to none. This is due to several reasons due to high risk of side effects such as higher rates of infection and the significant risk of fatal infection as well as the expensive annual cost of approximately $200,000 (Thompson and Nidorf, 2018).

In this chapter the anti-inflammatory profile of PRH S163C:S177C has been examined. Two VGF relevant inflammatory scenarios were utilised TNFα-activation and LSS. Monocyte recruitment is one of the earliest events in VGF (Yang, Chang and Wei, 2016). PRH S163C:S177C was able to prevent monocytes from adhering to TNFα-stimulated ECs. TNFα is a pleiotropic pro-inflammatory cytokine regulated at both the transcriptional and translational level. TNFα is produced by a variety of cell types such as macrophages, monocytes, endothelial cells, fibroblasts, and VSMCs (Ley *et al.,* 2007; Ozaki, 2007). It has been demonstrated to possess a pivotal role in vein graft neointima by triggering interactions between invading monocytes and vascular endothelial cells thereby activating inflammation-induced endothelial dysfunction and apoptosis (Ward *et al.,* 2017). Additionally, TNFα enhances adhesion molecules expression in human vascular endothelial cells (Ley *et al.,* 2007) and VSMCs (Yan *et al.,* 2017).

Following implantation into the arterial circulation system, the implanted vein graft undergoes haemodynamic adaptation that promotes graft stenosis. Several previous studies have implicated LSS in the development of EC inflammatory responses (Chiu *et al.,* 2011; Shyy *et al.,*1994; Dewey *et al.,*1981). At the site of the end-to-side anastomosis and venous valves, LSS on the endothelia-blood interface facilitates recruitment of circulating leukocytes and inflammatory cells. LSS often leads to EC activation and consequently impairs the function of the endothelium resulting in platelet aggregation and stimulate proliferative VSMCs (Kumar *et al.,* 2018). In support of this notion, LSS has been associated with increased expression of pro-inflammatory mediators and recruitment of leukocytes in response to release of cytokines including TNFa, whereas exposure to laminar blood flow and high shear stress are anti-inflammatory and thereby atheroprotective (Yoshizumi *et al.,* 2003).

As observed with TNFα-stimulation, under LSS culture conditions, there was decreased monocyte adhesion to HSVECs infected with Ad: PRH S163C:S177C. In activated endothelial cells, upregulation and presentation of adhesion molecules VCAM-1 and ICAM-1 has been reported to facilitate monocyte adhesion (Chen and Yeh, 2017). Moreover, several studies have reported an upregulation of these adhesion molecules in the context of VGF (Zhang *et al.,* 2013; George *et al.,* 2011; Hölschermann *et al.,* 2006). Since endothelial cell activation is mediated by combinatorial factors, this current study selected to investigate the effects of PRH S163C:S177C on the endothelial expression of adhesion molecules, VCAM-1 and ICAM-1 as these are recognised to play a critical role in mediating firm adhesion of circulating leukocyte into the vascular endothelium under pathological conditions (Sans *et al.,* 1999). On the other hand, well-known markers of inflammation, IL-6 and MCP-1 were selected to be examined owing to their recognised pro-inflammatory role in VGF (Fu *et al.,*2012; Christiansen *et al.,* 2004). For instance, studies have described the critical role of IL-6 stimulation in MCP-1

secretion and recruitment of monocytic cells (Su *et al.,* 2017). In response to PRH S163C:S177C overexpression, transcript and protein levels of these two inflammatory proteins were downregulated in HSVECs. Thus, validating a novel, anti-inflammatory role for PRH S163C:S177C. It is important to note that since PRH S163C:S177C is known to be important in multiple cell types, this work has important implications for the emerging role of highly conserved serine/threonine kinase CK2 in immunity (Gibson and Benveniste, 2019). As described in the previous chapters, PRH S163C:S177C is a mutant version of wild-type PRH that represses CK2 phosphorylation (Jayaraman *et al.,* 2018; Siddiqui *et al.,* 2017; Wadey *et al.,* 2017). Recent work on inflammatory diseases has reported CK2 augments inflammation signifying inhibition may warrant anti-tumour immunity. For example, glomerulonephritis is a progressive inflammation and CK2 expression have been identified to be markedly increased at the inflammatory sites in rat glomerulonephritis model (Yamada *et al.,* 2005). Conversely, the decline in pro-inflammatory cytokine secretion of IL-6 was mediated by pharmacologic inhibition of CK2 using Silmitasertib (CX-4945) in inflammatory breast cancer xenograft models (Drygin *et al.,* 2011). Often linked to chronic inflammation, hepatocellular cancer (HCC) has been associated with overexpression of CK2α. In particular, the oncogenic role of CK2α in HCC has been demonstrated by its ability to enhance proliferation, colony formation, migration, and invasion *in vitro* (Zhang *et al.,* 2015).

Under normal circumstances, the quiescent endothelium protects the vascular tree by promoting anti-coagulant and anti-inflammatory properties and mediates endothelial permeability preventing thrombus formation (Chiu *et al.,* 2011). The exposure of the endothelium in vascular injury may cause endothelial barrier disruption and increased vascular permeability which has been linked to ICAM-1 expression (Sumagin, Lomanika and Sarelius, 2008). Previous data have demonstrated that uPA increases EC permeability through VEGF signalling although binding of uPA to wild-type PRH inhibits their capacity to repress promoter activity of vehgr1 and vehgr2 (Stepanova *et al.,* 2016) highlighting PRH S163C:S177C to potentially regulate the control of vascular permeability. In this study, following confirmation of an anti-inflammatory response to PRH S163C:S177C in cultured HSVECs, endothelial permeability was examined in unstimulated HSVECs although there were no significant differences observed across all conditions. Perhaps pre-treatment of HSVECs with TNFα to destabilize endothelial junctions would have yielded a role for PRH S163C:S177C in restoring barrier function in activated endothelial cells. Interestingly, a previous report demonstrated Silmitasertib-treatment int mice post TNFα stimulation was associated with decreased microvascular permeability. Although, under non-stimulated conditions, the CK2 inhibitor Silmitasertib which acts to restore wild-type PRH was unable to modify permeability and EC-leukocyte binding (Ampofo *et al.,* 2015).

4.4.3 Chapter Summary

To date, no study has comprehensively examined the relationship between PRH S163C:S177C and inflammatory markers in endothelial cells. This project has illustrated that to achieve a similar infection efficiency in HSVECs and HSV VSMCs different doses of adenovirus are required. The results indicate that PRH S163C:S177C is unlikely to significantly disrupt re-endothelialisation, though it is unlikely to assist it either. Interestingly, PRH has demonstrated efficacy in attenuating inflammatory mediators of VGF suggesting the anti-inflammatory properties of Ad: PRH S163C:S177C. These findings may represent an exciting and unexplored strategy for improving vein graft outcome, with PRH emerging as a potential therapeutic approach for localised inhibition of inflammation at the time of vein grafting.

5.

OVEREXPRESSION OF PRH S163C:S177C ATTENUATED INTIMAL THICKENING IN MURINE CAROTID-ARTERY LIGATION MODEL

5.1 INTRODUCTION

Autologous HSV grafts conduits are the most favoured for revascularisation of the distal cardiac tissue (Harskamp *et al.,* 2013). Despite the frequent use of HSV, the risks of thrombotic occlusions, intimal thickening and superimposed atherosclerotic lesions within grafted conduits during 10 years after surgery persists to be a major clinical problem (Wan *et al.,* 2012). To date, there are 2,600 gene therapy clinical trials with a remarkable upsurge in the number of trials entering late phases, demonstrating the promise of this exciting therapeutic approach (Ginn *et al.,* 2018). The previous chapters revealed that overexpression of a modified form of the transcription factor PRH to a more stable form resistant to CK2 phosphorylation in endothelial cells and VSMCs yielded beneficial properties that could result in reduced intimal thickening and thereby retard VGF. To directly assess the efficacy of PRH S163C:S177C to reduce intimal thickening *in vivo* use of an animal is required.

Studies utilising animal models of intimal thickening have enabled researchers to better evaluate the potential of novel therapies for vein graft failure as well as unravel the molecular mechanisms behind restenosis (Holt and Tulis, 2013). For example, vascular injury induced by balloon angioplasty in rats has served as a powerful tool for studying vascular remodelling (Li *et al.,*2017). The mouse model of femoral artery denudation injury is another established model of intimal thickening (Lindner and Kumar, 1997) which stimulates arterial injury via endothelial denudation and arterial stretch (Le *et al.,*2015). Although in comparison to the other two models, ligation of the carotid artery is a robust and reproducible method. Firstly, a complete ligation of the vessel near the carotid bifurcation in a mouse disrupts the blood flow hence, inducing rapid VSMC proliferation and intimal thickening distal to the ligation site (Smolock and Berck, 2012). Secondly, it is highly achievable, reproducible injury model that stimulates intimal thickening without causing injury to the tunica media of the blood vessel. Lastly, this model differs from others as it does not require mechanical trauma and protects the endothelium (Xu, 2004; Ku, 1985). In line with this notion, there are an accumulating evidence from our group demonstrating the utility of a murine model for vascular occlusion using carotid artery ligation in C57BL6/J mice to induce intimal thickening. For example, Brown and colleagues were able to demonstrate that Wnt4-mediated proliferation is unaffected by age using the same model of stenosis (Brown *et al.,*2017). In a study by Curtis and colleagues, overexpression of the dominant negative N-cadherin using an adenovirus permitted significant suppression of intimal thickening in the mouse carotid artery ligation model (Hulin-Curtis *et al.,* 2017). Similarly, we employed the use of C57BL6/J mice which has the advantages of strain stability and ease of breeding that makes them predominantly useful in our study. It is inexpensive and the easiest model to use because lesions are typically

acquired precipitously, and it does not demand much equipment (Xu, 2004). For these reasons, this *in vivo* model of intimal thickening in particular has proven to be successful in testing functions of the target genes, thus, an attractive preliminary tool and experimental system to elucidate knowledge concerning the pathogenesis of vein graft intimal thickening.

The potential of PRH S163C:S177C in suppressing VSMC proliferation and migration has been demonstrated in chapter 3. Additionally, PRH S163C:S177C augmented the VSMCs phenotypic differentiation into the 'contractile' state with high levels of calponin and smoothelin. Moreover, PRH S163C:S177C exerted anti-inflammatory properties in HSVECs without influencing endothelial repair capacity through proliferation, migration and apoptosis. Together this provides strong *in vitro* data implicating that artificial modulation of PRH S163C:S177C possess the ability to impede the VSMC pathogenic phenotype without detrimental effects on endothelial cells. Consequently, assessment of the ability of PRH S163C:S177C to retard intimal thickening in a pre-clinical model is warranted. Utilisation of the mouse carotid artery ligation model enabled evaluation of the ability of PRH S163C:S177C to disrupt intimal thickening and examine its effects on VSMC behaviour and phenotype *in vivo*.

5.2 HYPOTHESIS

The hypothesis for this chapter were:

Overexpression of PRH S163C:S177C in ligated mouse carotid arteries *in vivo*:

- suppresses ligation-induced intimal thickening,
- upregulates contractile proteins and thereby may prevent VSMC de-differentiation,
- does not significantly reduce endothelial coverage.

This hypothesis was tested by:

- Examining the effect of PRH S163C:S177C overexpression on intimal thickening in the murine carotid artery ligation model via assessing:
    - intimal:medial ratio, lumen occlusion, proliferation, migration, and intimal and medial cell density in both intimal by histological staining and immunohistochemistry for BrdU.
- expression of contractile markers smoothelin and calponin by immunohistochemistry,
- endothelial coverage by immunohistochemistry for CD31

5.3 RESULTS

5.3.1 Attenuation of intimal thickening, I/M ratio, and lumen occlusion by overexpression of Ad: PRH S163C:S177C in the murine carotid artery ligation model

The first aim was to determine the effect of PRH S163C:S177C on intimal thickening *in vivo* was assessed in a reproducible and established model of restenosis which is routinely employed in our laboratory (Williams *et al.,* 2011). The model entails ligation of the left common carotid artery near the carotid bifurcation to induce intimal thickening. However, before embarking on the 28-day study it was important to ensure expression of c-myc-tagged PRH S163:S177C protein at 7 days after adenovirus delivery and ligation. In the pilot study, a total of 7 mice (4 males and 3 females) underwent ligation surgery. Following ligation, arteries were surrounded by 100ul of 30% (w/v) Pluronic F-127 (Sigma Aldrich) gel containing 1.33 x 10^8 pfu/mL replication-defective adenoviral constructs encoding either an empty vector (Ad: Control) or c-myc-tagged S163C:S177C PRH. After 7 days left carotid arteries were removed for immunofluorescence detection of c-myc-tagged PRH S163C:S177C. Immunofluorescence confirmed no expression of c-myc-tagged protein in left carotid arteries from mice infected with Ad: Control 7 days after infection, while c-myc-tagged PRH S163C:S177C protein was observed within the left carotid arteries 7 days post ligation infected with Ad: PRH S163C:S177C (FIGURE 5.1 A&B). As expected, the detected c-myc-tagged PRH S163C:S177C protein was exclusively detected within nuclei (FIGURE 5.1 B). Sections incubated with non-immune rabbit IgG detected no c-myc-tagged protein (FIGURE 5.1 C&D, demonstrating the specificity of the protocol.

For the analysis of intimal thickening in the 28-day study, 14 mice in each group (7 males and 7 females) underwent ligation surgery. Following ligation, arteries were surrounded by 30% (w/v) Pluronic F-127 (Sigma Aldrich) gel containing 1 x 10^8 pfu/mL replication-defective adenoviral constructs encoding either an empty vector (Ad: Control) or c-myc-tagged S163C:S177C PRH. After carotid ligation injury, mini-osmotic pump was implanted sub-cutaneously to deliver BrdU and enable proliferation and migration to be quantified. Intimal thickening was allowed for 28 days before retrieval of left carotid arteries. Out of the 28 mice that underwent ligation, two mice died during surgery due to the anaesthetic and prior to addition of the adenovirus, and one mouse in the Ad: Control group was excluded from analysis due to an incomplete artery ligation. Thus, in total, 13 and 12 ligated left carotid arteries were analysed in the Ad: Control and Ad: PRH S163C:S177C groups, respectively.

Miller's Elastic van Giesen (EVG) staining revealed intimal thickening formation 28 days post ligation in the longitudinally oriented formalin-fixed and paraffin-embedded carotid arteries. The intimal area, intimal-medial ration and % occlusion was measured as described in 2.12.2.2. A significant reduction in intimal area in carotid arteries infected with Ad: PRH S163C:S177C with respect to the empty vector (Ad: Control) (FIGURE 5.2). The intimal-medial ratio was markedly greater in the Ad: Control group compared to the Ad: PRH S163C:S177C group (FIGRUE 5.2). Furthermore, the Ad: Control group exhibited 80% lumen occlusion whilst the % occlusion observed in the Ad: PRH S163C:S177C group was significantly lower at approximately 40% (FIGURE 5.2).

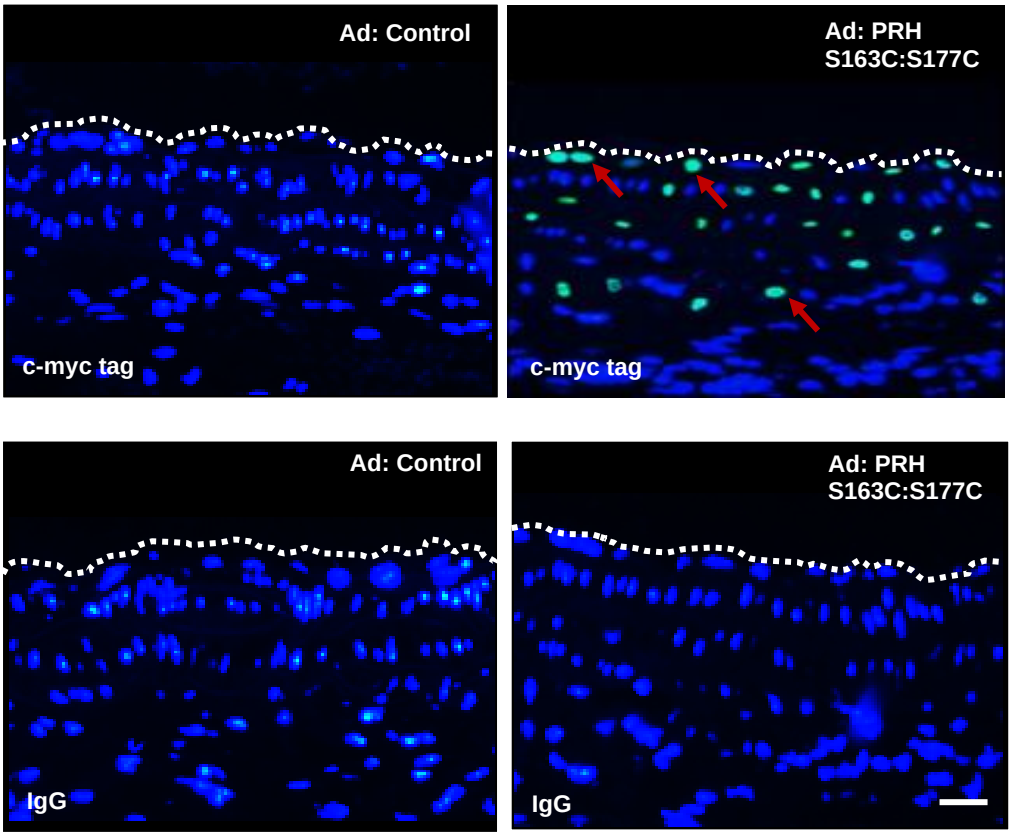

FIGURE 5.1: Overexpression of c-myc-tagged PRH S163C:S177C protein in ligated carotid arteries

Carotid arteries were ligated in C57BL6/J mice then infected with Ad: Control or Ad: PRH S163C:S177C.

Representative images of immunofluorescence for c-myc-tagged protein at day 7 post ligation and infection. White dashed line indicates the intima-lumen boundary. Positive cells have green nuclei (some are indicated with red arrows); negative cells are stained with DAPI and have blue nuclei. Scale bar represents 25 μm and applies to all panels. n=3 (Ad: Control) and n=4 (Ad: PRH S163C:S177C).

FIGURE 5.2: Overexpression of PRH S163C:S177C protein attenuated neointimal area, I/M ratio and % occlusion of the lumen

Ligated mouse carotid arteries received adventitial delivery of Ad: Control (n=13) or Ad: PRH S163C:S177C (n=13). After 28 days the arteries removed and subjected to EVG staining. Representative images of EVG-stained left carotid arteries (**A**) Ad: Control and (**B**) Ad: PRH S163C:S177C. Scale bar represents 200 μm (top panels) and 50 μm (bottom panels). The intimal area (**C**), intimal:medial (I/M) ratio (**D**) and percentage occlusion of the lumen (**E**) were measured. * indicates $p<0.05$, **** indicates $p<0.0001$, unpaired, two-tailed Student's *t*-test, n=13 (Ad: Control) and n=12 (Ad: PRH S163C:S177C). Error bars indicate SEM.

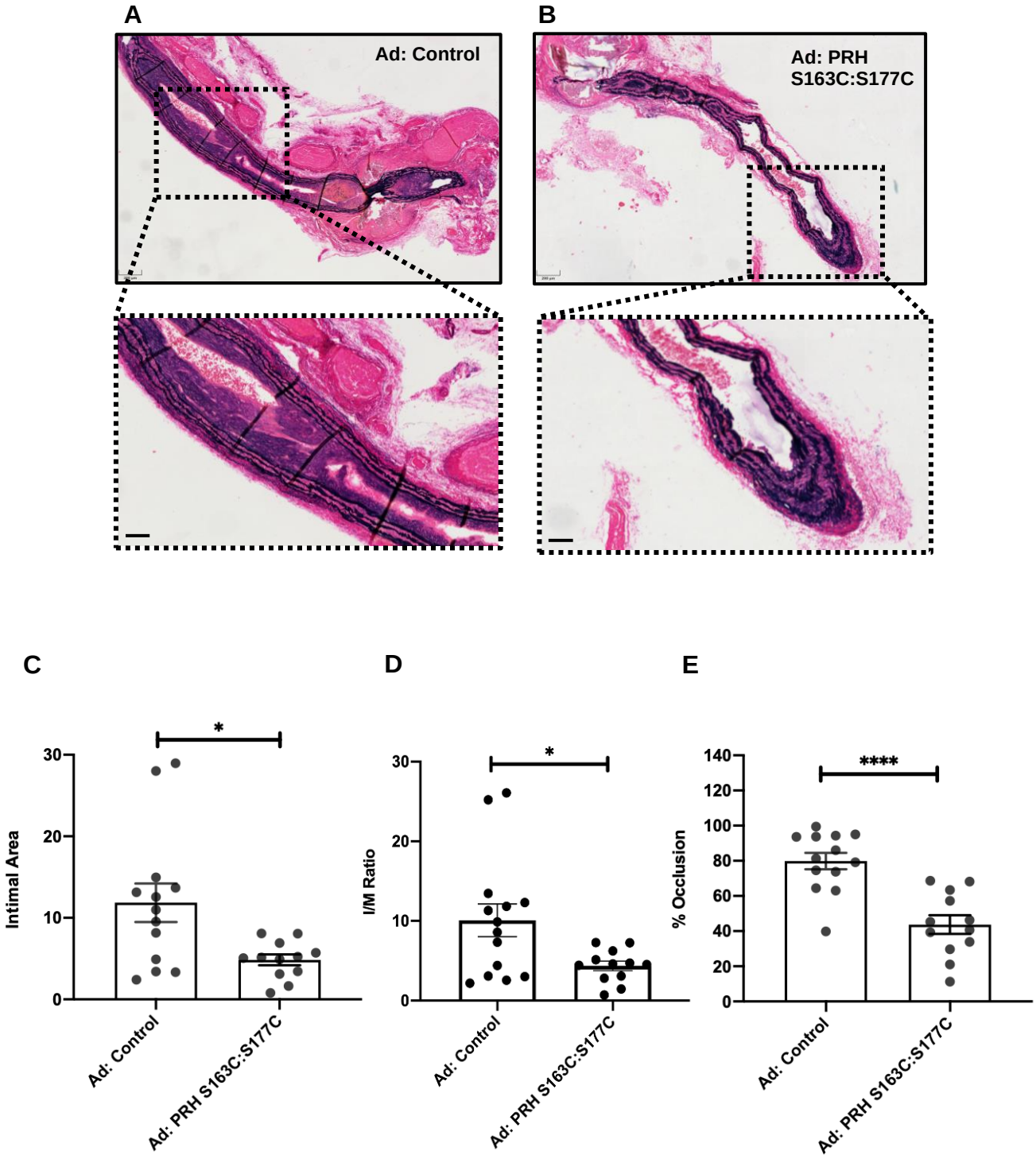
A
Ad: Control
B
Ad: PRH
S163C:S177C
C
Intimal Area
30
20
10
0
*
Ad: Control
Ad: PRH S163C:S177C
D
I/M Ratio
30
20
10
0
*
Ad: Control
Ad: PRH S163C:S177C
E
% Occlusion
140
120
100
80
60
40
20
0
****
Ad: Control
Ad: PRH S163C:S177C

5.3.2 Overexpression of PRH S163C:S177C attenuated intimal proliferation without affecting the cell density

It was observed in chapter 3 that overexpression of PRH S163C:S177C inhibited proliferation of isolated HSV VSMCs (see section 3.3.2). To determine whether PRH S163C:S177C suppression of VSMC proliferation *in vivo*, mini-osmotic pumps containing BrdU were implanted subcutaneously at the time of ligation. BrdU release from the mini-osmotic pump enabled quantification of the fraction of cells undergoing replication in the media and intima using immunohistochemistry for incorporated BrdU. Furthermore, intimal cell density was calculated by counting DAPI-stained nuclei and normalising this value by the intimal area. In addition, to provide an estimate of intimal-directed VSMC migration, non-proliferative, BrdU-negative cells were quantified and normalised by the length of the intimal thickening.

The proportion of proliferative BrdU-positive nuclei in the media and intima was significantly lower in the Ad: PRH S163C:S177C group than in the Ad: Control group (FIGURE 5.3A&B). The estimated number of migratory cells (BrdU-negative nuclei in the intima) was also significantly lower in the Ad: PRH S163C:S177C group than in the Ad: Control group (FIGURE 5.3C). Sections incubated with non-immune mouse IgG showed minimal staining. Overexpression of PRH S163C:S177C did not however affect the cell density in both the medial and intimal layers (FIGURE 5.4). Together, these data suggest that Ad: PRH S163C:S177C inhibits medial and intimal VSMC proliferation as well as migration of cells into the intima, and thereby retards intimal thickening.

FIGURE 5.3: Overexpression of PRH S163C:S177C attenuated cell proliferation and migration in ligated carotid arteries

Carotid arteries were ligated in C57B/L6 mice to induce intimal thickening then infected with Ad: Control (**A**) or Ad PRH S163C:S177C (**B**). Representative images of immunohistochemistry for BrdU at day 28. Black dashed line indicates the intima-media boundary. BrdU-positive cells have brown nuclei (some are indicated with red arrows); BrdU-negative cells are stained with haematoxylin and have grey/blue nuclei for Ad: Control (**C**) and Ad PRH S163C:S177C (**D**) (some are indicated with black arrows). The scale bar represents 50 μm and applies to all images.

Proliferation was quantified in the media (**E**) and intima (**F**) and expressed as the percentage of BrdU-positive cells. The rate of migration (**G**) was estimated by quantifying the number of BrdU-negative nuclei in the intima divided by the length of the intimal thickening. NS denotes not significant, * indicates $p<0.05$, ** indicates $p<0.01$, unpaired, two-tailed Student's *t*-test, n=6. Error bars indicate SEM.

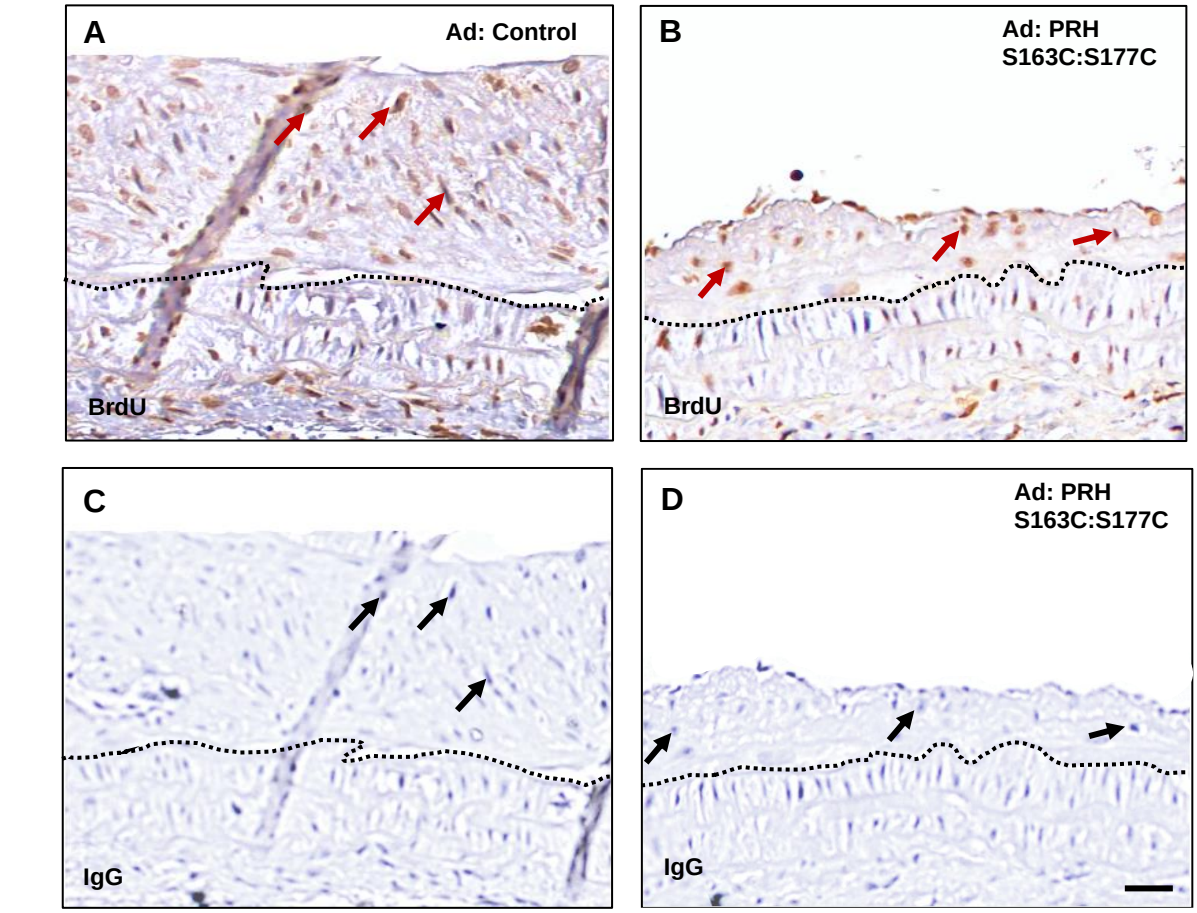
A
Ad: Control
BrdU
B
Ad: PRH
S163C:S177C
BrdU
C
IgG
D
Ad: PRH
S163C:S177C
IgG

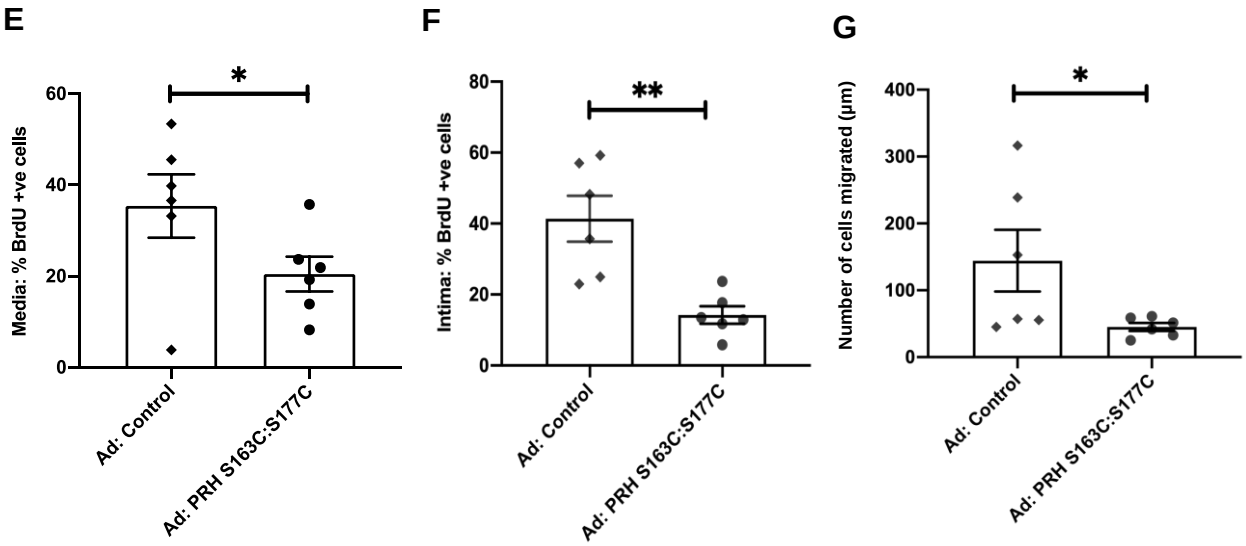
E
Media: % BrdU +ve cells
60
40
20
0
*
Ad: Control
Ad: PRH S163C:S177C
F
Intima: % BrdU +ve cells
80
60
40
20
0
**
Ad: Control
Ad: PRH S163C:S177C
G
Number of cells migrated (µm)
400
300
200
100
0
*
Ad: Control
Ad: PRH S163C:S177C

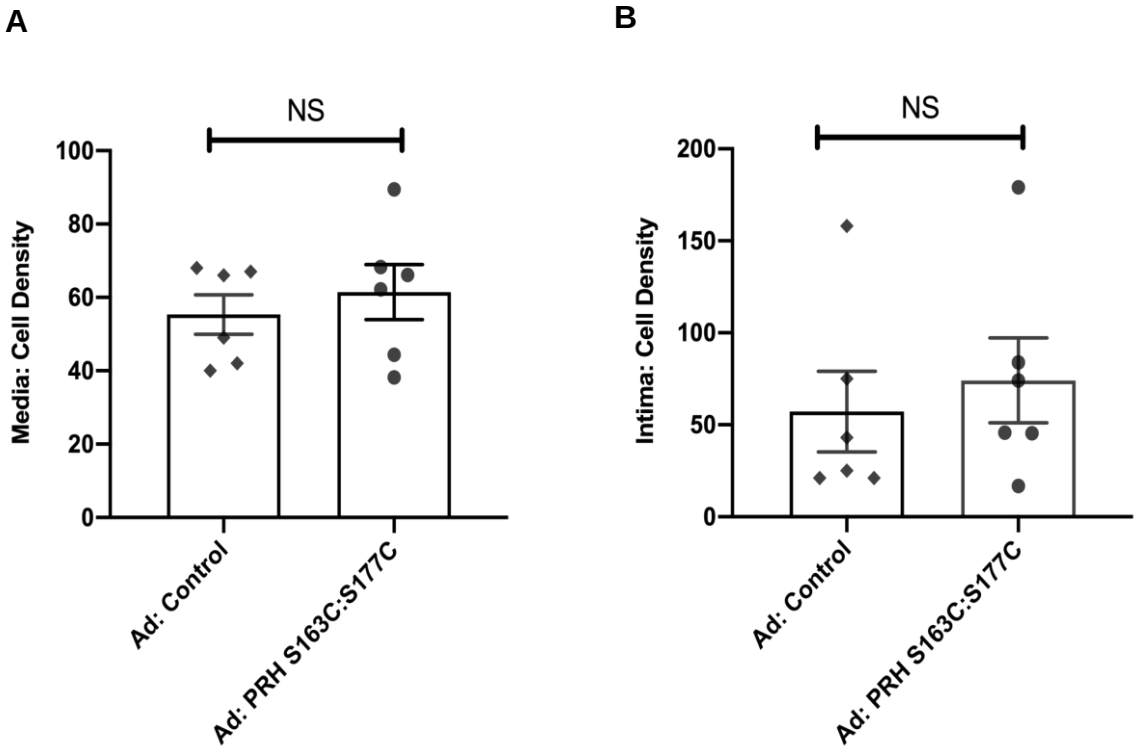

FIGURE 5.4 Overexpression of PRH S163C:S177C did not affect cellular density in ligated carotid arteries

Carotid arteries were ligated in C57B/L6 mice to induce intimal thickening then infected with Ad: Control or Ad PRH S163C:S177C. Quantification of cell density in the medial **(A**) and intimal (**B**) layers 28 days after ligation. Data is expressed as the number of cells per mm^2 of neointima. NS denotes not significant, unpaired, two-tailed Student's *t*-test, n=6. Error bars indicate SEM.

5.3.3 Overexpression of PRH S163C:S177C did not influence expression of α smooth muscle cell actin

To identify VSMCs in the ligated left carotids, sections were subjected to immunofluorescence detection of αSMA. Almost all cells in the media and the intima (except some on the intimal surface) were αSMA positive. There was no significant difference was noted in αSMA density between Ad: Control and Ad: PRH S163C:S177C groups (FIGURE 5.5). Negative control sections probed with non-immune mouse IgG showed no staining.

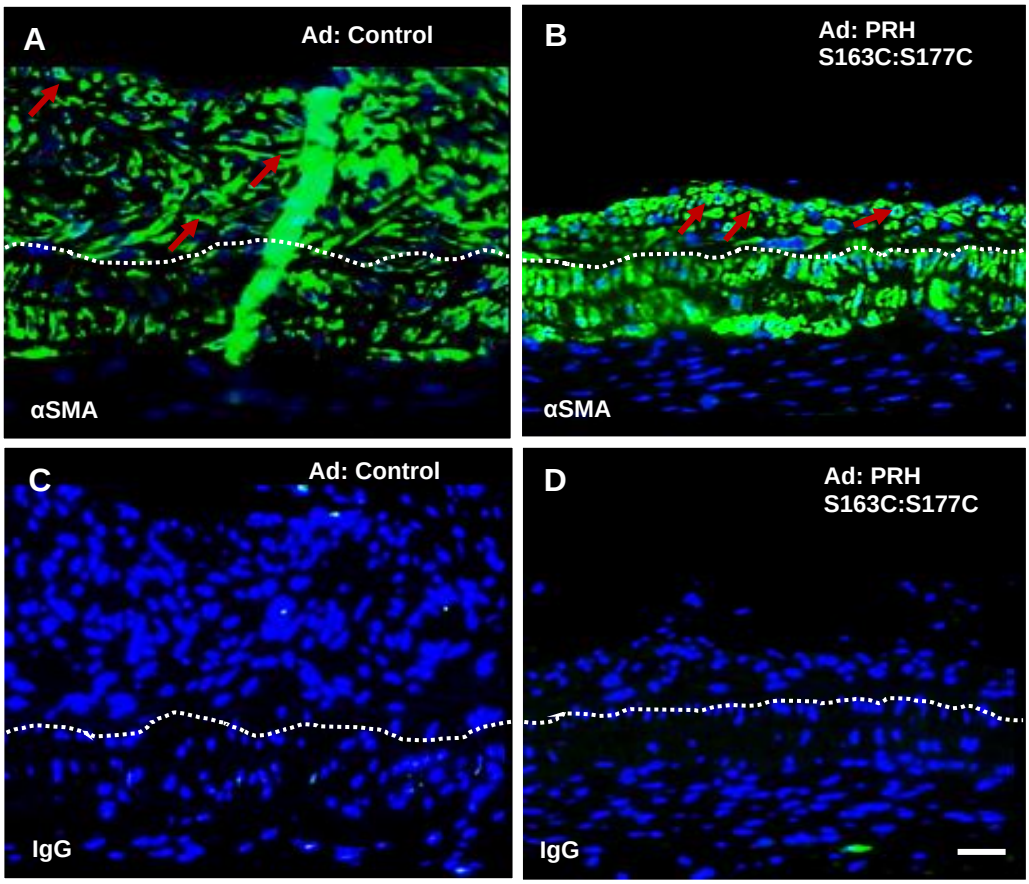

FIGURE 5.5: Overexpression of PRH S163C:S177C did not influence expression of αSMA protein in ligated carotid arteries

Carotid arteries were ligated in C57B/L6 mice to induce intimal thickening then infected with Ad: Control (**A&C**) or Ad PRH S163C:S177C (**B&D**).

Representative images of immunofluorescence for αSMA (**A&B**) and non-immune IgG (**C&D**), 28 days after ligation. αSMA -positive cells are stained green (some are indicated with red arrows) and the nuclei of all cells are stained blue/grey with DAPI. White dashed line indicates the intima-media boundary. Scale bar represents 25 μm and applies to all panels.

5.3.4 Overexpression of PRH S163C:S177C did not influence expression of the contractile markers smoothelin and calponin

In a healthy vessel wall, VSMCs exhibit a ‘contractile’ state which is less proliferative and migratory. Injury to the vessel facilitates the transformation of contractile VSMCs to the synthetic phenotype, where they rapidly proliferate and migrate, and increase their synthesis and secretion of ECM proteins (Petsophonsakul *et al.,* 2019; Biswas *et al.,* 2014). In Chapter 3 it was observed that infection of cultured HSV VSMCs with Ad: PRH S163C:S177C promoted the contractile state of VSMCs by upregulating their expression of contractile markers smoothelin and calponin. To investigate whether this effect was also observed *in vivo* in the murine carotid artery ligation model, retrieved carotids were subjected to immunohistochemistry for smoothelin and calponin. Results showed that there was no difference in the expression of these contractile markers between Ad: Control and Ad: PRH S163C:S177C groups. Negative control sections probed with non-immune rabbit IgG showed no staining.

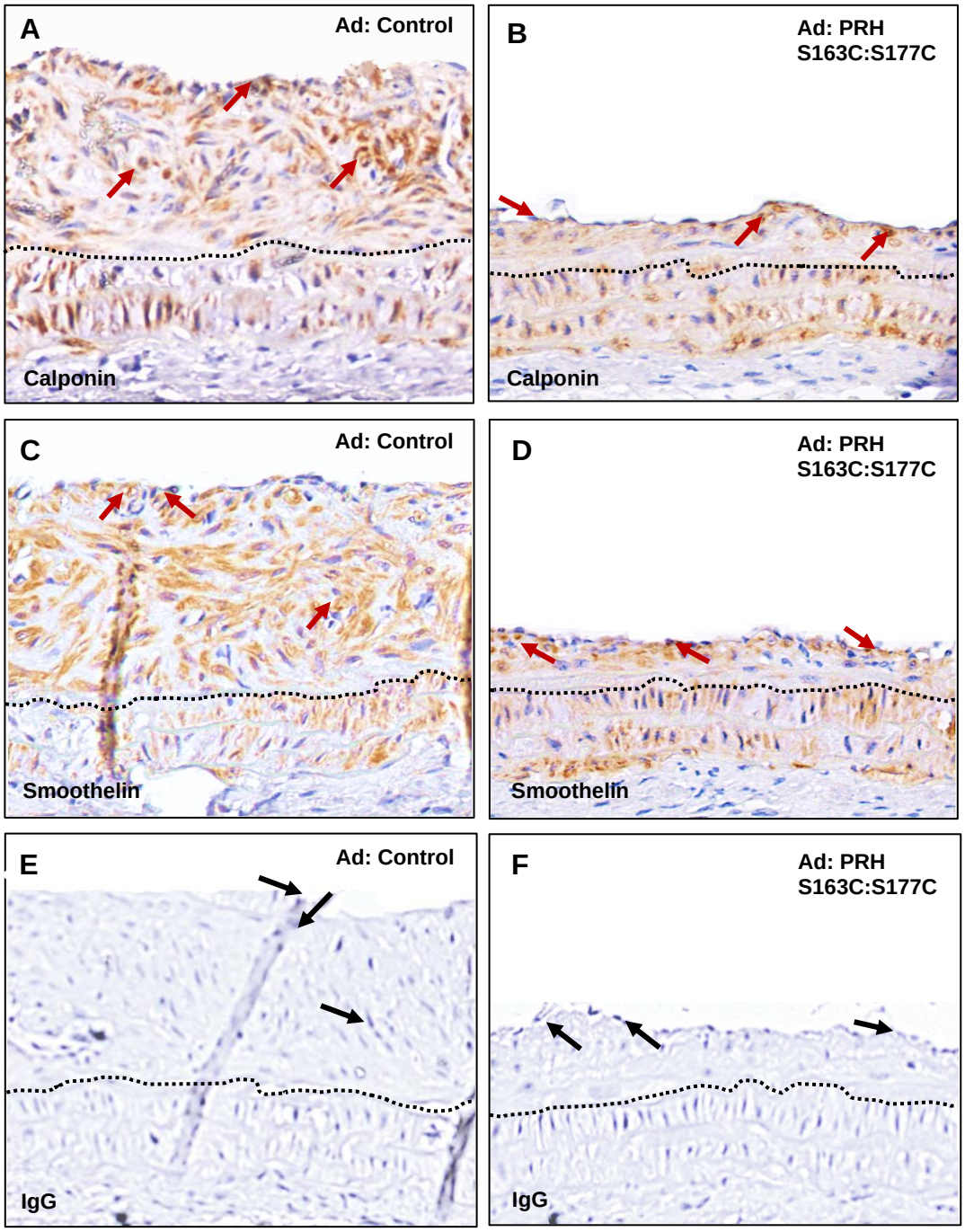

FIGURE 5.6: Overexpression of PRH S163C:S177C did not influence expression of smoothelin and calponin proteins

Carotid arteries were ligated in C57B/L6 mice to induce intimal thickening then infected with Ad: Control (**A,C&E**) or Ad PRH S163C:S177C (**B,D&F**). Representative images of immunofluorescence for calponin (**A&B**), smoothelin (**C&D)** and non-immune IgG (**E&F**) 28 days after ligation. Smoothelin- or calponin-positive cells are stained brown (some are indicated with red arrows); the nuclei of all cells are stained blue/grey with haematoxylin. Black dashed line indicates intimal: medial boundary. Scale bar represents 25 μm and applies to all panels.

5.3.5 Overexpression of PRH S163C:S177C did not influence endothelial coverage

It is vital that a therapeutic intervention for vein graft failure must not disrupt the endothelium as well as retard the development of intimal thickening (Ward *et al.,*2017). In Chapter 4, it was observed that infection of cultured HSVECs with Ad: PRH S163C:S177C did not affect endothelial cell behaviour such as proliferation and migration. To investigate whether Ad: PRH S163C:S177C affected endothelial coverage *in vivo* in the murine carotid artery ligation model, retrieved carotids were subjected to immunohistochemistry for cluster of differentiation 31 (CD31) which is an established marker of endothelial cells. Results showed that there was no difference in the expression of CD31 between Ad: Control and Ad: PRH S163C:S177C groups. Negative control sections probed with non-immune rabbit IgG showed no staining.

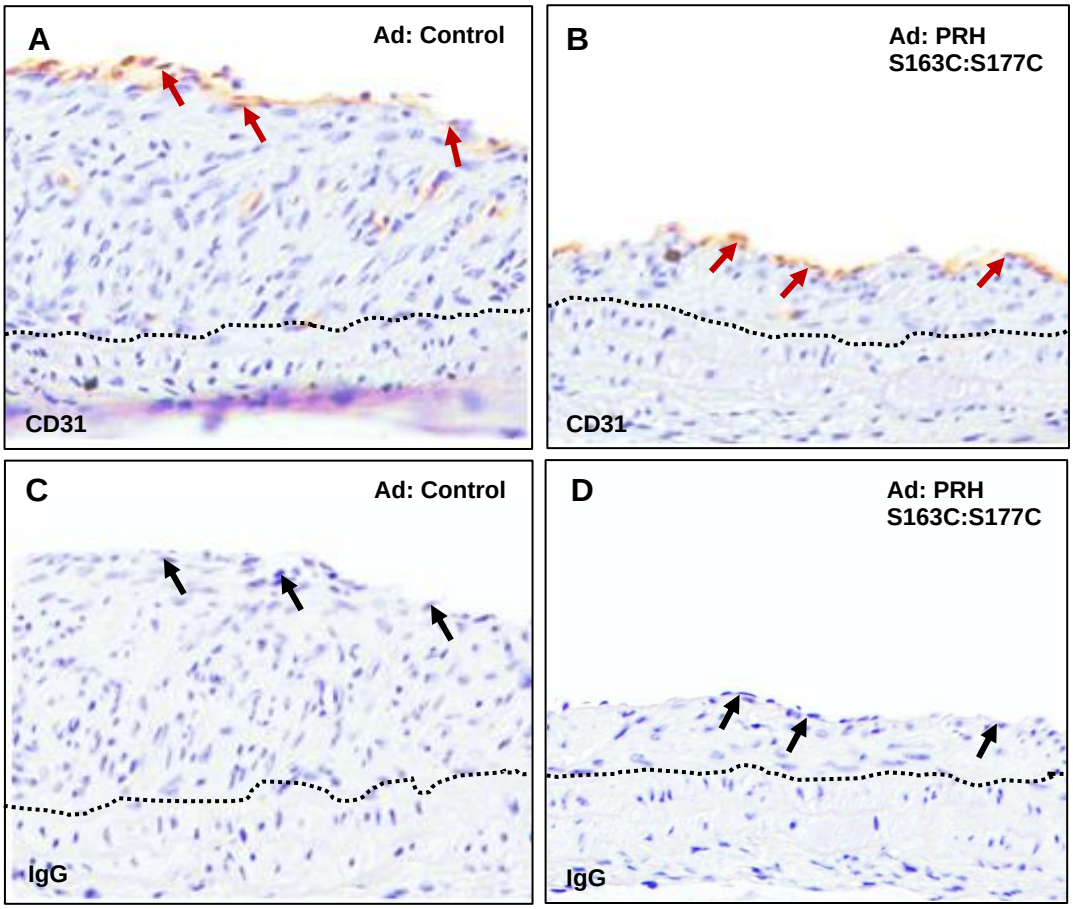

FIGURE 5.7: Overexpression of PRH S163C:S177C did not influence endothelial coverage

Carotid arteries were ligated in C57B/L6 mice to induce intimal thickening then infected with Ad: Control (**A&C**) or Ad PRH S163C:S177C (**B&D**). Representative images of immunofluorescence for CD31 (**A&B**) and non-immune IgG (**C&D**) 28 days after ligation. CD31-positive cells are stained brown (some are indicated with red arrows); the nuclei of all cells are stained blue/grey with haematoxylin. Black dashed line indicates intimal: medial boundary. Scale bar represents 25 μm and applies to all panels.

5.4 DISCUSSION

To investigate the ability of PRH S16C:S177C overexpression to reduce intimal thickening and thereby elucidate its potential as a therapeutic intervention for VGF, the effect of overexpression of these proteins *in vivo* was investigated using a murine carotid artery ligation model of intimal thickening.

5.4.1 Inhibition of intimal thickening by PRH 163C:177C

The findings of chapters 3 and 4 illustrated that overexpression of PRH S163C:S177C can impede VSMC proliferation, migration without inducing damaging effects on endothelial function *in vitro.* Therefore, it was hypothesized that overexpression of PRH S163C:S177C would result in reduced intimal thickening and resultant luminal narrowing in the established murine carotid artery ligation model. To date, the effect of PRH S163C:S177C overexpression in VGF and restenosis has not been investigated *in vivo*. These findings would strengthen the current reports on the therapeutic benefits of PRH S163C:S177C overexpression in human organ cultures *ex vivo*.

The central findings of this chapter clearly demonstrate the ability of PRH S163C:S177C overexpression in attenuating pathological intimal thickening. Morphological analysis of intimal thickening 4 weeks post-carotid artery ligation revealed that occlusion of the arterial lumen, intimal area and intima:media ratios were all significantly more pronounced in arteries subjected to infection with adenovirus encoding an empty vector versus those infected with Ad: PRH S163C:S177C. The influence of PRH S163C:S177C in reducing intimal thickening was first proposed by Wadey and colleagues, describing Ad: PRH S163C:S177C and CK2 inhibitors as suppressors of VSMC proliferation and intimal thickening in human saphenous vein organ cultures (Wadey *et al.,* 2017). Although the study by Wadey and colleagues utilised human saphenous vein organ culture in order to model intimal thickening, direct experimental testing in prospective animal models of human disease is essential to verify the potential of PRH S163C:S177C in pre-clinical research and support the proposition of investigations in larger animal models of VGF prior to clinical trials.

In this study, a murine carotid artery ligation model was employed in order to tackle the obstacles in understanding whether and how overexpression of PRH S163C:S177C might influence intima thickening *in vivo*. In this model, the left carotid artery is ligated near the carotid bifurcation and stenotic lesions begin to develop approximately 2-4 weeks post-surgery (Brown *et al.,* 2018). This model was selected as it is a well-established robust model that reproducibly leads to intimal thickening as a result of VSMC migration and proliferation

(Williams *et al.,* 2016; Williams *et al.,* 2014; Tsaousi *et al.,* 2011) and it is amenable to adenovirus-mediated gene therapy (Hulin-Curtis *et al.,* 2017). This reproducible and simple model has become a widely appealing tool with minimal mechanical trauma, low ischemic injury, and absence of a major inflammatory response (Xu, 2004). However, it has been widely postulated that stenotic lesions form at sites of altered haemodynamic or low sheer stress (Ley *et al.,* 2007); for this reason, the carotid ligation model may fail to completely replicate all of the relevant conditions that lead to VGF in humans (Hulin-Curtis *et al.,* 2017; Xu, 2004). Nevertheless, our *in vivo* murine model of carotid artery ligation remains to be a very suitable model for evaluating potential therapies for suppression of VGF and studying the mechanisms behind proliferation and migration of VSMCs.

Over-reliance on male mice in scientific animal research has led to female subjects becoming underappreciated; this is due to belief that inclusion of females leads to more data variability (Beery, 2018; Beery and Zucker, 2011). Utilisation of exclusively male mice was hence rationalised as being a means of producing more reproducible data and thereby being more cost-effective (Beery, 2018). However, emerging studies claim that gender influences the results and may alter data interpretation, thus, new ARRIVE guidelines stipulate that *in vivo* research must involve inclusion and balance of both male and female subjects and must not be limited to one gender (Percie du Sert *et al.,* 2020). It has also been assumed that female subjects exhibit more variability than males (Beery, 2018), although this has been challenged by a meta-analysis centring on neuroscience research (Becker, 2016). Of interest, studies have shown that women are more susceptible to comorbid conditions post-CABG surgery highlighting the necessity to examine therapeutic interventions for CVD in both genders (Nicolini *et al.,* 2016; den Ruijter *et al.,* 2015; Alam *et al.,* 2013; Bukkapatnam *et al.,* 2010; Abramov *et al.,* 2000). In this study *in vivo* study, both male and female mice were included to account for potential differences in response to PRH S163C:S177C overexpression in both genders.

5.4.2 Attenuation of neointimal proliferation and migration by overexpression of PRH S163C:S177C

In vitro analysis revealed a notable reduction in HSV VSMCs proliferation, along with an induction in p21 protein expression and a reduction in cyclin D1 protein levels in response to PRH S163C:S177C overexpression. Data from the *in vivo* study showed that PRH S163C:S177C overexpression suppressed aberrant proliferation of medial and intimal cells in ligated carotid arteries. As such, this implicates the success and effectiveness of the

adventitial delivery of Ad: PRH S163C:S177C to achieve reduction proliferation that results in attenuated intimal thickening. In parallel, detailed analysis revealed that migration from the media into the intima was also impaired by infection with Ad: PRH S163C:S177C. However, this was only an estimation of cellular migration calculated by measuring the proportion of BrdU-negative nuclei in the intima divided by the intimal length. These data indicated that PRH S163C:S177C overexpression impaired intima development via antagonising intimal-directed migration as well as replication. Comparably, Wadey and colleagues reported adenovirus-mediated gene transfer of PRH S163C:S177C notably disrupted intimal thickening and proliferation *ex vivo* implicating possible translational aspirations into humans. Conflictingly, gene transfer of PRH S163C:S177C did not influence the rate of VSMC migration in human organ cultures (Wadey *et al.,* 2017). The discrepancy between the *in vivo* and *ex vivo* findings may be due to differences between the infection efficiencies and existence of other factors such as blood and vasoactivity *in vivo*. No significant changes were detected in medial and intimal VSMC density as determined by the haematoxylin staining and immunohistochemistry for α-smooth muscle cell actin.

It is shown in this chapter that PRH S163C:S177C which is a more stable form of PRH, lowers the migratory potential of artery cells whilst preventing the rate of VSMC replication in our *in vivo* model. In a clinical setting genetic transfer into the venous graft may occur peri-operatively prior to implantation of the graft due to its simplicity and it can avoid the systemic side-effects of medications. Therefore, it is important that PRH S163C:S177C is a stable protein since a single exposure to PRH S163C:S177C-encoding adenoviruses alone is only permitted for perivascular therapy in humans during the grafting surgical procedure.

5.4.3 PRH S163C:S177C did not affect the levels of αSMA, Calponin and Smoothelin

Upon vascular injury, VSMCs switch from the quiescent and differentiated contractile phenotype to the highly proliferative and de-differentiated synthetic phenotype (Petsophonsakul *et al.,* 2019; Biswas *et al.,* 2014). This process in is tightly controlled by the transcription factor serum responsive factor (SRF). SRF recognises and binds to CArG sequences and thereby activates a range of cytoskeletal and contractile genes (Miano, 2012). A smooth muscle and cardiac muscle-specific accessory factor called myocardin is recruited by SRF to induce the genes involved in VSMC differentiation and proliferation (Petsophonsakul *et al.,* 2019). These master regulators functions as a transcriptional switch with numerous reports implicating the loss of binding state between SRF and myocardin de-

activates expression of VSMC-specific contractile genes. Hence, promoting the de-differentiation phenotype which leads to abnormal proliferation, migration, and matrix production in VSMCs (Biswas *et al.,* 2014; Oyama *et al*., 2004). The only report associating PRH to VSMC phenotypic markers was by Oyama and colleagues who showed that PRH associates with SRF to induce SM22α and αSMA transcript levels in embryonic fibroblasts, which are markers of the VSMC contractile phenotype (Oyama *et al.,* 2004). Similarly, the *in vitro* findings earlier in this thesis have corroborated that gene transfer of PRH S163C:S177C drives VSMCs into their contractile state, in part, through upregulating the expression of calponin and smoothelin. In the current study, we have demonstrated that almost all of cells present in the intima and media are SMCs and therefore it is appropriate to state that the detected proliferation and estimate of migration largely relates to VSMCs.

αSMA is an established marker of VSMCs. In line with the findings of Wadey and colleagues (Wadey *et al.,* 2017), our current study found there was no significant difference in the αSMA density of cells overexpressing Ad: PRH S163C:S177C compared to the Ad: Control and uninfected control (FIGURE 5.5). However, previous studies have shown that αSMA is not a good marker of VSMC phenotype as it is not highly regulated during phenotypic switching but rather it is preserved in both synthetic and contractile VSMCs (Xu *et al.,* 2012; Aikawa *et al.,* 1993). In order to evaluate the effect of PRH S163C:S177C on VSMC phenotype, protein expression of calponin and smoothelin was examined in ligated carotid arteries, where calponin and smoothelin are markers of VSMC differentiation (Lepreux *et al.,* 2013. Although PRH S163C:S177C overexpression enhanced levels of calponin and smoothelin in primary cultures of human saphenous vein VSMCs, no significant changes in the levels of calponin and smoothelin were detected in the media or intima of ligated carotid arteries. The reason for the discrepancy is unclear. It is possible that the inconsistency in our findings may be a result of temporal factors: *in vitro*, HSV VSMCs were infected with Ad: PRH S163C:S177C for 18 hours and then cultured for a further 24 hours whereas *in vivo*, Ad: PRH S163C:S177C was administered for 28 days. Hence, it is possible that ability of PRH S163C:S177C to induce expression of the contractile markers smoothelin and calponin is time limited. To investigate this, one could retrieve and analyse vessels at an earlier time-point following carotid ligation in order to study the ability of PRH S163C:S177C to modulate VSMC phenotype at the early stages of intimal thickening. Another added consideration is that of, which was our vector of choice to deliver PRH S163C:S177C, high seroprevalence rates of pre-existing neutralizing antibodies against Ad5 (Bauer *et al.,* 2005; Sumida *et al.,* 1995) may have restricted infection efficiency and delivery of the PRH S163C:S177C transgene. It seems that gene transfer of S163C:S177C at 28 days is sufficient to mitigate the proliferative and migratory actions although sustained expression of the protein may be required to regulate the expression of

the contractile markers smoothelin and calponin. Utilisation of a novel adenovirus vector with amplified vascular transduction and improved resistance to serum neutralising antibodies (White *et al.,* 2013). It is also worth considering that intimal thickening occurs within 2 weeks of vascular injury, and that by day 28 when arteries were retrieved, VSMCs may have returned to their contractile phenotype (Kumar and Lindner 1997, Godin et al. 2000).

5.4.4 PRH S163C:S177C did not affect the endothelial coverage

Thrombosis, intimal thickening and superimposed atherosclerosis are direct consequences of endothelial dysfunction or impaired post-operative re-endothelialisation (Wadey *et al.,* 2017). In Chapter 4, we provide an in vitro evidence demonstrating that overexpression of PRH S163C:S177C did not significantly alter proliferation and migration but reduced apoptosis in HSVECs. Data from our in vivo study illustrates that overexpression of PRH S163C:S177C had no detrimental effect in the endothelium compared to the control empty virus 28 days post-ligation. Similarly, previous work from our laboratory have shown that PRH S163C:S177C did not affect endothelial cell coverage via immunohistochemistry for QBEND-10 in a 14-day human saphenous vein organ culture compared to the controls (unpublished data). With respect to these results, data from our current study strengthens the protective effects of PRH S163C:S177C overexpression to the endothelium making it an ideal preventative measure against VGF.

5.4.4 Chapter Summary

The long-term benefits of HSV grafts are compromised by intimal thickening. This study provides *in vivo* evidence for the therapeutic benefits of PRH overexpression to reduce proliferation and migration of VSMCs in the vessel wall following vascular injury using a robust and established model of intimal thickening. Though our evidence suggests that PRH S163C:S177C overexpression does not enhance the number of VSMCs exhibiting a contractile phenotype, the potential of this gene therapy approach to reduce intimal thickening and thereby VGF remains convincing. Overexpression of PRH S163C:S177C may therefore prolong viability of vein grafts and improve patency rates. Altogether, data is presented that shows for the first time that adenoviral gene delivery of PRH S163C:S177C can retard intimal thickening *in vivo* presenting a novel strategy to combat restenosis associated with CABG surgery. It is conceivable that these findings may have relevance to other pathologies such as in-stent restenosis.

6.

IDENTIFICATION OF NOVEL PRH S163C:S177C TARGET GENES USING NEXT GENERATION SEQUENCING

6.1 INTRODUCTION

Previous studies have revealed PRH regulates several genes directly (Soufi and Jayaraman, 2008). The first aim of this chapter is to utilise an unbiased transcriptomic approach to identify genes that are associated with the anti-mitotic activity of PRH S163C:S177C in VSMCs. The second aim is to directly examine the expression and function of some of the identified target genes. Next generation sequencing (NGS) was employed to compare mRNA expression in VSMCs and HSVECs overexpressing PRH S163C:S177C and thereby identify genes that are specifically regulated in VSMCs, but not in HSVECs. HSV VSMCs and HSVECs were infected with an empty vector adenovirus (Ad: Control) and PRH S163C:S177C-expressing recombinant adenovirus (Ad: PRH S163C:S177C). The function of identified VSMC-specific PRH S163C:S177C target genes identified using the NGS was investigated, and to characterise the effect of their up- or down-regulation by PRH additional analyses were undertaken. This could potentially identify new targets for therapeutic intervention using novel small molecules or repurposed pharmacological agents.

In 2003, Sanger sequencing or 'first-generation' DNA sequencing was used to accomplish the Human Genome Project (Hagermann, 2015). First described by Sanger in 1977, the chain-terminating dideoxynucleotides using DNA polymerase became the primary method for DNA sequencing for approximately four decades (Sanger, Nicklen and Coulson, 1977). Since then, there has been an extensive demand for low-cost and high-throughput sequencing methods. The commercial introduction of NGS in 2005 has transformed identification of novel genes progressively more practical where an individual's entire genome can be sequenced inexpensively ($0.001/kb) within 2 days (Fogel *et al.,* 2016). Contrary to the conventional capillary-based Sanger sequencing, the massively parallel sequencing capabilities of NGS allows for sequencing millions of DNA fragments per run. High sequencing coverage via NGS technology is now achievable, leading to a significant growth of novel gene discovery (Hagermann, 2015).

Our knowledge of PRH is fundamentally limited by the availability of reports in the literature and its novelty as a candidate gene in cardiovascular diseases. With the aim of closing this gap NGS enables the identification of target genes throughout the entire proteome. Fortunately, the progress in bioinformatic analysis allows us to better interpret the gene expression profiles as revealed using NGS. One advanced bioinformatic tool is the Ingenuity pathway analysis (IPA) software program, which can analyse the gene expression patterns using a build-in scientific literature-based database (according to IPA Ingenuity Web Site, www.ingenuity.com). The research in this chapter will integrate the potential of NGS approach for accelerating discovery of novel PRH target genes and to determine the molecular

mechanisms of the development of VGF and made aid the future development of improved approaches for coronary artery bypass grafts.

6.2 HYPOTHESIS

The hypothesis for this chapter were:

- PRH S163C:S177C specifically regulates some genes in VSMC which suppress VSMC proliferation and thereby intimal thickening.

This hypothesis was tested using:

- Infecting HSV VSMCs and HSVECs with Ad: Control or Ad: PRH S163C:S177C and purified RNA samples submitted to QIAGEN for NGS.
- Bioinformatic filtering utilising Ingenuity Pathway Analysis (IPA) software was applied to validate or exclude differentially expressed genes (DEGs) obtained from NGS.
- Validation of VSMC-specific PRH S163C:S177C-targets using *in vitro* and *in vivo* analyses.

6. 3 RESULTS

6.3.1 Next Generation Sequencing

HSV VSMCs were subjected to infection with 5 x 10^8 pfu/mL of adenovirus encoding either empty vector or c-myc-tagged PRH S163C:S177C, for 18 hours. HSVECs were subjected to infection with 1 x 10^8 pfu/mL of adenovirus encoding c-myc-tagged PRH S163C:S177C combined with 4 x 10^8 pfu/mL of adenovirus encoding empty vector or 5 x 10^8 pfu/mL of adenovirus encoding 5 x 10^8 pfu/mL empty vector, for 18 hours. Subsequently, cells were incubated for another 24 hours after replenishing the culture medium. Total RNA extraction, purification and quantification were performed and then submitted to QIAGEN Genomic Services (Germany) for NGS, as described in Section 2.14. Whole transcriptomic NGS sequencing libraries were successfully prepared, quantified and sequenced for all the samples. The collected reads were subjected to quality control, alignment and downstream analysis.

6.3.2 Data Annotation and Data Filtering

Analysing the unprecedented number of molecules identified through NGS is a significant challenge. To prioritise potential DEGs from such a large dataset, approximately $\geq$ 26, 000 molecules, a series of filtering strategies were implemented, as described in Section 2.14.2. To produce a smaller, more manageable dataset, bioinformatic filtering utilising IPA was performed. The first criterion used to prioritise the DEGs was to set the parameters of calculate metrics (e.g., fold change, p-value). Briefly, raw outcomes from the NGS analysis were first uploaded into QIAGEN's IPA system for data annotation and data filtering. Two datasets were utilised in this study; Dataset A (HSV VSMCs): Ad: Control vs Ad: PRH S163C:S177C and Dataset B (HSVECs): Ad: Control vs Ad: PRH S163C:S177C.

Two entities of the filtered datasets were uploaded into the 'Compare Data tool' for further filtering to obtain DEGs which are VSMC-specific and PRH S163C:S177C-regulated-specific. Analysis of genes enriched in HSV VSMCs expressing PRH S163C:S177C were sought by subtracting genes identified in HSVECs. IPA identified 2,121 DEGSs that were specifically PRH S163C:S177C-regulated in VSMCs. On the other hand, 652 DEGs were identified as specifically PRH S163C:S177C-regulated in HSVECs. There were 865 common DEGs shared between two datasets (FIGURE 6.1).

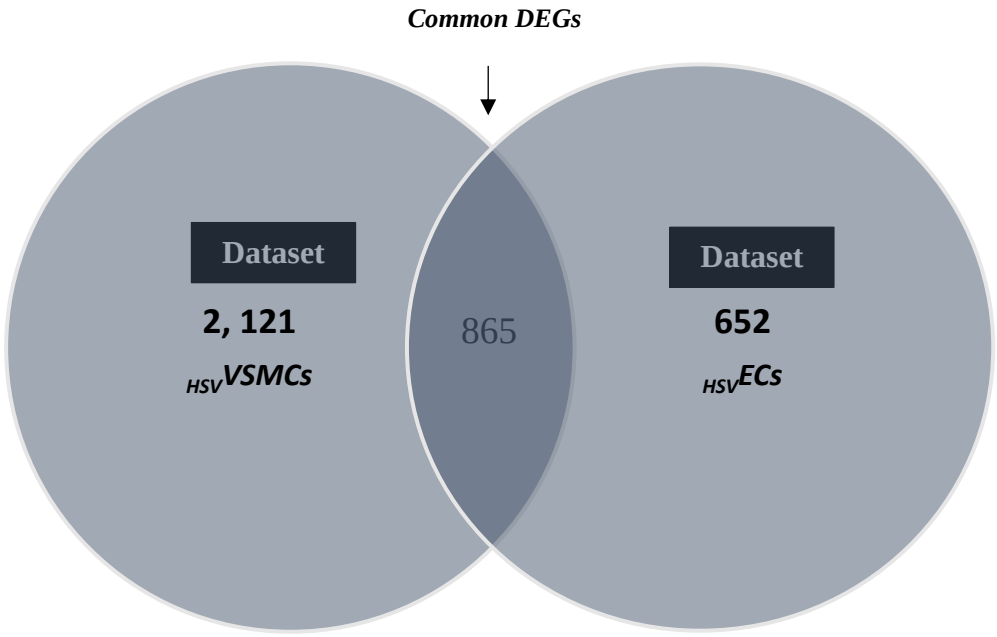

FIGURE 6.1: Venn diagram of PRH S163C:S177C-regulated DEGs

The previously filtered datasets were uploaded into the 'Compare Data tool' for further filtering of VSMC-specific and PRH S163C:S177C-specific DEGs. Dataset A: 2,121 DEGs that were specifically PRH S163C:S177C-regulated in VSMCs. Dataset B: 652 DEGs were identified as specifically PRH S163C:S177C-regulated in HSVECs. 865 DEGs were shared between the datasets.

6.3.3 Top-enriched canonical pathways of PRH S163C:S177C-regulated genes

In the next filtering step, the 2,121 VSMC-specific PRH-regulated DEGs were submitted in IPA for core analysis to explore the molecular mechanisms underlying the effects of PRH S163C:S177C. IPA identified canonical pathways, diseases and functions, and gene networks that are most significant to NGS outcomes and to categorize DEGs in specific diseases and functions. The differentially expressed genes were categorized to related canonical pathways based on IPA. The statistically significant enriched canonical pathways with a p-value less than 10^{-3} as well as representative DEGs in each canonical pathway are listed in Figure 6.2. A total of 369 DEGs (Supplementary Data 1) were identified in the Top 15 Canonical Pathways. This analysis suggests that PRH S163C:S177C may modulate several cellular pathways, which are associated with Carcinoma, Cardiac Hypertrophy, Fibrosis etc. (Table 6.1).

Further stratification of DEGs was undertaken on the 369 DEGs identified. An extensive literature review by means of biological analysis was performed as described in Section 2.14.2.6. As the focus of this analysis was intracellular signalling DEGs that were extracellular were eliminated as non-priority and transcription factors or transcriptional regulators were prioritised. An in-depth literature review produced a smaller subset of potential DEG which are expressed intracellularly and had published data related to features and biological/clinical significance of VGF. This strategy prioritised a smaller subset of potential DEGs (Supplementary Data 2).

FIGURE 6.2 – Top enriched canonical pathways following PRH S163C:S177C overexpression in VSMCs

The significant Canonical Pathways for the dataset that were identified are displayed along the y-axis. By default, the x-axis displays the -log of the p-value which is calculated using the right-tailed Fisher's Exact Test, such that larger bars equate to increased significance. The yellow line indicates the threshold value. The orange bars in the bar chart indicate predicted pathway activation or predicted inhibition, respectively, via another statistic: the z-score. Grey bars indicate pathways for which no prediction can be made due to insufficient evidence in the Knowledge Base for confident activity predictions across datasets.

Table 6.1: The top enriched PRH S163C:S177C-regulated canonical pathways in VSMCs based on IPA

Ingenuity Canonical Pathways	-log(p-value)	Ratio	No. of Molecules
Axonal Guidance Signalling	12.2	0.196	94
Breast Cancer Regulation by Stathmin1	11	0.179	105
Cardiac Hypertrophy Signalling (Enhanced)	9.01	0.179	86
Synaptogenesis Signalling Pathway	8.38	0.199	61
Hepatic Fibrosis Signalling Pathway	7.78	0.185	67
Hepatic Fibrosis / Hepatic Stellate Cell Activation	7.04	0.22	40
Role of Macrophages, Fibroblasts and Endothelial Cells in Rheumatoid Arthritis	6.46	0.183	56
Gα12/13 Signalling	6.26	0.238	30
Calcium Signalling	6.21	0.204	41
Glioblastoma Multiforme Signalling	6.15	0.218	35
Neuropathic Pain Signalling in Dorsal Horn Neurons	5.49	0.248	24
G-Protein Coupled Receptor Signalling	5.47	0.18	.48
Human Embryonic Stem Cell Pluripotency	5.41	0.222	29
Regulation of the Epithelial-Mesenchymal Transition Pathway	5.36	0.198	37
Agranulocyte Adhesion and Diapedesis	5.3	0.197	37

P- value is calculated using Fischer's exact test indicates the probability of the involvement of the genes in the dataset in a given pathway. Ratios represent the number of molecules in the dataset that are found in a given pathway, divided by total number of molecules that make up that pathway. Molecules are shown in the dataset (≥1.3 -log (p-value) and p≤0.05).

6.3.4 Functional analysis of PRH S163C:S177C-regulated genes

Further analysis was also conducted in IPA to understand the enriched and significant biological functions of genes identified in this dataset. Significantly enriched molecular and cellular functions were identified by means of this analysis, using a p-value threshold of 0.001. Among them, the p-value significance was shown to be higher for functions associated with cellular movement, survival, cellular growth, development, and proliferation (Table 6.2). These top functions appear to be linked with cellular proliferation which was supported by the presence of canonical cancer or fibrosis pathways and other-related pathways. Of interest, the tool determined that 135 DEGs within our dataset were associated with proliferation and migration of smooth muscle cells. In line with our previous findings, PRH S163C:S177C have been shown to reduce the proliferation and migration of VSMCs. As previously, any DEGs that were extracellular were eliminated as non-priority and transcription factors or transcriptional regulators were prioritised. An in-depth literature review produced a smaller subset of potential DEGs which are expressed intracellularly and had published data related to features and biological/clinical significance of VGF (Supplementary Data 3).

It is crucial to confirm the gene expression findings obtained from our NGS data. Thus, experimental validation using Western blotting was performed to study the effect of PRH S163C:S177C on all the prioritised DEGs. Any DEGs with protein expression that could not be confirmed or correlate to NGS data were eliminated as non-priority. Finally, this study identified two final target DEGs, STAT-1 and HDAC-9, associated with Cardiac Hypertrophy, Calcium Signalling and Fibrosis which were considered for further experimental validation.

Table 6.2: Enriched biological functions identified using IPA in VSMCs overexpressing PRH S163C:S177C

Categories	Molecular and Cellular Functions	No. of molecules	P-value
Skeletal and Muscular System Development and Function	Muscle contraction	73	1.01E-12
Inflammatory Response, Respiratory Disease	Inflammation of respiratory system component	142	4.62E-14
Cellular Movement, Skeletal and Muscular System Development and Function	Migration of smooth muscle cells	54	2.02E-14
Cellular Function and Maintenance	Function of phagocytes	80	1.32E-15
Cellular Development, Cellular Growth and Proliferation	Proliferation of smooth muscle cells	81	1.62E-13
Cellular Development, Cellular Growth and Proliferation	Proliferation of muscle cells	102	3.88E-13
Cellular Development, Cellular Growth and Proliferation	Cell proliferation of tumor cell lines	410	4.33E-22
Cell Death and Survival	Cell death of tumor cell lines	361	1.04E-17
Cell Death and Survival	Apoptosis of tumor cell lines	298	4.24E-17
Cell Cycle	Cell cycle progression	247	4.09E-16
Cardiovascular System Development	Development of endothelial tissue	115	1.1E-17
Cardiovascular Disease	Peripheral vascular disease	126	5.46E-16
Cancer, Organismal Injury and Abnormalities	Cancer		9.06E-100
Cancer, Organismal Injury and Abnormalities	Breast or pancreatic cancer	925	1.05E-41

P-value of inclusion is ≤0.001. The biological functions predicted to be regulated by PRH S163C:S177C in VSMCs.

6.3.5 Identification of STAT-1 as a novel PRH S163C:S177C-regulated gene

STAT-1 was identified as one of the putative targets of PRH S163C:S177C using the bioinformatic analysis. The observation of decreased amounts of STAT-1 mRNA from NGS warranted further validation with regards to its protein expression. To validate the findings obtained from NGS and determine whether PRH S163C:S177C regulates translation of STAT-1 protein, analysis was performed using Western blotting. HSV VSMCs were subjected to infection with 5 x 10^8 pfu/ml of adenovirus encoding either empty vector or c-myc-tagged PRH S163C:S177C or left uninfected. Subsequently, cells were incubated for another 24 hours after replenishing the culture medium. STAT-1 was detected at similar levels in uninfected VSMCs and those infected with Ad: Control. However, the level of STAT-1 protein detected in VSMCs infected with Ad: PRH S163C:S177C-infected VSMCs was significantly lower than that detected in uninfected VSMCs and VSMCs infected with Ad: Control (FIGURE 6.3). This finding indicates that overexpression of PRH S163C:S177C reduces the protein expression of STAT-1 in VSMCs.

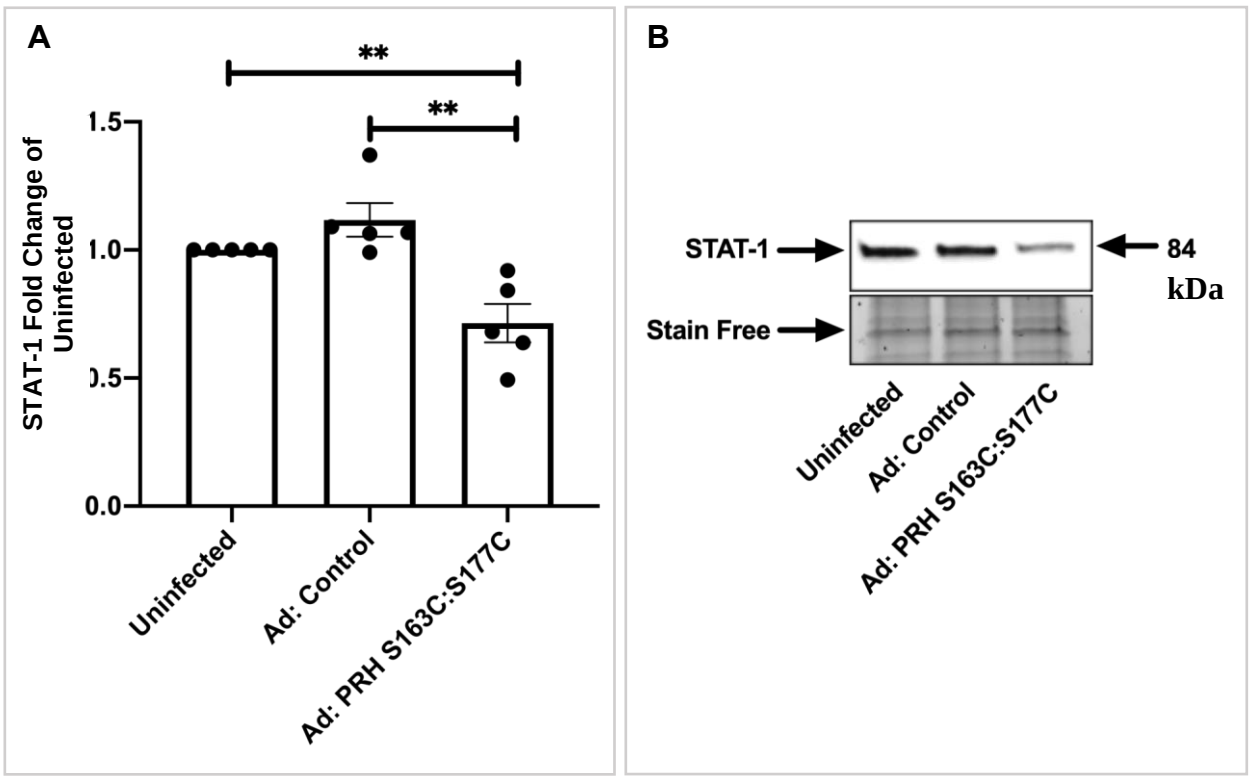

FIGURE 6.3 – Overexpression of PRH S163C:S177C downregulated STAT-1 protein in HSV VSMCs

HSV VSMCs were infected with Ad: Control or Ad: PRH S163C:S177C or left uninfected.

(A) Quantification of STAT-1 protein expression using Western blotting. Data was normalised using stain-free bands and expressed as a fold change from uninfected control. ** indicates $p<0.01$ vs. uninfected or Ad: Control, ANOVA, Student-Newman-Keuls Multiple Comparisons Test, n=5. Error bars indicate SEM.

(B) Representative Western blot for STAT-1. Stain-free bands served as a loading control. Approximate molecular weight of detected protein band is indicated on the right in kDa.

6.3.6 Inhibition of STAT-1 using fludarabine attenuated HSV VSMC proliferation

To directly investigate the role of STAT-1 in VSMC proliferation, HSV VSMCs were treated with 50 μM fludarabine (STAT-1 inhibitor) or DMSO (control). The dose of 50 μM fludarabine was selected as established by previous reports (Torella *et al.,* 2007). Assessment of cell growth was performed using measuring EdU incorporation 24 hours later. Treatment with 50 μM fludarabine significantly decreased VSMC proliferation compared to the DMSO control (FIGURE 6.4). Western blotting analysis for the cell cycle proteins, p21 and cyclin D1, revealed that fludarabine significantly decreased cyclin D1 levels (FIGURE 6.5). However, there fludarabine did not significantly affect the level of p21 protein in HSV VSMCs (FIGURE 6.6).

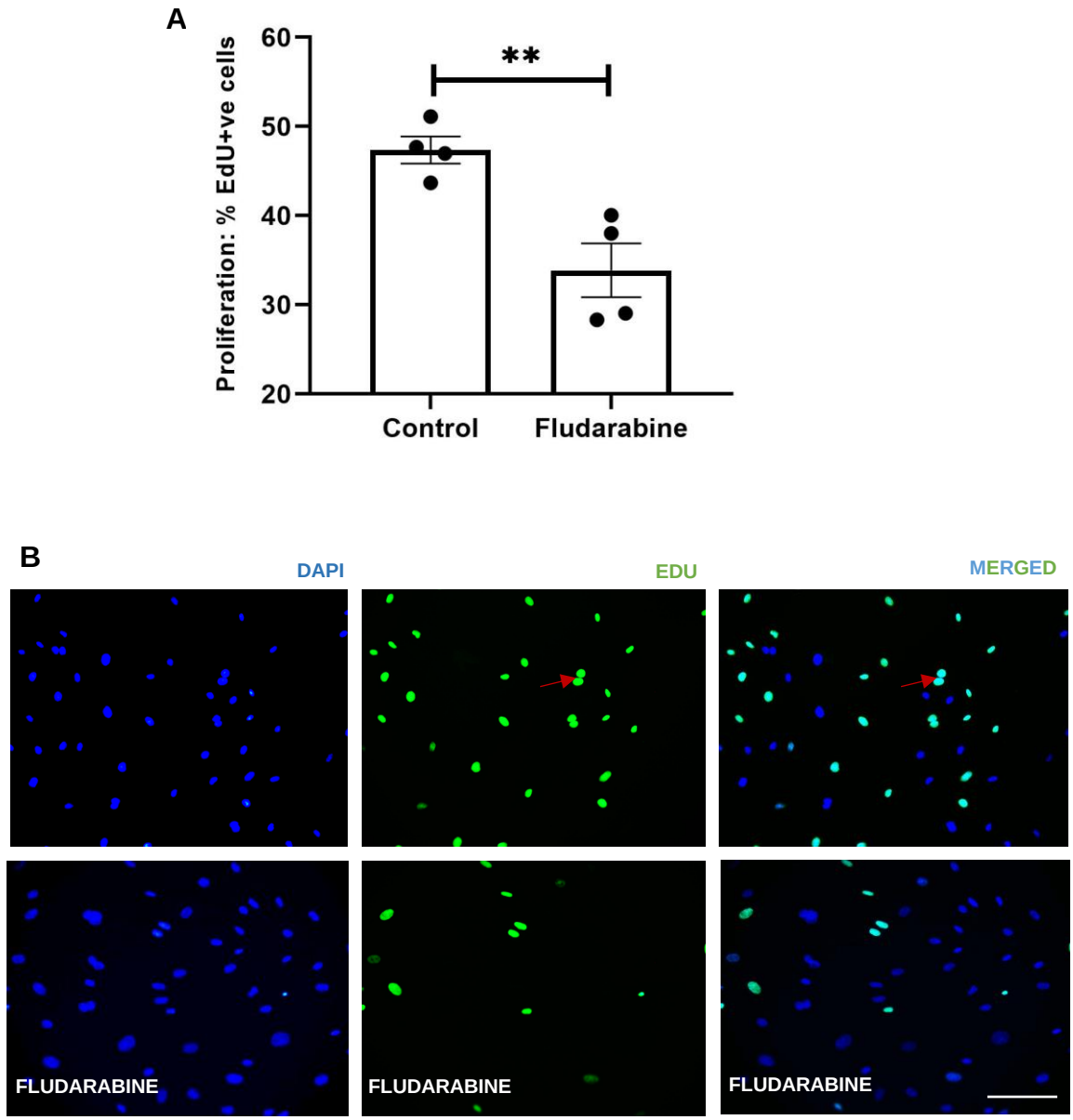

FIGURE 6.4 – Fludarabine retarded HSV VSMC proliferation detected using quantification of EdU incorporation

HSV VSMCs were cultured with 50 μM fludarabine in DMSO or DMSO control alone.

(A) EdU incorporation was quantified and expressed as the percentage of EdU-positive cells. ** indicates $p<0.01$, paired, two-tailed Student's t-Test, n=4. Error bars indicate SEM.

(B) Representative images of Click-iT EdU assay. Positive cells are green (some positive cells are indicated by red arrows), and all nuclei are stained blue with DAPI. Scale bar measures 50 μM and applies to all panels.

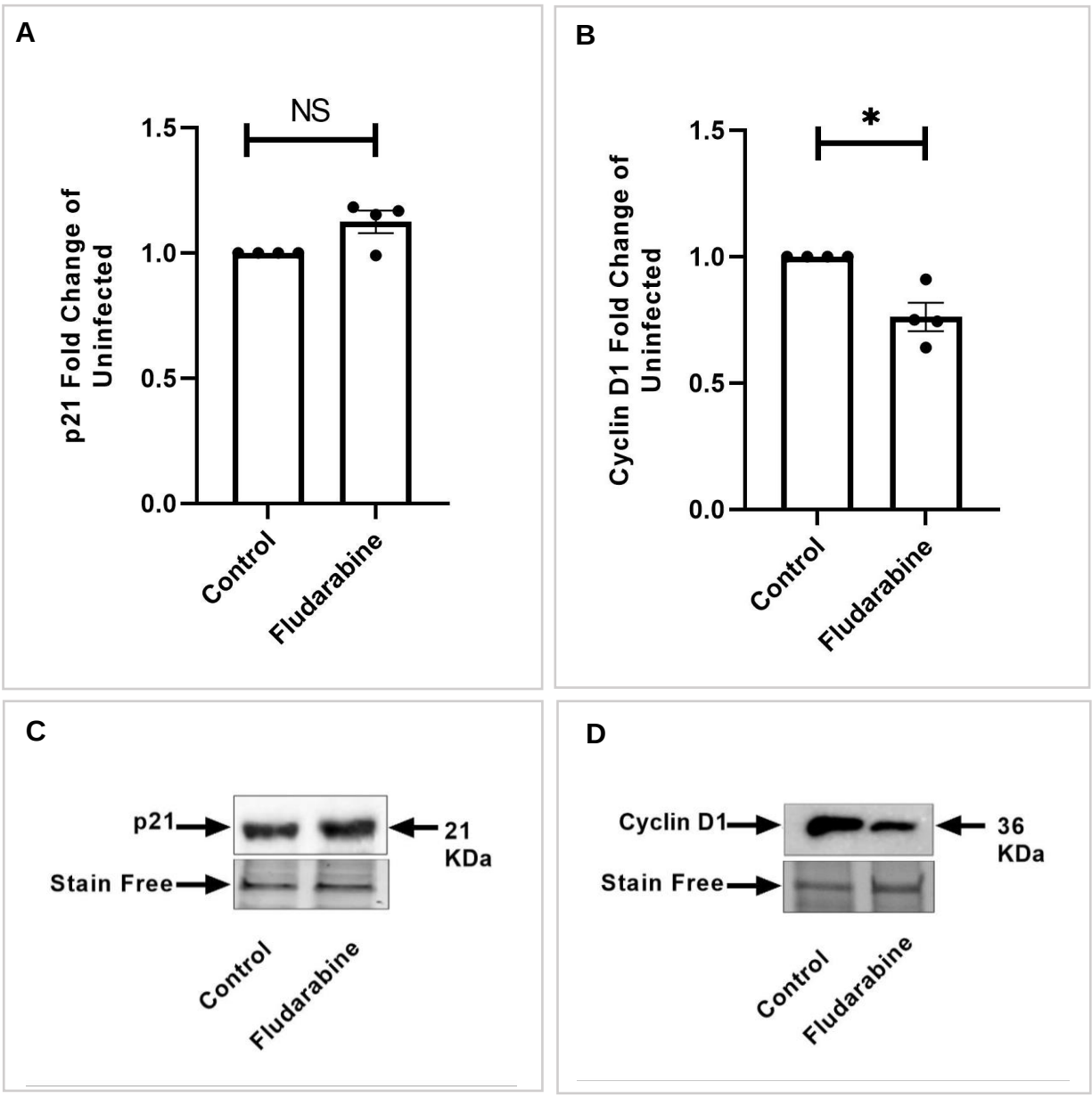

FIGURE 6.5 – Fludarabine reduced cyclin D1 protein levels in HSV VSMCs

HSV VSMCs were cultured with 50 μM fludarabine in DMSO or DMSO control alone. Quantification of p21 protein (**A**) and cyclin D1 protein (**B**) using Western blotting; data was normalised using stain-free bands and expressed as a fold change from uninfected control. NS denotes not significant, * indicates $p<0.05$, paired, two-tailed Student's t-Test, n=4.Error bars indicate SEM. Representative Western blot for p21 protein (**C**) and cyclin D1 (**D**). Stain-free bands served as a loading control. Approximate molecular weight of detected protein bands are indicated on the right in kDa.

6.3.7 Inhibition of STAT-1 using fludarabine did not affect HSV VSMC apoptosis

To assess whether fludarabine affects VSMC apoptosis, HSV VSMCs were treated with 50 μM fludarabine (STAT-1 inhibitor) or DMSO (control) for 24 hours. As a positive control, cells were incubated with 200 ng/mL human recombinant Fas-ligand in 2% serum-free media. Subsequently, apoptosis was assessed via immunofluorescence for cleaved caspase-3. As expected, Fas ligand significantly induced apoptotic cell death with respect to uninfected control (FIGURE 6.6). Quantification of cleaved caspase-3 positive cells showed that fludarabine treatment did not affect the rate of apoptosis in HSV VSMCs.

FIGURE 6.6: Fludarabine did not affect apoptosis

HSV VSMCs were subjected to treatment of with or without 50 μM fludarabine. Fas ligand was used as a positive control.

A – The rate of apoptosis was quantified and expressed as the percentage of cleaved caspase-3-positive cells. NS denotes not significant, paired, two-tailed Student's T-Test, n=4.

B – Representative images of immunocytochemistry for cleaved caspase-3 (CC-3). Positive cells (red arrow) are green, and all nuclei are stained blue with DAPI. Scale bar measures 25 μM and applies to all panels. CC-3 denotes cleaved caspase-3.

A

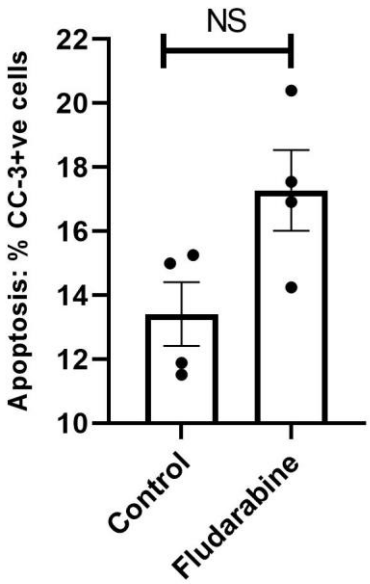
NS
Apoptosis: % CC-3+ve cells
22
20
18
16
14
12
10
Control
Fludarabine

B

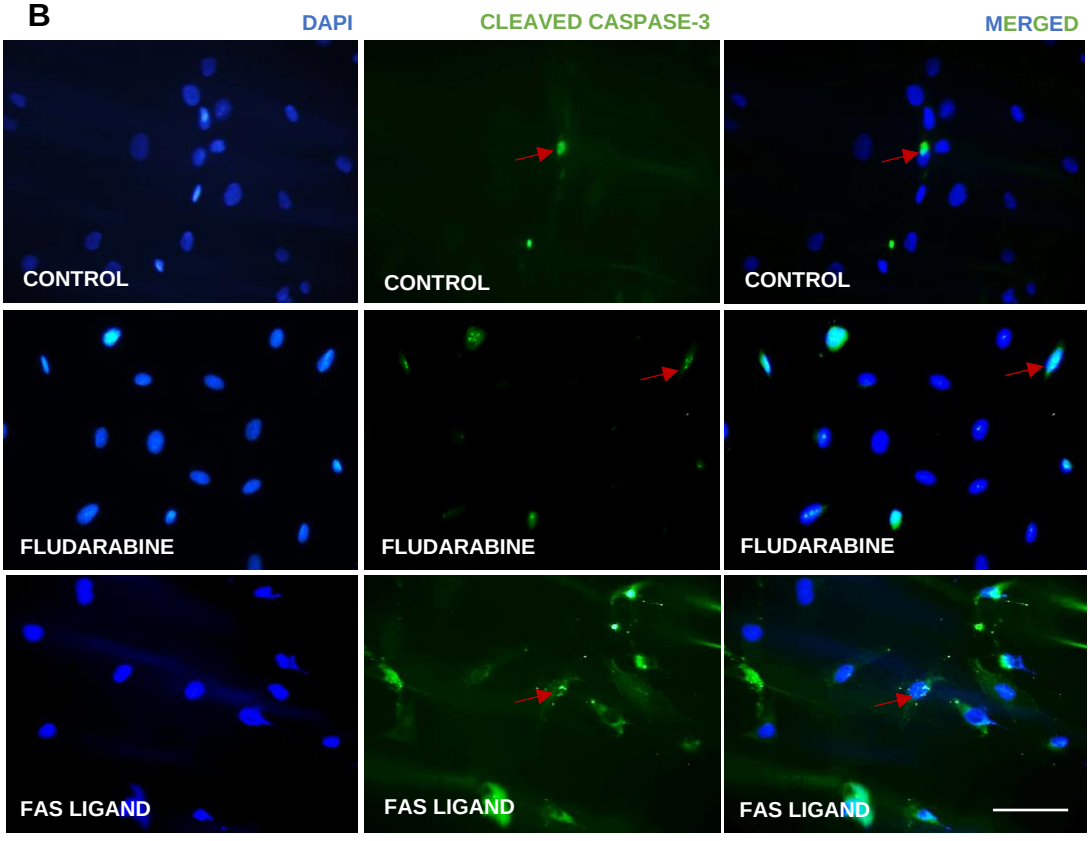
DAPI
CLEAVED CASPASE-3
MERGED
CONTROL
CONTROL
CONTROL
FLUDARABINE
FLUDARABINE
FLUDARABINE
FAS LIGAND
FAS LIGAND
FAS LIGAND

6.3.8 Inhibition of STAT-1 using fludarabine did not affect HSV VSMC migration

To assess whether fludarabine affects VSMC migration, HSV VSMCs were treated with 50 μM fludarabine (STAT-1 inhibitor) or DMSO (control). Subsequently, confluent HSV VSMCs were wounded then incubated for a further 24 hours. Treatment with 2 mM hydroxyurea in 10% FBS/DMEM inhibited cell proliferation. The distance migrated was quantified using measuring the wound at 0- and 24-hours post-wounding. No significant difference in distance migrated was observed in fludarabine treated VSMCs compared to control VSMCs (FIGURE 6.7).

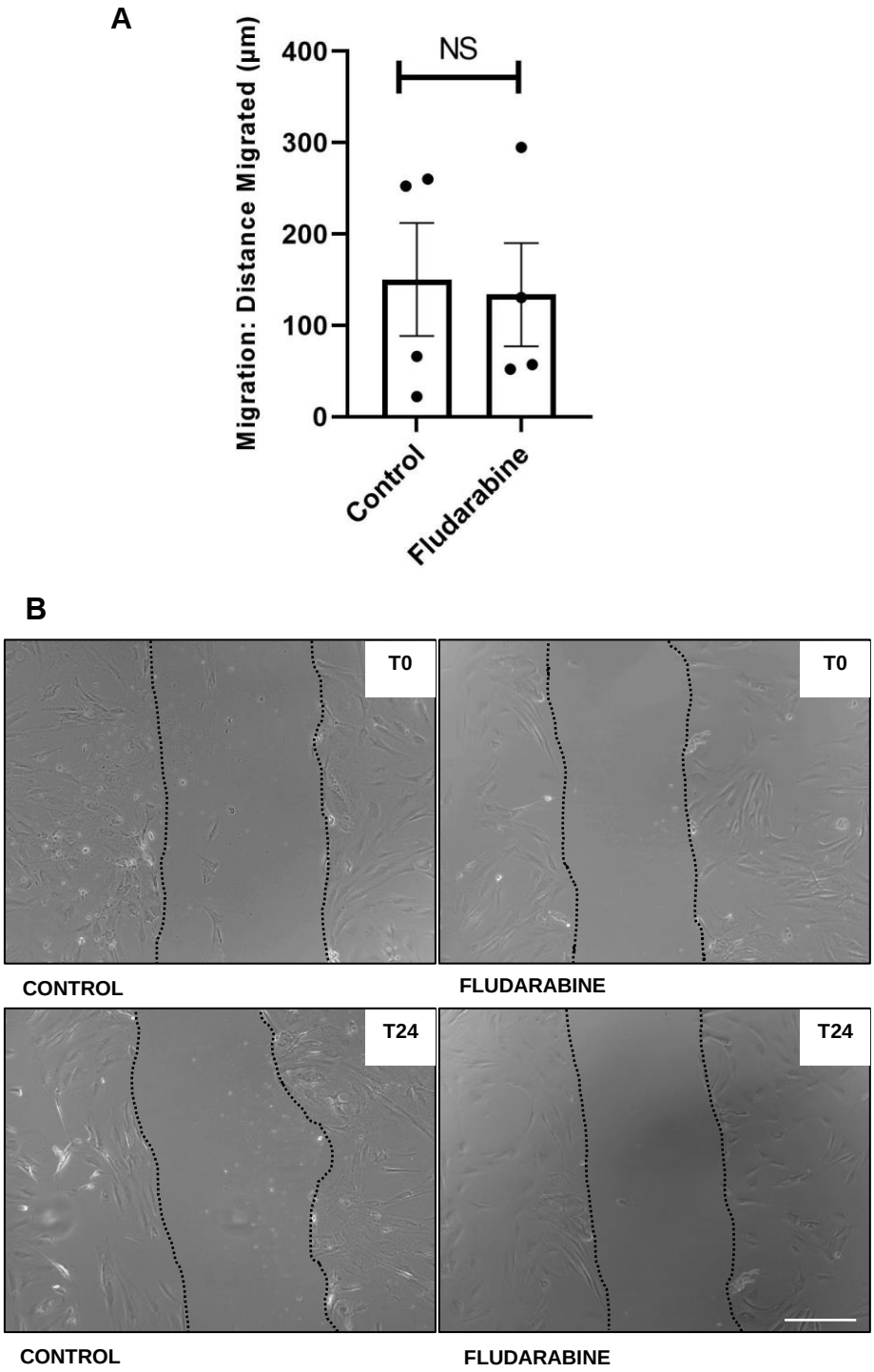

FIGURE 6.7– Fludarabine did not affect migration of HSV VSMCs

Migration of HSV VSMCs treated with 50 µM fludarabine in DMSO or DMSO control was assessed using the scratch wound assay. **(A)** Migration was quantified and expressed as distance migrated (µM); NS denotes not significant, paired, two-tailed Student's T-Test, n=4. Error bars indicate SEM. **(B)** Representative images of scratch wound assay. Dashed line indicates wound edge. T0 indicates Time = 0 hr; T24 indicates Time = 24 hr. Scale bar represents 1 mm and applies to all panels.

6.3.9 Inhibition of STAT-1 using fludarabine did not affect contractile proteins in HSV VSMC

To investigate the role of STAT-1 in the regulation of VSMC contractile protein markers, HSV VSMCs were treated with 50 μM fludarabine (STAT-1 inhibitor) or DMSO (control) in 10% FBS/DMEM. After 24 hours, cells were lysed for Western blotting analysis of the VSMC-specific contractile proteins, calponin and smoothelin. The level of calponin and smoothelin proteins detected in the fludarabine treated VSMCs was not significantly different from that detected in the control VSMCs treated with control alone (FIGURE 6.8).

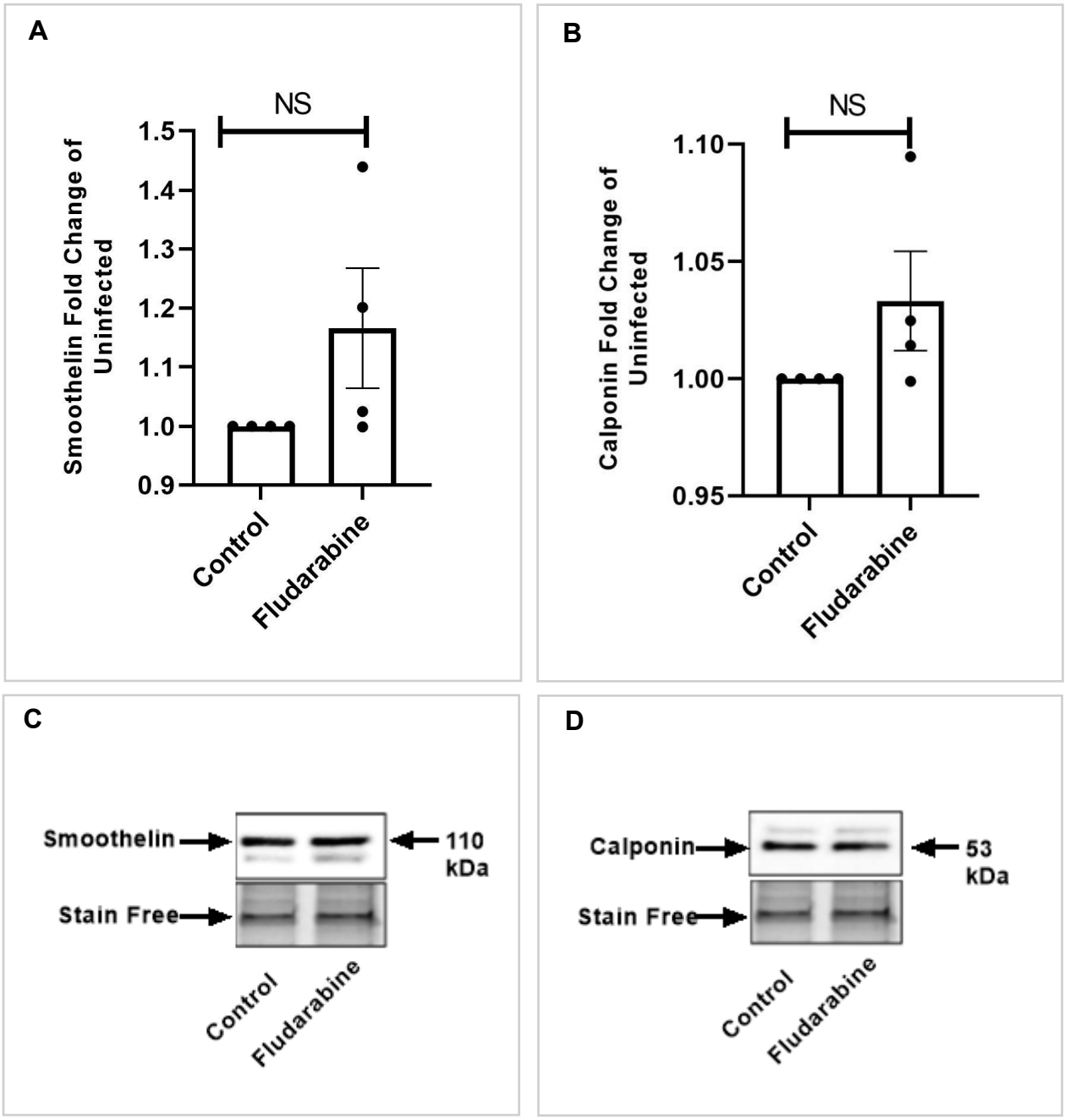

FIGURE 6.8 – Fludarabine did not regulate the level of contractile protein markers in HSV VSMCs

HSV VSMCs were cultured with 50 μM fludarabine in DMSO or DMSO control alone. Quantification of smoothelin (**A**) and calponin (**B**) proteins using Western blotting. Data was normalised using stain-free bands and expressed as a fold change from control. NS denotes not significant, paired, two-tailed Student's t-Test, n=4.. Error bars indicate SEM. Representative Western blots for smoothelin (**C**) and calponin (**D**). Stain-free bands served as a loading control. Approximate molecular weights of detected bands are indicated on the right in kDa

6.3.10 STAT-1 protein *in vivo*

To identify whether STAT-1 protein was expressed in control mouse carotid arteries (unligated) and those subjected to ligation for 7 days to initiate intimal thickening, immunohistochemistry for STAT-1 protein was performed (FIGURE 6.10A). In addition, immunohistochemistry for STAT-1 protein was performed on sections of mouse ligated carotid arteries at 7 days after infection with Ad: Control and Ad: PRH S163C:S177C to determine whether overexpression of PRH S163C:S177C protein affects the level of STAT-1 protein. The positively stained tissue detected using ImageJ analysis was calculated as a fold change from that detected in the Ad: Control. The results have shown that unligated mice carotids had a significantly lower HDAC-9 levels in comparison to the ligated carotids (FIGURE 6.9B and C). STAT-1 protein levels appeared slightly lower in the ligated carotid arteries infected with Ad: PRH S163C:S177C compared to ligated carotid arteries infected with Ad: Control (FIGURE 6.9A and C) however the difference did not reach significance. Negative control sections probed with non-immune mouse IgG showed no staining.

FIGURE 6.9 – STAT-1 protein in unligated and ligated left carotid arteries after 7 days with and without infection with Ad: Control or Ad: PRH S163:S177C

Mouse carotid arteries were ligated in C57B/L6 mice to induce intimal thickening then subjected to infection with adenoviruses encoding either Ad: Control or Ad: PRH S163C:S177C. The right carotid arteries were used as an unligated controls.

A - Quantification of STAT-1 protein in Ad: Control vs. Ad: PRH S163C:S177C infected ligated carotid arteries, expressed as the fold change, ns indicates not significant, unpaired, two-tailed Student's t-test, n=3. Error bars indicate SEM.

B - STAT-1 expression in ligated vs unligated mice carotids was quantified and expressed as the fold change, NS denotes not significant, * indicates $p<0.05$, paired, two-tailed Student's t-test, n=4Student's t-Test, unpaired, two-tailed Student's t-test, n=4 (ligated), n=5 (unligated).

C - Representative images of immunohistochemistry for STAT-1 protein at day 7. Positive cells have brown nuclei (red arrow); negative cells are stained with haematoxylin and have blue nuclei (black arrow). Scale bar represents 50μM and applies to all panels.

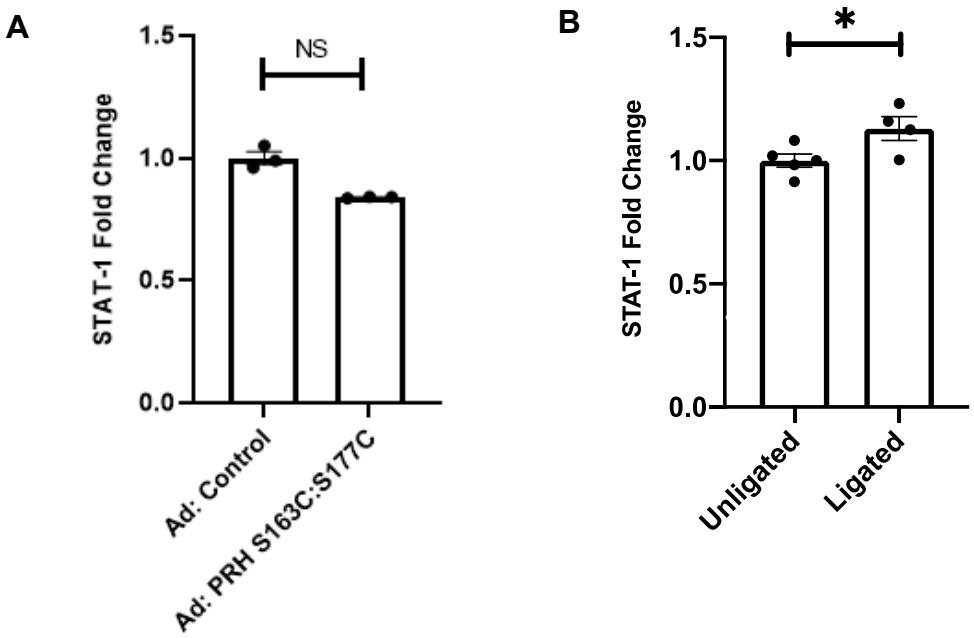
A
1.5
1.0
0.5
0.0
STAT-1 Fold Change
NS
Ad: Control
Ad: PRH S163C:S177C
B
1.5
1.0
0.5
0.0
STAT-1 Fold Change
*
Unligated
Ligated

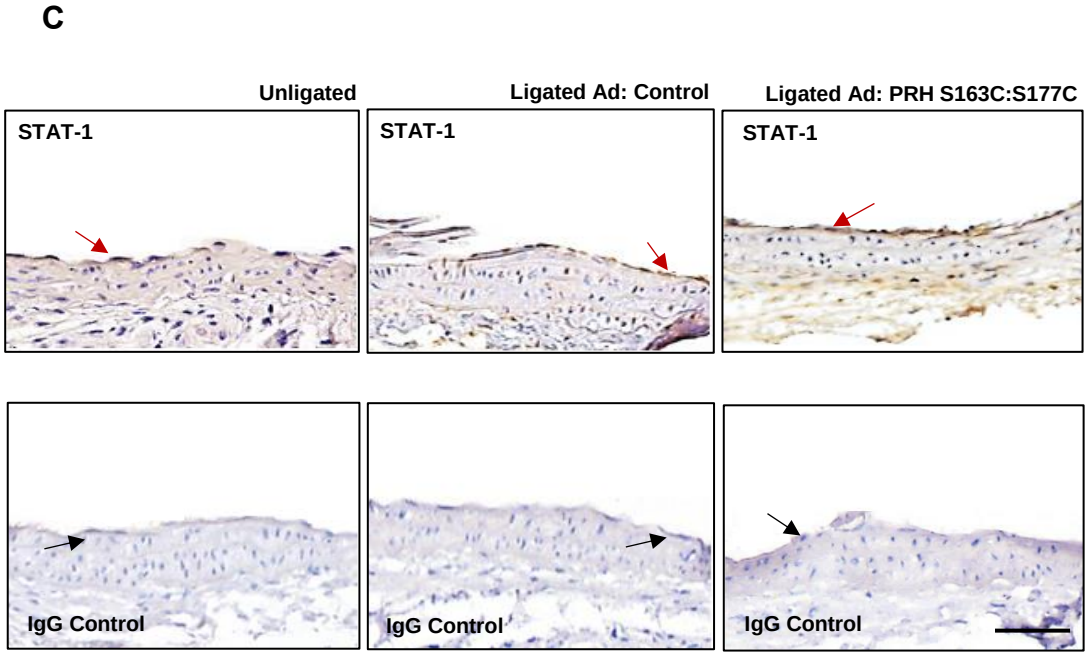
C
Unligated
Ligated Ad: Control
Ligated Ad: PRH S163C:S177C
STAT-1
STAT-1
STAT-1
IgG Control
IgG Control
IgG Control

6.3.11 Identification of HDAC-9 as a novel PRH S163C:S177C-regulated gene

In addition to the discovery of STAT-1, HDAC-9 was identified as one of the putative targets of PRH S163C:S177C. The first aim was to determine whether the observed depleted levels of HDAC-9 mRNA detected using NGS could be confirmed at the protein level and therefore Western blotting for HDAC-9 protein was employed. HSV VSMCs were subjected to infection with 5 x 10^8 pfu/ml of Ad: Control or Ad: PRH S163C:S177C, or left uninfected, for 18 hours. Subsequently, cells were incubated for another 24 hours after replenishing the culture medium. HDAC-9 protein was detected at a similar level in uninfected VSMCs and those infected with Ad: Control. Whilst HDAC-9 protein was significantly lower in VSMCs infected with Ad: PRH S163C:S177C compared to both the uninfected VSMCs and VSMCs infected with the control virus (FIGURE 6.10).

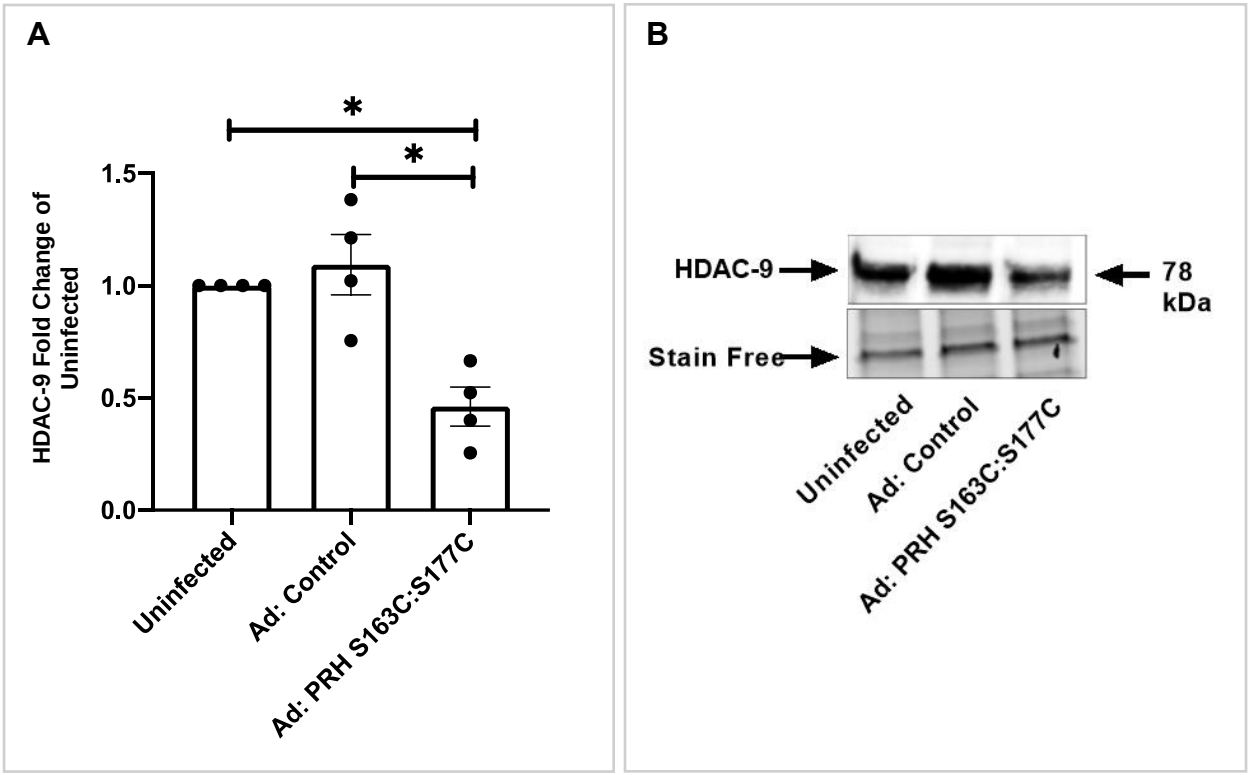

FIGURE 6.10 – Overexpression of PRH S163C:S177C reduced HDAC-9 protein in HSV VSMCs

HSV VSMCs were infected with Ad: Control or Ad: S163C:S177C PRH or left uninfected.

(A) Quantification of HDAC-9 protein using Western blotting. Data was normalised using stain-free bands and expressed as a fold change from uninfected control. * indicates $p<0.05$, ANOVA, Student-Newman-Keuls Multiple Comparisons Test, n=5. Error bars indicate SEM.

(B) Representative Western blot for HDAC-9. Stain-free bands served as a loading control. Approximate molecular weight of detected protein bands are indicated on the right in kDa.

6.3.12 Inhibition of HDAC-9 using TMP269 attenuated HSV VSMC proliferation

To investigate the role of HDAC-9 in VSMC proliferation, HSV VSMCs were treated with 50 nM TMP269 (HDAC-9 inhibitor) in DMSO or DMSO alone (control). In addition, 10% FBS/DMEM were supplemented with 10 μM EdU for Click-iT EdU analysis. Assessment of cell growth was performed using measuring EdU incorporation 24 hours later. Treatment with 50nM significantly decreased VSMC proliferation compared to the DMSO control (FIGURE 6.11). Western blotting analysis for the cell cycle proteins, p21 and cyclin D1, revealed that TMP269 significantly decreases cyclin D1 levels albeit at a non-significant level although significantly upregulates p21 protein expression (FIGURE 6.12).

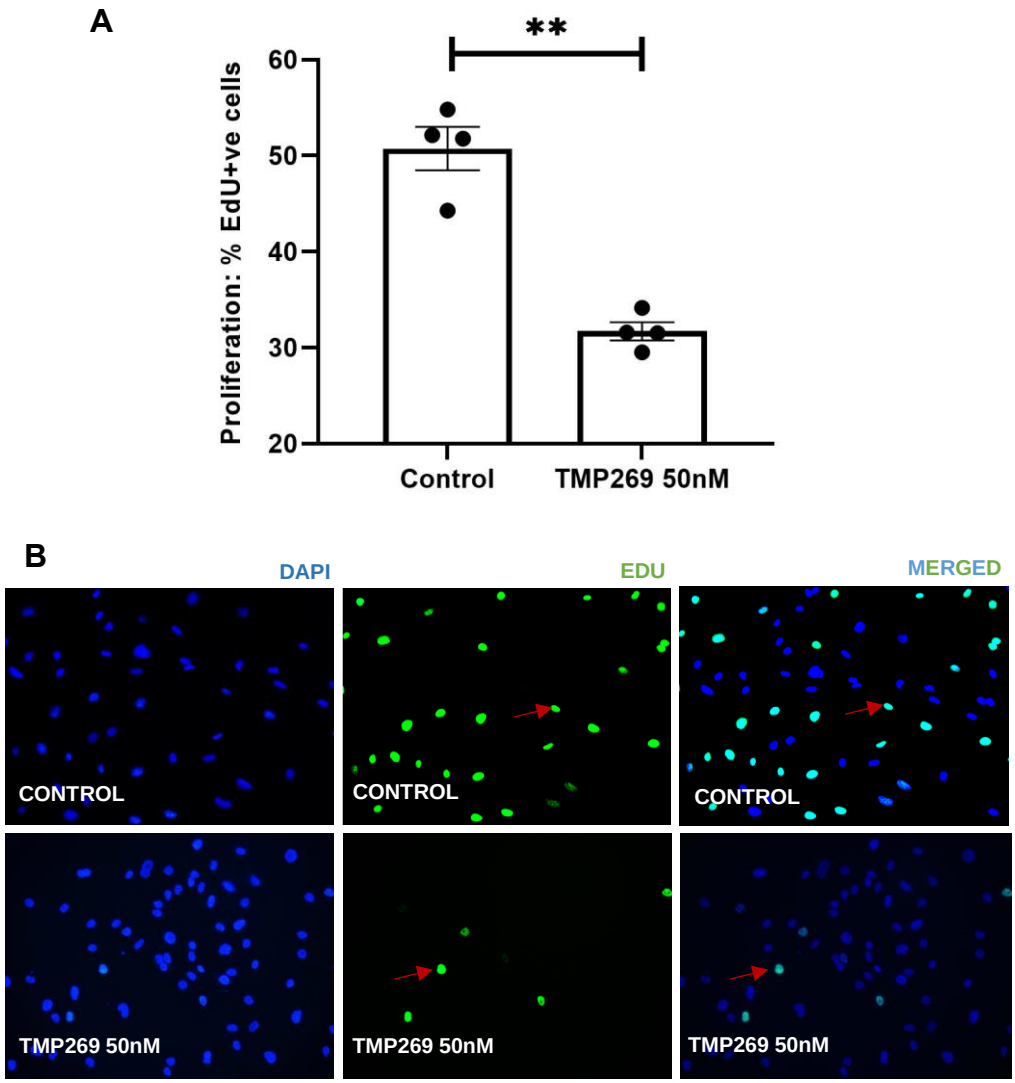

FIGURE 6.11 – TMP269 retarded HSV VSMC proliferation detected using quantification of EdU incorporation

HSV VSMCs were cultured with 50 nM TMP269 in DMSO or DMSO control alone.

A - EdU incorporation was quantified and expressed as the percentage of EdU-positive cells. ** indicates $p<0.01$, paired, two-tailed Student's t-test, n=4. Error bars indicate SEM.

B - Representative images of Click-iT EdU assay. Positive cells are green (some positive cells are indicated by red arrows), and all nuclei are stained blue with DAPI. Scale bar measures 50 μM and applies to all panels.

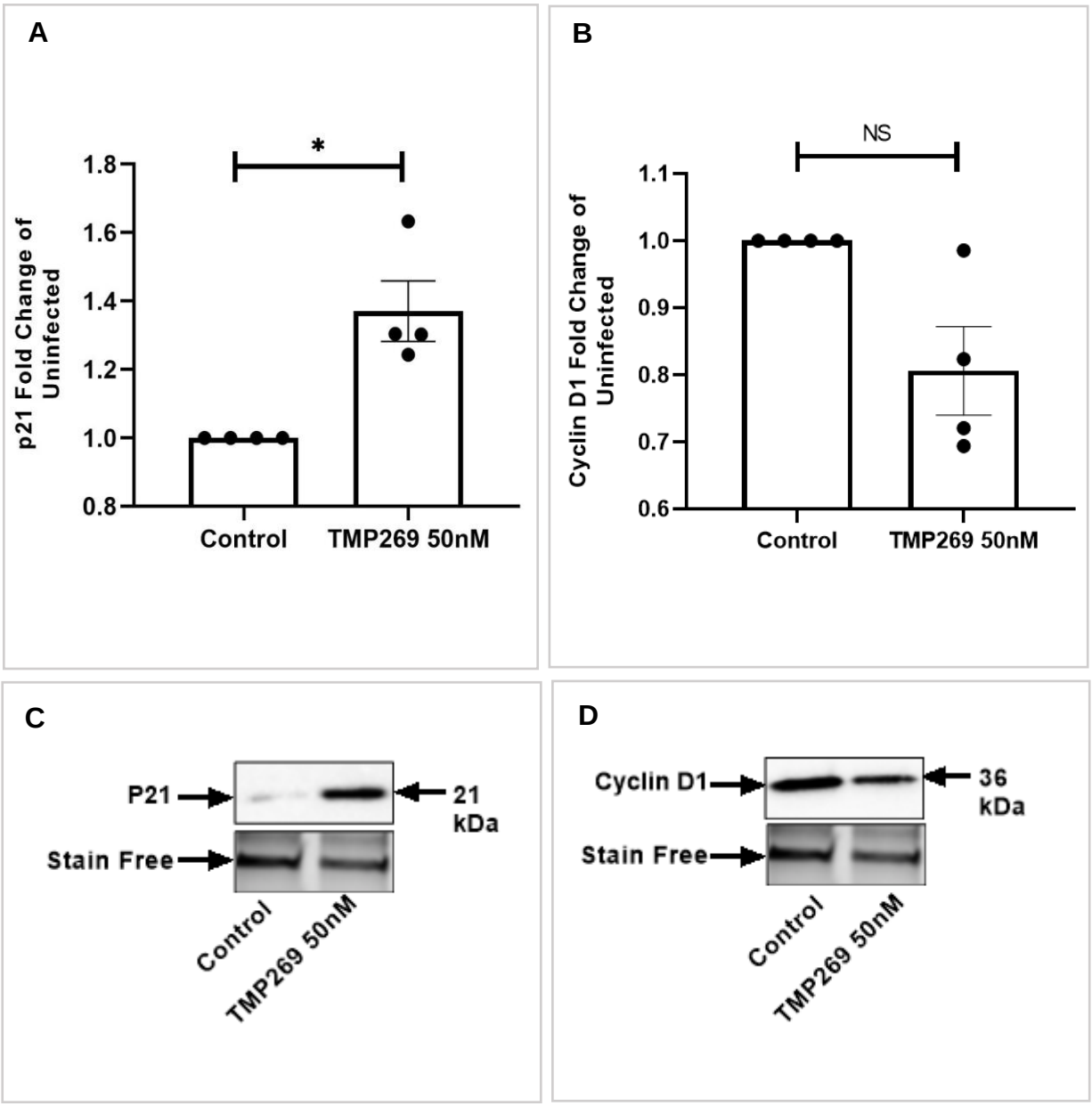

FIGURE 6.12 – TMP269 reduced cyclin D1 protein levels in HSV VSMCs

HSV VSMCs were cultured with 50 nM TMP269 in DMSO or DMSO control alone. Quantification of p21 protein (**A**) and cyclin D1 protein (**B**) using Western blotting; data was normalised using stain-free bands and expressed as a fold change from uninfected control. NS denotes not significant, * indicates $p<0.05$, paired, two-tailed Student's t-Test, n=4.Error bars indicate SEM. Representative Western blot for p21 protein (**C**) and cyclin D1 (**D**). Stain-free bands served as a loading control. Approximate molecular weight of detected protein bands are indicated on the right in kDa.

6.3.13 Inhibition of HDAC-9 using TMP269 did not affect HSV VSMC apoptosis

To assess whether fludarabine affects VSMC apoptosis, HSV VSMCs were treated with 50 nM TMP269 (HDAC-9 inhibitor) or DMSO (control) for 24 hours. As a positive control, cells were incubated with 200 ng/mL human recombinant Fas-ligand in 2% serum-free media. Subsequently, apoptosis was assessed via immunofluorescence for cleaved caspase-3. As expected, Fas ligand significantly induced apoptotic cell death with respect to uninfected control (FIGURE 6.13). Quantification of cleaved caspase-3 positive cells showed that rate of apoptosis in HSV VSMCs was not affected with TMP269 treatment.

FIGURE 6.13 - TMP269 in HSV VSMCs had no effect on apoptosis

HSV VSMCs were subjected to treatment of with or without 50 nM TMP269. Fas ligand was used as a positive control.

A – The rate of apoptosis was quantified and expressed as the percentage of cleaved caspase-3-positive cells. NS denotes not significant, paired, two-tailed Student's t-Test, n=4.

B – Representative images of immunocytochemistry for cleaved caspase-3 (CC-3). Positive cells (red arrow) are green, and all nuclei are stained blue with DAPI. Scale bar measures 10μM and applies to all panels. CC-3 denotes cleaved caspase-3.

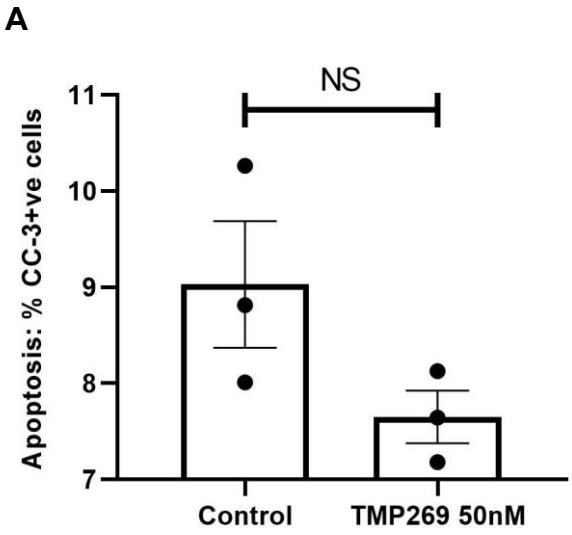
A
NS
11
10
9
8
7
Apoptosis: % CC-3+ve cells
Control
TMP269 50nM

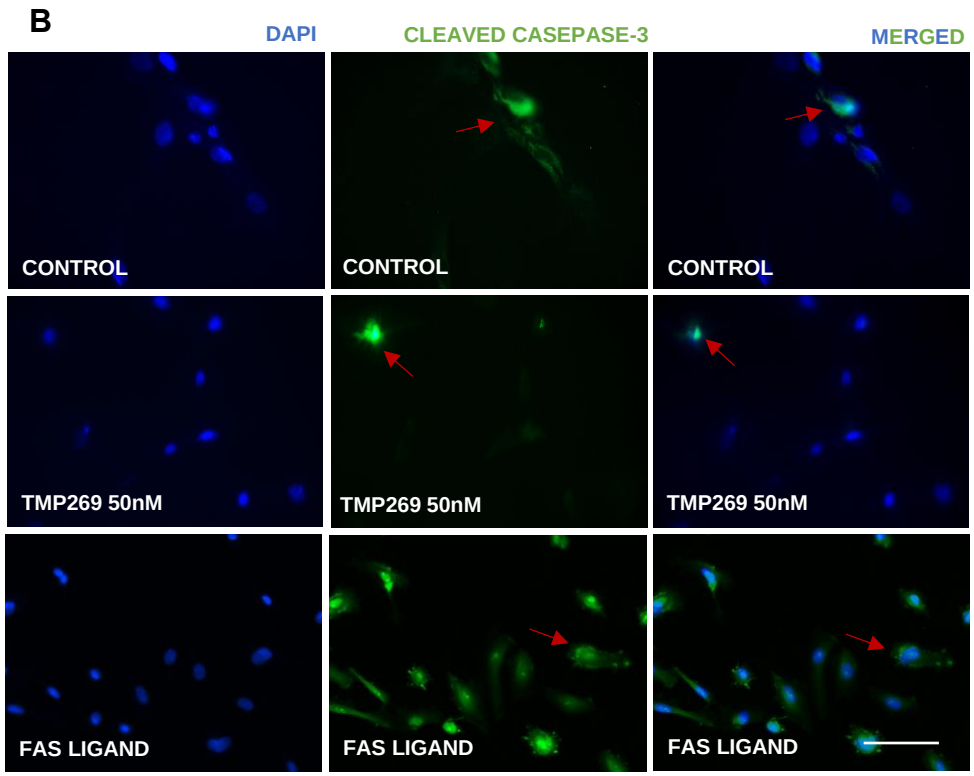
B
DAPI
CLEAVED CASEPASE-3
MERGED
CONTROL
CONTROL
CONTROL
TMP269 50nM
TMP269 50nM
TMP269 50nM
FAS LIGAND
FAS LIGAND
FAS LIGAND

6.3.14 Inhibition of HDAC-9 using TMP269 attenuated HSV VSMC migration

To assess whether HDAC-9 affects VSMC migration, HSV VSMCs were treated with 50 nM TMP269 in DMSO (HDAC-9 inhibitor) or DMSO alone (control). Subsequently, confluent HSV VSMCs were wounded then incubated for a further 24 hours. Treatment with 2 mM hydroxyurea inhibited cell proliferation. The distance migrated was quantified by measuring the wound at 0- and 24-hours post-wounding. Quantification of the migrated distance from the wound revealed that TMP269 significantly attenuated HSV VSMCs migration compared to VSMCs treated with the control (FIGURE 6.14).

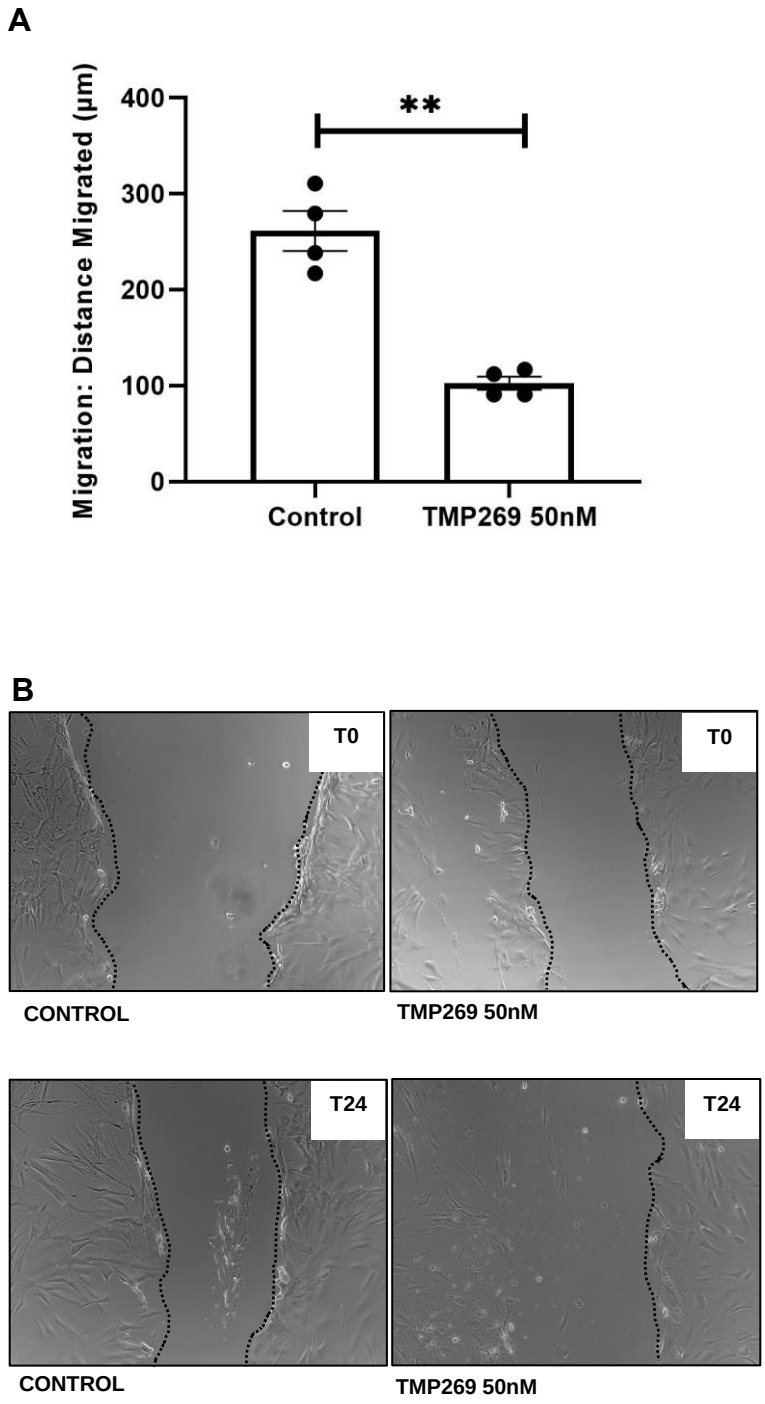

FIGURE 6.14 TMP269 reduced migration of primary HSV VSMCs

Migration of HSV VSMCs treated with 50 nM TMP269 in DMSO or DMSO control was assessed using the scratch wound assay. **(A)** Migration was quantified and expressed as distance migrated (µM); ** indicates $p<0.01$, paired, two-tailed Student's t-test, n=4. Error bars indicate SEM. **(B)** Representative images of scratch wound assay. Dashed line indicates wound edge. T0 indicates Time = 0 hr; T24 indicates Time = 24 hr. Scale bar represents 1 mm and applies to all panels.

6.3.15 Inhibition of HDAC-9 using TMP269 increased contractile marker proteins

To investigate the role of HDAC-9 in the regulation of VSMC contractile protein markers, HSV VSMCs were treated with 50 nM TMP269 (HDAC-9 inhibitor) in DMSO or DMSO alone (control) in 10% FBS/DMEM. After 24 hours, cells were lysed for Western blotting analysis of the VSMC-specific contractile proteins, calponin and smoothelin. The level of smoothelin and calponin proteins detected in the TMP269-treated VSMCs was significantly higher than that detected in the control VSMCs treated with control alone (FIGURE 6.15).

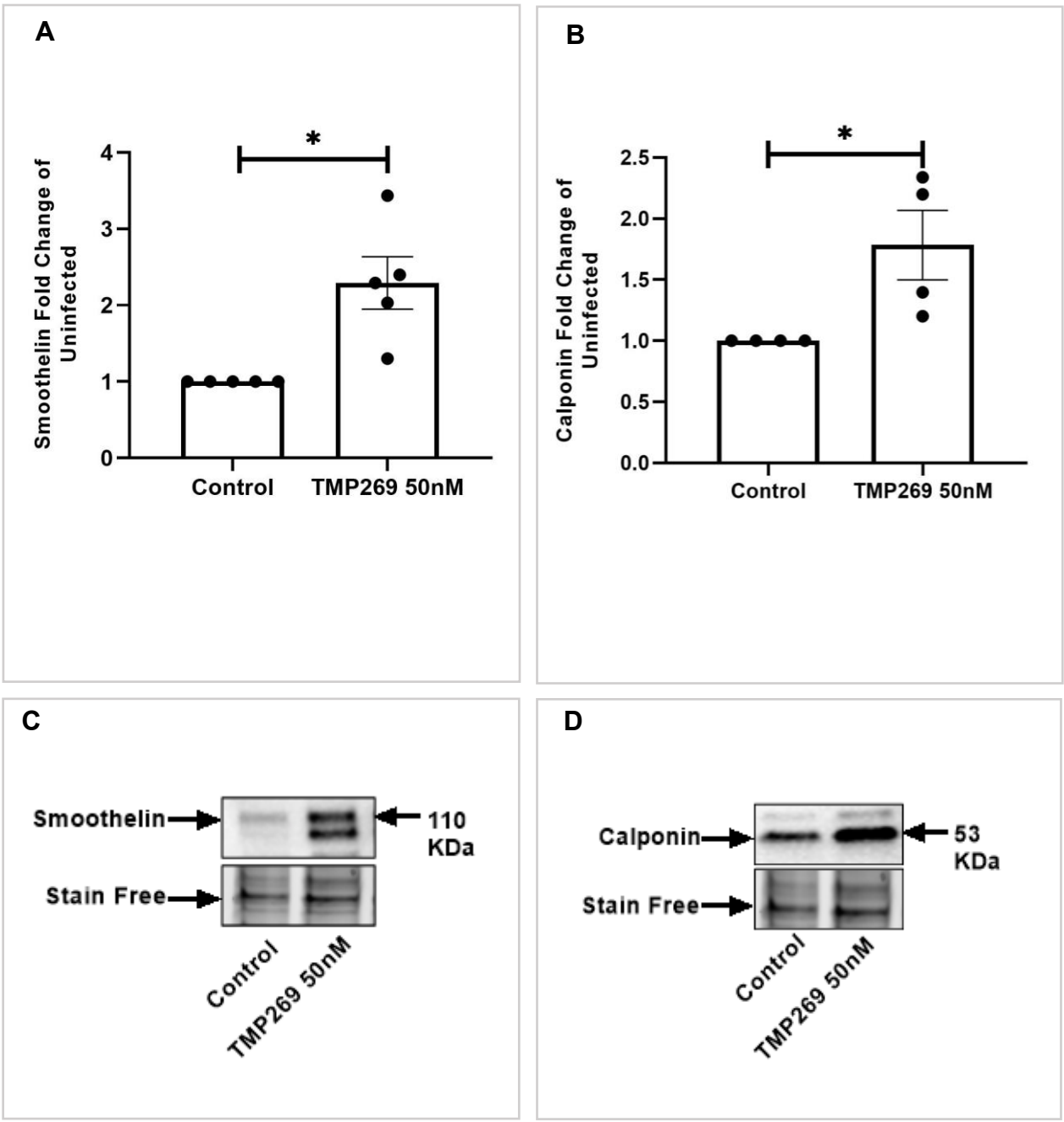

FIGURE 6.15 – The effect of TMP269 on contractile protein markers in HSV VSMCs

HSV VSMCs were cultured with 50 nM TMP269 in DMSO or DMSO control alone. Quantification of smoothelin (**A**) and calponin (**B**) proteins using Western blotting. Data was normalised using stain-free bands and expressed as a fold change from control. * indicates $p<0.05$ vs. uninfected, paired, two-tailed Student's t-test, n=4. Representative Western blots for smoothelin (**C**) and calponin (**D**). Stain-free bands served as a loading control. Approximate molecular weights are indicated on the right in kDa.

6.3.17 HDAC-9 protein *in vivo*

To identify the expression of HDAC-9 in the 7-day ligated left carotids, sections were immunostained for HDAC-9 and the percentage of positively stained tissue was calculated using Image-J analysis. Interestingly, HDAC-9 expression was significantly downregulated in the Ad: PRH S163C:S177C group vs control group (FIGURE 6.16A and C). Next, we examined the HDAC-9 expression in unligated vs ligated mice carotids. Our results have shown that unligated mice carotids had a significantly lower HDAC-9 levels in comparison to the ligated carotids (FIGURE 6.16B and C). Negative control sections probed with non-immune mouse IgG showed no staining.

FIGURE 6.16 – HDAC-9 protein in unligated and ligated left carotid arteries after 7 days with and without infection with Ad: Control or Ad: PRH S163:S177C

Mouse carotid arteries were ligated in C57B/L6 mice to induce intimal thickening then subjected to infection with adenoviruses encoding either Ad: Control or Ad: PRH S163C:S177C. The right carotid arteries were used as an unligated controls.

A - Quantification of HDAC-9 protein in Ad: Control vs. Ad: PRH S163C:S177C infected ligated carotid arteries, expressed as the fold change, NS denotes not significant, unpaired, two-tailed Student's t-test, n=3. Error bars indicate SEM.

B - HDAC-9 expression in ligated vs unligated mice carotids was quantified and expressed as the fold change, * indicates $p<0.05$, unpaired, two-tailed Student's t-test, n=4 (ligated), n=5 (unligated).

C - Representative images of immunohistochemistry for HDAC-9 protein at day 7. Positive cells have brown nuclei (red arrow); negative cells are stained with haematoxylin and have blue nuclei (black arrow). Scale bar represents 50μM and applies to all panels.

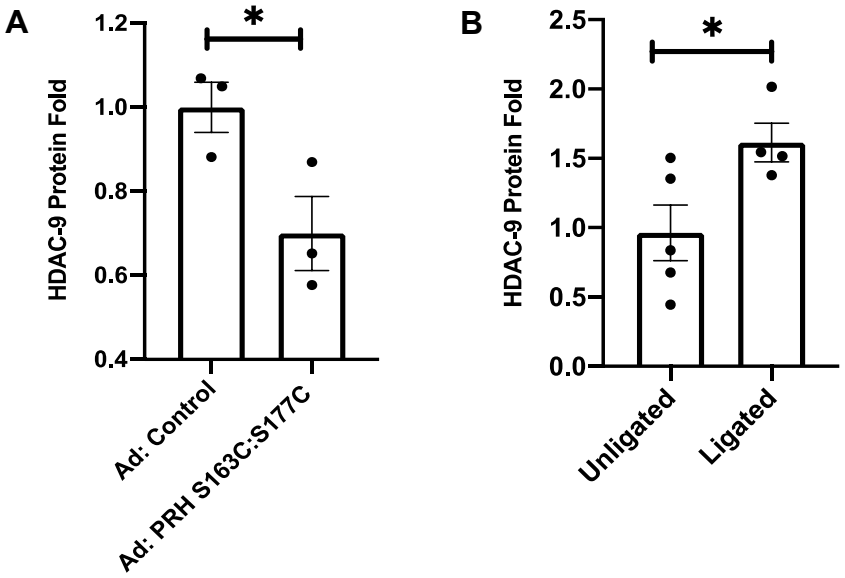
A
1.2
1.0
0.8
0.6
0.4
HDAC-9 Protein Fold
*
Ad: Control
Ad: PRH S163C:S177C
B
2.5
2.0
1.5
1.0
0.5
0.0
HDAC-9 Protein Fold
*
Unligated
Ligated

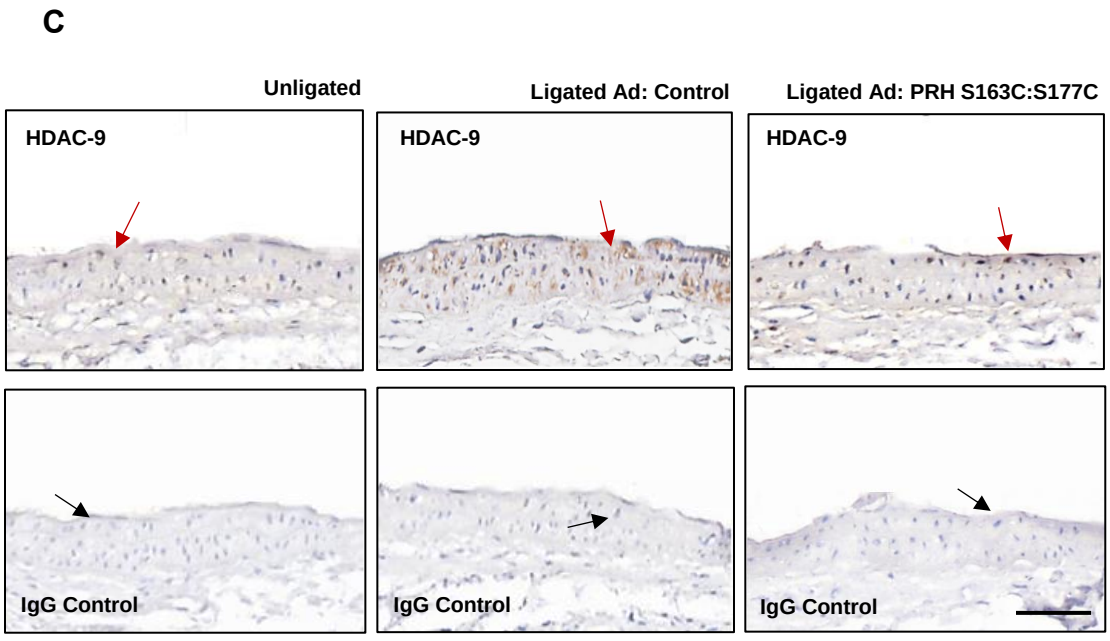
C
Unligated
Ligated Ad: Control
Ligated Ad: PRH S163C:S177C
HDAC-9
HDAC-9
HDAC-9
IgG Control
IgG Control
IgG Control

6. 4 DISCUSSION

It was previously observed that overexpression of PRH S163C:S177C caused cessation of VSMC proliferation, migration, apoptosis, and de-differentiation *in vitro*. Additionally, gene transfer of PRH S163C:S177C markedly decreased intimal thickening in the mouse carotid artery ligation model. The mechanism underlying this phenotype is partly related to PRH S163C:S177C mediated upregulation of p21 expression and downregulation of cyclin D1. Activation of PRH:CC induces a cell cycle block at G1 to S phase transition by inhibition of p21 degradation, leading to a rise in cellular p21 protein levels, and consequent inhibition of cyclin D1. However, the underlying intracellular signalling pathway responsible for modulation of p21 and cyclin D1 have not been elucidated.

In this chapter, IPA was used to identify and validate genes regulated by PRH S163C:S177C. This research utilised NGS data analysis, stringent bioinformatics filtering strategies and literature reviewing. Dysregulated transcriptional hubs, including transcription factors and their gene expression signatures are characteristic of mechanisms which may fundamentally elucidate pathological processes and underlying mechanisms. Thus, for the purpose of this study, we have focused on identifying potential transcription factors and transcriptional regulators regulated by PRH S163C:S177C. Further IPA analysis narrowed down the candidate DEG list, with the potential of identifying novel PRH target genes including STAT-1 and HDAC-9.

6.4.1 Identification of STAT-1 as a downstream target of PRH S163C:S177C

The Signal Transducer and Activator of Transcription (STAT) proteins are intracellular facilitators of cell growth, apoptosis and lineage-specific differentiation. To date, seven well-conserved members of the STAT family have been discovered (Akira, 1999). Under normal conditions, transient activation of STATs is stimulated by extracellular signals although such activation is often selective and bind to the promoters of specific target (Dorritie, McCubrey and Johnson *et al.,* 2013). Post-transcriptional modifications of these transcription factors can regulate their transcriptional activity. Accumulating evidence suggests that phosphorylation of STATs can occur upon activation by endogenous receptor tyrosine kinases, Src and abl and serine/threonine kinases including protein kinase CK2 and mitogen-activated protein kinase (MAPK) (Aparicio-Siegmund *et al.,* 2014).

In this study, NGS and bioinformatic analysis identified STAT-1 as a potential downstream target of PRH S163C:S177C. Data from NGS analysis demonstrated downregulation of STAT-1 at the mRNA level as a result of PRH S163C:S177C overexpression. In agreement with this finding, Western blot analysis showed a marked reduction of STAT-1 at the protein level. It has been formerly reported that induction of janus kinases and STATs, STAT-1 and STAT-3, was evident within intimal thickenings one week after balloon-injury of rat arteries and subsequently declined at day 14 (Seki, 2000). To explore whether the levels of STAT-1 protein was modulated during intimal thickening induced by carotid ligation immunohistochemistry was performed on mouse carotid arteries 7 days after ligation and compared with unligated arteries. There was no statistical difference in the amount of STAT-1 protein in the ligated carotid controls compared to the unligated carotid controls. However, the sample sizes for the groups were small due to the lack of suitable samples and it would be beneficial to repeat this analysis with increased numbers of samples in the future. Immunohistochemical detection of STAT-1 was employed in the ligated left carotids of mice treated with either Ad: Control or Ad: PRH S163C:S177C for 7 days. Interestingly, although fails to reach a significant level, it seems that STAT-1 expression was downregulated in the left carotids which received adenoviral-mediated PRH S163C:S177C gene delivery in comparison to the control group. It is important to highlight that data was conducted for this experiment base on n=3 as these samples were prepared for the pilot study to evaluate efficiency of gene delivery and not powered to detect altered protein expression.

Hence, we hypothesize that PRH S163C:S177C overexpression mediates VSMC proliferation and function, in part, by repressing the activation of STAT-1 activity. Having said this, the role of STAT-1 in VSMC function and other cell types remains unclear.

6.4.2 Suppression of VSMC proliferation using Fludarabine

Fludarabine, also known as Fludara®, is an established specific inhibitor of STAT-1 (Feng *et al.,* 2017), which is a standard chemotherapy treatment for patients suffering with chronic lymphocytic leukaemia (CLL) (Lukenbill and Kalaycio, 2013). In the present study, incorporating fludarabine was employed to specifically inhibit the function of the STAT-1 in HSV VSMCs.

To date, only one publication exists reporting the protective role of the STAT-1 inhibitor in dysregulated growth of VSMCs. Fludarabine is a selective STAT-1 inhibitor which have been previously reported to arrest rat VSMC growth (Torella *et al.,* 2007). These results agree with the findings of this chapter in which data demonstrates that STAT-1 suppressed HSV VSMC

growth without affecting the migratory capabilities of VSMC. The effect of fludarabine on cell cycle regulatory proteins demonstrated its ability to decrease cyclin D1 significantly. On the other hand, fludarabine did not affect p21 which may be due to the timings or reveal that PRH affects multiple pathways and it is the combined affects that lead to most effective inhibition of proliferation and changes in cell cycle proteins. Hence, the Western blotting results corroborate the EdU analysis and are strengthened by the existing report on the anti-proliferative actions of STAT-1 in rat primary VSMCs. To support our data, using A10 tTA-IRES-Neo cells, heparin inhibited VSMC proliferation and this is mediated via STAT-1 phosphorylation on serine 727 via activation protein kinase, RNA activated leading to the cell cycle arrest of VSMCs (Handy and Patel, 2013). Despite the anti-atherogenic potential of STAT-1 inhibitors, the potential of fludarabine is hampered by its toxicity due to its purine (adenine) nucleoside analogue (Sikorski *et al.,* 2011). However, our findings illustrated that fludarabine treatment did not affect apoptotic cell death. Nonetheless, these contrasting findings may serve as a basis for designing novel therapeutic regiments which are less toxic for STAT-1 inhibition. Engineering an improved therapy to outwit the development of vein graft disease or restenosis by creating inhibitors to stall DNA replication of VSMCs will provide a better understanding of the molecular mechanisms associated to the pathophysiology of the disease and may enhance the long-term patency of grafts.

6.4.3 Fludarabine did not affect VSMC phenotype

Under pathological conditions, VSMCs de-differentiate into a pro-proliferative, pro-migratory and synthetic phenotype. Contrary to this under normal conditions, quiescent VSMCs usually exhibit a contractile phenotype. Since PRH S163C:S177C promoted the contractile VSMC phenotype it was of interest to determine whether STAT-1 contributed to the regulation of the contractile proteins, smoothelin and calponin. The results showed that STAT-1 inhibition did not regulate smoothelin and calponin protein levels and therefore may not contribute for the phenotypic switching of VSMCs to the protective contractile phenotype.

In conclusion, the findings suggest that STAT-1 inhibition retards VSMC proliferation and therefore may be responsible at least in part for the anti-proliferative effects of PRH S163C:S177C. It does not, however, appear mediate the effects of PRH S163C:S177C-associated phenotypic switching which may perhaps occur through a different mechanism and other PRH S163C:S177C-regulated targets may be involved instead in this process. One possible mechanism could be that although STAT-1 does not alter the expression of

contractile markers, PRH:CC may modulate VSMC contractility through interacting directly or indirectly with other molecules which warrants further studies to be conducted.

6.4.4 Histone deacetylases (HDACs) and Histone deacetylases Inhibitors (HDACis)

In non-dividing cells, the DNA is tightly bound to prevent and govern binding of transcription factors. Eukaryotes package their DNA into a highly ordered structure with proteins called chromatin. Within chromatin lies the core nucleosome which is comprised of positively charged proteins termed histones that form an octamer; $(H3–H4)_2$ tetramer and two H2A-H2B dimers (Haggarty and Tsai, 2012). The structure of chromatin is not inert, post-transcriptional modification (PTMs) of the histones occur and alter the chromatin structure and thereby influence gene transcription. A myriad of different PTMs including methylation, phosphorylation, SUMOylation, ubiquitination, and acetylation occur. Acetylation is the most extensively characterised type of modification (Wolffe and Hayes, 1999). In 1964, Allfrey and colleagues first documented histone acetylation which requires the interplay and opposing actions between histone deacetylases (HDACs) and histone acetyltransferases (HATs) (Allfrey *et al.,* 1964). In an open chromatin conformation, HATs recruit acetyl coA as a cofactor to acetylate lysine residues residing on histone proteins forming ε-N-acetyllysine and relaxes the highly ordered chromatin architecture. This increases the specific DNA-binding activity and access to transcription factors. For the maintenance of a closed chromatin conformation, HDACs counterbalance the effects of HATs and catalyse the removal of the acetyl moiety (deacetylation) from lysine residues in both histone and non-histone substrates, thus, restoring lysine's positive charge and thereby stabilise the histone-DNA interaction (Xhemalce, Dawson and Bannister, 2011; Peserico and Simone, 2011; Choudhary et al., 2009). HDACs are a group of chromatin-modifying enzymes which play a critical role in the regulation of gene expression. In mammals, eighteen HDACs have been discovered and the members of the HDACs family are categorised into four classes based on their structure, function and tissue distribution: class I (HDAC-1, 2, 3, and 8), class IIa (HDAC-4, 5, 7, and 9), class IIb (HDAC-6 and 10), class III (sirtuins1-7), and class IV (HDAC-11) (Peserico and Simone, 2011). Moreover, aberrant gene transcription regulation of HDACs have been extensively studied to be involved in regulating cellular homeostasis including proliferation, apoptosis and DNA repair (Telles and Seto, 2014).

In disease states such as cancer, abnormal HDAC upregulation has been linked to diverse malignancies in gastrointestinal, prostate and breast carcinomas (Liu *et al.,* 2019).

Accordingly, HDAC inhibitors (HDACi) which block/interfere with the function of HDACs have emerged as an attractive approach for cancer therapy. To date, there are seven HDACis in clinical trials for various diseases (Table 6.3) and four HDACis are US-FDA approved for clinical use (Lyu et al., 2019). Moreover, HDACis continue to be developed as anti-cancer drugs based on their ability to induce cytotoxic effects and repress proliferation especially in cancer cells (Lyu *et al.,* 2019). Cumulative evidence also implicates a role of HDACs in modulation of cardiovascular diseases, opening up the possibility of therapeutic potential of HDACis (Chen *et al.,* 2020; Pickell *et al.,* 2020). Firstly, studies have revealed that HDAC inhibition also repressed myocardial hypertrophy and fibrosis (Lyu at al., 2019; Eom and Cook*,* 2015). The Class I HDACi (HDAC 1, 2, 3 and 8), valproic acid (VPA), inhibited cardiac hypertrophy and fibrosis via acetylation of the mineralocorticoid receptor (Jung *et al.,* 2018; Kang *et al.,* 2015). In a more recent paper by Barbosa and colleagues, the HDAC I/II inhibitor, Rhein, was reported to inhibit collagen contraction and cardiac remodelling thereby suggesting it is protective against cardiac hypertrophy and progression of fibrosis (Barbosa *et al.,* 2020). It has been suggested that the HDAC inhibitor, Butyrate, modulates VSMC proliferation through H3 posttranslational modification by H3K9 acetylation, reduced H3K9 dimethylation and low levels of H3S10 phosphorylation (Matthew *et al.,* 2010). This implied that inhibition of HDACs could potentially reduce intimal thickening. Indeed, it was recently described that trichostatin A, a pan-inhibitor of HDAC Class I/II, suppressed intimal hyperplasia induced by balloon-injury of the rat carotid artery (Kee *et al.,* 2011). Of interest, another Class IIa HDAC, HDAC-4, has been previously reported to play a role in the regulation of intimal thickening (Chen *et al.,* 2020). Silencing HDAC-4 using siRNA resulted in inhibition of aberrant VSMC proliferation and migration (Chen *et al.,* 2020; Zhang *et al.,* 2019; Usui *et al.,* 2014). Consistent with these findings, it was also shown that the HDAC Class IIa inhibitor, MC1568, prohibited intimal thickening induced by ligation of the carotid artery in mice (Usui *et al.,* 2014). Tubastatin A, an inhibitor of HDAC-6, was also reported to attenuate intimal thickening in a balloon-injured rat artery (Zhang *et al.,* 2018). These findings suggest that class I and class II HDACs at least in part mediate intimal thickening. Since HDACs are now beginning to be appreciated in cardiovascular disease processes (Chen *et al.,* 2020; Liu at al., 2019), the utility of HDACis have also been implicated in pre-clinical studies for stroke, cardiac arrest, myocardial infarction and fibrosis (Pickell *et al.,* 2020). However, to date clinical trials using HDACis in cardiovascular and fibrotic diseases have not been reported.

Table 6.3: HDAC Inhibitors in Clinical Trials

HDACi	Class	HDAC Target	Clinical Usage	Phase	Reference
Vorinostat	Hydroxamates	Class I, II, and IV	CTCL	Phase II	Duvic *et al.,* 2007
(SAHA, Zolinza®)			Soft tissue sarcomas	Phase II	Schmitt *et al.,* 2016
			Sickle cell disease	Phase I/II	Okam *et al.,* 2015
			Melanoma	Phase II	Haas *et al.,* 2014
			Gastrointestinal cancer	Phase I	Doi *et al.,* 2013
			Follicular and mantle cell lymphoma	Phase I	Watanabe *et al.,* 2010
			Prostate cancer	Phase II	Bradley *et al.,* 2009
			Glioblastoma multiforme	Phase II	Galanis *et al.,* 2009
			HIV infection	Phase II	Elliot *et al.,* 2014
Panobinostat	Hydroxymates	Class I and II	MDS or AML	Phase 3	Bug *et al.,* 2017
(LBH589, Farydac®)			Metastatic melanoma	Phase I	Ibrahim *et al.,* 2016
			Neuroendocrine tumors	Phase II	Jin *et al.,* 2016
			Solid tumors	Phase I	Jones *et al.,* 2011
			HIV infection	Phase I/II	Olesen *et al.,* 2015

Belinostat **(Beleodaq™, PXD101)**	Hydroxymates	Class I and II	Lymphoma PTCL Liver cancer Ovarian cancer	Phase II Phase II Phase I/II Phase II	Puvvada *et al.,* 2017 O'Connor *et al.,* 2015; Foss *et al.,* 2015 Wang *et al.,* 2013; Yeo *et al.,* 2012 Dizon *et al.,* 2012
Givinostat **(ITF2357)**	Hydroxymates	Class I and II	Duchenne muscular dystrophy Polycythemia vera Myeloproliferative diseases	Phase I/II Phase II Phase IIA	Bettica *et al.,* 2016 Finazzi *et al.,* 2013 Rambaldi *et al.,* 2010
Romidepsin **(FK228, Istodax®)**	Cyclic tetrapeptide	Class I and II	PTCL Non–small-cell lung cancer HIV infection	Phase II Phase I Phase I	Shustov *et al.,* 2017 Gerber *et al.,* 2015 Sogaard *et al.,* 2015
Entinostat **(MS-275)**	Benzamides	Class I	Metastatic colorectal cancer Breast cancer Hodgkin lymphoma Myeloid neoplasm	Phase II Phase II Phase II Phase II	Azad *et al.,* 2017 Connolly *et al.,* 2017 Batlevi *et al.,* 2016 Prebet *et al.,* 2016; Fandy *et al.,* 2009

Valproic acid (VPA)	Short-chain fatty acid	Class I	Gastric cancer Non-small cell lung cancer Rectal cancer	Phase II Phase I Phase I/II	Fushida *et al.,* 2016 Chu *et al.,* 2013 Avallone *et al.,* 2014

Keywords: AML, acute myeloid leukemia; CTCL, cutaneous T-cell lymphoma; HIV, human immunodeficiency virus; MDS, myelodysplastic syndrome; PTCL, peripheral T-cell lymphoma. Table adapted from Lyu *et al.,* 2019

6.4.5 Identification of HDAC-9 as a downstream target of PRH S163C:S177C

Previous genome-wide association studies have shown that genetic polymorphisms in HDAC-9 are linked to several cardiovascular diseases including coronary artery disease (Nelson *et al.,* 2017), atherosclerotic stroke (Malik *et al.,* 2018) and atherosclerotic aortic calcification (Malhotra *et al.,* 2019), suggestive of a role in disease pathogenesis. Consistent with these observations, expression of HDAC-9 was upregulated in carotid atherosclerotic plaques compared to atherosclerosis free left internal thoracic artery controls (Markus *et al.,* 2013). HDAC-9 knockout mice induced a stable atherosclerotic plaque phenotype by reducing proinflammatory responses in the arterial wall, in part by deacetylation of inhibitory kappa B kinase (Asare *et al.,* 2020). This present study is the first to identity HDAC-9 as a downstream target of PRH S163C:S177C. RNA sequencing performed to analyse RNA expression revealed that PRH S163C:S177C significantly downregulated the mRNA expression of HDAC-9 by approximately 4-fold in HSV VSMCs. In the top-enriched canonical pathways, HDAC-9 was discovered in both Cardiac Hypertrophy and Calcium Signalling. Previous studies have revealed an association between VSMC contractility and the intracellular calcium signalling control (Zhu *et al.,* 2019; Brozovich *et al.,* 2016; Lipskaia *et al.,* 2012). For these reasons, confirmation of HDAC-9 downregulation at the protein level was performed. These findings highlight a direct transcriptional regulation by PRH S163C:S177C. The *in vivo* results show for the first time that HDAC-9 expression upregulated by ligation of the carotid artery in mice and induction of intimal thickening and is downregulated in the ligated left carotid arteries which received Ad: PRH S163C:S177C in comparison to the control left carotids receiving the control virus.

6.4.6 Pharmacologic inhibition of HDAC-9 as a novel strategy to repress VSMC proliferation and migration

Unwarranted proliferative and migratory action of VSMCs are hallmark features of several vascular pathologies and occlusive diseases such as atherosclerosis, hypertension, and arterial and in-stent restenosis. Besides having the ability to deacetylate signal mediators including STAT-3, Smad family member 7 and β-catenin (Eom and Kook 2014), there had been early reports of the role of HDACs in regulating cell cycle progression since HDACs act redundantly to promote deacetylation of p53-, E2 factor (E2F)-, and Rb protein (pRb)- cell proliferation transcription factors thereby coordinating cell cycle arrest during G0 (relative to S phase) (Glozak *et al.,* 2005). For example, histone deacetylase-mediated transcriptional

inhibition can arise from retinol binding protein 1 (RBP1) employing HDACs to catalyse formation of the E2F-pRb-RBP1-Sin3-HDAC complex situated at the promoter region of the E2F-responsive gene (Lai *et al.,* 2001). Due to the lack of isoform-specific HDAC-9 inhibitor, the therapeutic potential of inhibiting HDAC-9 was evaluated using the novel HDAC Class IIa inhibitor, TMP269, and whether TMP269 can substantiate the previous *in vitro* findings governed by PRH S163C:S177C. TMP269 is a novel and selective class IIa HDACi with IC_{50}s of 157 nM, 97 nM, 43 nM and 23 nM for HDAC-4, HDAC-5, HDAC-7 and HDAC-9, respectively.

In this study, the biological impact of the class IIa HDAC inhibitor using 50 nM TMP269. The following dose had been chosen with the aim of specifically inhibiting the activity of HDAC-9. The data illustrated that compared to HSV VSMCs incubated in 10% FCS with DMSO (Control), HSV VSMCs treated with TMP269 exhibited a significantly lower mitotic activity of VSMCs and modulation of p21 protein levels. This is in line with the prior data from Chapter 3, highlighting the capability of PRH S163C:S177C as a negative regulator of cell proliferation by repressing cyclin proteins and inducing the cell cycle inhibitors p21. Contrary to PRH S163C:S177C, TMP269 did not have any effect on cyclin D1 protein expression. A recent paper by Malhotra and colleagues highlighted the possible physiological role of HDAC-9 activity in VSMCs, siRNA, suppression of HDAC-9 reduced human aortic VSMC proliferation by over 50% (Malhotra *et al.,* 2019). In support of the role of HDAC-9 in the cell cycle regulation, Zhang and co-workers previously reported that knockdown of HDAC-9 coordinated the cell cycle arrest during G1 phase in retinoblastoma cells (Zhang *et al.,* 2016). In pancreatic cancer, TMP269 treatment at 57.5 μM also prevented cell growth via p21 induction, cyclin D1/D2 and CDK 2/4/6 inhibition in pancreatic AsPC-1 cells (Usami *et al.,* 2020). Clearly, these data suggest inhibiting HDAC class IIa resulted in cell growth suppression in various cell types. To add, TMP269 prevents cell cycle progression, DNA synthesis, and proliferation by modulating the cell cycle proteins, thereby, inducing cellular arrest. TMP269 additionally suppressed the migration of VSMCs. Importantly, hydroxyurea was added to the VSMCs as an anti-proliferative agent, hence, any changes observed in VSMC migration was restricted to that alone. Interestingly, trophoblast cell line migration was enhanced by HDAC-9 overexpression via TIMP-3 (Xie *et al.,* 2019). Li and colleagues also demonstrated silencing HDAC-9 can attenuate the migration activity of pancreatic cell lines (Li *et al.,* 2020). To date, no previous data exists associating TMP269 with modulating VSMC motility. Collectively, these data implicate the ability of TMP269 in supressing both VSMC proliferation and migration via HDAC-9 inhibition and support the proposition that PRH S163C:S177C inhibits VSMC proliferation and migration and intimal thickening via suppression of HDAC-9 levels.

Moreover, it reveals the potential utility of TMP269 for the reduction of intimal thickening and vein graft failure.

Because TMP269 inhibits all the members in the HDAC class IIa family, future work may seek to determine whether specific knockdown of HDAC-9 mRNA levels with siRNA (siHDAC-9) was sufficient to validate the findings observed in TMP269 *in vitro* experiments.

6.4.7 Pharmacologic inhibition of HDAC-9 promoted the contractile phenotype in VSMCs

VSMC phenotypic switching is a crucial determinant of atherosclerosis and late vein graft failure (Wadey *et al.,* 2018). Further investigation was warranted to elucidate the precise mechanism by which PRH S163C:S177C regulates the phenotypic state of VSMCs, consequently whether HDAC-9 inhibition by TMP269 induced the expression of VSMC contractile phenotype markers was examined. The first study to associate HDAC-9 in phenotypic switching was by Cardenas and co-workers which investigated the role of HDAC-9 in thoracic aortic aneurysm (Cardenas *et al.,* 2018). Smooth muscle cell phenotypic modulation is a key contributing factor to the development of aortic aneurysm (Petsophonsakul *et al.,* 2019). Disruption of HDAC-9 and long noncoding RNA (lncRNA) Metastasis Associated Lung Adenocarcinoma Transcript 1 (MALAT-1) has been illustrated to inhibit aneurysm growth by improving VSMC contractility. Their outcomes have shown that the HDAC-9-MALAT1-BRG1 complex represses VSMC contractile genes TGF-beta receptor type-2 (TGFR2) and ACTA2 expression (Cardenas *et al.,* 2018). Whether or how pharmacological inhibition of HDAC-9 by TMP269 regulates VSMC dedifferentiation has not been investigated. Whether HDAC-9 and TMP269 regulate the expression of any of the contractile proteins was previously unknown. In our study, TMP269 substantially induced the expression of VSMC contractile phenotype markers, with prominently enhanced protein levels of calponin ($\geq$ 1.5-fold) and smoothelin ($\geq$ 2-fold). The current study was the first to demonstrate that addition of TMP269 can not only reduce VSMC proliferation and VSMC migration, but it can also augment VSMC contractility and thus reduce the phenotypic switching from contractile to the synthetic phenotype. Moreover, the findings represent that TMP269 elicits increased by regulating the contractile proteins calponin and smoothelin. These observations are consistent with the unanticipated findings described in Chapter 3 that PRH S163C:S177C overexpression induced similar levels of induction in calponin ($\geq$ 1.5-fold) and smoothelin ($\geq$ 2-fold). It can be speculated that there is a mechanistic link in which PRH S163C:S177C plays a role in the VSMC differentiation by supressing the translational activity of HDAC-9. As a result, VSMCs

sustains and exhibit a ‘contractile’ or differentiated phenotype which is associated with the low rate of proliferation, low synthetic activity, and expression of contractile phenotype proteins. This differentiated phenotype is a powerful inhibitor of VSMC mitotic activity and migratory properties, hence, suppresses the formation of intimal thickening that underlies late vein graft failure.

The role of HDACs in phenotypic switching remains an incompletely explored territory. Having said this, the HDAC family seems to play a dual role in the VSMC phenotypic transformation. For example, targeted inhibition of HDAC-6 (Class IIb) using Tubastatin A, but not inhibition of HDAC-3 (Class I) using RGFP966, considerably stimulated α-SM actin expression at a significant level both *in vitro* and *in vivo* (Zhang *et al.,* 2018). Both inhibitors did not upregulate SMHC expression. However, their data also demonstrated that pharmacological inhibition using RGFP966 reduced α-SM actin expression at a significant level (Zhang *et al.,* 2018). The results in this chapter are consistent with the literature that HDAC-9 inhibition promotes the contractile phenotype in VSMCs. However, this study is the first to show that TMP269 can promote the contractile phenotype of VSMC by upregulating the expression of smoothelin and calponin. In accordance with the study by Cardenas and colleagues, it seems that the role of TMP269 in phenotypic modulation is not restricted to governing the expression of calponin and smoothelin alone. Rather, an interesting further investigation could include looking at the effect of TMP269 in other repertoire of VSMC-restricted contractile proteins including smooth muscle alpha actin, h-caldesmon, transgelin, and smooth muscle myosin heavy chain.

6.4.8 Chapter Summary

Collectively, this chapter identified that PRH S163C:S177C-regulated downstream target genes as a result of transcriptomic profiling and bioinformatics filtering analysis. STAT-1 and HDAC-9 were identified as candidates involved in governing the underlying the effects of PRH S163C:S177C in the regulation of VSMC behaviour. In this study, fludarabine, a specific STAT-1 inhibitor, repressed VSMC growth but not migration of VSMC phenotype. With regards to investigating the potential of HDAC-9 as another PRH S163C:S177C target gene, the data strongly suggest that HDAC-9 modulates, at least in part, the effects of PRH S163C:S177C-mediated regulation via specific mechanisms concerning VSMC proliferation, migration, and contractile responses. Of course, a question arises as to whether the outcomes from TMP269 treatment in our study were mediated specifically by HDAC-9. This scenario is highly likely considering the following facts. Although the HDACi TMP269 binds to Class IIa HDACs, there is an exception: its selectivity for HDAC-4, HDAC-5, HDAC-7 and HDAC-9 exhibiting IC_{50}s of 157 nM, 97 nM, 43 nM and 23 nM, respectively. In this study, low-dose

treatment using 50 nM TMP269 was sufficient to for inhibition of VSMC growth and migration whilst promoting SMC phenotypic modulation to the contractile phenotype. Unlike fludarabine, TMP269 seems to be more favourable to conduct further intensive investigation because it can promote contractile phenotypic modulation in VSMCs. Furthermore, the observed increase in HDAC-9 expression during intimal thickening induction with ligation highlights therapeutic potential. The combined treatments using HDAC-9 inhibitor, TMP269, and STAT-1 inhibitor, Fludarabine, should be investigated in the future as a combined approach may be beneficial.

Further stratification of the mechanistic link between the PRH S163C:S177C and HDAC-9 is an attractive direction to be taken for future studies. For instance, IPA's upstream regulator analysis revealed HDAC-9 as an upstream regulator of NPPA, SLC2A4, MYH7, CCNB1, RGS2 and CEBPA with an algorithm of a negative z-score (-2.0) which reflects the overall predicted inhibition state of the regulator. This analysis was able to determine genes within our dataset which are directly regulated by HDAC-9; NPPA, CEBPA, SLC2A4, and have association to govern cardiac fibrosis and apoptosis of cardiomyocytes. In as much as HDAC-9 inhibition by TMP269 also attenuates VSMC proliferation and migration and preserves the contractile phenotype, controlling HDAC-9 activity may open a new method to retard intimal thickening by abrogating "full-spectrum" VSMC pathogenic phenotypes. In line with this theory, further validation experiments focusing on the HDAC-9 targets could be performed to aid with this notion.

7.

GENERAL DISCUSSION

7.1 SUMMARY OF THESIS AIMS

The aims of this thesis were:

7. To determine the effect of overexpression of non-phosphorylatable PRH S163C:S177C on human SV (HSV) EC and VSMC proliferation, migration and apoptosis *in vitro*.

8. To determine the effect of overexpression of non-phosphorylatable PRH S163C:S177C on phenotypic switching in HSV VSMCs *in vitro*.

9. To determine the effect of overexpression of non-phosphorylatable PRH S163C:S177C on vascular inflammation in HSV ECs *in vitro*.

10. To compare PRH target genes in HSV VSMCs and ECs and thereby identify genes that specifically repress VSMC proliferation.

11. To validate PRH target genes repress HSV VSMC proliferation *in vitro*.

12. To determine the effect of overexpression of non-phosphorylatable PRH S163C:S177C on intimal thickening and EC coverage *in vivo*.

7.2. SUMMARY OF THE MAIN FINDINGS OF THIS THESIS AND FUTURE DIRECTIONS

7.2.1 Regulation of HSV VSMCs and intimal thickening by (Aims 1, 2 and 6)

There is a continued reliance on saphenous veins as the most preferred graft conduits for coronary revascularization although they possess a poor lifespan owing to their susceptibility to degenerate within a decade (Harskamp *et al.,* 2013). The de-differentiation of VSMCs to the synthetic phenotype and subsequent migration and proliferation of VSMCs into the intima are the underlying cause of intimal thickening and thereby progressive saphenous vein graft failure. It was hypothesised that PRH S163C:S177C can retard excessive VSMC accumulation and migration in primary human cells harvested form the saphenous veins of CABG surgical patients. Prior to the commencement of this PhD, previous work in our laboratory demonstrated that overexpression of the PRH S163C:S177C mutant with putative, enhanced stability can mitigate excessive and uncontrolled proliferation and migration in rat VSMCs (Wadey *et al.,* 2017). Primarily, it was necessary to validate these previous findings *in vitro* using human VSMCs and *in vivo*. This present study demonstrated that artificially augmenting the levels of PRH S163C:S177C can suppress the mitotic action and migratory capabilities of human saphenous vein VSMCs comparable to control cells, indicating that the anti-proliferative and anti-migratory effects are not restricted to rat VSMCs. PRH S163C:S177C did not, however, significantly affect the rate of apoptosis, which corroborated the findings by Wadey and colleagues (Wadey *et al.,* 2017). Data presented in Chapter 4 of this report illustrated that PRH S163C:S177C overexpression resulted in downregulation of Cyclin D1 accompanied by elevation of p21, indicating inhibition of the G1/S cell cycle transition. Clearly, augmenting the levels of PRH S163C:S177C mutant robustly effects on VSMC behaviour.

A novel finding of this thesis is the observation that PRH S163C:S177C overexpression resulted in upregulation, of the SMC-specific contractile phenotype markers calponin and smoothelin *in vitro*. This indication of phenotypic switching to the contractile phenotype was substantiated in functional assessments using the collagen contraction assay which demonstrated augmented contractile capacity in VSMCs overexpressing PRH S163C:S177C.

In this thesis, ligation of the mouse left carotid artery was performed to examine the effect of PRH S163C:S177C overexpression on intimal thickening. In Chapter 5, it was shown that the

adenoviral gene transfer of PRH S163C:S177C was achieved via adventitial delivery and this caused a significant attenuation of proliferation and intimal thickening. Following occlusion of the mouse left carotid artery fas a result of the vessel ligation, cell replication occurs in the intimal layer of the vessel and also in the media. The overexpression of PRH S163C:S177C inhibited proliferation in both the intima and media. Additionally, migration can be estimated by means of quantifying the number of BrdU negative cells divided by the length of the intima. Using this approach, it was apparent that VSMC migration was retarded by PRH S163C:S177C, corroborating the *in vitro* migration assay results. It is important to note however, that this is an estimate of migration as it is technically difficult to directly measure VSMC migration *in vivo*. Together these findings from *in vitro* and *in vivo* analyses provide evidence for the potential of PRH S163C:S177C regulate the behaviour of VSMCs which may be beneficial in the goal to inhibit intimal thickening.

Despite the positive results in terms of inhibition of intimal thickening, the question remains regarding the long-term efficacy of PRH S163C:S177C due to the transient nature of Ad-based gene therapy. Previous report demonstrated the potential of an Ad-based TIMP-3 in supressing porcine vein graft occlusion at 3 months despite lack of TIMP-3 expression at this point (George *et al.,* 2011). Because there is a therapeutic window early after implantation, inhibiting the early detrimental remodelling via PRH could enable the graft to adapt and ECs to regrow. Hence, longer term expression of the transgene is not needed. Though results from TIMP-3 is promising, one novel finding from our study suggests that PRH S163C:S177C promotes VSMC contractility. Another advantage is the beneficial effects of PRH S163C:S177C on HSVECs although this was not directly assessed in TIMP-3. Prior to continuing with our approach, further investigation exploring the durability of PRH S163C:S177C expression is necessary to prevent aberrant vein graft intimal thickening at a longer time point is necessary. Although we have confirmed the benefit of Ad-based gene transfer of PRH at 28 days using a mouse ligation model, it would be of great interest to perform future studies using a porcine model, employing either an interpositional or coronary vein graft, for up to 3 months to validate our findings and assess the efficacy for long-term graft patency. Although, these studies may take time due to the inherent difficulties and cost of expenses. In a clinical setting, hindering the development of intimal thickening must occur outside of the patient's body. This implies that a perioperative intervention presents a unique window of opportunity to directly deliver Ad: PRH S163C:S177C to the arterial wall in solution prior to the venous graft implantation.

7.2.2 Identification and investigation of downstream genes regulated by PRH S163C:S177C in VSMCs: STAT-1 and HDAC-9 (Aims 4 and 5)

The mechanisms underlying how PRH S163C:S177C modulates inhibition of VSMC proliferation and migratory may lead to the discovery of novel therapeutic targets for the alleviation of intimal hyperplasia during vein graft disease which circumvent the need for adenoviral gene delivery but permit the use of pharmacological approaches. In Chapter 6, transcriptomic profiling data obtained from NGS identified STAT-1 and HDAC-9 as downstream genes modulated by PRH S163C:S177C overexpression.

To investigate the role of STAT-1 in VSMC proliferation and support the proposal that STAT-1 contributes to the anti-proliferative effects of PRH S163C:S177C, *in vitro* experiments were performed by means of pharmacological inhibition. This approach also gave the opportunity to evaluate whether the use of a STAT-1 inhibitor could be investigated as a pharmacological inhibitor of intimal thickening and provide similar effects to PRH S163C:S177C. Fludarabine was employed to specifically block STAT-1 activity. The experiments conducted in Chapter 6 demonstrated that VSMC proliferation, but not migration, was markedly suppressed upon treatment with Fludarabine. Notably, an apparent downregulation of Cyclin D1 was a shared feature with PRH S163C:S177C emphasizing its anti-proliferative role. Having observed the pro-contractile phenotype induction as a result of PRH S163C:S177C overexpression in VSMCs, the effect of Fludarabine on phenotype was investigated. In contrast to PRH S163C:S177C overexpression, fludarabine did not upregulate the expression of smoothelin and calponin proteins. Whilst this finding did not support the role of STAT-1 in the PRH S163C:S177C mediated effects on VSMC contractility and migration, they are able to provide initial insight into the mechanisms of the anti-proliferative role of PRH S163C:S177C. However, further examination different ways of inhibiting STAT-1, such as siRNA or other inhibitors, could be a possible approach to help broaden the understanding of its role in modifying VSMC behaviour. Quantification of the post-translational modification, such as phosphorylation levels would be beneficial to expand our understanding of its involvement and determine whether STAT-1 downstream genes or proteins are regulated, and which biological processes are significantly enriched.

HDAC-9 was also identified as a downstream target of PRH S163C:S177C overexpression and it has been identified as a major risk locus for vasculopathies (Prestel *et al.,* 2019). In this study a Class IIa HDACi, TMP-269 was identified as the most suitable pharmacological

inhibitor due to lack of a specific HDAC-9 inhibitor. To date, there are no existing reports associating the link between HDAC-9 and PRH. Excitingly, the data presented in Chapter 6 suggested TMP-269 can inhibit VSMC proliferation and, for the first time it was shown that it also retards migration of human saphenous vein VSMCs, mirroring the effects observed with PRH S163C:S177C overexpression. Further analysis observed that treatment of TMP-269 considerably increased the SMC-specific contractile markers calponin and smoothelin which again was comparable to the data observed from PRH S163C:S177C overexpression. Hence, providing a pathway by which PRH S163C:S177C modulates the VSMC proliferation, migration, and differentiation to the contractile phenotype. As stated previously, the 'contractile' effect of PRH S163C:S177C is restricted to regulating smoothelin and calponin expression except other markers of the contractile phenotype demonstrating that contractile mechanisms within VSMCs may be more diverse than usual. The role of TMP-269 in activating other contractile markers is currently unknown and represents an interesting route for further investigation. Excitingly, these data offer the first mechanistic link between PRH S163C:S177C and HDAC-9 which could be involved in smooth muscle contraction vasculopathies such as aortic aneurysms. As described in Chapter 3, the effect of PRH S163C:S177C in modulation the contractile phenotype of VSMCs was not apparent *in vivo*. As a future direction, myograph studies can be conducted to test contraction in whole vessels. From the evidence generated in this thesis it is indicated that blocking the HDAC-9 pathway may be the best candidate to reduce diseases related to smooth muscle phenotypic switching within the vasculature including vein graft disease, atherosclerosis, abdominal aortic aneurysm and pulmonary arterial hypertension, however, future studies are needed to verify this point of view.

Having said this, TMP269 is a potent inhibitor which is specific to class IIa HDACs with IC_{50} values of 23 nM for HDAC-9. Therefore, it will be important to determine whether the effect was solely due to HDAC-9. Additional work using siRNA experiments to silence HDAC-9 may be valuable to test the role of HDAC-9 in the observed effects of PRH S163C:S177C. Examining the physical interaction between PRH S163C:S177C and HDAC-9 by immunoprecipitation studies may also be valuable parameters to assess. Alternatively, HDAC-9 heterozygous knockout mice or TMP-269-treated mice subjected to left carotid artery ligation could be studied to strengthen the *in vitro* data. Thus, we consider that pharmacological inhibition through TMP-269 has a potential protective role in abrogating a thickened VSMC-rich intima by controlling the VSMC phenotype, proliferation and migration. Further to this, it is necessary for continuation of this work to execute a collagen gel contraction assay in human saphenous vein VSMCs treated with TMP-269 to substantiate our findings.

Future experiments concentrating on efficient delivery of TMP-269 to vein grafts would also be a considerable undertaking. This report has not explored innovative methods for periadventitial drug delivery of biotherapeutics. The use of polymer hydrogels (Terry et al., 2012), sheaths/wraps (Sanders et al., 2012), microspheres (Rajathurai et al., 2010) and nanoparticles materials is accumulating and revealing an exciting direction for translational drug delivery (Tee *et al.,* 2019; Chaudhary *et al.,* 2017). By way of demonstration, polylactic-polyglycolic acid (PLGA) wraps incorporated around the porcine external jugular vein have been shown to be effective in mitigating intimal thickening (Sanders *et al.,* 2012). In our laboratory, the utility of integrating anti-proliferative inhibitors into a biodegradable polylactic-polyglycolic acid (PLGA) sheaths or microspheres are currently being investigated to eliminate off-target drug infusion and improve sustained compound release. Currently, we are delivering CK2 inhibitors that are known to increase PRH levels and have been shown to reduce proliferation and migration (Brown *et al.,* unpublished data). To assess *in vivo* sheaths/wraps or microspheres containing TMP-269 could be produced from dissolving PLGA in dichloromethane (DCM) and delivered into porcine saphenous vein grafts. There are also opportunities to test in the *ex vivo* flow model which was developed in our laboratory. Alternatively, the success of 'nanocarriers' strategy has been formerly demonstrated in the delivery of microRNA-145-loaded PLGA nanoparticles to VSMCs (Nishio *et al.,* 2019). Promising preventative measures of this delivery system remarkably arrested venous neointimal hyperplasia *in vivo*. With respect to further translational aspirations, future research may aim to consider immersing porcine jugular veins into TMP-269-loaded PLGA nanoparticles solution to yield the desired therapeutic effects with local and sustained TMP-269 release that may prolong graft patency.

7.2.3 The anti-inflammatory effects of PRH S163C:S177C as a beneficial effect for enhancing vein graft patency (Aim 3)

As a direct effect of HSV bypass grafting, endothelial cells become activated, causing disruption of the vascular endothelium function which may predispose grafts to early and late vein graft failure (Ward *et al.,* 2017). Data from our laboratory previously demonstrated that overexpression PRH S163C:S177C mutant had no detrimental effect on the human umbilical vein endothelial cell proliferation, migration or survival (Wadey *et al.,* 2017). The results presented in Chapter 4 corroborated these findings in HSV ECs, showing that the normal cell cycle functions such as proliferation, motility and viability were not different between cells overexpressing PRH S163C:S177C and the control groups. These findings implicate that gene transfer of PRH S163C:S177C did not impair the capacity for re-endothelialisation, via

migration and proliferation, that is important for vein graft patency. Consequently, the results prompted the investigation of other aspects of endothelial function. Release of cytokines, chemokines and other inflammatory mediators and monocyte adherence are important regulators of intimal thickening (Yang, Chang and Wei, 2016). Therefore, the discovery that PRH S163C:S177C can act as a biological mediator to achieve anti-inflammatory responses is both intriguing and potentially of high importance. The suppression of interleukin-6 and MCP-1 proteins by PRH S163C:S177C overexpression, which are critical molecules controlling monocyte recruitment to endothelium, combined with reduced monocyte adhesion and expression of VCAM-1 and ICAM-1 highlight the possibility that PRH could retard inflammation within the vein graft. Moreover, the reduced permeability highlights the potential to reduce monocyte invasion and plasma lipid infiltration. It would be of great interest to determine whether these benefits are realised in vivo post PRH S163C:S177C overexpression in endothelial cells. Crucially, these data unveiled the potential benefit of artificially enhancing levels of PRH S163C:S177C to effectively avert endothelial dysfunction and inflammation associated to the pathogenesis of intimal thickening and vein graft failure.

The ever-persistent clinical demand for bioengineered blood vessels has been acknowledged due poor selection of vascular conduits (Song *et al.,* 2019). Excitingly, local method of genetically manipulating the saphenous vein using the multifunctional transcription factor PRH S163C:S177C incorporated into endothelial cells or perivascular VSMCs prior to implantation of the conduit provides an exciting opportunity for future studies. To minimize graft rejection, patient-derived autologous cells could be isolated for therapeutic efficacy. Alternatively, a previous study demonstrated that induced pluripotent stem cells (iPSCs) have been successfully differentiated into functional SMCs (Lee *et al.,* 2010). iPSC-derived endothelial cells or smooth muscle cells infected with the adenovirus-encoding PRH S163C:S177C could be seeded into the vascular grafts vessels to recapitulate the anti-proliferative and anti-inflammatory function of PRH within a vein graft.

7.2.4 Identifying endothelial cell-specific PRH S163C:S177C downstream targets that may modulate its protective role in the vascular endothelium

Having established the anti-inflammatory capabilities of PRH S163C:S177C, it remains unknown as to how PRH S163C:S177C regulates the endothelial cell behaviour and function. DEGs identified as specifically PRH S163C:S177C-regulated in HSV ECs represent an

unknown and a vital part for the continuance of this project. Firstly, similar bioinformatic filtering strategies as described in Chapter 2 may be performed focusing on the 652 genes identified to be specifically regulated in endothelial cells (Supplementary Material). Secondly, such findings require validation at the protein level. Western blotting or immunocytochemistry experiments may be performed to confirm whether PRH S163C:S177C affects their protein expression. Lastly, pharmacological strategies, overexpression or knockdown experiments could be conducted to evaluate the functional effect of these target genes in HSV ECs. To assess the therapeutic efficacy of these targets, similar *in vitro* experiments examining its anti-inflammatory role are necessary for continuation of this work.

7.3 LIMITATIONS OF THE STUDY

Relevant findings in animals are difficult to associate with humans because of animal-to-human translational success rates are frequently low. The carotid artery ligation model in mice is an attractive method to induce vascular injury and intimal thickening in order to address research questions. However, several inherent limitations have to be acknowledged as the clinical relevance of the carotid artery ligation model remains problematic. Firstly, the model features an intact endothelium which does not mimic clinical conditions observed in CABG patients where graft harvesting, distension and implantation causes endothelial damage and denudation (Holt and Tulis, 2013). Secondly, complete occlusion of the vessel from ligation restricts the ability to analyse the effect of haemodynamic forces which is an important contributing factor in early vein graft stenosis (Ward *et al.,* 2017; Ley *et al.,* 2007; Fernandez *et al.,*2004). Thirdly, the effect of macrophages and vascular inflammation is difficult to analyse using this model and in Chapter 4, PRH S163C:S177C was shown to have a protective role against vascular inflammation. To overcome these shortcomings, more appropriate animal models are desirable. A clinically more relevant model to investigate intimal thickening in the vein graft is the porcine saphenous vein-to-carotid artery interposition grafts (Rajathurai *et al.,* 2010). Although the potential benefits of porcine model include the ongoing issues of its technical complexity and high cost (Caramori *et al.,* 1997). Therefore, the mouse carotid artery ligation model remains to be a robust and established pre-clinical model model which permits substantial understanding of adenoviral-mediated gene therapy of restenosis in vein graft degeneration.

An additional limitation of the current study was the decision to focus on the transcription factors within VSMC-specific regulated DEGs due to the limited time to follow up on all of the regulated genes from NGS. Evidence presented in this thesis suggests the anti-inflammatory

role of PRH S163C:S177C in endothelial cells. Therefore, future work on the analysis of HSVEC-specific regulated DEGs from NGS would be optimal to provide a mechanistic link on the effect of PRH S163C:S177C in the endothelium. Although *in vitro* work in this thesis relied on isolated cells, patients with vein grafts have lots of risk factors including diabetes, age and high lipids (McKavanagh *et al.,* 2017). Future experiments may look into *ex vivo* bioreactor studies where cells are embedded in the native matrix.

The 7-day *in vivo* pilot study was originally set up to confirm the viral protein expression of PRH S163C:S177C transgene in the ligated mouse carotids. Due to the disruption caused by coronavirus (COVID-19) on this project (i.e., national lockdown and laboratory closures), we've faced difficulties in setting up the animal studies. Therefore, we had to move forward with the 28-days *in vivo* main study. As a future direction, more animals could be set up to look at the effect of PRH S163C:S177C overexpression at an earlier-point in the 7-day mouse carotid artery ligation model.

7.4 FINAL REMARKS

The fundamental goal of this thesis to evaluate the potential of PRH S163C:S177C as a therapeutic modality for long term venous graft patency is extremely clinically relevant. Together the data presented in this thesis clearly demonstrate the benefit of an adenoviral-based overexpression of the mutant and stabilised form PRH (S163C:S177C). In conclusion, evidence that PRH S163C:S177C may reduce vein graft failure by inhibiting intimal thickening through modulation of VSMC behaviour at least in part mediated by STAT-1 and HDAC-9, and reduction of endothelial inflammation. Hence, a clinically applicable strategy for delivering PRH S163C:S177C can limit the requirement for repeat revascularisation procedures in patients undertaking arterial reconstruction each year. Alternatively, the utilisation of pharmacological inhibitors of STAT-1 and HDAC-9 may be beneficial for the suppression of late vein graft failure.

FIGURE 7.1: Overexpression of PRH S163C:S177C can retard the development of intimal thickening

Schematic diagram illustrating PRH S163C:S177C can effectively retard VSMC proliferation and migration while promoting VSMC contractility without damaging endothelial function. Next Generation Sequencing (NGS) identified HDAC-9 as a novel PRH S163C:S177C-regulated target gene. Pharmacological inhibition of HDAC-9 using TMP269 inhibited VSMC proliferation and migration via promoting VSMC phenotypic switching from synthetic to contractile phenotype. Figure created from Biroender.com

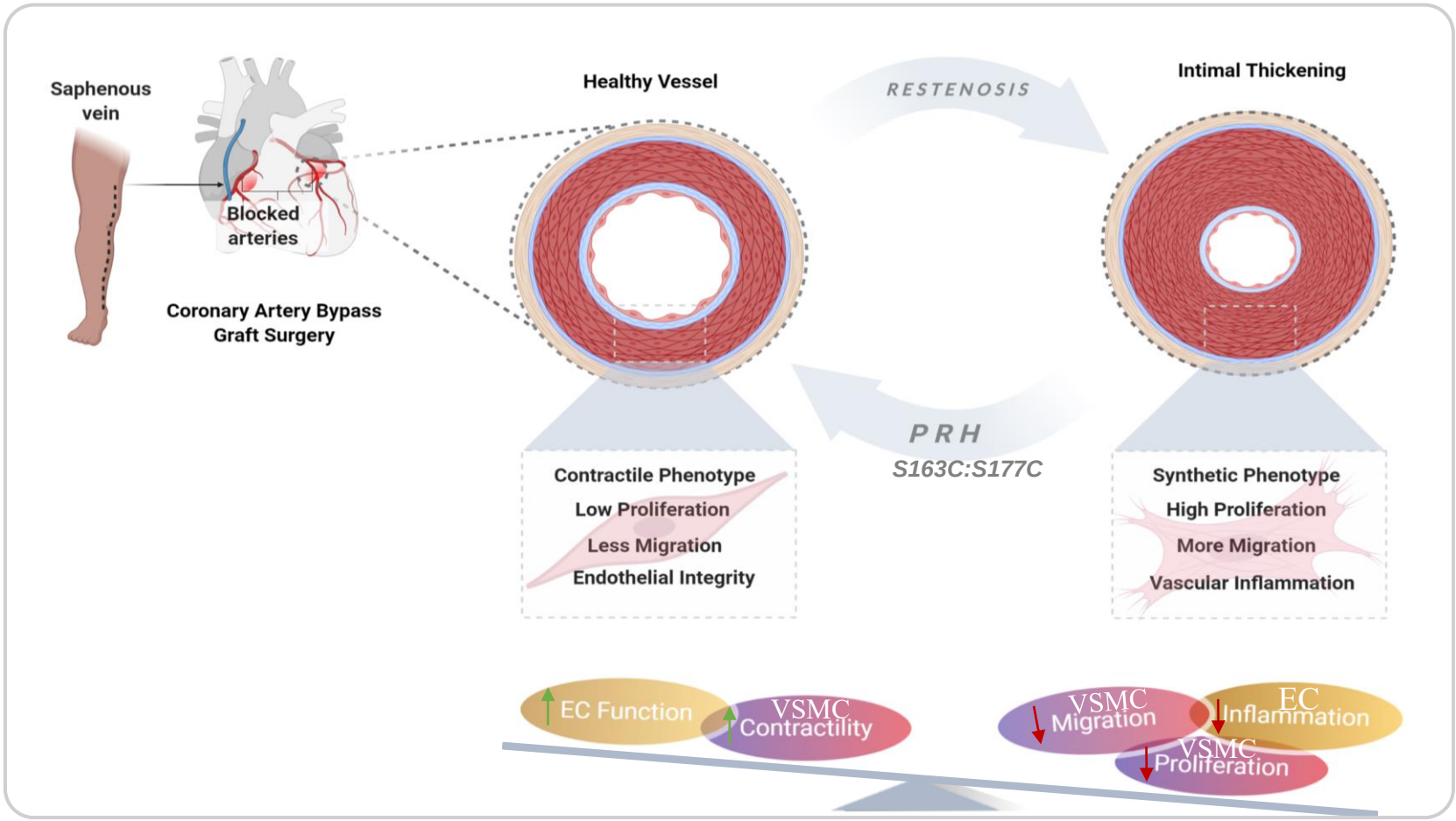
Saphenous vein
Blocked arteries
Coronary Artery Bypass Graft Surgery
Healthy Vessel
RESTENOSIS
Intimal Thickening
PRH
S163C:S177C
Contractile Phenotype
Low Proliferation
Less Migration
Endothelial Integrity
Synthetic Phenotype
High Proliferation
More Migration
Vascular Inflammation
EC Function
VSMC Contractility
VSMC Migration
EC Inflammation
VSMC Proliferation

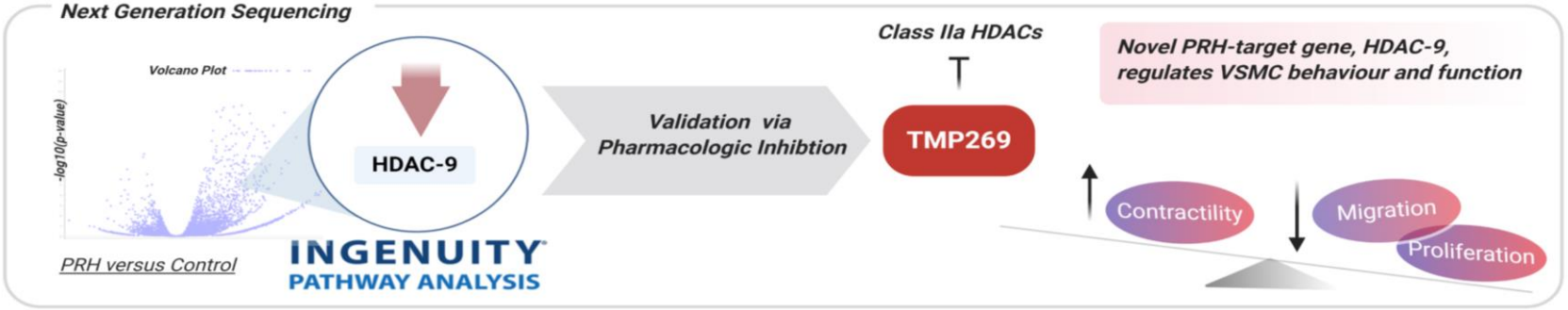
Next Generation Sequencing
Volcano Plot
-log10(p-value)
HDAC-9
PRH versus Control
INGENUITY PATHWAY ANALYSIS
Validation via Pharmacologic Inhibtion
Class IIa HDACs
TMP269
Novel PRH-target gene, HDAC-9, regulates VSMC behaviour and function
Contractility
Migration
Proliferation

8.

APPENDIX

Supplementary Data 1: The top enriched PRH S163C:S177C regulated canonical pathways based on Ingenuity Pathway Analysis (IPA).

P-value for inclusion here is ≤ .05. P- value is calculated using Fischer's exact test indicates the probability of the involvement of the genes in the dataset in a given pathway. Ratios represent the number of molecules in the dataset that are found in a given pathway, divided by total number of molecules that make up that pathway. Molecules are shown in the dataset (≥1.3 -log (p-value) and p ≤ 0.05). DEGs; Differentially expressed genes.

Supplementary Data 1: The top enriched PRH S163C:S177C regulated canonical pathways based on Ingenuity Pathway Analysis (IPA)

Ingenuity Canonical Pathways	-log(p-value)	Ratio	Molecules
Axonal Guidance Signalling	12.2	0.196	ABLIM1ABLIM2ADAM23 ADAM33 ADAMTS1 ADAMTS17 ADAMTS6 ADAMTS8 BAIAP2 BDNF BMP8B CXCL12 EFNA4 EFNB1 EFNB2 EFNB3 EGF EPHA3 EPHA7 EPHB2 EPHB3 EPHB4 EPHB6 FZD7 FZD9 GLIS2 GNAZ GNG12 GNG2 ITGA2 ITGA3 ITSN1 KCNJ12 MET MMP11 MMP9 MRAS MYL10 MYL2 MYL3 MYL4 MYL7 NFATC1 NTN5 NTNG2 PAPPA SEMA3A SEMA3B SEMA3F SEMA5A SEMA6A SEMA6B SHH SLIT2 SRGAP1 UNC5A VEGFA VEGFC WNT1 WNT10A WNT10B WNT11 WNT3 WNT3A WNT6 WNT9B
Breast Cancer Regulation by Stathmin1	11	0.179	ACKR3 ADGRA1 ADGRB1 ADGRG1 ADGRG6 ADGRL1 ADGRL4 ADRA1B ADRA2B APLNR ARHGEF4 AURKB BDKRB2 CAMK1D CAMK2A CASR CCR10 CCR7 CCRL2 CDK1 CELSR1 CELSR2 CHRM1 CHRM4 CRHR1 CRHR2 CX3CR1 EGF F2RL2 FFAR2 FFAR3 FGF2 FOXM1 FPR2 FZD7 FZD9 GALR2 GLP1R GLP2R GNG12 GNG2 GPR150 GPR153 GPR157 GPR162 GPR19 GPR20 GPR37L1 GPR4 GPR65 GPR78 GPR83 GPR84 GPRC5C GRM4 GRM8 GRPR HCRTR1 HGF HRH2 HTR2A HTR7 KISS1R LPAR1 LPAR2 MC1R MC5R MCHR1 MMP9 MRAS NTSR1 OPRD1 P2RY1 P2RY11 P2RY2 PDGFB PIK3C2B PIK3CD PIK3R3 PLCB2 PPP2R3B PRKCB PRKCD PRKCZ PRKD1 PTGER2 PTGER4 PTGFR RALA RRAS2 S1PR2 S1PR5 SLC52A1 SSTR1 SSTR2 SSTR3 STMN1 SUCNR1 TBXA2R TUBA1A TUBA1C TUBA4A TUBA8 TUBB4A VEGFA VEGFC
Cardiac Hypertrophy Signalling (Enhanced)	9.01	0.179	ADCY4 ADRA1B ADRA2B AGT CACNA1A CAMK2A CD70 DIAPH3 EDN1 FGF11 FGF18 FGF19 FGF2 FGF21 FGF3 FGFR4 FZD7 FZD9 GNG2 HAND1 HAND2 HDAC9 IFNLR1 IL12RB1 IL17RC IL1A IL1B IL21R IL27RA IL33 IL4R IL6 ITGA ITGA3 ITPR3 LEP LTA MAP3K20 MAP3K5 MEF2A MEF2C MEF2D MRAS MYOCD NFATC1 NPPA PDE3A PDE4A PDE4C PDE5A PDE6C PDE7B PDE8B PIK3C2B PIK3CD PIK3R3 PLCB2 PLCD1 PLCG2 PLCH2 PLCL1 PLN PRKCB PRKCD PRKCZPRKD1 RALA RRAS2 RYR1 SMPDL3B STAT1 TGFB3 TGFBR2 TNF TNFRSF11B TNFSF13 TNFSF14 TNFSF15 TNFSF4 TNFSF9WNT1 WNT10A WNT10B WNT11 WNT3 WNT3A WNT6 WNT9B

Synaptogenesis Signalling Pathway	8.38	0.199	ADCY4 APOE BDNF CACNB4 CAMK2A CDH10 CDH18 CDH2 CDH22 CDH23 CDH24 CDH3 CDH5 CDH6 CDH8 CNTNAP1 CPLX1 EFNA4 EFNB1 EFNB2 EFNB3 EPHA3 EPHA7 EPHB2 EPHB3 EPHB4 EPHB6 FGR GRIA1 GRIN1 GRIN2A GRIN2C GRM4 GRM8 ITSN1 MRAS NECTIN3 NLGN1 NRXN3 PIK3C2B PIK3CD PIK3R3 PLCG2 PRKCD RALA RASGRF1 RASGRP2 RELN RRAS2 SHC2 SHF SNCB SNCG STX1B STXBP5 SYN3 SYNGAP1 SYT11 SYT2 SYT3 SYT5 SYT7
Hepatic Fibrosis Signalling Pathway	7.78	0.185	AGT CACNA1A CCL2 CCN2 COL11A2 COL18A1 COL2A1 DIRAS3 EDN1 FGF2 FLT4 FZD7 FZD9 GLIS2 IL1A IL1B IL1RN IL33 IRAK2 ITGA2 ITGA3 LEF1 LEP MRAS MYL10 MYL2 MYL3 MYL4 MYL7 MYLK2 NFKBIE PDGFA PDGFB PIK3C2B PIK3CD PIK3R3 PLCG2 PRKCB PRKCD PRKCZ PRKD1 RALA RHOD RHOF RHOU RHOV RND3 RRAS2 SHH SNAI1 SOD2 SUCNR1 TF TGFB3 TGFBR2 TLR4 TNF TNFRSF11B VEGFA VEGFC WNT1 WNT10A WNT10B WNT11 WNT3 WNT3A WNT6 WNT9B
Hepatic Fibrosis / Hepatic Stellate Cell Activation	7.04	0.22	AGT CCL2 CCN2 CCR7 COL11A2 COL18A1 COL27A1 COL2A1 COL9A2 CXCL2 EDN1 EGF EGFR FGF2 FLT4 HGF IL1A IL1B IL4R IL6 LBP LEP MET MMP9 MYH10 MYH11 MYH7 MYL2 MYL3 MYL4 MYL7 PDGFA PDGFB STAT1 TGFB3 TGFBR2 TLR4 TNF TNFRSF11B VEGFA VEGFC
Role of Macrophages, Fibroblasts and Endothelial Cells in Rheumatoid Arthritis	6.46	0.183	CAMK2A CCL2 CEBPA CEBPD CXCL12 DKK2 FGF2 FZD7 FZD9 IL16 IL17RC IL1A IL1B IL1RN IL33 IL6 IRAK2 LEF1 LTA MRAS NFATC1 NFKBIE NOS2 PDGFA PDGFB PIK3C2B PIK3CD PIK3R3 PLCB2 PLCD1 PLCG2 PLCH2 PLCL1 PRKCB PRKCD PRKCZ PRKD1 RALA RRAS2 SFRP1 SFRP4 SOCS3 TLR4 TLR5 TNF TNFRSF11B TRAF1 VEGFA VEGFC WNT1 WNT10A WNT10B WNT11 WNT3 WNT3A WNT6 WNT9B
Gα12/13 Signalling	6.26	0.238	CDH10 CDH18 CDH2 CDH22 CDH23 CDH24 CDH3 CDH5 CDH6 CDH8 F2RL2 LPAR1 LPAR2 MAP3K5 MEF2A MEF2C MEF2D MRAS MYL10 MYL2 MYL3 MYL4 MYL7 NFKBIE PIK3C2B PIK3CD PIK3R3 RALA RRAS2 TBXA2R VAV1
Calcium Signalling	6.21	0.204	ACTA1 ASPH ATP2B1 ATP2B2 ATP2B3 CACNA1A CACNA1H CACNA1I CACNA2D2 CACNB4 CACNG4 CAMK1D CAMK2A CHRNA3 CHRNA4 CHRNB1 CHRNB4 GRIA1 GRIN1

			GRIN2A GRIN2C HDAC9 ITPR3 MEF2A MEF2C MEF2D MYH10 MYH11 MYH7 MYL2 MYL3 MYL4 MYL7 NFATC1 RYR1 SLC8B1 TNNC1 TNNI3 TNNT2 TRPC4 TRPC6 TRPV6
Glioblastoma Multiforme Signalling	6.15	0.218	CDKN2A DIRAS3 EGF EGFR FZD7 FZD9 ITPR3 LEF1 MRAS NF2 PDGFA PDGFB PIK3C2B PIK3CD PIK3R3 PLCB2PLCD1 PLCG2 PLCH2 PLCL1 PRKCD RALA RHOD RHOF RHOU RHOV RND3 RRAS2 WNT1 WNT10A WNT10B WNT11 WNT3 WNT3A WNT6 WNT9B
Neuropathic Pain Signalling In Dorsal Horn Neurons	5.49	0.248	BDNF CAMK1D CAMK2A GRIA1 GRIN1 GRIN2A GRIN2C GRM4 GRM8 ITPR3 KCNH2 KCNQ2 KCNQ3 PIK3C2B PIK3CD PIK3R3 PLCB2 PLCD1 PLCG2 PLCH2 PLCL1 PRKCB PRKCD PRKCZ PRKD1
G-Protein Coupled Receptor Signalling	5.47	0.18	ADCY4 ADRA1B ADRA2B APLNR CAMK2A CHRM1 CHRM4 CRHR1 DUSP6 DUSP9 FFAR3 FPR2 GLP1R GRM4 GRM8 HRH2 HTR2A HTR7 LPAR1 MC1R MC5R MRAS NFKBIE NPR3 OPRD1 PDE3A PDE4A PDE4C PDE5A PDE6C PDE7B PDE8B PIK3C2B PIK3CD PIK3R3 PLCB2 PRKCB PTGER2 PTGER4 RALA RAP1GAP RAPGEF3 RGS2 RPS6KA1 RRAS2 SMPDL3B SSTR3 SYNGAP1 TBXA2R
Human Embryonic Stem Cell Pluripotency	5.41	0.222	BDNF BMP8B FGF2 FGFR4 FZD7 FZD9 INHBA LEF1 LEFTY2 MRAS PDGFA PDGFB PIK3C2B PIK3CD PIK3R3 POU5F1 S1PR2 S1PR5 SMAD6 SOX2 TGFB3 TGFBR2 WNT1 WNT10A WNT10B WNT11 WNT3 WNT3A WNT6 WNT9B
Regulation of the Epithelial-Mesenchymal Transition Pathway	5.36	0.198	CDH2 EGF EGFR EGR1 FGF11 FGF18 FGF19 FGF2 FGF21 FGF3 FGFR4 FZD7 FZD9HGF HMGA2 JAG2 LEF1 LOX MET MMP9 MRAS NOTCH1 PIK3C2B PIK3CD PIK3R3 RALA RRAS2 SNAI1 TGFB3 TGFBR2 WNT1 WNT10A WNT10B WNT11 WNT3 WNT3A WNT6 WNT9B
Agranulocyte Adhesion and Diapedesis	5.3	0.197	ACTA1 AOC3 CCL11 CCL19 CCL2 CCL20 CCL22 CD34 CDH5 CLDN1 CLDN12 CLDN18 CLDN2 CX3CL1 CXCL1 CXCL12 CXCL16 CXCL2 CXCL3 CXCL5 IL1A IL1B IL1RN IL33 ITGA2 ITGA3 MMP11 MMP9 MYH10 MYH11 MYH7 MYL2 MYL3 MYL4 MYL7 PF4 SDC4 TNF

Supplementary Data 2: DEGs prioritised from the top-enriched canonical pathways approach.

Gene	Protein	Function	Fold Change	P-value
HDAC-9	Histone Deacetylase 9	transcription regulator/ repressor	-3.318	5.14E-05
NFATC-1	Nuclear Factor of Activated T Cells 1	transcription factor	3.783	2.80E-05
STAT-1	Signal Transducer and Activator of Transcription 1	transcription factor	-2.369	6.54E-03
HAND-1	Heart and Neural Crest Derivatives Expressed 1	transcription factor	121.350	1.48E-05
CEBPD	CCaAT Enhancer Binding Protein delta	transcription factor	-2.043	2.31E-02

Supplementary Data 1: DEGs prioritised from the canonical pathways approach.

P-value for inclusion here is ≤ .05. P- value is calculated using Fischer's exact test indicates the probability of the involvement of the genes in the dataset in either 'proliferation' and 'migration'. The direction of the fold change represents the upregulation or downregulation of a specific DEG. DEGs; Differentially expressed genes.

Supplementary Data 3: DEGs prioritised from the 'proliferation' and 'migration' disease and function approach.

Gene	Protein	Function	Fold Change	P-value
STAT-1	Signal Transducer and Activator of Transcription 1	transcription factor	-2.369	6.54E-03
FOXM-1	Forkhead Box M1	transcription factor	-1.877	1.20E-02
NFATC-1	Nuclear Factor of Activated T Cells 1	transcription factor	3.783	2.80E-05
CEBPA	CCaAT Enhancer Binding Protein alpha	transcription factor	10.992	1.64E-03
KLF-11	Kruppel Like Factor 11	transcription factor	2.411	7.33E-03

Supplementary Data 1: DEGs prioritised from the 'proliferation' and 'migration' disease and function approach.

P-value for inclusion here is ≤ .05. P- value is calculated using Fischer's exact test indicates the probability of the involvement of the genes in the dataset in either 'proliferation' and 'migration'. The direction of the fold change represents the upregulation or downregulation of a specific DEG. DEGs; Differentially expressed genes.

9.

REEFERENCES

REFERENCES

Abramov, D. (2000). Tamariz MG, Sever JY, Christakis GT, Bhatnagar G, Heenan AL, Goldman BS, Fremes SE. *The influence of gender on the outcome of coronary artery bypass surgery. Ann Thorac Surg*, *70*, 800-805.

Ahmed, K., Gerber, D. A., & Cochet, C. (2002). Joining the cell survival squad: an emerging role for protein kinase CK2. *Trends in cell biology*, *12*(5), 226-230.

Aikawa, M., Sivam, P. N., Kuro-o, M., Kimura, K., Nakahara, K. I., Takewaki, S. I., ... & Periasamy, M. (1993). Human smooth muscle myosin heavy chain isoforms as molecular markers for vascular development and atherosclerosis. *Circulation research*, *73*(6), 1000-1012.

Akira, S. (1999). Functional roles of STAT family proteins: lessons from knockout mice. *Stem cells*, *17*(3), 138-146.

Akowuah, E. F., Gray, C., Lawrie, A., Sheridan, P. J., Su, C. H., Bettinger, T., Brisken, A. F., Gunn, J., Crossman, D. C., Francis, S. E., Baker, A. H. and Newman, C. M. (2005). "Ultrasound-mediated delivery of TIMP-3 plasmid DNA into saphenous vein leads to increased lumen size in a porcine interposition graft model." *Gene Therapy 12*(14): 1154-1157

Alam, M., Bandeali, S. J., Kayani, W. T., Ahmad, W., Shahzad, S. A., Jneid, H., ... & Virani, S. S. (2013). Comparison by meta-analysis of mortality after isolated coronary artery bypass grafting in women versus men. *The American journal of cardiology*, *112*(3), 309-317.

Allfrey, V. G., Faulkner, R., & Mirsky, A. E. (1964). Acetylation and methylation of histones and their possible role in the regulation of RNA synthesis. *Proceedings of the National Academy of Sciences of the United States of America*, *51*(5), 786.

Al-Sabti, H. A., Al Kindi, A., Al-Rasadi, K., Banerjee, Y., Al-Hashmi, K., & Al-Hinai, A. (2013). Saphenous vein graft vs. radial artery graft searching for the best second coronary artery bypass graft. *Journal of the Saudi Heart Association*, *25*(4), 247-254.

Ampofo, E., Rudzitis-Auth, J., Dahmke, I. N., Rössler, O. G., Thiel, G., Montenarh, M., ... & Laschke, M. W. (2015). Inhibition of protein kinase CK2 suppresses tumor necrosis factor (TNF)-α-induced leukocyte–endothelial cell interaction. *Biochimica et Biophysica Acta (BBA)-Molecular Basis of Disease*, *1852*(10), 2123-2136.

Anderson, R. D., Haskell, R. E., Xia, H., Roessler, B. J. and Davidson, B. L. (2000). "A simple method for the rapid generation of recombinant adenovirus vectors. *Gene Therapy 7*(12): 1034-1038

Angelini, G. D., Soyombo, A. A., & Newby, A. C. (1991). Smooth muscle cell proliferation in response to injury in an organ culture of human saphenous vein*. European journal of vascular surgery, 5*(1), 5-12.

Angelini, G. D., Passani, S. L., Breckenridge, I. M., & Newby, A. C. (1987). Nature and pressure dependence of damage induced by distension of human saphenous vein coronary artery bypass grafts. *Cardiovascular research*, *21*(12), 902-907.

Andrés, V. (2004). Control of vascular cell proliferation and migration by cyclin-dependent kinase signalling: new perspectives and therapeutic potential. *Cardiovascular research*, *63*(1), 11-21.

Aparicio-Siegmund, S., Sommer, J., Monhasery, N., Schwanbeck, R., Keil, E., Finkenstädt, D., ... & Garbers, C. (2014). Inhibition of protein kinase II (CK2) prevents induced signal transducer and activator of transcription (STAT) 1/3 and constitutive STAT3 activation. *Oncotarget*, *5*(8), 2131.

Asare, Y., Campbell-James, T. A., Bokov, Y., Yu, L. L., Prestel, M., El Bounkari, O., ... & Dichgans, M. (2020). Histone deacetylase 9 activates IKK to regulate atherosclerotic plaque vulnerability. *Circulation Research*, *127*(6), 811-823.

Avallone, A., Piccirillo, M. C., Delrio, P., Pecori, B., Di Gennaro, E., Aloj, L., ... & Budillon, A. (2014). Phase 1/2 study of valproic acid and short-course radiotherapy plus capecitabine as preoperative treatment in low-moderate risk rectal cancer-V-shoRT-R3 (Valproic acid-short RadioTherapy-rectum 3rd trial). *BMC cancer*, *14*(1), 1-12.

Azad, N. S., El-Khoueiry, A., Yin, J., Oberg, A. L., Flynn, P., Adkins, D., ... & Ahuja, N. (2017). Combination epigenetic therapy in metastatic colorectal cancer (mCRC) with subcutaneous 5-azacitidine and entinostat: a phase 2 consortium/stand up 2 cancer study. *Oncotarget*, *8*(21), 35326.

Barbosa, D. M., Fahlbusch, P., de Wiza, D. H., Jacob, S., Kettel, U., Al-Hasani, H., ... & Knebel, B. (2020). Rhein, a novel Histone Deacetylase (HDAC) inhibitor with antifibrotic potency in human myocardial fibrosis. *Scientific reports*, *10*(1), 1-13.

Batlevi, C. L., Kasamon, Y., Bociek, R. G., Lee, P., Gore, L., Copeland, A., ... & Younes, A. (2016). ENGAGE-501: phase II study of entinostat (SNDX-275) in relapsed and refractory Hodgkin lymphoma. *Haematologica*, *101*(8), 968-975.

Bauer, U., Flunker, G., Bruss, K., Kallwellis, K., Liebermann, H., Luettich, T., ... & Seidel, W. (2005). Detection of antibodies against adenovirus protein IX, fiber, and hexon in human sera by immunoblot assay. *Journal of clinical microbiology*, *43*(9), 4426-4433.

Beamish, J. A., He, P., Kottke-Marchant, K., & Marchant, R. E. (2010). Molecular regulation of contractile smooth muscle cell phenotype: implications for vascular tissue engineering. Tissue engineering. *Part B, Reviews, 16*(5), 467–491. https://doi.org/10.1089/ten.TEB.2009.0630

Becker, J. B., Prendergast, B. J., & Liang, J. W. (2016). Female rats are not more variable than male rats: a meta-analysis of neuroscience studies. *Biology of sex differences*, *7*(1), 1-7.

Bedford, F. K., Ashworth, A., Enver, T., & Wiedemann, L. M. (1993). HEX: a novel homeobox gene expressed during haematopoiesis and conserved between mouse and human. *Nucleic acids research*, *21*(5), 1245-1249.

Beery, A. K. (2018). Inclusion of females does not increase variability in rodent research studies. *Current opinion in behavioral sciences*, *23*, 143-149.

Beery, A. K., & Zucker, I. (2011). Sex bias in neuroscience and biomedical research. *Neuroscience & Biobehavioral Reviews*, *35*(3), 565-572.

Bettica, P., Petrini, S., D'Oria, V., D'Amico, A., Catteruccia, M., Pane, M., ... & Mercuri, E. (2016). Histological effects of givinostat in boys with Duchenne muscular dystrophy. *Neuromuscular disorders*, *26*(10), 643-649.

Betts, J. G. (2013). *Anatomy & physiology*. Retrieved from: https://opentextbc.ca/anatomyandphysiology/chapter/20-1-structure-and-function-of-blood-vessels/

Bhatnagar, P., Wickramasinghe, K., Williams, J., Rayner, M., & Townsend, N. (2015). The epidemiology of cardiovascular disease in the UK 2014. *Heart, 101*(15), 1182-1189.

Bhave, V. S., Mars, W., Donthamsetty, S., Zhang, X., Tan, L., Luo, J., ... & Michalopoulos, G. K. (2013). Regulation of liver growth by glypican 3, CD81, hedgehog, and Hhex. *The American journal of pathology*, *183*(1), 153-159.

Bischof, O., Purbey, P. K., Notani, D., Urlaub, H., Dejean, A., & Galande, S. (2007). Functional interaction between PML and SATB1 regulates chromatin-loop architecture and transcription of the MHC class I locus. *Nature cell biology*, *9*(1), 45.

Bochaton-Piallat, M. L., Ropraz, P., Gabbiani, F., & Gabbiani, G. (1996). Phenotypic heterogeneity of rat arterial smooth muscle cell clones: implications for the development of experimental intimal thickening. *Arteriosclerosis, thrombosis, and vascular biology*, *16*(6), 815-820.

Bond, M., Sala-Newby, G. B., Wu, Y. J., & Newby, A. C. (2006). Biphasic effect of p21Cip1 on smooth muscle cell proliferation: role of PI 3-kinase and Skp2-mediated degradation. *Cardiovascular research, 69*(1), 198-206.

Bourassa, M. G., Fisher, L. D., Campeau, L., Gillespie, M. J., McConney, M., & Lesperance, J. (1985). Long-term fate of bypass grafts: the Coronary Artery Surgery Study (CASS) and Montreal Heart Institute experiences. *Circulation*, *72*(6 Pt 2), V71-8.

Bradley, D., Rathkopf, D., Dunn, R., Stadler, W. M., Liu, G., Smith, D. C., ... & Hussain, M. (2009). Vorinostat in advanced prostate cancer patients progressing on prior chemotherapy (National Cancer Institute Trial 6862) Trial results and interleukin-6 analysis: A study by the Department of Defense Prostate Cancer Clinical Trial Consortium and University of Chicago Phase 2 Consortium. *Cancer*, *115*(23), 5541-5549.

Bradshaw, P. J., Jamrozik, K., Le, M., Gilfillan, I., & Thompson, P. L. (2002). Mortality and recurrent cardiac events after coronary artery bypass graft: long term outcomes in a population study. *Heart*, *88*(5), 488-494.

Brickman, J. M., Jones, C. M., Clements, M., Smith, J. C., & Beddington, R. S. (2000). Hex is a transcriptional repressor that contributes to anterior identity and suppresses Spemann organiser function. *Development*, *127*(11), 2303-2315.

Brozovich, F. V., Nicholson, C. J., Degen, C. V., Gao, Y. Z., Aggarwal, M., & Morgan, K. G. (2016). Mechanisms of Vascular Smooth Muscle Contraction and the Basis for Pharmacologic Treatment of Smooth Muscle Disorders. *Pharmacological reviews*, *68*(2), 476–532. https://doi.org/10.1124/pr.115.010652

Brown, B. A., Williams, H., Bond, A. R., Angelini, G. D., Johnson, J. L., & George, S. J. (2018). Carotid artery ligation induced intimal thickening and proliferation is unaffected by ageing. *Journal of cell communication and signaling*, *12*(3), 529-537.

Brown, B. A., Williams, H., & George, S. J. (2017). Evidence for the involvement of matrix-degrading metalloproteinases (MMPs) in atherosclerosis. In *Progress in molecular biology and translational science* (Vol. 147, pp. 197-237). Academic Press.

Bug, G., Burchert, A., Wagner, E. M., Kröger, N., Berg, T., Güller, S., ... & Ottmann, O. G. (2017). Phase I/II study of the deacetylase inhibitor panobinostat after allogeneic stem cell transplantation in patients with high-risk MDS or AML (PANOBEST trial). *Leukemia*, *31*(11), 2523-2525.

Buxton, B. F., Komeda, M., Fuller, J. A., & Gordon, I. (1998). Bilateral internal thoracic artery grafting may improve outcome of coronary artery surgery. Risk-adjusted survival. *Circulation*, *98*(19 Suppl), II1-6.

Cannan, C. R., Yeh, W., Kelsey, S. F., Cohen, H. A., Detre, K., & Williams, D. O. (1999). Incidence and predictors of target vessel revascularization following percutaneous transluminal coronary angioplasty: a report from the National Heart, Lung, and Blood Institute Percutaneous Transluminal Coronary Angioplasty Registry. *American Journal of Cardiology*, *84*(2), 170-175.

Captur, G. (2004). Memento for René Favaloro. *Texas Heart Institute Journal*, *31*(1), 47.

Caramori, P. R. A., Eggers, E. E., Silva-Filho, A. D. P. F. D., Uchôa, D. D. M., Jung, F., Zago, A. C., ... & Zago, A. J. (1997). Postangioplasty restenosis: a practical model in the porcine carotid artery. *Brazilian journal of medical and biological research*, *30*(9), 1087-1091.

Cardenas, C. L. L., Kessinger, C. W., Cheng, Y., MacDonald, C., MacGillivray, T., Ghoshhajra, B., ... & Lindsay, M. E. (2018). An HDAC9-MALAT1-BRG1 complex mediates smooth muscle dysfunction in thoracic aortic aneurysm. *Nature communications*, *9*(1), 1-14.

Cardiovascular Disease Statistics 2020. (2020). Retrieved from https://www.bhf.org.uk/what-we-do/our-research/heart-statistics

Chaudhary, M. A., Guo, L. W., Shi, X., Chen, G., Gong, S., Liu, B., & Kent, K. C. (2016). Periadventitial drug delivery for the prevention of intimal hyperplasia following open surgery. *Journal of controlled release*, *233*, 174-180.

Chen, X., He, Y., Fu, W., Sahebkar, A., Tan, Y., Xu, S., & Li, H. (2020). Histone Deacetylases (HDACs) and Atherosclerosis: A Mechanistic and Pharmacological Review. *Frontiers in cell and developmental biology*, *8*, 581015. https://doi.org/10.3389/fcell.2020.581015

Chen, H. R., & Yeh, T. M. (2017). In vitro assays for measuring endothelial permeability by transwells and electrical impedance systems. *Bio Protoc*, *7*(9), e2273.

Chen, S. J., Wilson, J. M., & Muller, D. W. (1994). Adenovirus-mediated gene transfer of soluble vascular cell adhesion molecule to porcine interposition vein grafts. *Circulation*, *89*(5), 1922-1928.

Chettimada, S., Joshi, S. R., Dhagia, V., Aiezza, A., Lincoln, T. M., Gupte, R., ... & Gupte, S. A. (2016). Vascular smooth muscle cell contractile protein expression is increased through protein kinase G-dependent and-independent pathways by glucose-6-phosphate dehydrogenase inhibition and deficiency. *American Journal of Physiology-Heart and Circulatory Physiology, 311*(4), H904-H912.

Choudhary, C., Kumar, C., Gnad, F., Nielsen, M. L., Rehman, M., Walther, T. C., ... & Mann, M. (2009). Lysine acetylation targets protein complexes and co-regulates major cellular functions. *Science*, *325*(5942), 834-840.

Chiu, J. J., & Chien, S. (2011). Effects of disturbed flow on vascular endothelium: pathophysiological basis and clinical perspectives. *Physiological reviews*, *91*(1), 327-387.

Christiansen, J. F., Hartwig, D., Bechtel, J. M., Klüter, H., Sievers, H. H., Schönbeck, U., & Bartels, C. (2004). Diseased vein grafts express elevated inflammatory cytokine levels compared with atherosclerotic coronary arteries. *The Annals of thoracic surgery*, *77*(5), 1575-1579.

Chu, B. F., Karpenko, M. J., Liu, Z., Aimiuwu, J., Villalona-Calero, M. A., Chan, K. K., ... & Otterson, G. A. (2013). Phase I study of 5-aza-2′-deoxycytidine in combination with valproic acid in non-small-cell lung cancer. *Cancer chemotherapy and pharmacology*, *71*(1), 115-121.

Cong, R., Jiang, X., Wilson, C. M., Hunter, M. P., Vasavada, H., & Bogue, C. W. (2006). Hhex is a direct repressor of endothelial cell-specific molecule 1 (ESM-1). *Biochemical and biophysical research communications*, *346*(2), 535-545.

Conte, M. S. (2010). Challenges of distal bypass surgery in patients with diabetes: patient selection, techniques, and outcomes. *Journal of vascular surgery*, *52*(3), 96S-103S.

Connolly, R. M., Li, H., Jankowitz, R. C., Zhang, Z., Rudek, M. A., Jeter, S. C., ... & Stearns, V. (2017). Combination epigenetic therapy in advanced breast cancer with 5-azacitidine and entinostat: a phase II National Cancer Institute/Stand Up to Cancer Study. *Clinical Cancer Research*, *23*(11), 2691-2701.

Cooper, D. K. (2011). Open Heart: The Radical Surgeons Who Revolutionized Medicine. *Annals of the Royal College of Surgeons of England*, *93*(7), 557.

Crompton, M. R., Bartlett, T. J., MacGregor, A. D., Manfioletti, G., Buratti, E., Giancotti, V., & Goodwin, G. H. (1992). Identification of a novel vertebrate homeobox gene expressed in haematopoietic cells. *Nucleic acids research*, *20*(21), 5661-5667.

Cuminetti, G., Gelsomino, S., Curello, S., Lorusso, R., Maessen, J. G., & Hoorntje, J. C. (2017). Contemporary use of arterial and venous conduits in coronary artery bypass grafting: anatomical, functional and clinical aspects. *Netherlands heart journal : monthly journal of the Netherlands Society of Cardiology and the Netherlands Heart Foundation*, *25*(1), 4–13. https://doi.org/10.1007/s12471-016-0919-2

den Ruijter, H. M., Haitjema, S., van der Meer, M. G., Van der Harst, P., Rouleau, J. L., Asselbergs, F. W., ... & IMAGINE Investigators. (2015). Long-term outcome in men and women after CABG; results from the IMAGINE trial. *Atherosclerosis*, *241*(1), 284-288.

Desjobert, C., Noy, P., Swingler, T., Williams, H., Gaston, K., & Jayaraman, P. S. (2009). The PRH/Hex repressor protein causes nuclear retention of Groucho/TLE co-repressors. *Biochemical Journal*, *417*(1), 121-132.

Developed with the special contribution of the European Association for Percutaneous Cardiovascular Interventions (EAPCI), Wijns, W., Kolh, P., Danchin, N., Di Mario, C., Falk, V., ... & Knuuti, J. (2010). Guidelines on myocardial revascularization: the task force on myocardial revascularization of the European Society of Cardiology (ESC) and the European Association for Cardio-Thoracic Surgery (EACTS). *European heart journal*, *31*(20), 2501-2555.

Dewey, C. F., Jr, Bussolari, S. R., Gimbrone, M. A., Jr, & Davies, P. F. (1981). The dynamic response of vascular endothelial cells to fluid shear stress. *Journal of biomechanical engineering*, *103*(3), 177–185. https://doi.org/10.1115/1.3138276

Dhawan, S. S., Avati Nanjundappa, R. P., Branch, J. R., Taylor, W. R., Quyyumi, A. A., Jo, H., McDaniel, M. C., Suo, J., Giddens, D., & Samady, H. (2010). Shear stress and plaque development. *Expert review of cardiovascular therapy*, *8*(4), 545–556. https://doi.org/10.1586/erc.10.28

Dizon, D. S., Damstrup, L., Finkler, N. J., Lassen, U., Celano, P., Glasspool, R., ... & Penson, R. T. (2012). Phase II activity of belinostat (PXD-101), carboplatin, and paclitaxel in women

with previously treated ovarian cancer. *International Journal of Gynecologic Cancer*, *22*(6), 979-986.

Doi, T., Hamaguchi, T., Shirao, K., Chin, K., Hatake, K., Noguchi, K., ... & Ohtsu, A. (2013). Evaluation of safety, pharmacokinetics, and efficacy of vorinostat, a histone deacetylase inhibitor, in the treatment of gastrointestinal (GI) cancer in a phase I clinical trial. *International Journal of Clinical Oncology*, *18*(1), 87-95.

Donella-Deana, A., Cesaro, L., Sarno, S., Ruzzene, M., Brunati, A. M., Marin, O., ... & Pinna, L. A. (2003). Tyrosine phosphorylation of protein kinase CK2 by Src-related tyrosine kinases correlates with increased catalytic activity. *Biochemical Journal*, *372*(Pt 3), 841.

Dorritie, K. A., McCubrey, J. A., & Johnson, D. E. (2014). STAT transcription factors in hematopoiesis and leukemogenesis: opportunities for therapeutic intervention. *Leukemia*, *28*(2), 248-257.

Drygin, D., Ho, C. B., Omori, M., Bliesath, J., Proffitt, C., Rice, R., ... & Anderes, K. (2011). Protein kinase CK2 modulates IL-6 expression in inflammatory breast cancer. *Biochemical and biophysical research communications*, *415*(1), 163-167.

Duhaylongsod, F. G., Mayfield, W. R., & Wolf, R. K. (1998). Thoracoscopic harvest of the internal thoracic artery: a multicenter experience in 218 cases 1. *The Annals of thoracic surgery*, *66*(3), 1012-1017.

Duvic, M., Talpur, R., Ni, X., Zhang, C., Hazarika, P., Kelly, C., ... & Frankel, S. R. (2007). Phase 2 trial of oral vorinostat (suberoylanilide hydroxamic acid, SAHA) for refractory cutaneous T-cell lymphoma (CTCL). *Blood*, *109*(1), 31-39.

Elliott, J. H., Wightman, F., Solomon, A., Ghneim, K., Ahlers, J., Cameron, M. J., ... & Lewin, S. R. (2014). Activation of HIV transcription with short-course vorinostat in HIV-infected patients on suppressive antiretroviral therapy. *PLoS Pathog*, *10*(11), e1004473.

Englberger, L., Streich, M., Tevaearai, H., & Carrel, T. P. (2008). Different anticoagulation strategies in off-pump coronary artery bypass operations: a European survey. *Interactive cardiovascular and thoracic surgery*, *7*(3), 378-382.

Eom, G. H., & Kook, H. (2015). Role of histone deacetylase 2 and its posttranslational modifications in cardiac hypertrophy. *BMB reports*, *48*(3), 131.

Eom, G. H., & Kook, H. (2014). Posttranslational modifications of histone deacetylases: implications for cardiovascular diseases. *Pharmacology & therapeutics*, *143*(2), 168-180.

Fandy, T. E., Herman, J. G., Kerns, P., Jiemjit, A., Sugar, E. A., Choi, S. H., ... & Carraway, H. E. (2009). Early epigenetic changes and DNA damage do not predict clinical response in an overlapping schedule of 5-azacytidine and entinostat in patients with myeloid malignancies. *Blood, The Journal of the American Society of Hematology*, *114*(13), 2764-2773.

Favaloro, R. G. (1998). Critical analysis of coronary artery bypass graft surgery: a 30-year journey. *Journal of the American College of Cardiology*, *31*(4 Supplement 2), 1B-63B.

Favero, G., Paganelli, C., Buffoli, B., Rodella, L. F., & Rezzani, R. (2014). Endothelium and its alterations in cardiovascular diseases: lifestyle intervention. *BioMed research international*, *2014*, 801896. https://doi.org/10.1155/2014/801896

Feng, Z., Zheng, W., Tang, Q., Cheng, L., Li, H., Ni, W., & Pan, X. (2017). Fludarabine inhibits STAT1-mediated up-regulation of caspase-3 expression in dexamethasone-induced osteoblasts apoptosis and slows the progression of steroid-induced avascular necrosis of the femoral head in rats. *Apoptosis*, *22*(8), 1001-1012.

Finazzi, G., Vannucchi, A. M., Martinelli, V., Ruggeri, M., Nobile, F., Specchia, G., ... & Rambaldi, A. (2013). A phase II study of G ivinostat in combination with hydroxycarbamide in patients with polycythaemia vera unresponsive to hydroxycarbamide monotherapy. *British journal of haematology*, *161*(5), 688-694.

Fischman, D. L., Leon, M. B., Baim, D. S., Schatz, R. A., Savage, M. P., Penn, I., ... & Cleman, M. (1994). A randomized comparison of coronary-stent placement and balloon angioplasty in the treatment of coronary artery disease. *New England Journal of Medicine*, *331*(8), 496-501.

Fitzgibbon, G. M., Kafka, H. P., Leach, A. J., Keon, W. J., Hooper, G. D., & Burton, J. R. (1996). Coronary bypass graft fate and patient outcome: angiographic follow-up of 5,065 grafts related to survival and reoperation in 1,388 patients during 25 years. *Journal of the American College of Cardiology*, *28*(3), 616-626.

Fogel, B. L., Lee, H., Strom, S. P., Deignan, J. L., & Nelson, S. F. (2016). Clinical exome sequencing in neurogenetic and neuropsychiatric disorders. *Annals of the New York Academy of Sciences*, *1366*(1), 49.

Foss, F., Advani, R., Duvic, M., Hymes, K. B., Intragumtornchai, T., Lekhakula, A., ... & Pohlman, B. (2015). A Phase II trial of Belinostat (PXD 101) in patients with relapsed or refractory peripheral or cutaneous T-cell lymphoma. *British journal of haematology*, *168*(6), 811-819.

French, B. A., Mazur, W., Ali, N. M., Geske, R. S., Finnigan, J. P., Rodgers, G. P., Roberts, R., & Raizner, A. E. (1994). Percutaneous transluminal in vivo gene transfer by recombinant adenovirus in normal porcine coronary arteries, atherosclerotic arteries, and two models of coronary restenosis. *Circulation*, *90*(5), 2402–2413. https://doi.org/10.1161/01.cir.90.5.2402

Fu, C., Yu, P., Tao, M., Gupta, T., Moldawer, L. L., Berceli, S. A., & Jiang, Z. (2012). Monocyte chemoattractant protein-1/CCR2 axis promotes vein graft neointimal hyperplasia through its signaling in graft-extrinsic cell populations. *Arteriosclerosis, thrombosis, and vascular biology*, *32*(10), 2418-2426.

Fushida, S., Kinoshita, J., Kaji, M., Oyama, K., Hirono, Y., Tsukada, T., ... & Ohta, T. (2016). Paclitaxel plus valproic acid versus paclitaxel alone as second-or third-line therapy for advanced gastric cancer: a randomized Phase II trial. *Drug design, development and therapy*, *10*, 2353.

Galanis, E., Jaeckle, K. A., Maurer, M. J., Reid, J. M., Ames, M. M., Hardwick, J. S., ... & Buckner, J. C. (2009). Phase II trial of vorinostat in recurrent glioblastoma multiforme: a north central cancer treatment group study. *Journal of clinical oncology*, *27*(12), 2052.

Gaston, K., Tsitsilianos, M. A., Wadey, K., & Jayaraman, P. S. (2016). Misregulation of the proline rich homeodomain (PRH/HHEX) protein in cancer cells and its consequences for tumour growth and invasion. *Cell & bioscience*, *6*(1), 12.

George, S. J., Wan, S., Hu, J., MacDonald, R., Johnson, J. L., & Baker, A. H. (2011). Sustained reduction of vein graft neointima formation by ex vivo TIMP-3 gene therapy. *Circulation*, *124*(11 suppl 1), S135-S142.

George, S. J., Baker, A. H., Angelini, G. D., & Newby, A. C. (1998). Gene transfer of tissue inhibitor of metalloproteinase-2 inhibits metalloproteinase activity and neointima formation in human saphenous veins. *Gene therapy*, *5*(11), 1552.

George, S. J., Lloyd, C. T., Angelini, G. D., Newby, A. C., & Baker, A. H. (2000). Inhibition of late vein graft neointima formation in human and porcine models by adenovirus-mediated overexpression of tissue inhibitor of metalloproteinase-3. *Circulation*, *101*(3), 296-304.

Gerber, D. E., Boothman, D. A., Fattah, F. J., Dong, Y., Zhu, H., Skelton, R. A., ... & Schiller, J. H. (2015). Phase 1 study of romidepsin plus erlotinib in advanced non-small cell lung cancer. *Lung cancer*, *90*(3), 534-541.

Gibson, S. A., & Benveniste, E. N. (2018). Protein Kinase CK2: An Emerging Regulator of Immunity. *Trends in immunology*, *39*(2), 82–85. https://doi.org/10.1016/j.it.2017.12.002

Ginn, S. L., Amaya, A. K., Alexander, I. E., Edelstein, M., & Abedi, M. R. (2018). Gene therapy clinical trials worldwide to 2017: An update. *The journal of gene medicine*, *20*(5), e3015.

Glozak, M. A., Sengupta, N., Zhang, X., & Seto, E. (2005). Acetylation and deacetylation of non-histone proteins. *gene*, *363*, 15-23.

Godin, D., Ivan, E., Johnson, C., Magid, R., & Galis, Z. S. (2000). Remodeling of carotid artery is associated with increased expression of matrix metalloproteinases in mouse blood flow cessation model. *Circulation*, *102*(23), 2861-2866.

Goetz, R. H., Rohman, M. H. J. D., Haller, J. D., Dee, R., & Rosenak, S. S. (1961). Internal mammary-coronary artery anastomosis. A nonsuture method employing tantalum rings. *The Journal of thoracic and cardiovascular surgery*, *41*, 378.

Goodings, C., Smith, E., Mathias, E., Elliott, N., Cleveland, S. M., Tripathi, R. M., ... & Hamid, R. (2015). Hhex is required at multiple stages of adult hematopoietic stem and progenitor cell differentiation. *Stem Cells*, *33*(8), 2628-2641.

Gosling, M., Golledge, J., Turner, R. J., & Powell, J. T. (1999). Arterial flow conditions downregulate thrombomodulin on saphenous vein endothelium. *Circulation*, *99*(8), 1047-1053.

Guiral, M., Bess, K., Goodwin, G., & Jayaraman, P. S. (2001). PRH represses transcription in hematopoietic cells by at least two independent mechanisms. *Journal of Biological Chemistry*, *276*(4), 2961-2970.

Gulielmos, V. (2004). *Beating Heart Bypass Surgery and Minimally Invasive Conduit Harvesting*. Steinkopff.

Guller, S., & LaChapelle, L. (1999, March). The role of placental Fas ligand in maintaining immune privilege at maternal-fetal interfaces. In Seminars in reproductive endocrinology (Vol. 17, No. 01, pp. 39-44). Copyright© 1999 by Thieme Medical Publishers, Inc..

Hagemann, I. S. (2015). Overview of technical aspects and chemistries of next-generation sequencing. In *Clinical Genomics* (pp. 3-19). Academic Press.

Haggarty, S. J., & Tsai, L. H. (2011). Probing the role of HDACs and mechanisms of chromatin-mediated neuroplasticity. *Neurobiology of learning and memory*, *96*(1), 41-52.

Hallaq, H., Pinter, E., Enciso, J., McGrath, J., Zeiss, C., Brueckner, M., ... & Jiang, X. (2004). A null mutation of Hhex results in abnormal cardiac development, defective vasculogenesis and elevated Vegfa levels. *Development*, *131*(20), 5197-5209.

Han, J. H., Lee, S. G., Jung, S. H., Lee, J. J., Park, H. S., Kim, Y. H., & Myung, C. S. (2015). Sesamin inhibits PDGF-mediated proliferation of vascular smooth muscle cells by upregulating p21 and p27. *Journal of agricultural and food chemistry, 63*(33), 7317-7325.

Handy, I., & Patel, R. C. (2013). STAT1 requirement for PKR-induced cell cycle arrest in vascular smooth muscle cells in response to heparin. *Gene*, *524*(1), 15-21.

Harskamp, R. E., Williams, J. B., Hill, R. C., de Winter, R. J., Alexander, J. H., & Lopes, R. D. (2013). Saphenous vein graft failure and clinical outcomes: Toward a surrogate end point in patients following coronary artery bypass surgery?. *American heart journal*, *165*(5), 639-643.

Haas, N. B., Quirt, I., Hotte, S., McWhirter, E., Polintan, R., Litwin, S., ... & Oza, A. (2014). Phase II trial of vorinostat in advanced melanoma. *Investigational new drugs*, *32*(3), 526-534.

Heo, S. K., Yun, H. J., Park, W. H., & Park, S. D. (2008). Emodin inhibits TNF-α-induced human aortic smooth-muscle cell proliferation via caspase-and mitochondrial-dependent apoptosis. *Journal of cellular biochemistry, 105*(1), 70-80.

Hillis, L. D., Smith, P. K., Anderson, J. L., Bittl, J. A., Bridges, C. R., Byrne, J. G., ... & Jessen, M. E. (2012). 2011 ACCF/AHA guideline for coronary artery bypass graft surgery: executive summary: a report of the American College of Cardiology Foundation/American Heart Association Task Force on Practice Guidelines. *The Journal of thoracic and cardiovascular surgery*, *143*(1), 4-34.

Hinokiyama, K., Valen, G., Tokuno, S., Vedin, J. B., & Vaage, J. (2006). Vein graft harvesting induces inflammation and impairs vessel reactivity. *The Annals of thoracic surgery*, *82*(4), 1458-1464.

Ho, C. Y., Houart, C., Wilson, S. W., & Stainier, D. Y. (1999). A role for the extraembryonic yolk syncytial layer in patterning the zebrafish embryo suggested by properties of the hex gene. *Current biology*, *9*(19), 1131-S4.

Hoch, J. R., Stark, V. K., Hullett, D. A., & Turnipseed, W. D. (1994). Vein graft intimal hyperplasia: leukocytes and cytokine gene expression. *Surgery*, *116*(2), 463.

Hölschermann, H., Stadlbauer, T. H., Wagner, A. H., Fingerhuth, H., Muth, H., Rong, S., ... & Hecker, M. (2006). STAT-1 and AP-1 decoy oligonucleotide therapy delays acute rejection and prolongs cardiac allograft survival. *Cardiovascular research*, *71*(3), 527-536.

Holt, A. W., & Tulis, D. A. (2013). Experimental Rat and Mouse Carotid Artery Surgery: Injury and Remodeling Studies. *ISRN minimally invasive surgery*, *2013*.

Hong, Y. J., Jeong, M. H., Ahn, Y., Kang, J. C., Mintz, G. S., Kim, S. W., ... & Waksman, R. (2013). Impact of lesion location on intravascular ultrasound findings and short-term and five-year long-term clinical outcome after percutaneous coronary intervention for saphenous vein graft lesions. *International journal of cardiology*, *167*(1), 29-33.

Hossainy, S., & Prabhu, S. (2008). A mathematical model for predicting drug release from a biodurable drug-eluting stent coating. *Journal of Biomedical Materials Research Part A*, *87*(2), 487-493.

Hromas, R., Radich, J., & Collins, S. (1993). PCR cloning of an orphan homeobox gene (PRH) preferentially expressed in myeloid and liver cells. *Biochemical and biophysical research communications*, *195*(2), 976-983.

Hulin-Curtis, S., Williams, H., Wadey, K. S., Sala-Newby, G. B., & George, S. J. (2017). Targeting Wnt/β-Catenin Activated Cells with Dominant-Negative N-cadherin to Reduce Neointima Formation. *Molecular Therapy-Methods & Clinical Development, 5*, 191-199.

Ibrahim, N., Buchbinder, E. I., Granter, S. R., Rodig, S. J., Giobbie-Hurder, A., Becerra, C., ... & Hodi, F. S. (2016). A phase I trial of panobinostat (LBH 589) in patients with metastatic melanoma. *Cancer medicine*, *5*(11), 3041-3050.

Ishiwata, S., Tukada, T., Nakanishi, S., Nishiyama, S., & Seki, A. (1997). Postangioplasty restenosis: platelet activation and the coagulation-fibrinolysis system as possible factors in the pathogenesis of restenosis. *American heart journal*, *133*(4), 387-392.

Jankovic, D., Gorello, P., Liu, T., Ehret, S., La Starza, R., Desjobert, C., ... & Mecucci, C. (2008). Leukemogenic mechanisms and targets of a NUP98/HHEX fusion in acute myeloid leukemia. *Blood*, *111*(12), 5672-5682.

Jayaraman, P. S., Wadey, K. S., George, S. J., & Gaston, K. (2018). Phosphorylation of PRH/HHEX by Protein Kinase CK2 Regulates Cell Proliferation and Cell Migration in Diverse Cell Types. In *Gene Expression and Regulation in Mammalian Cells-Transcription From General Aspects*. InTech.

Jeremy, J. Y., Gadsdon, P., Shukla, N., Vijayan, V., Wyatt, M., Newby, A. C., & Angelini, G. D. (2007). On the biology of saphenous vein grafts fitted with external synthetic sheaths and stents. *Biomaterials*, *28*(6), 895-908.

Jin, N., Lubner, S. J., Mulkerin, D. L., Rajguru, S., Carmichael, L., Chenv, H., ... & LoConte, N. K. (2016). A phase II trial of a histone deacetylase inhibitor panobinostat in patients with low-grade neuroendocrine tumors. *The oncologist*, *21*(7), 785.

Jones, S. F., Bendell, J. C., Infante, J. R., Spigel, D. R., Thompson, D. S., Yardley, D. A., ... & Burris 3rd, H. A. (2011). A phase I study of panobinostat in combination with gemcitabine in the treatment of solid tumors. *Clin Adv Hematol Oncol*, *9*(3), 225-30.

Jung, H., Lee, E., Kim, I., Song, J. H., & Kim, G. J. (2019). Histone deacetylase inhibition has cardiac and vascular protective effects in rats with pressure overload cardiac hypertrophy. *Physiological research*, *68*(5), 727-737.

Kang, S. H., Seok, Y. M., Song, M. J., Lee, H. A., Kurz, T., & Kim, I. (2015). Histone deacetylase inhibition attenuates cardiac hypertrophy and fibrosis through acetylation of mineralocorticoid receptor in spontaneously hypertensive rats. *Molecular pharmacology*, *87*(5), 782-791.

Kang, S., Liu, Y., & Liu, X. B. (2013). Effects of aggressive statin therapy on patients with coronary saphenous vein bypass grafts: a systematic review and meta-analysis of randomized, controlled trials. *Clinical therapeutics*, *35*(8), 1125-1136.

Kasamatsu, S., Sato, A., Yamamoto, T., Keng, V. W., Yoshida, H., Yamazaki, Y., ... & Noguchi, T. (2004). Identification of the transactivating region of the homeodomain protein, hex. *Journal of biochemistry*, *135*(2), 217-223.

Kee, H. J., Kwon, J. S., Shin, S., Ahn, Y., Jeong, M. H., & Kook, H. (2011). Trichostatin A prevents neointimal hyperplasia via activation of Krüppel like factor 4. *Vascular pharmacology*, *55*(5-6), 127-134.

Keng, V. W., Yagi, H., Ikawa, M., Nagano, T., Myint, Z., Yamada, K., ... & Sato, M. (2000). Homeobox gene Hex is essential for onset of mouse embryonic liver development and differentiation of the monocyte lineage. *Biochemical and biophysical research communications*, *276*(3), 1155-1161.

Kershaw, R. M., Siddiqui, Y. H., Roberts, D., Jayaraman, P. S., & Gaston, K. (2014). PRH/HHex inhibits the migration of breast and prostate epithelial cells through direct transcriptional regulation of Endoglin. *Oncogene*, *33*(49), 5592.

Khan, W., Farah, S., & Domb, A. J. (2012). Drug eluting stents: developments and current status. *Journal of controlled release*, *161*(2), 703-712.

Kirtane, A. J., Leon, M. B., Ball, M. W., Bajwa, H. S., Sketch Jr, M. H., Coleman, P. S., ... & Kandzari, D. E. (2013). The “final” 5-year follow-up from the ENDEAVOR IV trial comparing a zotarolimus-eluting stent with a paclitaxel-eluting stent. *JACC: Cardiovascular Interventions*, *6*(4), 325-333.

Kloc, M., & Ghobrial, R. M. (2014). Chronic allograft rejection: a significant hurdle to transplant success. *Burns & trauma*, *2*(1), 3.

Kluger, M. S. (2004). 6. Vascular endothelial cell adhesion and signaling during leukocyte recruitment. *Advances in dermatology*, *20*, 163-164.

Konstantinov, I. E. (2004). Vasilii I. Kolesov: A Surgeon to Remember. *Texas Heart Institute Journal*, *31*(4), 349–358.

Kritz, A. B., Yu, J., Wright, P. L., Wan, S., George, S. J., Halliday, C., ... & Baker, A. H. (2008). In vivo modulation of Nogo-B attenuates neointima formation. *Molecular Therapy, 16*(11), 1798-1804.

Ku, D. N., Giddens, D. P., Zarins, C. K., & Glagov, S. (1985). Pulsatile flow and atherosclerosis in the human carotid bifurcation. Positive correlation between plaque location and low oscillating shear stress. *Arteriosclerosis: An Official Journal of the American Heart Association, Inc.*, *5*(3), 293-302.

Kulik, A., Voisine, P., Mathieu, P., Masters, R. G., Mesana, T. G., Le May, M. R., & Ruel, M. (2011). Statin therapy and saphenous vein graft disease after coronary bypass surgery: analysis from the CASCADE randomized trial. *The Annals of thoracic surgery*, *92*(4), 1284-1291.

Kumar, A., Hung, O. Y., Piccinelli, M., Eshtehardi, P., Corban, M. T., Sternheim, D., Yang, B., Lefieux, A., Molony, D. S., Thompson, E. W., Zeng, W., Bouchi, Y., Gupta, S., Hosseini, H., Raad, M., Ko, Y. A., Liu, C., McDaniel, M. C., Gogas, B. D., Douglas, J. S., … Samady, H. (2018). Low Coronary Wall Shear Stress Is Associated With Severe Endothelial Dysfunction in Patients With Nonobstructive Coronary Artery Disease. *JACC. Cardiovascular interventions*, *11*(20), 2072–2080. https://doi.org/10.1016/j.jcin.2018.07.004

Kumar, A. and Lindner, V. (1997). Remodeling with neointima formation in the mouse carotid artery after cessation of blood flow. *Arterioscler Thromb Vasc Biol, 17*(10): 2238-2244.

Kupfer, J. M., Ruan, X. M., Liu, G., Matloff, J., Forrester, J., & Chaux, A. (1994). High-efficiency gene transfer to autologous rabbit jugular vein grafts using adenovirus–transferrin/polylysine–DNA complexes. *Human gene therapy*, *5*(12), 1437-1443.

Lai, A., Kennedy, B. K., Barbie, D. A., Bertos, N. R., Yang, X. J., Theberge, M. C., ... & Branton, P. E. (2001). RBP1 recruits the mSIN3-histone deacetylase complex to the pocket of retinoblastoma tumor suppressor family proteins found in limited discrete regions of the nucleus at growth arrest. *Molecular and cellular biology*, *21*(8), 2918-2932.

Le, V., Johnson, C. G., Lee, J. D., & Baker, A. B. (2015). Murine model of femoral artery wire injury with implantation of a perivascular drug delivery patch. *JoVE (Journal of Visualized Experiments)*, (96), e52403.

Lee, C. S., Bishop, E. S., Zhang, R., Yu, X., Farina, E. M., Yan, S., ... & He, T. C. (2017). Adenovirus-mediated gene delivery: potential applications for gene and cell-based therapies in the new era of personalized medicine. *Genes & diseases*, *4*(2), 43-63.

Lee, T. H., Song, S. H., Kim, K. L., Yi, J. Y., Shin, G. H., Kim, J. Y., Kim, J., Han, Y. M., Lee, S. H., Lee, S. H., Shim, S. H., & Suh, W. (2010). Functional recapitulation of smooth muscle cells via induced pluripotent stem cells from human aortic smooth muscle cells. *Circulation research*, *106*(1), 120–128. https://doi.org/10.1161/CIRCRESAHA.109.207902

Lepreux, S., Guyot, C., Billet, F., Combe, C., Balabaud, C., Bioulac-Sage, P., & Desmoulière, A. (2013). Smoothelin, a new marker to determine the origin of liver fibrogenic cells. *World Journal of Gastroenterology: WJG*, *19*(48), 9343.

Ley, K., Laudanna, C., Cybulsky, M. I., & Nourshargh, S. (2007). Getting to the site of inflammation: the leukocyte adhesion cascade updated. *Nature Reviews Immunology*, *7*(9), 678-689.

Li, H., Li, X., Lin, H., & Gong, J. (2020). High HDAC9 is associated with poor prognosis and promotes malignant progression in pancreatic ductal adenocarcinoma. *Molecular Medicine Reports*, *21*(2), 822-832.

Li, Y. Q., Wang, J. Y., Qian, Z. Q., Li, Y. L., Li, W. N., Gao, Y., & Yang, D. L. (2017). Osthole inhibits intimal hyperplasia by regulating the NF-κB and TGF-β1/Smad2 signalling pathways in the rat carotid artery after balloon injury. *European Journal of Pharmacology*, *811*, 232-239.

Lipskaia, L., Limon, I., Bobe, R., & Hajjar, R. (2012). Calcium cycling in synthetic and contractile phasic or tonic vascular smooth muscle cells. *Current Basic and Pathological Approaches to the Function of Muscle Cells and Tissues—From Molecules to Humans*, 27-43.

Loop, F. D., Lytle, B. W., Cosgrove, D. M., Stewart, R. W., Goormastic, M., Williams, G. W., ... & Proudfit, W. L. (1986). Influence of the internal-mammary-artery graft on 10-year survival and other cardiac events. *New England Journal of Medicine*, *314*(1), 1-6.

Lopes, R. D., Williams, J. B., Mehta, R. H., Reyes, E. M., Hafley, G. E., Allen, K. B., Mack, M. J., Peterson, E. D., Harrington, R. A., Gibson, C. M., Califf, R. M., Kouchoukos, N. T., Ferguson, T. B., Lorenz, T. J., & Alexander, J. H. (2012). Edifoligide and long-term outcomes after coronary artery bypass grafting: PRoject of Ex-vivo Vein graft ENgineering via Transfection IV (PREVENT IV) 5-year results. *American heart journal, 164*(3), 379–386.e1. https://doi.org/10.1016/j.ahj.2012.05.019

Lukenbill, J., & Kalaycio, M. (2013). Fludarabine: a review of the clear benefits and potential harms. *Leukemia research*, *37*(9), 986-994.

Lusis, A. J. (2000). Atherosclerosis. Nature, 407(6801), 233–241. http://doi.org/10.1038/35025203

Lyu, X., Hu, M., Peng, J., Zhang, X., & Sanders, Y. Y. (2019). HDAC inhibitors as antifibrotic drugs in cardiac and pulmonary fibrosis. *Therapeutic advances in chronic disease*, *10*, 2040622319862697.

Malhotra, R., Mauer, A. C., Cardenas, C. L. L., Guo, X., Yao, J., Zhang, X., ... & O'Donnell, C. J. (2019). HDAC9 is implicated in atherosclerotic aortic calcification and affects vascular smooth muscle cell phenotype. *Nature genetics*, *51*(11), 1580-1587.

Mali S. (2013). Delivery systems for gene therapy. *Indian journal of human genetics*, *19*(1), 3–8. https://doi.org/10.4103/0971-6866.112870

Malik, R., Chauhan, G., Traylor, M., Sargurupremraj, M., Okada, Y., Mishra, A., ... & Melander, O. (2018). Multiancestry genome-wide association study of 520,000 subjects identifies 32 loci associated with stroke and stroke subtypes. *Nature genetics*, *50*(4), 524-537.

Manfioletti, G., Gattei, V., Buratti, E., Rustighi, A., De Iuliis, A., Aldinucci, D., ... & Pinto, A. (1995). Differential expression of a novel proline-rich homeobox gene (Prh) in human hematolymphopoietic cells. *Blood*, *85*(5), 1237-1245.

Mann, M. J., Whittemore, A. D., Donaldson, M. C., Belkin, M., Conte, M. S., Polak, J. F., ... & Dzau, V. J. (1999). Ex-vivo gene therapy of human vascular bypass grafts with E2F decoy: the PREVENT single-centre, randomised, controlled trial. *The Lancet*, *354*(9189), 1493-1498.

Marfil, V., Blazquez, M., Serrano, F., Castell, J. V., & Bort, R. (2015). Growth-promoting and tumourigenic activity of c-Myc is suppressed by Hhex. *Oncogene, 34*(23), 3011.

Markus, H. S., Mäkelä, K. M., Bevan, S., Raitoharju, E., Oksala, N., Bis, J. C., ... & Lehtimäki, T. (2013). Evidence HDAC9 genetic variant associated with ischemic stroke increases risk via promoting carotid atherosclerosis. *Stroke*, *44*(5), 1220-1225.

Masłyk, M., Janeczko, M., Martyna, A., & Kubiński, K. (2017). CX-4945: the protein kinase CK2 inhibitor and anti-cancer drug shows anti-fungal activity. *Molecular and cellular biochemistry*, *435*(1-2), 193-196.

Mathew, O. P., Ranganna, K., & Yatsu, F. M. (2010). Butyrate, an HDAC inhibitor, stimulates interplay between different posttranslational modifications of histone H3 and differently alters G1-specific cell cycle proteins in vascular smooth muscle cells. *Biomedicine & Pharmacotherapy*, *64*(10), 733-740.

McCormack, M. P., Young, L. F., Vasudevan, S., de Graaf, C. A., Codrington, R., Rabbitts, T. H., ... & Curtis, D. J. (2010). The Lmo2 oncogene initiates leukemia in mice by inducing thymocyte self-renewal. *Science*, *327*(5967), 879-883.

McKavanagh, P., Yanagawa, B., Zawadowski, G., & Cheema, A. (2017). Management and Prevention of Saphenous Vein Graft Failure: A Review. *Cardiology and therapy*, *6*(2), 203-223.

Miano, J. M. (2012). Vascular smooth muscle cell phenotypic adaptation. In *Muscle* (pp. 1269-1278). Elsevier Inc..

Mills, N. L., & Everson, C. T. (1995). Vein graft failure. *Current opinion in cardiology*, *10*(6), 562-568.

Minami, T., Murakami, T., Horiuchi, K., Miura, M., Noguchi, T., Miyazaki, J. I., ... & Kodama, T. (2004). Interaction between hex and GATA transcription factors in vascular endothelial cells inhibits flk-1/KDR-mediated vascular endothelial growth factor signaling. *Journal of Biological Chemistry*, *279*(20), 20626-20635.

Mishra, S., Reichert, A., Cunnick, J., Senadheera, D., Hemmeryckx, B., Heisterkamp, N., & Groffen, J. (2003). Protein kinase CKIIα interacts with the Bcr moiety of Bcr/Abl and mediates proliferation of Bcr/Abl-expressing cells. *Oncogene, 22*(51), 8255.

Mitra, A. K., Gangahar, D. M., & Agrawal, D. K. (2006). Cellular, molecular and immunological mechanisms in the pathophysiology of vein graft intimal hyperplasia. *Immunology & Cell Biology*, *84*(2), 115-124.

Moliterno, D. J., & Topol, E. J. (1998). Restenosis: epidemiology and treatment. *Textbook of Cardiovascular Medicine, EJ Topol, ed.(Philadelphia, Lippincott-Raven Publ.), pp2065-2100*

Motwani, J. G., & Topol, E. J. (1998). Aortocoronary saphenous vein graft disease: pathogenesis, predisposition, and prevention. *Circulation*, *97*(9), 916-931.

Mudau, M., Genis, A., Lochner, A., & Strijdom, H. (2012). Endothelial dysfunction: the early predictor of atherosclerosis. *Cardiovascular journal of Africa*, *23*(4), 222–231. https://doi.org/10.5830/CVJA-2011-068

Mundi, S., Massaro, M., Scoditti, E., Carluccio, M. A., Van Hinsbergh, V. W., Iruela-Arispe, M. L., & De Caterina, R. (2018). Endothelial permeability, LDL deposition, and cardiovascular risk factors—a review. *Cardiovascular research*, *114*(1), 35-52.

Murray, G., Redmond Porcheron, J. H., & Roschlau, W. (1954). Anastomosis of a systemic artery to the coronary. *Canadian Medical Association Journal*, *71*(6), 594.

Nakagawa, T., Abe, M., Yamazaki, T., Miyashita, H., Niwa, H., Kokubun, S., & Sato, Y. (2003). HEX acts as a negative regulator of angiogenesis by modulating the expression of angiogenesis-related gene in endothelial cells in vitro. *Arteriosclerosis, thrombosis, and vascular biology*, *23*(2), 231-237.

Nelson, C. P., Goel, A., Butterworth, A. S., Kanoni, S., Webb, T. R., Marouli, E., ... & UK Biobank CardioMetabolic Consortium CHD working group. (2017). Association analyses based on false discovery rate implicate new loci for coronary artery disease. *Nature genetics*, *49*(9), 1385.

Newby, A. C. (2005). Dual role of matrix metalloproteinases (matrixins) in intimal thickening and atherosclerotic plaque rupture. *Physiological reviews*, *85*(1), 1-31.

Newman, C. S., Chia, F., & Krieg, P. A. (1997). The XHex homeobox gene is expressed during development of the vascular endothelium: overexpression leads to an increase in vascular endothelial cell number. *Mechanisms of development*, *66*(1-2), 83-93.

Newman, K. D., Dunn, P. F., Owens, J. W., Schulick, A. H., Virmani, R., Sukhova, G., ... & Dichek, D. A. (1995). Adenovirus-mediated gene transfer into normal rabbit arteries results in prolonged vascular cell activation, inflammation, and neointimal hyperplasia. *The Journal of clinical investigation*, *96*(6), 2955-2965.

Nicolini, F., Vezzani, A., Fortuna, D., Contini, G. A., Pacini, D., Gabbieri, D., ... & Gherli, T. (2016). Gender differences in outcomes following isolated coronary artery bypass grafting: long-term results. *Journal of cardiothoracic surgery*, *11*(1), 144.

Nishio, H., Masumoto, H., Sakamoto, K., Yamazaki, K., Ikeda, T., & Minatoya, K. (2019). MicroRNA-145-loaded poly (lactic-co-glycolic acid) nanoparticles attenuate venous intimal hyperplasia in a rabbit model. *The Journal of thoracic and cardiovascular surgery*, *157*(6), 2242-2251.

Noy, P., Gaston, K., & Jayaraman, P. S. (2012). Dasatinib inhibits leukaemic cell survival by decreasing PRH/Hhex phosphorylation resulting in increased repression of VEGF signalling genes. *Leukemia research*, *36*(11), 1434-1437.

Noy, P., Williams, H., Sawasdichai, A., Gaston, K., & Jayaraman, P. S. (2010). PRH/Hhex controls cell survival through coordinate transcriptional regulation of vascular endothelial growth factor signaling. *Molecular and cellular biology, 30*(9), 2120-2134.

Nguyen, A. T., Gomez, D., Bell, R. D., Campbell, J. H., Clowes, A. W., Gabbiani, G., … Owens, G. K. (2013). Smooth Muscle Cell Plasticity: Fact or Fiction? *Circulation Research*, *112*(1), 17–22.

O'Connor, O. A., Horwitz, S., Masszi, T., Van Hoof, A., Brown, P., Doorduijn, J., ... & Shustov, A. (2015). Belinostat in patients with relapsed or refractory peripheral T-cell lymphoma: results of the pivotal phase II BELIEF (CLN-19) study. *Journal of Clinical Oncology*, *33*(23), 2492.

Ohnaka, M., Marui, A., Yamahara, K., Minakata, K., Yamazaki, K., Kumagai, M., ... & Sakata, R. (2014). Effect of microRNA-145 to prevent vein graft disease in rabbits by regulation of smooth muscle cell phenotype. *The Journal of Thoracic and Cardiovascular Surgery*, *148*(2), 676-682.

Okam, M. M., Esrick, E. B., Mandell, E., Campigotto, F., Neuberg, D. S., & Ebert, B. L. (2015). Phase 1/2 trial of vorinostat in patients with sickle cell disease who have not benefitted from hydroxyurea. *Blood, The Journal of the American Society of Hematology*, *125*(23), 3668-3669.

Olesen, R., Vigano, S., Rasmussen, T. A., Søgaard, O. S., Ouyang, Z., Buzon, M., ... & Lichterfeld, M. (2015). Innate immune activity correlates with CD4 T cell-associated HIV-1 DNA decline during latency-reversing treatment with panobinostat. *Journal of virology*, *89*(20), 10176-10189.

Owens, C. D., Gasper, W. J., Rahman, A. S., & Conte, M. S. (2015). Vein graft failure. *Journal of vascular surgery*, *61*(1), 203–216. https://doi.org/10.1016/j.jvs.2013.08.019

Owens, G. K., Kumar, M. S., & Wamhoff, B. R. (2004). Molecular regulation of vascular smooth muscle cell differentiation in development and disease. *Physiological reviews*, *84*(3), 767-801.

Oyama, Y., Kawai-Kowase, K., Sekiguchi, K., Sato, M., Sato, H., Yamazaki, M., ... & Nagai, R. (2004). Homeobox Protein Hex Facilitates Serum Responsive Factor–Mediated Activation of the SM22α Gene Transcription in Embryonic Fibroblasts. *Arteriosclerosis, thrombosis, and vascular biology, 24*(9), 1602-1607.

Ozaki, C. K. (2007). Cytokines and the early vein graft: strategies to enhance durability. *Journal of vascular surgery*, *45*(6), A92-A98.

Padró, T., Mesters, R. M., Dankbar, B., Hintelmann, H., Bieker, R., Kiehl, M., ... & Kienast, J. (2002). The catalytic domain of endogenous urokinase-type plasminogen activator is required

for the mitogenic activity of platelet-derived and basic fibroblast growth factors in human vascular smooth muscle cells. *Journal of cell science*, *115*(9), 1961-1971.

Pahk, K., Joung, C., Jung, S. M., Song, H. Y., Park, J. Y., Byun, J. W., ... & Kim, W. K. (2017). Visualization of synthetic vascular smooth muscle cells in atherosclerotic carotid rat arteries by F-18 FDG PET. *Scientific reports*, *7*(1), 1-8.

Parker, A. L., White, K. M., Lavery, C. A., Custers, J., Waddington, S. N., & Baker, A. H. (2013). Pseudotyping the adenovirus serotype 5 capsid with both the fibre and penton of serotype 35 enhances vascular smooth muscle cell transduction. *Gene therapy*, *20*(12), 1158-1164.

Percie du Sert, N., Hurst, V., Ahluwalia, A., Alam, S., Avey, M. T., Baker, M., ... & Würbel, H. (2020). The ARRIVE guidelines 2.0: Updated guidelines for reporting animal research. *Journal of Cerebral Blood Flow & Metabolism*, *40*(9), 1769-1777.

Peserico, A., & Simone, C. (2011). Physical and functional HAT/HDAC interplay regulates protein acetylation balance. *Biomed Research International*, *2011*.

Petsophonsakul, P., Furmanik, M., Forsythe, R., Dweck, M., Schurink, G. W., Natour, E., ... & Schurgers, L. (2019). Role of Vascular Smooth Muscle Cell Phenotypic Switching and Calcification in Aortic Aneurysm Formation: Involvement of Vitamin K-Dependent Processes. *Arteriosclerosis, thrombosis, and vascular biology*, *39*(7), 1351-1368.

Pickell, Z., Williams, A. M., Alam, H. B., & Hsu, C. H. (2020). Histone Deacetylase Inhibitors: A Novel Strategy for Neuroprotection and Cardioprotection Following Ischemia/Reperfusion Injury. *Journal of the American Heart Association*, *9*, e016349.

Prebet, T., Sun, Z., Ketterling, R. P., Zeidan, A., Greenberg, P., Herman, J., ... & Eastern Cooperative Oncology Group and North American Leukemia intergroup. (2016). Azacitidine with or without Entinostat for the treatment of therapy-related myeloid neoplasm: further results of the E1905 North American Leukemia Intergroup study. *British journal of haematology*, *172*(3), 384-391.

Prestel, M., Prell-Schicker, C., Webb, T., Malik, R., Lindner, B., Ziesch, N., ... & Dichgans, M. (2019). The atherosclerosis risk variant rs2107595 mediates allele-specific transcriptional regulation of HDAC9 via E2F3 and Rb1. *Stroke*, *50*(10), 2651-2660.

Potter, C. M., Lundberg, M. H., Harrington, L. S., Warboys, C. M., Warner, T. D., Berson, R. E., Moshkov, A. V., Gorelik, J., Weinberg, P. D., & Mitchell, J. A. (2011). Role of shear stress

in endothelial cell morphology and expression of cyclooxygenase isoforms. *Arteriosclerosis, thrombosis, and vascular biology*, *31*(2), 384–391. https://doi.org/10.1161/ATVBAHA.110.214031

Puvvada, S. D., Guillén-Rodríguez, J. M., Rivera, X. I., Heard, K., Inclan, L., Schmelz, M., ... & Persky, D. O. (2017). A phase II exploratory study of PXD-101 (Belinostat) followed by Zevalin in patients with relapsed aggressive high-risk lymphoma. *Oncology*, *93*(6), 401-405.

Rajathurai, T., Rizvi, S. I., Lin, H., Angelini, G. D., Newby, A. C., & Murphy, G. J. (2010). Periadventitial rapamycin-eluting microbeads promote vein graft disease in long-term pig vein-into-artery interposition grafts. *Circulation: Cardiovascular Interventions*, *3*(2), 157-165.

Rambaldi, A., Dellacasa, C. M., Finazzi, G., Carobbio, A., Ferrari, M. L., Guglielmelli, P., ... & Barbui, T. (2010). A pilot study of the Histone-Deacetylase inhibitor Givinostat in patients with JAK2V617F positive chronic myeloproliferative neoplasms. *British journal of haematology*, *150*(4), 446-455.

Ridker, P. M., Everett, B. M., Thuren, T., MacFadyen, J. G., Chang, W. H., Ballantyne, C., Fonseca, F., Nicolau, J., Koenig, W., Anker, S. D., Kastelein, J., Cornel, J. H., Pais, P., Pella, D., Genest, J., Cifkova, R., Lorenzatti, A., Forster, T., Kobalava, Z., Vida-Simiti, L., … CANTOS Trial Group (2017). Antiinflammatory Therapy with Canakinumab for Atherosclerotic Disease. *The New England journal of medicine, 377*(12), 1119–1131. https://doi.org/10.1056/NEJMoa1707914

Sabik, J. F. (2011). Understanding saphenous vein graft patency.

Sanders, W. G., Hogrebe, P. C., Grainger, D. W., Cheung, A. K., & Terry, C. M. (2012). A biodegradable perivascular wrap for controlled, local and directed drug delivery. *Journal of controlled release: official journal of the Controlled Release Society*, *161*(1), 81–89. https://doi.org/10.1016/j.jconrel.2012.04.029

Sanger, F., Nicklen, S., & Coulson, A. R. (1977). DNA sequencing with chain-terminating inhibitors. *Proceedings of the national academy of sciences*, *74*(12), 5463-5467.

Sans, M., Panés, J., Ardite, E., Elizalde, J. I., Arce, Y., Elena, M., ... & Piqué, J. M. (1999). VCAM-1 and ICAM-1 mediate leukocyte-endothelial cell adhesion in rat experimental colitis. *Gastroenterology*, *116*(4), 874-883.

Sano, K., Mintz, G. S., Carlier, S. G., Fujii, K., Yasuda, T., Kimura, M., ... & Moussa, I. (2006). Intravascular ultrasonic differences between aorto-ostial and shaft narrowing in saphenous

veins used as aortocoronary bypass grafts. *American Journal of Cardiology*, *97*(10), 1463-1466.

Schepers, A., Eefting, D., Bonta, P. I., Grimbergen, J. M., De Vries, M. R., Van Weel, V., De Vries, C. J., Egashira, K., Van Bockel, J. H. and Quax, P. H. A. (2006). "Anti-MCP-1 gene therapy inhibits vascular smooth muscle cells proliferation and attenuates vein graft thickening both in vitro and in vivo." *Arteriosclerosis Thrombosis and Vascular Biology 26*(9): 2063-2069

Schmitt, T., Mayer-Steinacker, R., Mayer, F., Grünwald, V., Schütte, J., Hartmann, J. T., ... & Egerer, G. (2016). Vorinostat in refractory soft tissue sarcomas–Results of a multi-centre phase II trial of the German Soft Tissue Sarcoma and Bone Tumour Working Group (AIO). *European Journal of Cancer*, *64*, 74-82.

Seki, Y., Kai, H., Shibata, R., Nagata, T., Yasukawa, H., Yoshimura, A., & Imaizumi, T. (2000). Role of the JAK/STAT pathway in rat carotid artery remodeling after vascular injury. *Circulation research*, *87*(1), 12-18.

Sekiguchi, K., Kurabayashi, M., Oyama, Y., Aihara, Y., Tanaka, T., Sakamoto, H., ... & Iijima, H. (2001). Homeobox protein Hex induces SMemb/nonmuscle myosin heavy chain-B gene expression through the cAMP-responsive element. *Circulation research*, *88*(1), 52-58.

Sena, C. M., Pereira, A. M., & Seiça, R. (2013). Endothelial dysfunction—a major mediator of diabetic vascular disease. *Biochimica et Biophysica Acta (BBA)-Molecular Basis of Disease*, *1832*(12), 2216-2231.

Serruys, P. W., De Jaegere, P., Kiemeneij, F., Macaya, C., Rutsch, W., Heyndrickx, G., ... & Belardi, J. (1994). A comparison of balloon-expandable-stent implantation with balloon angioplasty in patients with coronary artery disease. *New England Journal of Medicine*, *331*(8), 489-495.

Shapira, O. M., Xu, A., Aldea, G. S., Vita, J. A., Shemin, R. J., & Keaney, J. F. (1999). Enhanced nitric oxide–mediated vascular relaxation in radial artery compared with internal mammary artery or saphenous vein. *Circulation*, *100*(suppl 2), II-322.

Shuhaiber, J. H., Evans, A. N., Massad, M. G., & Geha, A. S. (2002). Mechanisms and future directions for prevention of vein graft failure in coronary bypass surgery. *European journal of cardio-thoracic surgery*, *22*(3), 387-396.

Shustov, A., Coiffier, B., Horwitz, S., Sokol, L., Pro, B., Wolfson, J., ... & Bates, S. (2017). Romidepsin is effective and well tolerated in older patients with peripheral T-cell lymphoma: analysis of two phase II trials. *Leukemia & lymphoma*, *58*(10), 2335-2341.

Shyy, Y. J., Hsieh, H. J., Usami, S., & Chien, S. (1994). Fluid shear stress induces a biphasic response of human monocyte chemotactic protein 1 gene expression in vascular endothelium. *Proceedings of the National Academy of Sciences of the United States of America*, *91*(11), 4678–4682. https://doi.org/10.1073/pnas.91.11.4678

Siddiqui, Y. H., Kershaw, R. M., Humphreys, E. H., Junior, E. A., Chaudhri, S., Jayaraman, P. S., & Gaston, K. (2017). CK2 abrogates the inhibitory effects of PRH/HHEX on prostate cancer cell migration and invasion and acts through PRH to control cell proliferation. *Oncogenesis*, *6*(1), e293.

Sikorski, K., Czerwoniec, A., Bujnicki, J. M., Wesoly, J., & Bluyssen, H. A. (2011). STAT1 as a novel therapeutical target in pro-atherogenic signal integration of IFNγ, TLR4 and IL-6 in vascular disease. *Cytokine & growth factor reviews*, *22*(4), 211-219.

Smith, S., Beasley, M., Hodes, R., Hall, H., Biel, E., & Huth, E. W. (1957). Auxiliary myocardial vascularization by prosthetic graft implantation. *Surgery, gynecology & obstetrics*, *104*(3), 263-268.

Smolock, E., & Berk, B. C. (2012). Vascular smooth muscle cell remodeling in atherosclerosis and restenosis. In *Muscle* (pp. 1301-1309). Academic Press.

Søgaard, O. S., Graversen, M. E., Leth, S., Olesen, R., Brinkmann, C. R., Nissen, S. K., ... & Tolstrup, M. (2015). The depsipeptide romidepsin reverses HIV-1 latency in vivo. *PLoS Pathog*, *11*(9), e1005142.

Song, H. H. G., Rumma, R. T., Ozaki, C. K., Edelman, E. R., & Chen, C. S. (2018). Vascular tissue engineering: progress, challenges, and clinical promise. *Cell stem cell*, *22*(3), 340-354.

Soufi, A., Sawasdichai, A., Shukla, A., Noy, P., Dafforn, T., Smith, C., ... & Gaston, K. (2010). DNA compaction by the higher-order assembly of PRH/Hex homeodomain protein oligomers. *Nucleic acids research*, *38*(21), 7513-7525.

Soufi, A., Noy, P., Buckle, M., Sawasdichai, A., Gaston, K., & Jayaraman, P. S. (2009). CK2 phosphorylation of the PRH/Hex homeodomain functions as a reversible switch for DNA binding. *Nucleic acids research*, *37*(10), 3288-3300.

Soufi, A., & Jayaraman, P. S. (2008). PRH/Hex: an oligomeric transcription factor and multifunctional regulator of cell fate. *Biochemical Journal*, 412(3), 399-413.

Soufi, A., Gaston, K., & Jayaraman, P. S. (2006). Purification and characterisation of the PRH homeodomain: removal of the N-terminal domain of PRH increases the PRH homeodomain–DNA interaction. *International journal of biological macromolecules*, *39*(1-3), 45-50.

Soufi, A., Smith, C., Clarke, A. R., Gaston, K., & Jayaraman, P. S. (2006). Oligomerisation of the developmental regulator proline rich homeodomain (PRH/Hex) is mediated by a novel proline-rich dimerisation domain. *Journal of molecular biology*, *358*(4), 943-962.

Southerland, K. W., Frazier, S. B., Bowles, D. E., Milano, C. A., & Kontos, C. D. (2013). Gene therapy for the prevention of vein graft disease. *Translational Research*, *161*(4), 321-338.

Sousa, J. E., Costa, M. A., Abizaid, A., Abizaid, A. S., Feres, F., Pinto, I. M., ... & Falotico, R. (2001). Lack of neointimal proliferation after implantation of sirolimus-coated stents in human coronary arteries. *Circulation, 103*(2), pp.192-195.

Souza, D. S., Johansson, B., Bojö, L., Karlsson, R., Geijer, H., Filbey, D., ... & Dashwood, M. R. (2006). Harvesting the saphenous vein with surrounding tissue for CABG provides long-term graft patency comparable to the left internal thoracic artery: results of a randomized longitudinal trial. *The Journal of thoracic and cardiovascular surgery*, *132*(2), 373-378.

Souza, D. S., Dashwood, M. R., Tonazi, A., Johansson, B., Buffolo, E., Lima, R., ... & Bomfim, V. (2003). Preparation of the saphenous vein for coronary artery bypass grafting: a new technique" no touch" that maintains the vein wall integral and provides high immediate patency. *Brazilian Journal of Cardiovascular Surgery*, *18*(4), 303-311.

Souza, D. (2002a). *Harvesting of saphenous vein for coronary artery bypass grafting: an improved technique that maintains vein wall integrity and provides a high early patency rate* (Doctoral dissertation, Acta Universitatis Upsaliensis).

Souza, D. S., Dashwood, M. R., Tsui, J. C., Filbey, D., Bodin, L., Johansson, B., & Borowiec, J. (2002b). Improved patency in vein grafts harvested with surrounding tissue: results of a randomized study using three harvesting techniques. *The Annals of thoracic surgery*, *73*(4), 1189-1195.

Stepanova, V., Jayaraman, P. S., Zaitsev, S. V., Lebedeva, T., Bdeir, K., Kershaw, R., ... & Tkachuk, V. A. (2016). Urokinase-type plasminogen activator (uPA) promotes angiogenesis by attenuating proline-rich homeodomain protein (PRH) transcription factor activity and de-

repressing vascular endothelial growth factor (VEGF) receptor expression. *Journal of Biological Chemistry*, *291*(29), 15029-15045.

Stepanova, V., Jerke, U., Sagach, V., Lindschau, C., Dietz, R., Haller, H., & Dumler, I. (2002). Urokinase-dependent human vascular smooth muscle cell adhesion requires selective vitronectin phosphorylation by ectoprotein kinase CK2. *Journal of Biological Chemistry*, *277*(12), 10265-10272.

Su, H., Lei, C. T., & Zhang, C. (2017). Interleukin-6 signaling pathway and its role in kidney disease: an update. *Frontiers in immunology*, *8*, 405.

Su, J., You, P., Zhao, J. P., Zhang, S. L., Song, S. H., Fu, Z. R., ... & Hu, Y. P. (2012). A potential role for the homeoprotein Hhex in hepatocellular carcinoma progression. *Medical Oncology*, *29*(2), 1059-1067.

Sumagin, R., Lomakina, E., & Sarelius, I. H. (2008). Leukocyte-endothelial cell interactions are linked to vascular permeability via ICAM-1-mediated signaling. *American Journal of Physiology-Heart and Circulatory Physiology*, *295*(3), H969-H977.

Sumida, S. M., Truitt, D. M., Lemckert, A. A., Vogels, R., Custers, J. H., Addo, M. M., ... & Barouch, D. H. (2005). Neutralizing antibodies to adenovirus serotype 5 vaccine vectors are directed primarily against the adenovirus hexon protein. *The Journal of Immunology*, *174*(11), 7179-7185.

Swingler, T. E., Bess, K. L., Yao, J., Stifani, S., & Jayaraman, P. S. (2004). The proline-rich homeodomain protein recruits members of the Groucho/Transducin-like enhancer of split protein family to co-repress transcription in hematopoietic cells. *Journal of Biological Chemistry*, *279*(33), 34938-34947.

Szasz, T., Thakali, K., Fink, G. D., & Watts, S. W. (2007). A comparison of arteries and veins in oxidative stress: producers, destroyers, function, and disease. *Experimental Biology and Medicine*, *232*(1), 27-37.

Taggart, D. P., D'Amico, R., & Altman, D. G. (2001). Effect of arterial revascularisation on survival: a systematic review of studies comparing bilateral and single internal mammary arteries. *The Lancet*, *358*(9285), 870-875.

Tan, P. H., Chan, C., Xue, S. A., Dong, R., Ananthesayanan, B., Manunta, M., ... & Taylor, K. M. (2004). Phenotypic and functional differences between human saphenous vein (HSVEC) and umbilical vein (HUVEC) endothelial cells*. Atherosclerosis, 173*(2), 171-183.

Tanaka, T., Inazu, T., Yamada, K., Myint, Z., Keng, V. W., Inoue, Y., ... & Noguchi, T. (1999). cDNA cloning and expression of rat homeobox gene, Hex, and functional characterization of the protein. *Biochemical Journal*, *339*(Pt 1), 111.

Tanaka, H., Yamamoto, T., Ban, T., Satoh, S. I., Tanaka, T., Shimoda, M., ... & Noguchi, T. (2005). Hex stimulates the hepatocyte nuclear factor 1α-mediated activation of transcription. *Archives of biochemistry and biophysics, 442*(1), 117-124.

Taniwaki, M., Stefanini, G. G., Silber, S., Richardt, G., Vranckx, P., Serruys, P. W., ... & RESOLUTE All-Comers Investigators. (2014). 4-year clinical outcomes and predictors of repeat revascularization in patients treated with new-generation drug-eluting stents: a report from the RESOLUTE All-Comers trial (A Randomized Comparison of a Zotarolimus-Eluting Stent With an Everolimus-Eluting Stent for Percutaneous Coronary Intervention). *Journal of the American College of Cardiology*, *63*(16), 1617-1625.

Tee, J. K., Yip, L. X., Tan, E. S., Santitewagun, S., Prasath, A., Ke, P. C., ... & Leong, D. T. (2019). Nanoparticles' interactions with vasculature in diseases. *Chemical Society Reviews*, *48*(21), 5381-5407.

Telles, E., & Seto, E. (2012). Modulation of cell cycle regulators by HDACs. *Frontiers in bioscience (Scholar edition)*, *4*, 831.

Terry, C. M., Li, L., Li, H., Zhuplatov, I., Blumenthal, D. K., Kim, S. E., ... & Cheung, A. K. (2012). In vivo evaluation of the delivery and efficacy of a sirolimus-laden polymer gel for inhibition of hyperplasia in a porcine model of arteriovenous hemodialysis graft stenosis. *Journal of controlled release*, *160*(3), 459-467.

Thomas J. L. (1999). The Vineberg legacy: internal mammary artery implantation from inception to obsolescence. *Texas Heart Institute journal*, *26*(2), 107–113.

Thomas, A. C., Angelini, G. D., & Zakkar, M. (2016). Strategies to Extend the Life of Saphenous Vein Grafts. In *Coronary Graft Failure* (pp. 581-593). Springer, Cham.

Thompson, P. L., & Nidorf, S. M. (2018). Anti-inflammatory therapy with canakinumab for atherosclerotic disease: lessons from the CANTOS trial. *Journal of Thoracic Disease*, *10*(2), 695.

Topisirovic, I., Culjkovic, B., Cohen, N., Perez, J. M., Skrabanek, L., & Borden, K. L. (2003). The proline-rich homeodomain protein, PRH, is a tissue-specific inhibitor of eIF4E-dependent cyclin D1 mRNA transport and growth. *The EMBO journal*, *22*(3), 689-703.

Torella, D., Curcio, A., Gasparri, C., Galuppo, V., Serio, D. D., Surace, F. C., ... & Indolfi, C. (2007). Fludarabine prevents smooth muscle proliferation in vitro and neointimal hyperplasia in vivo through specific inhibition of STAT-1 activation. *American Journal of Physiology-Heart and Circulatory Physiology*, *292*(6), H2935-H2943.

Tsaousi, A., Williams, H., Lyon, C. A., Taylor, V., Swain, A., Johnson, J. L., & George, S. J. (2011). Wnt4/β-catenin signaling induces VSMC proliferation and is associated with intimal thickening. *Circulation research, 108*(4), 427-436.

Tsui, J. C. S., & Dashwood, M. R. (2002). Recent strategies to reduce vein graft occlusion: a need to limit the effect of vascular damage. *European journal of vascular and endovascular surgery*, *23*(3), 202-208.

Tucker, R. P., Henningsson, P., Franklin, S. L., Chen, D., Ventikos, Y., Bomphrey, R. J., & Thompson, M. S. (2014). See-saw rocking: an in vitro model for mechanotransduction research. *Journal of The Royal Society Interface*, *11*(97), 20140330.

Turner, N. A., O'regan, D. J., Ball, S. G. and Porter, K. E. (2005). "Simvastatin inhibits MMP-9 secretion from human saphenous vein smooth muscle cells by inhibiting the RhoA/ROCK pathway and reducing MMP-9 mRNA levels." *Faseb Journal 19*(2): 804-815

Usami, M., Kikuchi, S., Takada, K., Ono, M., Sugama, Y., Arihara, Y., ... & Kato, J. (2020). FOXO3a Activation by HDAC Class IIa Inhibition Induces Cell Cycle Arrest in Pancreatic Cancer Cells. *Pancreas*, *49*(1), 135-142.

van Buul, J. D., Kanters, E., & Hordijk, P. L. (2007). Endothelial signaling by Ig-like cell adhesion molecules. *Arteriosclerosis, thrombosis, and vascular biology*, *27*(9), 1870–1876. https://doi.org/10.1161/ATVBAHA.107.145821

Vigl, B., Zgraggen, C., Rehman, N., Banziger-Tobler, N. E., Detmar, M., & Halin, C. (2009). Coxsackie-and adenovirus receptor (CAR) is expressed in lymphatic vessels in human skin and affects lymphatic endothelial cell function in vitro. *Experimental cell research, 315*(2), 336-347.

Vineberg, A. M. (1949). Development of anastomosis between the coronary vessels and a transplanted internal mammary artery. *The Journal of thoracic surgery*, *18*(6), 839.

Vlodaver, Z., & Edwards, J. E. (1971). Pathologic changes in aortic-coronary arterial saphenous vein grafts. *Circulation*, *44*(4), 719-728.

Wadey, K. S., Brown, B. A., Sala-Newby, G. B., Jayaraman, P. S., Gaston, K., & George, S. J. (2017). Protein kinase CK2 inhibition suppresses neointima formation via a proline-rich homeodomain-dependent mechanism. *Vascular pharmacology*, *99*, 34-44.

Wallentin, L., Becker, R. C., Budaj, A., Cannon, C. P., Emanuelsson, H., Held, C., ... & Mahaffey, K. W. (2009). Ticagrelor versus clopidogrel in patients with acute coronary syndromes. *New England Journal of Medicine*, *361*(11), 1045-1057.

Wan, S., George, S. J., Berry, C., & Baker, A. H. (2012). Vein graft failure: current clinical practice and potential for gene therapeutics. *Gene therapy*, *19*(6), 630.

Wang, L. Z., Ramírez, J., Yeo, W., Chan, M. Y. M., Thuya, W. L., Lau, J. Y. A., ... & Goh, B. C. (2013). Glucuronidation by UGT1A1 is the dominant pathway of the metabolic disposition of belinostat in liver cancer patients. *PloS one*, *8*(1), e54522.

Wang, J. C., Waltner-Law, M., Yamada, K., Osawa, H., Stifani, S., & Granner, D. K. (2000). Transducin-like enhancer of split proteins, the human homologs of Drosophila groucho, interact with hepatic nuclear factor 3β. *Journal of Biological Chemistry*, *275*(24), 18418-18423.

Ward, A. O., Caputo, M., Angelini, G. D., George, S. J., & Zakkar, M. (2017). Activation and inflammation of the venous endothelium in vein graft disease. *Atherosclerosis*, *265*, 266-274.

Watanabe, T., Kato, H., Kobayashi, Y., Yamasaki, S., Morita-Hoshi, Y., Yokoyama, H., ... & Tobinai, K. (2010). Potential efficacy of the oral histone deacetylase inhibitor vorinostat in a phase I trial in follicular and mantle cell lymphoma. *Cancer science*, *101*(1), 196-200.

West, N. E. J., Qian, H. S., Guzik, T. J., Black, E., Cai, S. J., George, S. E. and Channon, K. M. (2001). "Nitric oxide synthase (nNOS) gene transfer modifies venous bypass graft remodeling - Effects on vascular smooth muscle cell differentiation and superoxide production." *Circulation 104*(13): 1526-1532.

White, K. M., Alba, R., Parker, A. L., Wright, A. F., Bradshaw, A. C., Delles, C., ... & Baker, A. H. (2013). Assessment of a novel, capsid-modified adenovirus with an improved vascular gene transfer profile. *Journal of cardiothoracic surgery*, *8*(1), 1-8.

Wickham, T. J., Mathias, P., Cheresh, D. A., & Nemerow, G. R. (1993). Integrins αvβ3 and αvβ5 promote adenovirus internalization but not virus attachment. *Cell, 73*(2), 309-319.

Wijns, W., Steg, P. G., Mauri, L., Kurowski, V., Parikh, K., Gao, R., ... & Rademaker-Havinga, T. (2014). Endeavour zotarolimus-eluting stent reduces stent thrombosis and improves clinical

outcomes compared with cypher sirolimus-eluting stent: 4-year results of the PROTECT randomized trial. *European heart journal*, *35*(40), 2812-2820.

Williams, H., Mill, C. A., Monk, B. A., Hulin-Curtis, S., Johnson, J. L., & George, S. J. (2016). Wnt2 and WISP-1/CCN4 induce intimal thickening via promotion of smooth muscle cell migration. *Arteriosclerosis, thrombosis, and vascular biology*, ATVBAHA-116.

Williams, H., Mill, C. A., Curtis, S., Johnson, J. L., & George, S. J. (2014). Wnt inducible soluble protein 1 (WISP-1) promotes VSMC migration and intimal thickening. *Atherosclerosis, 232*(2), e2.

Williams, P. D., & Kingston, P. A. (2011). Plasmid-mediated gene therapy for cardiovascular disease. *Cardiovascular research, 91*(4), 565-576.

Williams, H., Jayaraman, P. S., & Gaston, K. (2008). DNA wrapping and distortion by an oligomeric homeodomain protein. *Journal of molecular biology*, *383*(1), 10-23.

World Heart Day 2017. (2018). Retrieved from http://www.who.int/cardiovascular_diseases/world-heart-day-2017/en/

Wolffe, A. P., & Hayes, J. J. (1999). Chromatin disruption and modification. *Nucleic acids research*, *27*(3), 711-720.

Xhemalce, B., Dawson, M. A., & Bannister, A. J. (2011). Histone Modifications. Encyclopedia of Molecular Cell Biology and Molecular Medicine.

Xie, D., Zhu, J., Liu, Q., Li, J., Song, M., Wang, K., ... & Li, T. (2019). Dysregulation of HDAC9 represses trophoblast cell migration and invasion through TIMP3 activation in preeclampsia. *American journal of hypertension*, *32*(5), 515-523.

Xie, N., Chen, M., Dai, R., Zhang, Y., Zhao, H., Song, Z., ... & Wang, L. (2017). SRSF1 promotes vascular smooth muscle cell proliferation through a Δ133p53/EGR1/KLF5 pathway. *Nature communications, 8*, 16016.

Xu, S., Shriver, A. S., Jagadeesha, D. K., Chamseddine, A. H., Szőcs, K., Weintraub, N. L., ... & Miller Jr, F. J. (2012). Increased expression of Nox1 in neointimal smooth muscle cells promotes activation of matrix metalloproteinase-9. *Journal of vascular research*, *49*(3), 242-248.

Xu Q. (2004). Mouse models of arteriosclerosis: from arterial injuries to vascular grafts. *The American journal of pathology*, *165*(1), 1–10. https://doi.org/10.1016/S0002-9440(10)63270-1

Xu, Y. J., Rathi, S. S., Chapman, D. C., Arneja, A. S., & Dhalla, N. S. (2003). Mechanisms of Lysophosphatidic Acid–induced DNA Synthesis in Vascular Smooth Muscle Cells. *Journal of cardiovascular pharmacology*, *41*(3), 381-387.

Yamada, M., Katsuma, S., Adachi, T., Hirasawa, A., Shiojima, S., Kadowaki, T., Okuno, Y., Koshimizu, T. A., Fujii, S., Sekiya, Y., Miyamoto, Y., Tamura, M., Yumura, W., Nihei, H., Kobayashi, M., & Tsujimoto, G. (2005). Inhibition of protein kinase CK2 prevents the progression of glomerulonephritis. *Proceedings of the National Academy of Sciences of the United States of America*, *102*(21), 7736–7741. https://doi.org/10.1073/pnas.0409818102

Yamaoka, T., Yonemitsu, Y., Komori, K., Baba, H., Matsumoto, T., Onohara, T., & Maehara, Y. (2005). Ex vivo electroporation as a potent new strategy for nonviral gene transfer into autologous vein grafts. *American journal of physiology. Heart and circulatory physiology*, *289*(5), H1865–H1872. https://doi.org/10.1152/ajpheart.00353.2005

Yan, L. J., Yang, H. T., Duan, H. Y., Wu, J. T., Qian, P., Fan, X. W., & Wang, S. (2017). Myricitrin inhibits vascular adhesion molecule expression in TNF-α-stimulated vascular smooth muscle cells. *Molecular Medicine Reports*, *16*(5), 6354-6359.

Yang, X., Chang, Y., & Wei, W. (2016). Endothelial Dysfunction and Inflammation: Immunity in Rheumatoid Arthritis. *Mediators of inflammation*, *2016*, 6813016. https://doi.org/10.1155/2016/6813016

Yang, Z., Oemar, B. S., Carrel, T., Kipfer, B., Julmy, F., & Lüscher, T. F. (1998). Different proliferative properties of smooth muscle cells of human arterial and venous bypass vessels: role of PDGF receptors, mitogen-activated protein kinase, and cyclin-dependent kinase inhibitors. *Circulation*, *97*(2), 181-187.

Yap, C. H., Sposato, L., Akowuah, E., Theodore, S., Dinh, D. T., Shardey, G. C., ... & Mohajeri, M. (2009). Contemporary results show repeat coronary artery bypass grafting remains a risk factor for operative mortality. *The Annals of thoracic surgery*, *87*(5), 1386-1391.

Yeo, W., Chung, H. C., Chan, S. L., Wang, L. Z., Lim, R., Picus, J., ... & Goh, B. C. (2012). Epigenetic therapy using belinostat for patients with unresectable hepatocellular carcinoma: a multicenter phase I/II study with biomarker and pharmacokinetic analysis of tumors from patients in the Mayo Phase II Consortium and the Cancer Therapeutics Research Group. *Journal of Clinical Oncology*, *30*(27), 3361.

Yoshizumi, M., Abe, J. I., Tsuchiya, K., Berk, B. C., & Tamaki, T. (2003). Stress and vascular responses: atheroprotective effect of laminar fluid shear stress in endothelial cells: possible

role of mitogen-activated protein kinases. *Journal of pharmacological sciences*, *91*(3), 172-176.

Young JL, Dean DA. Electroporation-mediated gene delivery. *Adv Genet*. 2015;89:49-88. doi:10.1016/bs.adgen.2014.10.003

Zamparini, A. L., Watts, T., Gardner, C. E., Tomlinson, S. R., Johnston, G. I., & Brickman, J. M. (2006). Hex acts with β-catenin to regulate anteroposterior patterning via a Groucho-related co-repressor and Nodal. *Development*, *133*(18), 3709-3722.

Zaromitidou, M., Siasos, G., Papageorgiou, N., Oikonomou, E., & Tousoulis, D. (2017). Atherosclerosis and Coronary Artery Disease: From Basics to Genetics. In *Cardiovascular Diseases* (pp. 3-24).

Zhang, B., Dong, Y., Liu, M., Yang, L., & Zhao, Z. (2019). miR-149-5p Inhibits Vascular Smooth Muscle Cells Proliferation, Invasion, and Migration by Targeting Histone Deacetylase 4 (HDAC4). *Medical science monitor: international medical journal of experimental and clinical research*, *25*, 7581.

Zhang, M., Urabe, G., Little, C., Wang, B., Kent, A. M., Huang, Y., Kent, K. C., & Guo, L. W. (2018). HDAC6 Regulates the MRTF-A/SRF Axis and Vascular Smooth Muscle Cell Plasticity. *JACC. Basic to translational science*, *3*(6), 782–795. https://doi.org/10.1016/j.jacbts.2018.08.010

Zhang, Q., Gerlach, J. C., Schmelzer, E., & Nettleship, I. (2017). Effect of Calcium-Infiltrated Hydroxyapatite Scaffolds on the Hematopoietic Fate of Human Umbilical Vein Endothelial Cells. *Journal of vascular research*, *54*(6), 376–385. https://doi.org/10.1159/000481778

Zhang, Y., Wu, D., Xia, F., Xian, H., Zhu, X., Cui, H., & Huang, Z. (2016). Downregulation of HDAC9 inhibits cell proliferation and tumor formation by inducing cell cycle arrest in retinoblastoma. *Biochemical and biophysical research communications*, *473*(2), 600-606.

Zhang, H. X., Jiang, S. S., Zhang, X. F., Zhou, Z. Q., Pan, Q. Z., Chen, C. L., ... & Weng, D. S. (2015). Protein kinase CK2α catalytic subunit is overexpressed and serves as an unfavorable prognostic marker in primary hepatocellular carcinoma. *Oncotarget*, *6*(33), 34800.

Zhang, S. M., Zhu, L. H., Chen, H. Z., Zhang, R., Zhang, P., Jiang, D. S., ... & Wang, P. X. (2014). Interferon regulatory factor 9 is critical for neointima formation following vascular injury. *Nature communications, 5*(1), 1-17.

Zhang, K., Cao, J., Dong, R., & Du, J. (2013). Early growth response protein 1 promotes restenosis by upregulating intercellular adhesion molecule-1 in vein graft. *Oxidative Medicine and Cellular Longevity*, *2013*.

Zhu, Y. (2019). Calcium in vascular smooth muscle cell elasticity and adhesion: novel insights into the mechanism of action. *Frontiers in physiology*, *10*, 852.

Zhou, H., Zeng, G., Zhou, A., Tang, J., Huang, Q., Chen, G., ... & Hu, B. (1995). Adenovirus mediated gene transfer of vascular smooth muscle cells and endothelial cells in vitro. *Chinese medical journal*, *108*(7), 493-496.